SYNTHESIS, CHARACTERIZATION AND CORROSION INHIBITION APPLICATIONS OF CERIUM (III) METAL COMPLEXES DERIVED FROM SOME SALICYALDEHYDE-BASED SCHIFF BASES

BY

ONU, UCHENNA LYNDA. (*BSc., IMSU; MSc., FUTO)*
Reg. No. 20144918688

SUBMITTED TO THE
POSTGRADUATE SCHOOL,
FEDERAL UNIVERSITY OF TECHNOLOGY, OWERRI.

JUNE, 2025

SYNTHESIS, CHARACTERIZATION AND CORROSION INHIBITION APPLICATIONS OF CERIUM (III) METAL COMPLEXES DERIVED FROM SOME SALICYALDEHYDE- BASED SCHIFF BASES

BY

ONU, UCHENNA LYNDA
Reg. No. 20144918688

A THESIS SUBMITTED TO THE DEPARTMENT OF CHEMISTRY, POSTGRADUATE SCHOOL, FEDERAL UNIVERSITY OF TECHNOLOGY, OWERRI

IN PARTIAL FULFILLMENT OF THE REQUIREMENTS FOR THE AWARD OF DOCTOR OF PHILOSOPHY (Ph.D) IN INORGANIC CHEMISTRY

JUNE, 2025

CERTIFICATION

We, the undersigned, certify that this work entitled "**SYNTHESIS, CHARACTERIZATION AND CORROSION INHIBITION APPLICATIONS OF CERIUM (III) METAL COMPLEXES DERIVED FROM SOME SALICYALDEHYDE- BASED SCHIFF BASES**" was carried-out by the **Onu Uchenna Lynda** with registration number, **20144918688** in accordance with regulations governing the award of the degree of Doctor of Philosophy (Ph.D) in the postgraduate School at the Federal University of Technology, Owerri.

Dr. C.O. Akalezi
(Thesis Supervisor)
19/06/2025
Date

Dr. C.O. Alisa
(Co- supervisor)
19/06/2025
Date

Dr. C.I.A. Nwoko
(Co- supervisor)
19/06/25
Date

Prof. C.K. Enenebeaku.
(HOD, Chemistry Dept.)
19-06-25
Date

Prof. (Mrs.) C.E. Ogukwe
(Dean, School of Physical Sciences)
19/06/2025
Date

Prof. (Mrs.) J. N. Nwosu
(Dean, PG School)
Date

Prof. A. I. Onen
(External Examiner)
19-06-2025
Date

DEDICATION

This research work is dedicated to God Almighty, for His infinite mercies, Assistant Comptroller of Immigration (ACI). L. Onu (JP), whose strong support and immeasurable love encouraged me to achieve this milestone in my carrier. And finally, to the loving memory of my beloved immediate elder sister, Late Mrs. Doris I. Orji.

ACKNOWLEDGEMENTS

My sincere gratitude goes to the Soveign God, Whose mercy kept me till the completion of this work. My special thanks goes to my supervisor Dr. C.O. Akalezi, who guided me, and ensured that justice is done to this research. I also acknowledge the Co- supervisors. Dr. C.I.A. Nwoko. and Dr. C.O. Alisa, for their encouragement during the course of this work. A big thank you to the H.O.D of Chemistry Department, Prof. C.K., Enenebeaku, and the PG coordinator Dr. A.B. Ali, for their immense contributions and encouragement during all stages of this study. I appreciate the Dean of School of Physical Sciences, Prof. (Mrs.) C.E., Ogukwe of Chemistry Department for her professional advice and relentless guidance throughout the period of this programme. I also acknowledge Dr. I.C., Iwu, of Chemistry Department, all my colleagues from Chemistry Department, and Prof. C.I., Duruigbo of Department of Crop Science, FUTO for their positive roles. Words will not be enough to describe my immense gratitude to Dr. Peter D.M. Njamanze, Senior Consultant Obstetrician and Gynaecologist with Federal Teaching Hospital Owerri, for his medical care. My profound appreciation goes to my Course-mate, Dr. (Mrs.) N. P., Ebosie, of Chemistry Department, IMSU, Owerri, Mr. Chimobi, Mr. A. U. Anuo, the Chief Technologist of the laboratory section of Chemistry Department FUTO, as well as all the lab Staff for their collective effort. I extend my appreciation to my undergraduate students who assisted me in various ways, especially Mr. F.O. Izuagba. I am also grateful to Dr. C. Echereobia, director of FUTO Press, Prof. Okereke of Geology Department FUTO for their wise counsel. I would not fail to thank the Dean of PG School, Prof. (Mrs.) J.N Nwosu, the associate Dean of PG School, Prof. C.C. Egwuonwu, Chemistry Schedule Officer, Comr. Ebere Nwafor. Thanks to Post Graduate School lecturers, the Staff and Management of PG School for the good work they do.

A big thank you to my siblings, Mr. Henry Nnodim, Mr. Emeka Nnodim, Mr. Tochi Nnodim, Mrs. Henrietta Sylvanus for their love and support, and to everyone who put-in their effort to see that this work is achieved. Finally, my profound appreciation goes to my beloved husband, Assistant Comptroller of Immigration, Imo State Command (ACI). L. Onu. (JP), my awesome children: Master Solace Onu, Master Royal Onu, Miss Awesome Onu, Master Kaima Onu, and Master Jayden Onu, for their love, time, encouragement, and immeasurable contributions.

TABLE OF CONTENTS

COVER PAGE
TITLE PAGE i
CERTIFICATION ii
DEDICATION iii
ACKNOWLEDGEMENTS iv
TABLE OF CONTENTS v
LIST OF TABLES ix
LIST OF FIGURES xii
LIST OF SCHEMES xv
LIST OF ABBREVIATIONS xvi
ABSTRACT xvii

CHAPTER ONE: INTRODUCTION 1
1.1 Background Information 1
1.1.1 Compounds of Interest in the Present Study 1
1.1.2 Rare Earth Metal Chemistry 3
1.1.3 Chemistry of Cerium [Xe] $4f^1$ $5d^1$ $6s^2$ 4
1.2 Statement of the Problem 5
1.3 Aim and Objectives of the Study 5
1.4 Justification of the Study 6
1.5. Scope of this Study 6

CHAPTER TWO: LITERATURE REVIEW 8
2.1 Background Study 8
2.2 Biological Applications of Rare-earth Schiff base Metal Complexes 10
2.2.1 Antimicrobial Applications 10
2.2.2 Pharmaceutical and Biomedical Applications 12
2.3 Catalytic Activities of Transition Schiff base Metal complexes 15
2.4 Corrosion Inhibition Applications of Schiff-bases and Their Metal Complexes 16
2.4.1 Inorganic Inhibitors 19
2.4.2 Organic Inhibitors 20
2.5 Molecular Modelling Study Approach to Corrosion inhibition 20
2.6 Computational Studies on Corrosion Inhibition 21
2.7 Corrosion Inhibition by Weight-loss and Electrochemical Methods. 23

CHAPTER THREE: MATERIALS AND METHODS 26
3.1 Materials 26
3.1.1 Materials/Reagents 26
3.2 Methods 26
3.2.1 Sample Preparations 26
3.2.1.1 Synthesis of 2-hydroxyphenyl – phenylimine or (salicylideneaniline) SALAN 26
3.2.1.2 Synthesis of Bis (2-hydroxyphenyl) imine or (salicylidene-2-aminophenol) SAL2AP 27
3.2.1.3 Synthesis of Bis(2-hydroxyphenyl) – 1,2-benzenediimine (salicylidene1,2- phenylenediamine) SALPD 27
3.2.1.4 Synthesis of Lanthanide (III) Metal Complexes 28
3.2.3 Characterization Techniques 28

3.2.3.1 Elemental Microanalysis 28
3.2.3.2 pH Measurement 28
3.2.3.3 Conductivity Measurement 28
3.2.3.4 Electronic Absorption Spectroscopy 29
3.2.3.5 FT-IR Spectral Study 29
3.2.3.6 1H & 13C NMR Spectral Study 29
3.2.3.7 EDXRF Study 29
3.2.3.8 AFM Study 30
3.2.3.9 Magnetic Susceptibility Measurement 30
3.2.4 Corrosion Inhibition Test by Weight- Loss Method. 30
3.2.4.1 Preparation corrodent 30
3.2.4.2 Preparation of Specimen 30
3.2.5 Molecular Modeling 32

CHAPTER FOUR: RESULTS AND DISCUSSION 33
4.1 RESULTS 33
4.1.1 Physical Measurements for SALAN and CeSALAN 34
4.1.2 Spectral results for SALAN and CeSALAN 37
4.1.3 Inhibitive Action SALAN and CeSALAN 46
4.1.3.1 Gravimetric results 46
4.1.3.2: Effect of temperature on the performance of the inhibitors 55
4.1.4 Surface Studies Using AFM 62
4.1.5 Electrochemical Studies 64
4.2 Discussions on SALAN and CeSALAN 67
4.2.1 Physical Measurements 67
4.2.1.1 Colour 67
4.2.1.2 pH and Melting point Measurement 67
4.2.1.3 Solubility 67
4.2.1.4 Molar Conductivity and Magnetic Susceptibility Measurement 68
4.2.2 Spectral Studies 68
4.2.2.1 Uv-Vis spectral data of SALAN and CeSALAN 68
4.2.2.2 Analysis of SALAN and CeSALAN FTIR Spectral 68
4.2.2.3 Analysis of 1H-NMR Spectral of SALAN 69
4.2.2.4 Analysis of 13-C NMR of SALAN 69
4.2.2.5 Discussion on EDXRF of CeSALAN 70
4.2.3 Inhibitive Action of SALAN and CeSALAN. 70
4.2.3.1 Gravimetric Results 70
4.2.3.2 Analysis of the Results of the Mass-Loss Method 70
4.2.3.3 Analysis of Variation of IE with Immersion Time 71
4.2.3.4 Analysis of the effect of Temperature on the Performance of the Inhibitors 71
4.2.3.5 Analysis of Thermodynamics Parameters, ΔH, and ΔS 71
4.2.4 Adsorption Isotherm 72
4.2.5 Surface Analysis using AFM 73
4.2.6 Electrochemical Studies 74
4.2.6.1 Analysis of the results of Potentiodynamic Polarization Studies 74
4.2.6.2 Analysis of the results of EIS studies 74
4.1.2 Physical Measurements for SAL2AP and CeSAL2AP 75

4.1.3 Spectral Results for SAL2AP and CeSAL2AP 76
4.1.4 Inhibitive Action of SAL2AP and CeSAL2AP 86
4.1.4.1 Gravimetric Results 86
4.1.4.2: Effect of Temperature on the Inhibition Efficiency of the Inhibitor- compounds at the optimum concentration 95
4.1.5 Surface Studies Using AFM 102
4.1.6 Electrochemical Results 104
4.1.6.1 Potentiodynamic (PDP) Results 104
4.1.6.2 EIS Results 105
4.2.1 Discussion on SAL2AP and CeSAL2AP 107
4.2.1.1 Physical Measurements 107
4.2.1.1.1 Colour 107
4.2.1.1.2 Melting Point and pH Measurement 107
4.2.1.1.3 Solubility Analysis 107
4.2.1.1.4 Molar Conductivity and Magnetic Susceptibility Measurement 107
4.2.1.2 Spectral Measurements 108
4.2.1.2.1 UV-Vis Spectral data of SAL2AP and CeSAL2AP 108
4.2.1.2.2 FTIR Spectral Studies of SAL2AP and CeSAL2AP 108
4.2.1.2.3 Analysis of ^{1}H-NMR Spectral of SAL2AP 108
4.2.1.2.4 13-C NMR Spectra of SAL2AP Schiff Base 109
4.2.1.2.5 Energy Dispersive X- ray Fluorescence (EDXRF) Spectroscopy Analysis of CeSAL2AP 109
4.2.1.3 Inhibitive Action SAL2AP and CeSAL2AP 110
4.2.1.3.1 Analysis of Gravimetric Results 110
4.2.1.3.2 Analysis of variation of IE with Immersion time 110
4.2.1.3.3 Analysis of the effect of temperature on the performance of the inhibitors 110
4.2.1.3.4 Analysis of Thermodynamics Parameters, ΔH, and ΔS 111
4.2.1.4 Adsorption Isotherms 112
4.2.1.5 Surface Analysis using AFM 113
4.2.1.6 Electrochemical Studies 113
4.2.1.6.1 Analysis of the results of Potentiodynamic polarization studies 113
4.2.1.6.2 Analysis of the Results of EIS Studies 114
4.1.3 Physical Measurements for SALPD and CeSALPD 115
4.1.4 Spectral Results 116
4.1.5 Inhibitive Action of SALPD and CeSALPD. 126
4.1.5.1 Gravimetric Results 126
4.1.5.2: Effect of temperature on the performance of the inhibitors 135
4.1.6 Surface Analysis Using AFM 142
4.1.7 Electrochemical Results 144
4.1.7.1 Potentiodynamic (PDP) Results 144
4.2.2 Discussion on SALPD and CeSALPD 146
4.2.2.1 Physical Measurements 146
4.2.2.1.1 Colour 146
4.2.2.1.2 PH and Melting Points Measurement 146
4.2.2.1.3 Solubility Analysis 147
4.2.2.1.2 Molar Conductivity Measurement and Magnetic Susceptibility measurements 147
4.2.2.2 Spectral Measurements 147
4.2.2.2.1 Electronic Absorption Spectra Analysis of SALPD and CeSALPD 147
4.2.2.2.2 FTIR Spectral Studies of SALPD and CeSALPD 148

4.2.2.2.3 ^{1}H Spectral Study of SALPD 148
4.2.2.2.4 13-C NMR Spectral Study of SALPD 149
4.2.2.2.5 EDXRF Spectral Analysis of CeSALPD 149
4.2.2.3 Inhibitive Action SALPD and CeSALPD 150
4.2.2.3.1 Analysis of gravimetric Results 150
4.2.2.3.2 Analysis of variation of Inhibition Efficiency with Immersion Time 150
4.2.2.3.3 Analysis of the Effect of Temperature on the Performance of the Inhibitors 151
4.2.2.3.4 Analysis of Thermodynamics Parameters, Δ H and ΔS. 151
4.2.2.4 Adsorption Isotherm 152
4.2.2.5 Surface Analysis using AFM 153
4.2.2.6 Electrochemical Studies 154
4.2.2.6.1 Analysis of the Results of Potentiodynamic Polarization Studies 154
4.2.2.6.2 Analysis of the Results of EIS Studies 154
4.2.2.7 Molecular Modeling Study 163
4.2.2.8 Analysis of Molecular Modelling of Schiff Bases 168
4.2.2.8 HSAB-type Analysis 169
4.2.2.9 Inhibitor Adsorption Simulation. 170

CHAPTER FIVE: CONCLUSION AND RECOMMENDATIONS 172
5.1 Conclusion 172
5.2 Recommendations 173
5.3 Contributions to Knowledge 174

REFERENCES 175
APPENDIX 185

LIST OF TABLES

Table	Title	Page
4.1:	Physical Properties, Percentage Yield, and Elemental Analysis of SALAN and CeSALAN	34
4.2:	Solubility Tests for SALAN and CeSALAN	35
4.3:	Molar conductivity and Magnetic susceptibility for SALAN and CeSALAN	36
4.4:	^{1}H NMR Spectral Data of SALAN	42
4.5:	C-13 NMR Spectral Data of SALAN	44
4.6:	Gravimetric Data of Mild Steel in 1M HCl in the presence and absence of SALAN (Lagmuir Adsorption Isotherm)	46
4.7:	Gravimetric Data of Mild Steel in 1M HCl in the presence and absence of SALAN (Temkin Adsorption Isotherm)	48
4.8:	Gravimetric Data of Mild Steel in 1M HCl in the presence and absence of SALAN (Frumkin's Adsorption Isotherm)	49
4.9:	Gravimetric Data of Mild Steel in 1M HCl in the presence and absence of CeSALAN (Langmuir's Isotherm)	50
4.10:	Gravimetric Data of Mild Steel in 1M HCl in the presence and absence of CeSALAN (Temkin's Isotherm)	51
4.11:	Gravimetric Data of Mild Steel in 1M HCl in the presence and absence of CeSALAN (Frumkin's Isotherm)	52
4.12:	Regression Square (R^2) values obtained for Langmuir, Temkin, and Frumkim Adsorption Isotherms.	53
4.13:	Influence of Concentration on the Inhibition Efficiency of SALAN and CeSALAN during Mild Steel Corrosion in 1M HCl after 24-hour immersion.	53
4.14:	Effect of Temperature on the inhibition efficiency of SALAN and CeSALAN at optimum concentration	55
4.15:	Corrosion Data of BLANK, SALAN and CeSALAN for plot of log CR/T vs 1/T	57
4.16:	Values for E_a, ΔG_{ads}, ΔH, and ΔS for BLANK, SALAN and CeSALAN	60
4.17:	Variation of Inhibition Efficiency with Immersion Time of SALAN and CeSALAN	60
4.18:	AFM Parameter Data for Compounds	63
4.19:	PDP Parameters of Mild Steel immersed in the presence and absence of 0.8 mmol/dm^3 of the inhibitors in 1M HCl	64
4.20:	EIS parameters and Inhibition Efficiency at 30 °C of Mild steel in the absence and in the presence of 0.8 mmol/dm^3 concentrations of the inhibitors	66
4.21:	Inhibition efficiency values obtained for the various Analytical Technique	66
4.22:	Physical properties, percentage yield, and elemental analysis of	75
4.23:	Solubility Tests for Compounds	76
4.24:	Molar Conductivity and Magnetic Susceptibility of Compounds	76
4.25:	^{1}H NMR Spectral Data of SAL2AP	82
4.26:	C-13 NMR data of SAL2AP	84

4.27: Gravimetric data of Mild Steel in 1M HCl in the presence and absence of SAL2AP (Langmuir Adsorption Isotherm) 86
4.28: Gravimetric Data of Mild Steel in 1M HCl in the presence and absence of SAL2AP (Temkin Adsorption Isotherm) 88
4.29: Gravimetric Data of Carbon Steel in 1M HCl in the presence and absence of SAL2AP (Frumkin's Adsorption Isotherm) 89
4.30: Gravimetric Data of Mild Steel in 1M HCl in the presence and absence of CeSAL2AP (Langmuir's Isotherm) 90
4.31: Gravimetric Data of Mild Steel in 1M HCl in the presence and absence of CeSAL2AP (Temkin's Isotherm) 91
4.32: Gravimetric Data of Mild Steel in 1M HCl in the presence and absence of CeSAL2AP (Frumkin's Isotherm) 92
4.33: Regression Square values obtained for Langmuir, Temkin, and Frumkin Adsorption Isotherms. 93
4.34: Influence of Concentration on the Inhibition Efficiency of SAL2AP and CeSAL2AP during Mild Steel Corrosion in 1M HCl after 24-hour immersion. 93
4.35: Effect of Temperature on the Inhibition Efficiency of SAL2AP and CeSAL2AP at optimum concentration 95
4.36: Corrosion data of BLANK, SAL2AP and CeSAL2AP, for Plot of log C_R/T vs 1/T 97
4.37: Values for Ea, ΔGads, ΔH, and ΔS for Blank, SAL2AP and CeSAL2AP 100
4.38: Variation of Inhibition Efficiency with Immersion Time for SAL2AP and CeSAL2AP 100
4.39: AFM Parameters of Compounds 103
4.40: PDP parameters of Mild Steel immersed in the presence and absence of 0.8 mmol /dm^3 of the inhibitors in 1M HCl 104
4.41: EIS Parameters and Inhibition Efficiency at 30 °C of Mild Steel in the absence and in the presence of 0.8 mmol /dm3 concentrations of the inhibitors 106
4.42: Inhibition Efficiency values obtained for the various Analytical Techniques 106
4.43: Physical Properties, Percentage Yield, and Elemental Analysis of SALPD and CeSALPD 115
4.44: Solubility Tests for SALPD and CeSALPD in different Organic Solvents 115
4.45: Molar Conductivity and Magnetic Susceptibility of SALPD and CeSALPD in DMSO and DMF 116
4.46: ^{1}H NMR Spectral Data of SALPD f1(ppm) 123
4.47: C-13 NMR Data of SALPD 124
4.48: Gravimetric data of Mild Steel in 1M HCl in the presence and absence of SALPD (Lagmuir Adsorption Isotherm) 126
4.49: Gravimetric data of Mild Steel in 1M HCl in the presence and absence of SALPD (Temkin Adsorption Isotherm) 128
4.50: Gravimetric Data of Mild Steel in 1M HCl in the presence and absence of SALPD (Frumkin's Adsorption Isotherm) 129

4.51: Gravimetric Data of Mild steel in 1M HCl in the presence and absence of CeSALPD (Langmuir's Isotherm) 130
4.52: Gravimetric Data of Mild Steel in 1M HCl in the presence and absence of CeSALPD (Temkin's Isotherm) 131
4.53: Gravimetric data of Mild Steel in 1M HCl in the presence and absence of CeSALPD (Frumkin's Isotherm) 132
4.54: Regression Square values obtained for Langmuir, Temkin, and Frumkin adsorption isotherms. 132
4.55: Influence of concentration on the inhibition efficiency of SALPD and CeSALPD during Mild Steel corrosion in 1M HCl after 24-hour immersion. 133
4.56: Effect of Temperature on the inhibition efficiency of SALPD and CeSALPD at optimum concentration 135
4.57: Corrosion Data of BLANK, SALPD and CeSALPD for plot of log C_R/T vs 137
4.58: Values for E_a, ΔG_{ads}, ΔH, and ΔS for Blank, SALPD and CeSALPD 140
4.59: Effect of Immersion time on Inhibition Efficiency of SALPD and 140
4.60: AFM Parameters of Inhibitor Compounds 143
4.61: The PDP Parameters of Mild Steel immersed in the presence and absence of 0.8 mmol/dm^3 of the inhibitors in 1M HCl 144
4.62: EIS Parameters and Inhibition Efficiency at 30°C of Mild Steel in the absence and in the presence of 0.8mmol/dm^3 concentrations of the inhibitors 145
4.63: Inhibition Efficiency values obtained for the various Analytical Techniques 146
4.64: Quantum Chemical Parameter Data of Schiff Bases 165

LIST OF FIGURES

Figure	Title	Page
1.1	Structures of precursor compounds of interest applicable in this study.	3
4.1:	UV-Visible Spectrum of SALAN	37
4.2:	Uv –Visible Spectrum of CeSALAN	38
4.3:	Fourier Transform Infrared (FTIR) Spectrum of SALAN	39
4.4:	Fourier Transform Infrared (FTIR) Spectrum (FTIR) of CeSALAN	40
4.5:	Proton ^{1}H NMR Spectrum of SALAN	41
4.6:	Proton numbering in SALAN	42
4.7:	Carbon 13 (C-13) NMR Spectrum of SALAN	43
4.8:	Carbon numbering in SALAN	44
4.9:	EDXRF Spectra of CeSALAN	45
4.10:	Langmuir's Adsorption Plots for Mild Steel in 1 M HCl containing various concentrations of SALAN and CeSALAN.	47
4.11:	Influence of Concentration on the Inhibition Efficiency of SALAN and CeSALAN during Mild Steel Corrosion in 1M HCl after 24-hour immersion	54
4.12:	Arrhenius plots for Mild Steel in 1 M HCl solution free and systems inhibited by 0.8 mmol/dm^3 of the Inhibitors	56
4.13:	Plot of log (C_R/T) Vs 1/ T for BLANK, SALAN, and CeSALAN	58
4.14:	Effect of Temperature on the Inhibition efficiency of the compounds at the optimum concentration	59
4.15:	The Variation of Inhibition Efficiency of SALAN and CeSALAN with Immersion time	61
4.16 (a)	BLANK 2D AFM (1M HCl)	62
Figure 4.16 (b)	BLANK 3D AF(1M HCl)	62
4.16 (c)	SALAN 2D AFM	62
Figure 4.16 (d)	SALAN 3D AFM	62
4.16 (e)	CeSALAN 2D AFM	62
Figure 4.16 (f)	CeSALAN 3D AFM	62
4.17:	Polarization curves of Mild Steel in the absence and in the presence of 0.8 mmol/dm^3 each of SALAN and CeSALAN at 30 °C.	64
4.18:	Nyquist Curves of Mild Steel in the absence and presence of 0.8mmol/dm^3 Concentrations of SALAN and CeSALAN at 30 °C.	65
4.19:	UV-Vis. Spectrum of SAL2AP	77
4.20:	UV- Vis Spectrum of CeSAL2AP Wavenumber (cm-^{1})	79
4.21:	FTIR Spectrum of SAL2AP	79
4.22:	FTIR of CeSAL2AP	80
4.23:	SAL2AP ^{1}H- NMR	81
4.24:	Proton numbering in SAL2AP	82
4.25:	C-13 NMR OF SAL2AP	83
4.26:	Carbon numbering in SAL2AP	84
4.27:	Energy Dispersive X-Ray Fluorescence (EDXRF) Spectrum of CeSAL2AP	85
4.28:	Langmuir's Adsorption plots for Mild Steel in 1 M HCl containing various concentrations of SAL2AP and CeSAL2AP	87
4.29:	Influence of Concentration on the Inhibition Efficiency of SAL2AP and CeSAL2AP during Mild Steel Corrosion in 1M HCl after 24 hr. Immersion.	94

4.30: Arrhenius Plots for Mild Steel in 1 M HCl Solution free and Inhibited by 0.8 mmol/dm^3 of the Inhibitors 96
4.31: Plot of log of C_R/T vs I/T for Blank, SAL2AP and CeSAL2AP 98
4.32: Effect of Temperature on the Inhibition Efficiency of the compounds at Optimum Concentration 99
4.33: Variation of Inhibition Efficiency of SAL2AP, and CeSAL2AP with Immersion Time 101
4.34 (a) BLANK 2D AFM (1M HCl) Figure 4.34(b) BLANK 3D AFM (1 M HCl) 102
4.34 (c) SAL2AP 2D AFM Figure 4.34 (d) SAL2AP 3D AFM 102
4.34 (e) CeSAL2AP 2D AFM Figure 4.34 (f) CeSAL2AP 3D AFM 102
4.35: Polarization curves of Mild Steel in the absence and in the presence of 0.8 mmol/dm^3 each of SAL2AP and CeSAL2AP at 30 °C 104
4.36: Nyquist curves of Mild Steel in the Absence and Presence of 0.8 mmol /dm^3 concentrations at of SAL2AP and CeSAL2AP at 30 °C. 105
4.37: UV- VIS Spectrum of SALPD 117
4.38: UV-VIS. SPECTRUM OF CeSALPD 118
Wavenumber(cm^{-1}) 119
4.39: Furia Transform Infrared (FTIR) Spectrum of SALPD 119
4.40: Fourier Transform Infrared (FTIR) Spectrum of CeSALPD 120
4.41: Proton NMR (^{1}H- NMR) Spectrum of SALPD 121
4.42: Proton numbering in SALPD 122
4.43: Carbon-13 (C-13) NMR OF SALPD 123
4.44: Carbon numbering in SALPD 124
4.45: Energy Dispersive X-Ray Fluorescence (EDXRF) OF CeSALPD 125
4.46: Langmuir's Adsorption Plots for mild steel in 1 M HCl containing various concentrations of SALPD and CeSALPD 127
4.47: Effect of Concentration on the Inhibition Efficiency of SALPD and CeSALPD during Mild Steel Corrosion in 1M HCl after 24-hour immersion 134
4.48: Arrhenius plots for Mild Steel in 1 M HCl solution free and 136
4.49: Plot of log (CR/T) Vs 1/T 138
4.50: Effect of Temperature on the Inhibition Efficiency of the Compounds at the Optimum Concentration 139
4.51: Variation of Inhibition Efficiency of SALPD, and CeSALPD with Immersion Time 141
4.52: (a) 2D AFM FOR BLANK Figure 4.52: (b) 3D AFM FOR BLANK 142
4.52: (c) 2D AFM FOR SALPD Figure 4.52: (d) 3D AFM FOR SALPD 142
4.52: (e) 2D AFM FOR CeSALPD Figure 4.52: (f) 3D AFM FOR CeSALPD 142
4.53: Polarization curves of Mild Steel in the absence and presence of 0.8 mmol / dm3 each of SALPD and CeSALPD of at 30 °C. 144
4.54: Nyquisit Plot for inhibitors at 0.8 mmol/dm^3 145
4.55: Comparism Plot of the Inhibition Efficiency vs Concentration of the Schiff bases and their Metal Complexes 156
4.56: Plot of Inhibition Efficiency vs Concentration of the Schiff base Compounds after 24 hr. Immersion 157
4.57: Comparism plot of Inhibition Efficiency of the Cerium Metal Complexes 158
4.58: Comparism of Inhibition Efficiency of Compounds with Immersion Time 159

4.59: Proposed structure for Ce (III) - 2-hydroxyphenyl-phenylimine or (Cerium (III) Salicyalideneaniline) 160
4.60: Proposed Structure for Ce (III) -Bis (2-hydroxyphenyl) imine or (Cerium (III) Salicyalidene-2-aminophenol) 161
4.61: Proposed structure for Ce (III)- Bis (2-hydroxyphenyl) -1,2-Benzenediimine or (Cerium (III) Salicyalidene-O-phenylindiamine) 162
4.62: (a) (b) (c) OPTIMIZED STRUCTURE OF SALAN, SAL2AP and SALPD 164
4.63: (a) (b)(c) HOMO OF SALAN, SAL2AP and SALPD 164
4.64: (a) (b) (c) LUMO OF SALAN, SAL2AP, and SALPD 165
4.65: (a) (b) Top and Side view of adsorption mode of SALAN on Mild Steel surface 166
4.66 (a)(b) Top and Side views of adsorption mode of SAL2AP on Mild Steel surface 166
4.67: (a) (b) Top and Side views of Adsorption mode of SALPD on Mild Steel Surface 167

LIST OF SCHEMES

Scheme	Title	Page
1.1:	Reaction scheme for a Schiff base formation	9
3.1:	Synthesis of 2-hydroxyphenyl-Phenylimine.	26
3.2	Synthesis of Bis(2-hydroxyphenyl) imine.	27
3.3:	Synthesis of Bis (2-hydroxyphenyl) – 1, 2-benzenediimine.	27

LIST OF ABBREVIATIONS

(1)	UV. Vis Spectra	-	Ultra- Violet Visible Spectra
(2)	EDXRF	-	Electron Dispersive X-ray Fluorescence
(3)	FTIR	-	Fourier Transform Infrared Spectroscopy
(4)	AFM	-	Atomic Force Microscopy
(5)	NMR	-	Nuclear Magnetic Resonance
(6)	PDP	-	Potentio dynamic Polarization
(7)	EIS	-	Electrochemical Impedance Spectroscopy
(8)	ba	-	Tafel anodic Slope
(9)	bc	-	Tafel cathodic Slope
(10)	Rct	-	Resistance to Charge transfer
(11)	Cdl	-	Double layer Capacitance
(12)	Rs	-	System Resistance
(13)	Rp	-	Polarization Resistance
(14)	IE	-	Inhibition Efficiency
(15)	Ecorr	-	Corrosion Potential
(16)	I corr	-	Corrosion Current
(17)	ΔH	-	Change in Enthaipy
(18)	ΔS	-	Change in Entropy
(19)	ΔEa	-	Change in activation Energy
(20)	ΔGads	-	Gibb's Adsorption free Energy
(21)	EHOMO	-	Energy of highest Occupied Molecular Orbital
(22)	ELUMO	-	Energy of Lowest Unoccupied Molecular Orbital
(23)	ΔE	-	Energy gap
(24)	ΔN	-	Number of transferred Electrons -
(25)	I	-	Ionization potential
(26)	A	-	Absolute Electronegativity
(27)	SALAN	-	Salicylidene-aniline
(28)	CeSALAN	-	Cerium (III) Salicylidene-aniline
(29)	SAL2AP	-	Salicylalidene-2-Aminophenol
(30)	CeSAL2AP	-	Cerium (III) Salicylidene-2-Aminophenol
(31)	SALPD	-	Salicylidene-o-Phenylenediamine
(32)	CeSALPD	-	Cerium (III) Salicylidene-o-Phenylenediamine

ABSTRACT

This present research work focuses on the synthesis , characterization and corrosion inhibition efficiency of three synthesized salicylalde - based Schiff bases with their Cerium(III) complexes, namely: 2-hydroxyphenyl-phenylimine or (Salicyalideneaniline (SALAN)), Bis(2-hydroxyphenyl) imine or (Salicyalidene-2- aminophenol (SAL2AP)), Bis (2-hydroxyphenyl) -1,2-Benzenediimine or (Salicyalidene-*O*-phenylenediamine (SALPD)), Ce(III)-2-hydroxyphenyl-phenylimine (CeSALAN), Ce(III)-Bis(2-hydroxyphenyl) imine (CeSAL2AP), and Ce(III)-Bis (2-hydroxyphenyl) -1,2-Benzenediimine (CeSALPD) in 1 M HCl solution. The compounds were characterized by physicochemical methods such as colour, melting point, solubility test, molar conductivity measurement, magnetic susceptibility and elemental analysis. There is variation in colour, pH, melting point, conductivity, and elemental compositions of the of the Schiff bases compared to their metal complexes. Magnetic susceptibility measurements values recorded for the metal complexes shows their paramagnetic nature. The high molar conductivity values of the metal complexes (> 0.1 $mSCm^{-2}$) shows their electrolytic nature, while the Schiff bases were found to be non- electrolytic. The compounds were also analyzed spectrally by Uv. Vis. Spectroscopy, ^{1}H, and ^{13}C NMR, FTIR, and EDXRF. The effect of inhibitor- concentration, temperature, and immersion time, on the inhibition efficiency of the compounds were studied by weight loss methods. ElS technique was used to investigate the nature of the protective film, EIS measurement shows that the addition of the inhibitors into the corrosion medium inhibited corrosion by increasing the system resistance (Rs), transfer charge resistance (Rct) while reducing the double layer capacitance (Cdl). PDP polarization techniques were used to study the nature of the inhibitors, and they were found to be mixed- type inhibitors. The corrosion potentials (Ecorr), and corrosion current (Icorr) due to the blank was reduced in the presence of the inhibitors. Increase in IE was observed due to increase in concentration of the inhibitors, with highest I.E value of 82.95 % recorded for the overall best inhibitor–compound CeSALPD at concentration of 0.4 $mmol/dm^3$. Effect of temperature on IE of inhibitors at temperature of 30 ^{o}C, 40 ^{o}C, 50 ^{o}C, 60 ^{o}C, and 70 ^{o}C shows decrease in IE due to increasing temperature (i.e. physical adsorption process). Thermodynamics parameters calculated for the inhibited reaction system shows increase in values of enthalpy (ΔH), entropy (ΔS), and activation energy (ΔEa) compared to values for blank. This obtained positive values of Δ H shows endothermic nature of the reaction system, and negative values of ΔS shows reduction in disorderliness of the system due to the action of the inhibitors. Negative values for ΔG, obtained for the inhibited systems shows the spontaneous adsorption process. Effect of immersion time on IE of the compounds shows decrease in I.E with immersion time (i.e. physisorption adsorption process). Langmuir, Temkin, and Frumkin models were used to determine the adsorption mode of the compounds. Langmuir model with regression square (R^2) value upto 0.99, best suits the adsorption process. Generally, for all the analytical techniques employed for the study of the IE, i.e. (weight- loss method, PDP and EIS), the I.E of the metal complexes were found to be higher than those of the parent Schiff bases. The quantum chemical parameters obtained from the Computational analysis and modelling of the Schiff bases such as E_{HOMO}, E_{LUMO}, shows that the reactivity of the Schiff bases follow the order: SALPD > SALAN > SAL2AP. The result from the weight–loss method is in agreement with the computational analysis. Conclusively, the compounds under study performed excellently as inhibitors, however, due to physisorption process of adsorption of the inhibitor molecules on the mild- steel surface, the compounds may not efficiently inhibit corrosion for a long - term duration. Hence, synergism with nano particles such as metal oxides i.e., (ZnO, TiO_2, Al_2O_3), may enhance their IE for the long-term process.

Keywords: Corrosion, Schiff bases, Inhibitors, complexes, inhibition efficiency

CHAPTER ONE

INTRODUCTION

1.1 Background Information

Coordination chemistry of transition and lanthanide metal complexes is gaining much popularity in recent years due to their versatile applications in the various fields of chemical and medical sciences, and it comprises a large body of bio-inorganic chemistry research. It has inspired the chemical researchers to design and fabricate novel metal complexes all over the world. It was Werner, a Swiss chemist, who first recognized such a class of compounds and was awarded Nobel Prize in Chemistry in 1913 for his invaluable contributions to coordination chemistry (Brodowska and Łodyga-Chruscinska, 2014).

By the exploration of the chelating ability of Schiff bases, a novel class of metal complexes may be obtained, which may possess potential applications in industrial, pharmaceutical and catalytic fields. By elucidating the structures of the metal chelates and ligands using advanced tools and techniques, a proper correlation can be made with the structure and activity. Even though large number of Schiff bases have been prepared and the chelating efficacy of these compounds exploited, there still remains wide scope for the synthesis of novel Schiff bases which possess hetero atoms and their metal chelates. Literature survey showed that Schiff bases which are primarily derived from heterocyclic compounds such assalicylideneaniline, salicylidene-2-aminophenol and salicylidene-1, 2-phenylenediamine and their lanthanide metal chelates are not much explored nor reported.

1.1.1 Compounds of Interest in the Present Study

i. **Aniline** also called phenylamine or benzeneamine ($C_6H_5NH_2$) is an organic chemical compound, a primary aromatic amine. It consists of a benzene ring attached to an amino group, a liquid at room temperature. Aniline is oily and, although colourless, it can be slowly oxidized and resinified in air to form impurities which can give it a red brown tint. It is volatile with somewhat unpleasant odour of rotten fish, and a burning aromatic taste. Melting point of aniline is 6 ^oC and boiling point is 184 ^oC, and density is 8.5 g/cm^3. It is slightly soluble in water.

ii. **2-Aminophenol** also called 2-hydroxylaniline is an organic compound with the formular C_6H_7NO. Its isomers are 3-aminophenol and 4-aminophenol. It is an amphoteric molecule and a reducing agent used in synthesis of dyes and heterocyclic compounds. 2-

Aminophenol is a white powder, moderately soluble in alcohols and can be recrystallized from hot water. The compound exhibits intra and intermolecular hydrogen bonding involving the neighboring amine and hydroxyl groups, hence it has a rather high melting point compared with other compounds with a similar molecular mass such as methylphenol. Its molar mass is 109.13 g/mol, appearance is white orthorhombic pyramidal needles, density is 1.328 g/cm^3, and melting point is 174 ^{o}C. 2-Aminophenol is industrially prepared by reducing the corresponding nitrophenol with hydrogen in the presence of various catalysts.

iii. **1,2-Phenylenediamine** also called Benzen-1,2-diamine and *o*-phenylenediamine, is an organic compound with the formular, $C_6H_8N_2$. This aromatic diamine is an important precursor to many heterocyclic compounds. It is isomeric with *m*-phenylenediamine and *p*-phenylenediamine, commonly called OPP.

It has a molar mass 108.14 g/mol, density 1.031 g/cm^3, melting point 104 ^{o}C, and boiling point of 253 ^{o}C, and soluble in hot water. I,2-phenylenediamine is prepared by treating 2-nitrochloro benzene with ammonia and the resulting 2-aminonitro benzene is then hydrogenated.

$$ClC_6H_4NO_2 + 2NH_3 \longrightarrow H_2NC_6H_4NO_2 + NH_4Cl \quad 1.1$$

$$H_2NC_6H_4NO_2 \longrightarrow 3H_2H_2NC_6H_4NH_2 + 2H_2O. \quad 1.2$$

In coordination chemistry, phenylenediamine is an important ligand.

iv. **Salicylaldehyde** is called 2-hydroxylbenzaldehyde and *o*-hydroxybenzaldehyde. It is an organic compound with the formula $C_7H_6O_2$. It is part of the class of hydroxyl-aromatic aldehydes. The aromatic nucleus contains two functional groups, a hydroxyl and aldehyde. This colorless liquid has a bitter almond odour at higher concentrations. Salicylaldehyde is used as an important intermediate in the chemical industry, it is also used in making perfumes, fragrance, dyes, pharmaceuticals, etc. Salicyaldehydes and its derivatives can be used as preservatives in cosmetic products, fragrance, essential oils in various biological applications. Salicylaldehyde is an important intermediate in the manufacture of herbicides and pesticides. Also, salicylaldehyde and its derivatives are used for various reactions for the production of polymers and fibres. (Genta, Villa, Mariani and Laipy, 2002; Mounika, Anupama, Pragathi and Gyana kumara, 2010; Rajewar, Dhermale and Pingalkar, 2014). Salicyaldehyde is one of the three isomers of hydroxylbenzaldehyde, other two isomers include 3-hydroxybenzaldehyde and

4-hydroxybenzaldehyde. Its molar mass is 122.12 g/mol, density 1.146g/cm^3, melting point, -7.15 ^{o}C, boiling point 196-197 ^{o}C. Salicyaldehydeis prepared from phenol and chloroform by heating with sodium hydroxide or potassium hydroxide in a Reimer-Tiemann reaction.

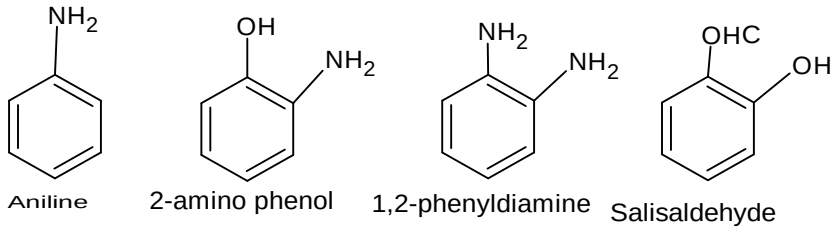

Figure 1.1 Structures of precursor compounds of interest applicable in this study.

1.1.2 Rare Earth Metal Chemistry

(a) General Properties

The lanthanides exhibit a number of features in their chemistry that differentiate them from the d-block metals. The reactivity of the elements is greater than that of the transition metals, because they exhibit a very wide range of coordination numbers, generally 6–12. Their coordination geometries are determined by the ligand steric factors rather than crystal field effects.

The lanthanides form labile 'ionic' complexes that undergo facile exchange of ligand. The 4f orbitals in the Ln^{3+} ion do not participate directly in bonding, being well shielded by the $5s^2$ and $5p^6$ orbitals. Their spectroscopic and magnetic properties are thus largely uninfluenced by the ligand. Lanthanides have small crystal-field splitting and very sharp electronic spectra in comparison with the d-block metals. They prefer anionic ligands with donor atoms of rather high electronegativity (e.g. O, F). They readily form hydrated complexes, on account of the high hydration energy of the small Ln^3+ ion and this can cause uncertainty in assigning coordination numbers. Insoluble hydroxides precipitate at neutral pH unless complexing agents are present. The chemistry is largely that of one (3+) oxidation state, certainly in aqueous solution. They do not form Ln = O or Ln ≡N multiple bonds of the type known for many transition metals and certain actinides. Unlike the transition metals, they do not form stable carbonyls and have virtually no chemistry in the zero-oxidation state.

Compared with transition metals, lanthanide elements have two distinct characteristics in terms of their coordination number.

(b) Coordination Numbers

i. Large coordination numbers. For example, the coordination number of 3d transition metals is generally four or six. However, the most common coordination number of lanthanide complexes is eight or nine. This number is close to the sum of the 6s, 6p, and 5d orbitals. Another factor responsible for the large coordination number of lanthanide complexes is the large ionic radius of the lanthanide.

ii. Variable coordination numbers. The coordinating stabilization energy (about 4.18 kJ/mol^{-1}) of lanthanide ions is much smaller than the crystal field stabilization energy of transition metals (typically-418 $kJ \cdot mol^{-1}$). Therefore, the coordinating bonds of lanthanide complexes are not directional and the coordination number varies from 3 to 12.

(c) Photophysical Properties

The ground state spectral terms of lanthanide elements in the periodic table can be sorted into two categories and these are divided by gadolinium. The first category consists of elements before gadolinium, which includes lanthanum, cerium, praseodymium, neodymium, promethium, samarium, europium, and gadolinium, while the second category contains the elements after gadolinium, which includes gadolinium, terbium, dysprosium, holmium, erbium, thulium, ytterbium, and lutetium.

Because the 4f shells of lanthanide elements are unfilled, different arrangements of 4f electrons generate different energy levels. The 4f electron transitions between the various energy levels, could generate numerous absorption and emission spectra. The ionic radii of Fe^{3+} and Co^{3+} are 55 and 54 pm, respectively for the coordination number six. However, the ionic radii of La^{3+}, Gd^{3+}, and Lu^{3+} are 103.2, 93.8, and 86.1 pm, respectively for the same coordination number.

1.1.3 Chemistry of Cerium [Xe] $4f^1$ $5d^1$ $6s^2$

Cerium (Ce) is a chemical element that is the most abundant of the rare-earth metals, it has atomic number of 58, atomic weight 140.116. Ce as the oxide (ceria) was discovered in 1803 by Swedish chemists, Jons Jacob Berzelius and Wilhelm Heisinger. Melting point 798 ^oC, boiling point is 3,443 ^oC, specific gravity (6.7704), oxidation state (+3, +4).

Ce occurs in bastnasite, monazite and many other complex ores. It is found among the fission products of uranium, plutonium and thorium. Ce is about as abundant as copper and nearly three times as abundant as lead in the igneous rocks of earth's crust.

Commercial grade cerium is iron-gray in colour, silvery when in a pure form, and about as soft and ductile as tin. It oxidizes in air at room temperature to form CeO_2. The metal slowly reacts with water, and it quickly dissolves in dilute acids, except hydrofluoric acid (HF). Ce turnings easily self-ignite in air, burning white-hot. Its pyrophoric nature accounts for one of its important metallurgical applications in lighter flints.

1.2 Statement of the Problem

As oil and gas reserves begin to deplete, there is a growing need to operate deeper, and consequently, hotter wells. One of the challenges of accessing such deep reservoirs is that they operate under much higher pressures and temperatures and are typically sourer than shallower formations. This typically leads to a much more corrosive environment and this problem is worsened by the fact that many traditional oilfield corrosion inhibitors are ineffective under such harsh conditions. Considering the above, the development of inhibitors with long durability for corrosion protection of steel stands the overall objective of this project. Regarding the search for new ecological alternatives in order to replace the hazardous Cr(VI) for metal protection against corrosion, lanthanides compounds, also identified as rare earth metals, are among the substances that have been hardly investigated by scientists in the last years. Lanthanides have low toxicity and their inhalation or ingestion has not been considered harmful.

1.3 Aim and Objectives of the Study

The aim of this present work is to synthesize, characterize and evaluate the corrosion inhibition efficiency of Cerium (III) metal complexes derived from some salicyladelyde based Schiff bases. The specific objectives are to:

i. synthesize three Schiff base ligands: salicylideneaniline, salicylidene-2-aminophenol and salicylidene-1,2-phenylenediamine;
ii. prepare Ce (III) complexes of the three ligands: salicylideneaniline, salicylidene-2-aminophenol and salicylidene-1,2-phenylenediamine;
iii. characterize the above ligands and their Ce(III) complexes by physical methods such as elemental analysis, melting point determination, solubility tests, conductivity test, and spectral methods such as UV-visible spectra, infra-red spectra, proton and carbon -13 Nuclear Magnetic Resonance (NMR);

iv. perform Density Functional Theory (DFT) computational studies for each of these ligands and evaluate their quantum chemical parameters;
v. evaluate the corrosion inhibition properties of these ligands and their respective cerium complexes on carbon mild steel in 1M hydrochloric acid by the conventional mass loss and electrochemical studies;
vi. investigate the mechanism of corrosion inhibition using Langmuir, Temkin and Frumkin adsorption isotherms;
vii. temperature effect on corrosion will be investigated by subjecting the immersed carbon steel to elevate temperature in order to determine thermodynamic parameters such as activation energy, enthalpy and entropy and
viii. molecular modelling characterization and simulation of the adsorption model of the Schiff bases on a metal substrate.

1.4 Justification of the Study

Due to health concerns arising from the use of chromium - based compounds as corrosion inhibitors, severe restriction has been placed on their use by international environmental standards. Therefore, rare- earth metal compounds are suggested as alternative materials for chromate, and Cerium- based compounds among all of the rare – earth compounds have proven to be very effective as an anti -corrosive materials for aluminum and mild steel alloys. Although organic inhibitors are ecologically friendly, but the permeation of oxygen, water, and corrosive ions through the organic inhibitors reduces their anti-corrosion performance when used alone as inhibitors. This situation leads to degradation of mild steel and its alloys over time even in the presence of the inhibitors. Hence, organic inhibitors don't have a long- term protective behaviour against the aggressive ions. Additionally, in many cases, large quantities of these organic inhibitors are required to be operative. To reduce the amount of organic inhibitors at the same time improve their anti-corrosion performance, incorporation of metals into the molecules of organic compounds might provide superior anti- corrosion properties in comparism with the individual constituents at the same concentration

1.5. Scope of this Study

a) Synthesis of three Schiff bases and their Cerium (III) complexes (total of six products).
b) Characterization of all six products using Uv- vis, FTIR, C-13 and proton NMR spectroscopy.
c) Corrosion inhibition assessment of all six products using:

i. One metal substrate
ii. One corrodent concentration (1M HCl)
iii. Eight inhibitor concentrations.

d) Determination of the effect of temperature at optimum inhibition efficiency concentrations.
e) Molecular dynamics characterization of the Schiff bases using dmol-3 module available in material studios.
f) Molecular simulation of the adsorption model of the Schiff bases.
g) Modelling the adsorption mechanism of all six products on three adsorption isotherms namely, Temkin, Frumkin and Langmuir isotherms.
h) Calculations of all relevant thermodynamics' parameters - activation energy(ΔEa), enthalpies(ΔH), entropies (ΔS) and Gibb's free energy (ΔG)

CHAPTER TWO

LITERATURE REVIEW

2.1 Background Study

In recent decades, a large volume of research works in chemistry have been dedicated to the synthesis, characterization and applications of metal complexes of Schiff bases (Hitesh, Blutadiya, Jabali and Toral, 2019; Shebl, 2014; Sherif and Abdel-Kader, 2014). Schiff base is the most familiar discovery of Hugo Schiff, who was called one of the founders of modern chemistry. After the novel work of Schiff in 1864, many researchers got involved in this research field and made successes in the synthesis and structural design of this class of compounds. Recent investigations in coordination chemistry regard Schiff base organic compounds as one of the most employed classes of ligands. The research area encompassing the coordination compounds with the azomethine group as the main character is widely expansive due to their potential interest aroused in various interdisciplinary fields. Metal coordination to organic ligands brings dramatic changes in the stability as well as the physiological and pharmacological profiles of chelated compounds. Schiff bases are presently the drug substances being used in medical sciences as chemotherapeutic agents. Chemotherapy, in general, refers to the treatment of diseases with chemicals. When used in reference to infectious diseases, the term is antimicrobial chemotherapy. Besides their chemotherapeutic applications, they have played major roles in other fields also. Simple preparative method and easy structural design further popularize Schiff bases and their metal complexes in the research field. Schiff bases comprise a group of the most widely used families of organic compounds, formed as the condensation product of the chemical reaction of the active carbonyl group and a primary amine. This class of compounds is mainly recognized by the presence of an active imine (-CH = N-) group that carry potential binding site for the metal ions through nonbonding electrons of the nitrogen atom (Da Silva et al., 2011). The structural unit of Schiff bases also possesses many other heteroatoms like oxygen and Sulphur as main component elements for chelate formation with metals. The nature of donor atoms that act as coordination sites, their electronegativity and steric factors largely determine the bonding ability of the ligands. By virtue of the presence of lone pair of electrons on N-atom, electron donating character of the double bond and low electronegativity of nitrogen, N-atom of the azomethine group (>C=N) acts as a very good donor site and Schiff bases are considered as active ligands (Kostova and Saso, 2013).

Schiff bases occupy a leading position in metal coordination chemistry and they are widely studied due to their simplicity in preparation, variation in properties, biomedical, and industrial applications (Prasad, Vedanayaki and Rajavel, 2016; Luz and Ramalho, 2010). There are several amines and carbonyl compounds in the library of organic chemistry that enable the synthesis of Schiff bases with diverse structural features. For the synthesis of Schiff bases, the basic carbonyl group may be aldehydes (aromatic or aliphatic) or a ketone. The stability of imine group is controlled by the presence of substituent groups attached to (>C=N) linkage. The general reaction for the formation of Schiff base is illustrated in the Scheme 1 below:

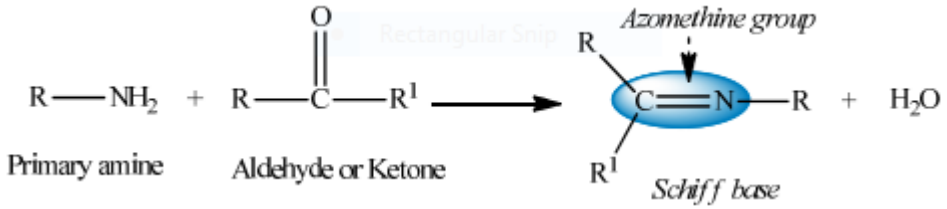

Scheme 1.1: Reaction scheme for a Schiff base formation

Where R represents an alkyl, aryl, cycloalkyl or heterocyclic group, which may be variably substituted and R^1 may be an alkyl, aryl group or H atom. The formation of a Schiff base is a reversible process and generally takes place by refluxing the mixture under the neutral condition or in the presence of acid or base catalysts. The formation is generally driven to completion by the separation of product or removal of water.

Besides the bio-medical applications, Schiff base metal complexes also bear various important applications in chemical, industrial and electronic fields. In the material science, they are found to have good corrosion inhibitory activity (Madkour & Elroby, 2015). This phenomenon is the spontaneous formation of a monolayer on the surface to be protected. A large number of Schiff base metal complexes are identified by an excellent catalytic activity in a variety of synthetic chemical reactions at high temperature (>100 °C) and in the presence of moisture. Many research reports display their use in homogeneous and heterogeneous catalysis. In many biological systems, Schiff bases and metal complexes show active participation in the synthesis of some life molecules like enzymes and biopolymers (Hameed,Al-Rashida, Uroos, Ali, & Khan, 2017). Numerous scientific publication reports, appearing annually in recent years, highlight the keen interest of researchers in metal complexes in which Schiff bases play a critical role as ligands. Due to excellent selectivity, sensitivity and stability of Schiff bases for specific metal ions, a large number of Schiff base ligands have been used as cation carriers in potentiometric sensors. In modern

technology fields, Schiff bases and metal complexes deliver important applications because of their photo- and thermochromic properties (Rawat, Mal, & Singh, 2015; Almi et al., 2025). They have applications in optical computers, to measure and control the intensity of radiation, in imaging systems, as well as in the molecular memory storage devices. Due to photochromic properties, they function as photo stabilizer, dyes for solar collectors and solar filters. Schiff bases can also be used as stationary phase in gas chromatography, due to their thermal stability (Brodowska & Łodyga-Chruscinska, 2014). This literature review highlights some areas of interest to Schiff bases and metal complexes based on their applications.

2.2 Biological Applications of Rare-earth Schiff base Metal Complexes

Schiff bases were reported to possess antibacterial, antifungal and antitumor activities. Several researchers have studied the synthesis, characterization and structure-activity relationships of Schiff bases (Abdel et al., 2012) Lanthanides and lanthanide compounds have attracted a great deal of interest in recent years because they have applications in medicinal inorganic chemistry and in materials science. In medicine, lanthanide complexes are exploited in study of diagnostic procedures and also as therapeutic drugs (Kapoor and Singh, 2012).

2.2.1 Antimicrobial Applications

In recent al years, there have been several reports about the studies on the preparation, characterization, and antimicrobial properties of rare earths combined with antibacterial materials (Zhang et al., 2010). These studies all indicate that rare earths can exhibit antibacterial properties. It has been established that the antibacterial materials containing rare earths can release many free hydroxylic radicals, which can kill bacteria efficiently.

Hitesh et al., (2019) prepared lanthanide complexes using Lanthande ions: La(III), Ce (III), and Pr(III) with N-salicylaldehyde-anthranilic acid Schiff base (NSAA) ligand and characterized it by spectral, magnetic elemental and thermal analyses. Catalytic effect of the complexes on Diel-Alder reaction was studied. The activation energy for thermal decomposition of the complexes and ligand were determined. Higher activation energy shown by the complexes indicated good thermal stability and therefore, good catalytic ability.

Waleed et al., 2013 investigated the antimicrobial activity of lanthanide complexes with a (N, N-bis (1- naphthaldehyde with o- phenylenediamine in a molar ratio 0f 2: 1. The lanthanide (III) elements used are La, Pr, Sm, Gd, Nd. La (III) and Pr (III) complexes were effective inhibitors against *Staphylococcus aureus*, Sm (III) complex was effective against *Serratia marcescens*, while Gd, La, and Nd (III) were found to be potent inhibitors against *Pseudomonas aeruginosa*.

Kawther and Naser, 2022 synthesized a Schiff base ligand by reacting4,4- methylenediaantipyrine with ethylenediamine. The Schiff base was complexed with various nitrate (III) salts, i.e. (Nd, La, Er, Gd, Dy). Antibacterial activities of the metal complexes were tested against Staphylococcus aureus, *Bacillus subtilis, Escherichia coli, and Klebsiella pneumonia*. Majority of the complexes demonstrated antibacterial activity.

Fatma and Gehad (2022) prepared, characterized, and studied antimicrobial as well as anticancer activity of Schiff base lanthanide complexes derived from ferrocene and L- histidine amino acid. The lanthanide elements used included: Er(III), La (III), and Yb (III). The compounds showed promising biological and anticancer activities. Yb(III) was confirmed to be effective drug for treatment of breast and colon cancer.

Kapoor and Singh in 2012 reported biological evaluation and DNA cleavage of lanthanide (III) complexes of a class of coumarin based imines. The metal complexes showed enhanced biological activities compared to the free ligands.

Ingale and co-workers in 2015, reported the synthesis of new divalent Schiff base -2-(E)-(4-methoxyphenylimino) methyl phenol (MPMP) and the lanthanide (III) complexes, with lanthanide ions such as La(III), Ce(III), Nd(III), Sm(III), Gd(III), Tb(III) and Dy(III). The structures of the Schiff base and their Lanthanide (III) complexes were characterized by analytical and spectral data using FTIR, HNMR, molar conductance, XRD and magnetic studies. $[Gd(MPMP)_2(H_2O)_2NO_3]$ showed toxicity against staphylococcus aureus in 500 ppm solution. The antibacterial and antifungal activity of the MPMP metal complexes were also studied.

Rajewar et al. (2014) had synthesized some solid complexes of La(III), Pr(III), Tb(III), Sm(III), and Nd (III) from a bidentate Schiff base, 2-(4-bromo-2,6-dichlorophenylimino) methyl)-4-6-diodophenol. These metal complexes were characterized by physiochemical studies, spectral studies, thermal studies, molar conductivites and X-ray diffraction. The IR spectral data reveal that the ligand is bidentate, coordinating through the (O, N) donor atom to the metal ion.

Binary complexes of La(III), Sm(III), Gd(III) and Dy(III) Lanthanide ions with the ligand FCA (Furan-2-carboxylic acid) have been prepared and reported by Gupta et al. (2012). The antibacterial and antifungal activities of the complexes were studied against some gram positive and gram-negative bacteria. The synthesized complexes showed an enhanced antibacterial and antifungal activities against some bacteria and fungi when compared to the parent ligand.

Almomani et al. (2013) prepared complexes of trivalent Lanthanide metals with Schiff base ligand synthesized from 2-hydroxy-1-naphthaldehyde with *O* -phenylenediamine. The antimicrobial

activity revealed that most complexes showed higher activity against some bacteria than the free ligand.

Kapoor et al. (2012), synthesized two octahedral complexes of Nd(III), Sm(III), and Gd(III) metal with two ligands, 3-acetylcoumarinthiosemicarbazone (ACTSZH) and 3-acetylcoumarinsemicarbazone (ACSZH). Antibacterial and antifungal studies showed that the Sm(III) complexes of both ligands have the highest biological activity than other complexes and parent ligands.

2.2.2 Pharmaceutical and Biomedical Applications

There are numerous publications covering the potential use of Schiff bases in therapeutic and biological fields either as potential drug candidates or diagnostic probes and analytical tools

(Mushtaq et al., 2024). Moreover, Schiff bases are present in various natural, semi-synthetic and synthetic compounds and have been demonstrated to be essential for their biological activities (Arjmand and Muddassir, 2011). The review article of Abu-Dief and Mohamed (2015); Prakash and Adhikari (2011), and Da Silva et al., (2011) have summarized the important applications of Schiff bases and their metal complexes. A huge number of Schiff base metal complexes are of potential biological interest because of their remarkable biomedical applications, being used as successful models of biological compounds. They have important applications as anticancer (Chakraborty et al., 2010), antibacterial (Keypour et al., 2014), antiviral (Shebl, 2014), antifungal (Sherif and Abdel-Kader, 2014), analgesics (Osowole and Balogun, 2012), anti–inflammatory and several others. Salicylaldehyde is a very important drug component found in many drugs that contain cyclic system.

Some piperazine derivatives are also known to possess anti malaria activities. To widen the applications of these classes of compounds, El-Sherif et al. (2012) have synthesized Schiff base ligand 1,4-bis[(2-hydroxybenzaldehyde) propyl]piperazine (BHPP) from salicylaldehyde and 1,4-bis(3-aminopropyl)piperazine. They further prepared the complexes of the ligand using three divalent metalions (Co^{2+}, Ni^{2+}, and Cu^{2+}) and investigated their structure and biological activity. The hexadentate Schiff base ligand (BHPP) was found to possess better antibacterial activity against both gram-positive and gram-negative bacteria. The three complexes also exhibited moderate activity against the fungal strains when compared with standard amphotericin. The Schiff base compound, salicylideneanthranilic acid (SAA) derived from salicylaldehyde and 2-substituted aniline and its three metal complexes with Cu (II), Ni (II) & Co (II) have been found

to possess good anti-inflammatory and anti-ulcer activity. However, the copper complex of this compound showed increased antiulcer activity.

Abdel-Rahman et al. (2016) have reported the synthesis of three tridentate Schiff base amino acids by the direct condensation of 3-methoxysalicylaldehyde and 4-diethylaminosalicylaldehyde with various α-amino acids. They were further complexed with copper and produced Cu (II) complexes. The experimental results suggested the octahedral geometry of Cu (II) complexes of Schiff bases amino acids. The *in- vitro* antimicrobial study of Schiff bases amino acids and their Cu(II) complexes with pathogenic bacterial and fungal strains revealed stronger antibacterial and antifungal efficiency compared to their corresponding ligands. Purine and triazole based organic compounds and their derivatives are reported to have relevant biological functions and many of them are naturally occurring compounds.

Amer et al. (2013) have prepared a series of Cu(II) complexes of Schiff bases derived from 7H-2,6-diaminopurine and 4H-3,5-diamino-1,2,4-triazole with 2-pyridinecarbaldehyde, salicylaldehyde, 2,4-dihydroxybenzaldehyde, and 2-hydroxy-1-naphthaldehyde. The tetradentate ligands were coordinated to the metal center through the N-atom of azomethine group and the nearest N-atom of it or O-atom of OH group. The *in - vitro* antibacterial and antifungal results showed moderate activity against *E. coli* and *S. aureus*. Similarly, the *in - vitro* antitumor activity of the complexes showed a moderate activity against the studied cell lines.

The metal-based antibiotics are reported to have better pharmacological properties. To derive additional knowledge about antibiotic action, Anacona et al. (2015) reported the isolation and characterization of metal (II) complexes containing a Schiff base ligand derived from the condensation of cephalothin and sulfadiazine. The antibacterial study revealed the higher bactericidal activity of Cu(II) and Zn(II) complexes than the un-complexed cephalothin and the sulfadiazine against the bacteria strains. The Mn (II), Co (II) and Ni (II) complexes proved to be less toxic than the two referenced drugs and the Schiff base ligand.

Cao et al. (2016) have synthesized and investigated the *in - vitro* anticancer activities of four new amino acid Schiff base oxovanadium(IV) complexes. X-ray structural analysis showed that the

V (IV) atoms in all four complexes are six-coordinated in a distorted octahedral environment. The anticancer study revealed moderate activities towards human lung carcinoma and human hepatoma cell lines.

Ceyhan et al. (2013) have reported the synthesis of three new Schiff base ligands derived from benzaldehyde derivatives and trans-1,4-cyclohexane diamine and also investigated the

electrochemical, photoluminescence, thermal and anticancer activity properties. These were screened for their cytotoxicity against HeLa and Vero and C6 cancer cell lines. The results showed that all of the compounds have cell selective activity against all the cell lines. Moreover, the Schiff base compound IGA3 has been found to show the highest antiproliferative activity against HeLa cell line. Anticancer property of copper complexes is conjectured to be less toxic and more potent. Copper is a biologically relevant metal as it is associated with various biomolecules related to essential physiological activities.

In a research work of Chakraborty et al. (2010), the anticancer activities of a family of Schiff base copper complexes of general formula [Cu(Pyimpy)Cl_2] were tested. The results indicated prominent anticancer properties *in - vitro* as well as in-vivo.

Negajothi and co-workers in 2012 synthesized Fe(III) complexes obtained by reacting *O*-phenylenediamine with salicyladehyde and Isatin/2-hydroxy Naphathaldehyde/acetylactone. The metal complexes were characterized by elemental analysis, molar conductance, magnetic susceptibility, thermal analyses and spectral analyses. The results of the antimicrobial studies confirm that the metal complexes are good antibacterial and antifungal agents. Schiff bases namely, viz, Salicyladehyde glycine, DL-2, 3-Diaminopropion-Salicyaldehyde, benzylidene glycine and 4-acetylamido benzylidene aniline have been prepared in basic media and reported (Navne et al., 2013). The complexes of these Schiff bases with Cu (II) were isolated, and their use as catalyst, polymer and dyes were studied. The Schiff bases were screened for antimicrobial, antifungal and antiviral activities and the result revealed that the Schiff bases exhibited good biological activities.

Similar research carried out by Vimal and co-workers (2014) on antimicrobial activity of Schiff base *P*-chloroaniline N-Salicylidene prepared by reacting Salicylaldehyde with *P*-chloroaniline. The Schiff base was complexed with the metal ions: Cu (II), Co (II) and Cd (II). Antimicrobial study on the Schiff base and its metal complexes confirmed that the metal complexes are more effective antimicrobial agents than the uncomplexed ligand.

Yousif et al. (2013) synthesized and characterized a novel metal complex derivatives of 2-N-Salicylidene-5-(*P*-nitrophenyl)-1,3,4-thiadiazole, HL with the metal ions: Vo (II), Co (II), Rh (III), Pd (II) and Au (III). The metal complexes proved to be better antibacterial agents compared to the ligand when the in - vitro antibacterial screening activities was studied.

Mounika et al. (2010) had prepared a new Schiff base 3-ethoxysalicylidenamino benzoic acid (ETSAN) from 3-ethoxysalicylaldehyde and 2-amino benzoic acid. Biological studies of the

ligand and its Ni(II), Cu(II) and Zn(II) complexes reveals that the metal complexes show a better biological activity compared to the uncomplexed ligand.

2.3 Catalytic Activities of Transition Schiff base Metal complexes

Transition Schiff base metal complexes are powerful catalysts for various organic transformations. They play important roles in oxidative processes employed in laboratory synthesis and chemical industries.

In recent years, Schiff bases and their metal complexes have been extensively investigated due to their wide range of applications as valuable catalysts. The Schiff base compounds have the ability to stabilize many metals in various oxidation states and control the performance of metals in several catalytic transformations.

Schiff bases and their transition metal derivatives are known to possess catalytic activity for the oxidation of alcohols and alkenes in several synthetic organic reactions because of their cheap, easy synthesis, their thermal and chemical stability.

Rhodium and Iridium complexes are mostly catalysts that have potential industrial applications to lead very efficient chemical processes.

Biswas et al. (2015) have synthesized novel Rhodium (III)-triphenylphosphine complex, $[Rh(PPh_3)(L)Cl_2](PF_6)$ with thioether containing NNS donor ligand ie, 2-(methylthio)-N-((pyridine-2-yl)methylene) benzenamine, and investigated its catalytic activity. The results showed that the complex effectively catalyzed the transfer hydrogenation reaction of ketones with high yield of 2-propanol.

In recent years, the interest in the vanadium complexes in coordination chemistry has grown enormously due to their multifaceted activities. Tahmasebi et al. (2016) have carried out the synthesis, characterization and crystal structure determination of oxovanadium Schiff base complexes. Additionally, they have studied and observed the catalytic activity of synthesized vanadium complexes in the epoxidation of alkenes. The results of this study showed that the epoxidation of alkenes takes place more efficiently even in a small concentration of oxovanadium catalyst.

Abdel et al. (2012) prepared and characterized complexes of N-Salicylidene-o-aminophenol(SaphH2) with Mn, Co, Ni, Cu, and Zn using FTIR, NMR, IR, UV- Vis., and ESR spectroscopy. The catalytic properties of the new complexes on aerial oxidation of benzaldehyde to benzoic acid were explored. The complexes showed good catalytic potentials.

2.4 Corrosion Inhibition Applications of Schiff-bases and Their Metal Complexes

Corrosion is simply described as destructive attacks of a material by its environment. It is gradual deterioration of metals due to environmental factors; therefore, it is a pervasive issue affecting numerous industries worldwide (Ahmed, 2024). Iron and its alloys (steel) are the important materials used in various industrial and engineering applications. However, their regular use in the industrial process requires cleaning of the metal surface and for this purpose, acid solutions are used to remove undesirable scale and corrosion products. To prevent from this acidic corrosion, some inhibitors are required which prevent the metal surface from acidic attack. Inhibitors prevent corrosion as well as cathodic and anodic reactions by adsorbing on the surface of metal in the form of a wall.

Some Schiff base compounds containing imine group and donor atoms like nitrogen, oxygen, and sulfur are effective to prevent corrosion of metal surface in acidic medium. There are interactions between O, N, S heteroatoms and the mild steel, which play important role in the anti-corrosion activity caused by the free electron pairs. The presence of azomithine (=C=N) group in different metal complexes enhances their stability and corrosion inhibiting activities. A coordination complex of specific geometries such as square planar, tetrahedral or octahedral is formed when negative ions and electron pairs are moved from the corrosion inhibitors to the metal d-orbitals of the corroding metal (Nidhi et al., 2025).

Saline medium is one of the leading agents that cause corrosion. The water produced during petroleum production in the deep oil wells contains a variety of dissolved organic and inorganic compounds. These compounds have aggressive properties to corrode the material substances and for this purpose, inhibitors are commonly used. Corrosion inhibitors block the active sites and enhance the adsorption process and thus decrease the corrosion rate to extend the life of equipment. Nitrogen-based organic surfactants have been used successfully as the corrosion inhibitor in the oil and gas fields even without an understanding of the inhibition mechanism.

Ammar et al. (2023) assessed the inhibitory activity of three prepared azo compounds derived from Schiff bases namely: bis[5(-(phenylazo)-2-hydroxybenzaldehyde]-4,4'-diaminophenylmethane (C1), bis [5-(4- methylphenylazo) -2- hydroxybenzaldehyde] – 4, 4'-diaminophenylmethane

(C2), and bis[5 – (4 – bromophenylazo) -2- hydroxybenzaldehyde] -4, 4'- diaminophenylmethane (C3) against corrosion of steel type XC70 in 1 M HCl. The inhibitory performances of the compounds are in the order: C3 < C1 < C2.

Nizor et al. (2024) synthesized and studied electrochemical, computational and corrosion inhibition potentials of novel thiazole- derived Schiff bases on mild steel in acidic media. The synthesized compounds showed promising inhibitory potentials, and there is correlation among the various techniques used for inhibition assessment.

Abdelbasset et al. (2025) reported the electrochemical, quantum chemical, and thermodynamic investigation of a Schiff base corrosion inhibitor for XC70 steel. using a Schiff base(Z)-2-((3-nitrobenzylidene)amino)phenol (NBAP). 89 % inhibition efficiency was recorded for NBAP at 10^{-4} M. NBAP acted as a mixed-type inhibitor, and adsorption mechanism obeyed Langmuir adsorption process.

Aouniti et al. (2016) have synthesized Schiff base (E)-2-methyl-N-(thiophen-2-ylmethylidene) aniline from 2-acetyl thiophene and studied its corrosion inhibition behavior on steel/1.0 M HCl interface by using gravimetric and electrochemical methods at 308 K. Their study revealed that the corrosion inhibition might have taken place through its adsorption at the metal/solution interface. The synthesized Schiff base demonstrated good inhibitive properties for mild steel corrosion and its efficiency increased with increasing concentration of the inhibitor.

Shivakumar and Mohana (2013) reported on the inhibition performance and adsorption behavior of (E)-2-(3-nitrobenzylidene) hydrazine carbothioamide and (E)-2-(4-(dimethylamino) benzylidene) hydrazine carbothioamide Schiff bases using gravimetric, potentiodynamic polarization and electrochemical impedance spectroscopy techniques. The Schiff bases were found to be efficient corrosion inhibitor for mild steel in industrial water.

Singh and Quraishi (2012) have reported the corrosion inhibitory efficiency of some satin - based bidentate Schiff bases for mild steel in 1.0 M HCl solution. The study revealed excellent inhibition effect on corrosion. They have explained the high inhibition efficiencies of Schiff bases which are attributed to the adherent adsorption of the inhibitor molecules on the mild steel surface.

El-Baradie et al. (2014) have synthesized Co(II), Ni(II) and Cu(II) complexes of L-histidine Schiff base derived from 2,4-dihydroxybenzaldehyde and 2-hydroxynaphthaldehyde and studied their corrosion inhibition effect on aluminum in 2M H_2SO_4 by weight loss method. The obtained data indicated these compounds as efficient corrosion inhibitors with increased inhibition efficiency on increasing the inhibitor concentration and temperature, which is suggestive of a chemical adsorption process. The Sulphur as a donor atom in the Schiff bases bears a strong affinity on transition metal surfaces.

Samide and Tutunaru, (2011), investigated a Schiff base, N-(2-hydroxybenzylidene) thiosemicarbazide (HBTC) as a corrosion inhibitor for carbon steel in saline water by using various electrochemical measurements. The investigators suggested that, the Schiff base compound, was good corrosion inhibitor of carbon steel in dilute acidic medium.

Hamak and Eissa (2013) have synthesized a series of Schiff bases by the condensation of 1,4-bis(3-aminopropyl)-piperazine and various aromatic aldehydes in ethanol in the presence of the acetic acid catalyst. Their oxazepine derivatives had been prepared by the treatment of Schiff base with phthalic anhydride. The corrosion inhibiting action of these compounds had been investigated on steel in 1M H_2SO_4 by electrochemical techniques. The study revealed the effective corrosion inhibiting activities of all the synthesized compounds.

Migahed et al. (2011) have synthesized a new family of Schiff base nonionic surfactants and evaluated their corrosion inhibition effect on X-65 type tubing steel in deep oil wells formation water. The results showed good inhibition properties for the corrosion. This is attributed to the strong adsorption ability of surfactant molecules on the metal surface.

Negm et al. (2011) have synthesized a new series of cationic Schiff bases and evaluated the corrosion inhibitory effect on carbon steel in acidic medium (2 M HCl) at 25 °C using the weight loss technique. The results showed decreasing corrosion rate by increasing the doses of Schiff base surfactants.

Zhang et al. (2019) reported the corrosion inhibition effect of three newly synthesized benzaldehydethiosemicarbazone derivatives, namely, benzaldehyde thiosemicarbazone (BST), 4-carboxyl benzaldehyde thiosemicarbazone (PBST) and 2-carboxyl benzaldehyde thiosemicarbazone (OCT) on mild steel in 0.5 M H_2SO_4 solution using gravimetric and electrochemical measurements. PBST was reported to have exhibited the highest inhibition efficiency of 96.6% among the investigated compounds at concentration of 300 μm. The three inhibitors acted as mixed- type inhibitors.

A new 8-hydroxyquinoline derivative, 1,3-bis(quinoline-8-dimethyformamide) propane (BQYP) was synthesized and characterized by Zahra and Aisha in 2019, using FTIR and NMR spectroscopic methods. The corrosion inhibition properties of the BQYP molecule against mild steel in 2 M H_2SO_4 acid was studied by electrochemical technique at a varied concentration and temperatures. Inhibition effect was observed to have improved with increase in concentration of the inhibitor and was reduced with increasing temperature.

Ebenso et al. (2010) synthesized three thiosemicarbazides, namely: 2-(2-aminophenyl)-N—Phenylhydrazinecarbothioamide (AP4PT), N,2-diphenylhydrazinecarbothiomide (D4PT) and 2-(2-hydroxyphenyihydrazinecarbothiomide (HP4PT). The inhibitory potentials of the synthesized compounds on corrosion of mild steel were investigated in H2SO4 solution using gravimetric and gasometric method. Their inhibition efficiency was observed to follow the order AP4PT. HP4PT >D4PT.

Although inhibitors are widely used industrially because they possess excellent anti-corrosive properties, most of them however, have adverse effects on the environment by releasing toxic substances which damage the environment. This situation necessitates the search for a more environmentally friendly inhibitor that will not posse risk to the environment such as inorganic and organic inhibitors (Negm, Mandile, Badr, Mohammed, 2012; Abdel-Gaber, Abd-El- Nabey, Khamis and Abd- El Khalek, 2011). Some inhibitors such as chromates have been replaced by molybdate compounds and rare earth metal salts like cerium chloride. Both organic and inorganic inhibitors are finding wide application in metal protection technology.

2.4.1 Inorganic Inhibitors

This class of inhibitors can be cathodic or anodic by action. Cathodic corrosion inhibitors act by preventing the cathodic reaction on the metal from taking place during corrosion processes. These inhibitors consist of metal ions that are capable of cathodic reaction due to alkalinity, which produces insoluble compounds (e.g. hydroxides, sulphides, etc.) that selectively precipitate at the cathodic sites. There is a restriction of in-flow of reducing species in the areas around the metal where there is a deposit of a compact and adherent film due to the action of cathodic inhibitors. A barrier is therefore created between the metal and its environment, thereby preventing corrosion. Cathodic inhibitors are independent of concentration and they are more secure than anodic inhibitor. Ions of magnesium, zinc, and nickel that form insoluble hydroxides ($Mg(OH)_2$, $Zn(OH)_2$, $Ni(OH)_2$) are deposited at the cathodic site of metal when they react with OH of water. Anodic inhibitors reduce anodic reaction supporting the natural reaction of passivation of metal surface also forming a film adsorbed on the metal. Anodic inhibitors react with corrosion products giving rise to a formation of a cohesive and insoluble film on the surface of the metal. Anodic inhibitors form insoluble hydroxides on reaction with metallic ions produced on the anode. The insoluble oxides and hydroxides are deposited as insoluble film on the metal surface impermeable to metallic ions. For anodic inhibitor effect, it is essential that the inhibitor concentration should be high enough in the solution. Inadequate amount of inhibitor affects the formation of film protection because the metal is not completely covered leading to a localized corrosion. Examples

are nitrates, molybdates, sodium chromates, phosphates, hydroxides and silicates (Tian et al., 2013)

2.4.2 Organic Inhibitors

Organic compounds may be used as inhibitors. They can be cathodic or anodic or can also act as both cathodic and anodic simultaneously. In general, organic inhibitors act through a process of surface adsorption thereby forming a film. There is high affinity of metal surfaces associated with organic inhibitors which leads to good inhibition efficiency accompanied by low risk to the environment. They act by building-up of a protective hydrophobic film of adsorbed molecules on the metal surface. This creates a barrier to the dissolution of the metal into the electrolyte. It is important for the organic inhibitor to be soluble or dispersible in the medium in which the metal is immersed. The presence of polar functional groups with S, O, and N atoms in the molecule of an organic inhibitor is related to its ability to work effectively as an inhibitor. The polar functional groups are the sites of reaction center for the establishment of the adsorption process. The corrosion inhibition by these organic inhibitors is achieved when the organic inhibitors consisting of oxygen, nitrogen or sulphur is adsorbed on the metallic surface thereby blocking the corrosion sites. Organic compounds containing pi-bond (π) have proven to be efficient inhibitors for the fact that the pi- bond provides an active reaction site site for the organic inhibitor to interact with (the metal), and effectively adsorb on the metal surface it is protecting. Examples of these compounds are amines, urea, mercaptobenzothiazole, aldehydes, heterocyclic nitrogen compounds, sulphur containing compounds extracts of natural substances.

2.5 Molecular Modelling Study Approach to Corrosion inhibition

The use of computational software for molecular modelling of organic compounds has proven to be a powerful approach for theoretical determination of corrosion inhibition potentials of organic compounds. The various methods applied in the theoretical studies of corrosion inhibition potentials and mechanism are Monte Carlo (MC) simulations, density functional theory (DFT), molecular dynamic (MD), artificial neutral networks (ANN), quantitative structure activation relationship (QSAR) method among others (Oguzie, Li, Wang, and Wang, 2011). Computational modelling gives an insight into the chemical reactivity and corrosion inhibition activities of organic compounds. The modelling approach has offered a better advantage since it gives an idea of the corrosion inhibition potentials of organic compounds prior to the laboratory synthesis. It saves time and it is also an environmental – friendly approach which can easily be used to predict the adsorption sites and structure of organic compounds. So many corrosion parameters can also

be predicted such as corrosion inhibition efficiency, nature of metal – inhibition interaction by applying theoretical descriptors (Ebenso et al., 2021). Computational method for corrosion inhibition has been widely studied due to inadequacy of conventional methods to describe vividly the interaction between the inhibitor molecule and the metal surface. The conventional method for determining the inhibition properties of an inhibitor involves weight loss method, electrochemical impedance spectroscopy, potentiodynamic polarization and cyclic voltammetry. However, these methods are time consuming and possesses health risks. Molecular simulation, first introduced by Berni Alder in 1956 while studying copper corrosion inhibition using alkyl ester compounds. MD describes the movement of atoms or molecules within a specified time frame by computational calculation. Equilibrium properties of the system are also obtained using MD (Verma et al.,2018; Ni et al., 2019; Jiang et al., 2019).

With improvement on hardware and software, computer simulation has become a powerful tool to investigate complex systems. Through investigation of structure, electron distribution, and adsorption process of molecules, inhibition mechanism has been deeply explored (Mohamed et al., 2010). In 1971, Vosta introduced quantum chemistry methods to investigate corrosion inhibition mechanism and founded quantum corrosion electrochemistry. Thereafter, the focus of quantum chemistry method was mainly on relations between molecular structures and inhibition efficiencies, and many valuable results have been reported. In the 1990s, researchers turned their interests to the interaction between inhibitor molecules and metal surfaces via molecular dynamic simulation. Quantum chemical methods have proven to be useful in studying the molecular structure as well as reactivity of inhibitors this could be applied in designing efficient inhibitors. The use of DFT- based quantum chemical computation is applied for theoretical investigation of inhibition mechanism. DFT helps to analyze quantum chemical descriptors such as, frontier molecular orbital, HOMO (higher occupied molecular orbital) energy, LUMO (lower unoccupied molecular orbital) energy, chemical potential, hardness, electronegativity and number of transferred electrons etc.(Khlood et al., 2021) Molecular and structural parameters derived through computational calculations such as chemical selectivity, reactivity and charge distribution are correlated to inhibition efficiency (Amin et al., 2010; Gece et al., 2010; Fu et al., 2010; Pirhadi et al., 2016 ; Gece, 2018).

2.6 Computational Studies on Corrosion Inhibition

El Arrouji et al. (2020) carried out an experiment on Monte Carlo and MD simulation to evaluate the corrosion inhibition of two pyrazole derivatives namely:(E)-N’ – benzylidene-2-(3,5-dimethyl-1H-pyrazol-1-yl) acetohydrazide(DPP) and (E)- N’-(4- chlorobenzylidene)- 2- (3,5-dimethyl-1H-

pyrazol-1-yl)acetohydrazide (4-CP) on steel in 1M HCl. Montecarlo simulation data revealed stronger adsorption of the 4-CP inhibitor on the surface of Fe (110) with -109.18 Kcal/mol adsorption energy compared to DPP inhibitor with -103.38 kcal/ mol adsorption energy respectively. This result was in good correlation with the experimental findings. According to the MD simulation result, the orientation of the overall molecule was not completely parallel.

Hongfu et al. (2020) reported on the corrosion inhibition mechanism of six 2-amino-5-alkyl-1,3,4-thiadazole compounds for mild steel surface protection.

The study was done by combining quantum chemistry, molecular mechanics and molecular dynamics simulation methods. Molecular reactivity parameters such as E_{Homo}, E_{Lumo}, Fukui index values were obtained. MD simulation data indicates that the equilibrium adsorption behavior of these thiadazole molecules on the metal surface and the calculated results agreed with the experimentally determined inhibition efficiencies.

Maryam et al. (2019) studied and reported the anticorrosion effect of a new Schiff base hydrazone named as (E-2-(4-(methyl(pyridine-2-yl) amino) ethoxylbenzylidene)- hydrazine-1- carboxamide (MPAH) against a mild steel surface in 1.0 M HCl by experimental methods, computational method and thermodynamic characterization. MPAH showed a good inhibition ability and the effectiveness enhanced by increase in concentration up to an optimal level of 5×10^{-3}M. DFT and molecular dynamics simulation were utilized in the investigation of the MPAH adsorption on metal surface.

Ahmed et al. (2019) reported on corrosion inhibition using 2-((2-hydroxy-5-methoxybenzylidene) amino) pyridine(HMAP) Schiff base, for mild steel (MS) protection in a 1 M HCl acidic media by weight loss, SEM technique, as well as quantum chemical method. Density functional theory (DFT) was performed on HMAP inhibitor and quantum chemical parameters were calculated. Data obtained revealed that HMAP functioned as a good inhibitor in the acidic environment. There was increase in inhibition efficiency with increase in concentration of HMAP inhibitor and decrease in efficiency with increase in temperature. The value of adsorption free energy (ΔG_{ads}) is suggestive of a physisorption/chemisorption adsorption process for HMAP inhibitor. DFT result correlates with experimental inhibition performance

Mohamed, Mohamed and Mohamed (2010) performed a density functional theory (DFT) at the B 3LYP/6-31G++(d,p) basis set level alongside calculation using the HF/6-31G++(d,p) and semi - empirical PM3 methods on four triazole derivatives used as corrosion inhibitors. These compounds include (5-amino1,2,4 triazole(5-ATA), 5-amino-3- mercapto 1,2,4, triazole(5-AMT), 5-amino-3-

methyl thio 1,2,4 triazole(5-AMeTT), 1-amino-3-methylthio-1,2,4- triazole(1-AMeTT). Their various inhibition efficiency was compared with their molecular structures. Molecular dynamics (MD) method was used to study the adsorption energies of the inhibitors with copper (110) surface. Quantum chemical parameters were calculated. Theoretical and experimental results were in agreement.

Khaled (2010) employed Fukui functions, computational simulation comprising of molecular mechanics and molecular dynamics to investigate the corrosion inhibition performance of three amino acids namely: L-methionine (MIT)L- methionine sulfoxide (MITO) and L- methionine sulfone(MITO2) on copper surface in 0.1 M nitric acid. Weight loss, de-polarization and AC impedance techniques were employed as experimental technique.

Jun et al., 2010 investigated the corrosion inhibition efficiency of four 1-R- 2- undecyl-imidazoline compounds namely R=CH_2COOH (A), CH_2CH_2OH (B), $CH_2CH_2NH_2$(C) and H(D) for carbon steel using both molecular mechanics and quantum chemistry methods. Results obtained is suggestive that molecular reactivity binding energy between self-assembled monolayer (SAM) and iron surface, and compactness of the inhibitor SAM are dependent on the hydrophilic groups. Theoretical results were found to be in correlation with experimental data.

2.7 Corrosion Inhibition by Weight-loss and Electrochemical Methods.

Sagar et al. (2013) investigated the inhibitive potential of a chiral ligand (CML) metal complexes of the type [M(PMINAP)(aa).$2H_2O$ on mild steel corrosion in 1M HCl using weight loss experimental technique, corrosion potential, potentiodynamic polarization and surface analytical techniques. M stands for Ni(II), PMINAP is sodium salt of *P*–methoxynitrosoacetophenone and aa is chiral amino acid. Inhibitor concentration of 100 ppm, 200 ppm and 500 ppm were used. The complexes were found to be effective inhibitors and the adsorption characteristics of the inhibitor were in line with Lagmuir adsorption isotherm.

Suraj, Balasaheb, Subhash, & Nana (2020) reported the inhibiting action of the Schiff base 2-[(1H-indol-3-yl methylene)]-4-methyl-phenol and their metal complexes [Ti(IV)AMPIA], [Zr(IV)AMPIA], [Cd(II) AMPIA], [Hg(II)AMPTA] against carbon steel in different acidic medium of HCl, HNO_3 and H_2SO_4 using weight loss method. Experimental data suggests that the Schiff bases and the metal complexes exhibits good inhibition potential. However, the inhibition action of the Schiff base and the metal complexes were enhanced in HCl acid medium compared with their inhibition action in HNO_3 and HSO_4 acid media.

Tahani & Khadijah (2016) synthesized the Pd(II), Hg(II), Cd(II)&Zn(II) metal complexes of the Schiff bases N-(2-hydroxyphenyl)-3-(2-hydroxyphenyl Iminobutanamide (H_2L1) and ethylacetoacetate-isonocotinoylthiosemicarbazidehydrozone (H_2L_2). Corrosion inhibition of the Schiff bases and their Pd(II), Hg(II), Cd(II) & Zn(II) compounds evaluated by hydrogen evolution measurements (HEM) and mass loss method (MLM), were found to be in correlation with each other, and the difference in inhibition efficiency of the Schiff bases were in relation with their chemical structures. Adsorption mechanism of the Schiff bases was found to follow Temkin adsorption isotherm.

Athira et al. (2021) reported on the corrosion inhibition potential of a heterocyclic ligand (HTAN) prepared by coupling diazotized 2-amino-3- caroxylethyl-4,5-dimethylthiophene with □-naphthol with the lanthanide (III) metal complexes using weight loss and open circuit potential (OCP) techniques. The lanthanides used are La(III), Ce(III), Pr(III), Nd(III), Sm(III), Eu(III) & Gd(III). The experimental result showed increase in inhibition efficiency with increase in concentration of inhibitors with enhanced inhibition due to complexation with metal ions.

Shobha et al. (2021) investigated the corrosion inhibition action of a synthesized Schiff base compounds N,N'-bis(Salicylidene)-4,4-diaminostilbene (SDS) and N,N'-bis(salicylidene)-4,4'-diaminoazobenzene (SDA) on alumunium 2024 in HCl using Potentiodynamic polarization, impedence technique, weight loss method and scanning electron microscope technique. The inhibition efficiency of the additives was found to increase with increase in concentration and decreased with an increase in temperature of the medium and immersion time. Both Schiff bases showed superior corrosion inhibition action with SDA giving a more effective inhibition compared to SDS and follows Langmuir adsorption isotherm model.

Bhawna et al. (2020) report on the inhibitive performance of four thiadazole bis-Schiff base derivatives N,N'-(1,phenylenebis(metanylylidene))bis(5-(methylthio)-1,3,4-thiadiazole-2-amine) (PMTTA),5,5'-((1,4-phenyenebis(methanyliylidene)) bis(azanylylidene)),bis(1,3,4-thiodiazole-2-thiol) (PATT), N,N'(1,4-Phenylenebis(methanylylidene)) bis(5-methyl-1,3,4-thiadizole-2-amine) (PMTA) and N,N'-(1,4-Phenylenebis(methanylylidene)) bis(-1,3,4-thiadizole-2-amine) (PTA) on mild steel corrosion in 1 M HCl have been investigated by weight loss method, potentiodynamic polarization, electrochemical impedance spectroscopy(EIS), scanning electron microscopy(SEM), X-ray diffraction and X-ray photoelectron spectroscopy analysis . Recorded data showed that the four synthesized thiadazole bis- Schiff base derivatives, PTA, PMTA, PATT, and PMTTA proved to be superior corrosion inhibitors for mild steel in HCl medium while

inhibition efficiency was in the order PMTAA> PATT > PMTA> PTA. Potentiodynamic polarization data revealed the mixed type nature of all inhibitors.

Preethi and Lavange (2021) synthesized the Schiff base N'-[4-(dimethylamino) benzylidene]-4-hydroxybenzohydrazine (SB) and studied its corrosion mitigating effect on mild steel (MS) in HCl acid medium using potentiodynamic polarization (PDP) technique, scanning electron microscopy (SEM) and atomic force microscopy. The effect of SB & HCl concentration and temperature effect on current density (i_{corr}) and inhibition efficiency (IE) where studied. The potential dynamic polarization measurements shows that the SB functioned as a good anti-corrosive agent.

CHAPTER THREE

MATERIALS AND METHODS

3.1 Materials

3.1.1 Materials/Reagents

All chemicals used for the investigation were of analytical grade and used without further purification. The ligand: Salicylaldehyde, 2aminophenol, 1-2-phenylenediimine, aniline, and the metal precursor, Cerium (III) nitrate hexahydrate ($Ce(NO_3)_36H_2O$), were all used as received from Aldrich. The solvents, absolute ethanol, diethyl ether, dimethyl sulphoxide (DMSO), methanol, HCl, ethylacetate were obtained from Merck and were used as received. The mild steel used in the corrosion studies was obtained from the Metallurgy and Materials (METMAT) Department of the Federal university of technology Owerri (FUTO). Some of the basic tools employed include, a thermometer, weighing balance, melting point apparatus, conductivity meter, ice bathe, volumetric flasks, capillary tubes etc.

3.2 Methods

3.2.1 Sample Preparations

3.2.1.1 Synthesis of 2-hydroxyphenyl – phenylimine or (salicylideneaniline) SALAN

SALAN was prepared by the condensation reaction of salicylaldehyde and aniline according to Onu et al. (2024). 1.525 g (0.0082 moles) of aniline dissolved in 40 mL ethanol was added to 2.0 g (0.0082 moles) of salicylaldehyde in 40 mL ethanol. The mixture was concentrated by heating to half of its volume and placed in an ice bath. The resultant yellow crystal product were filtered, recrystallized from ethanol, air-dried and weighed.

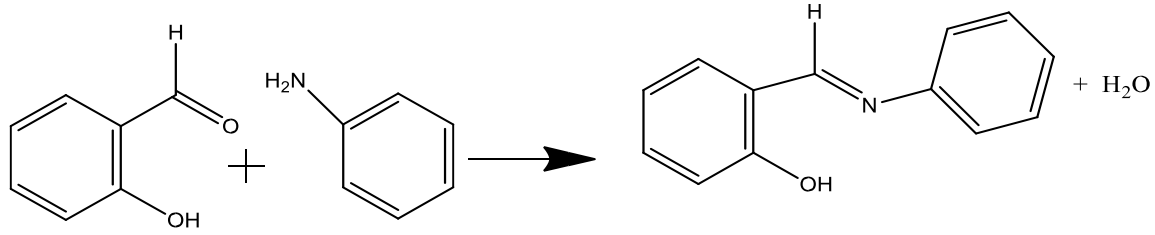

Salicylaldehyde Aniline 2-hydroxyphenyl-phenylimine

Scheme 3.1: Synthesis of 2-hydroxyphenyl-Phenylimine.

3.2.1.2 Synthesis of Bis (2-hydroxyphenyl) imine or (salicylidene-2-aminophenol) SAL2AP

SAL2AP was synthesized by the method of Onu et al. (2024), by the condensation reaction between salicylaldehyde and 2-aminophenol. 1.79 g (0.016 moles) of 2-aminophenol dissolved in 40 mL of ethanol was added to 2.0 g (0.016 moles) of salicylaldehyde in 40 mL of ethanol. The mixture was concentrated by heating to half of its volume and cooled in ice bath. The resultant product was filtered, washed with hot ethanol and recrystallized from ethanol, dried in vacuum desiccators and weighed as appropriate.

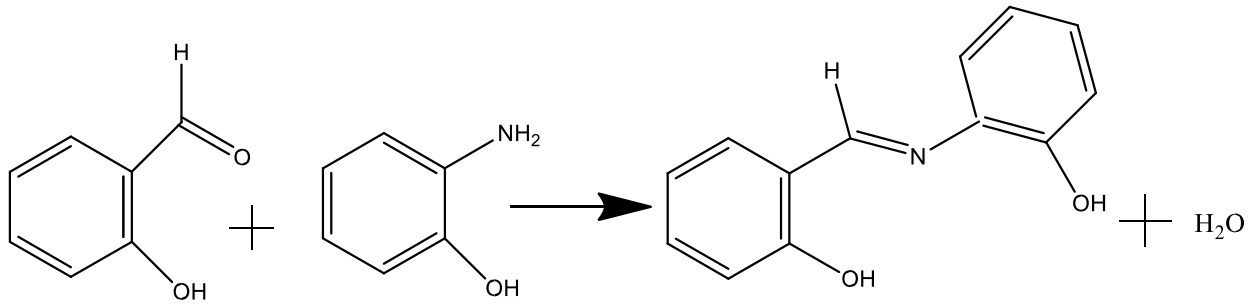

Salcylaldehyde 2- aminophenol Bis (2 hydroxyphenyl)imine

Scheme 3.2: Synthesis of Bis(2-hydroxyphenyl) imine.

3.2.1.3 Synthesis of Bis(2-hydroxyphenyl) – 1,2-benzenediimine (salicylidene1,2-phenylenediamine) SALPD

Bis(2-hydroxyphenyl)-1,2-phenyldiimine was prepared, by the condensation of salicylaldehyde with 1,2-phenylenediamine. 0.886g (0.01 mole) of 1,2-phenylenediamine was dissolved in 40 mL of ethanol and added to 2.0 g (0.016 moles) salicylaldehyde in 40 mL ethanol. The mixture was concentrated by heating to half of its volume and allowed to cool. The resultant orange crystals product was filtered, recrystallized from ethanol, air-dried and weighed (Onu et al.,2024).

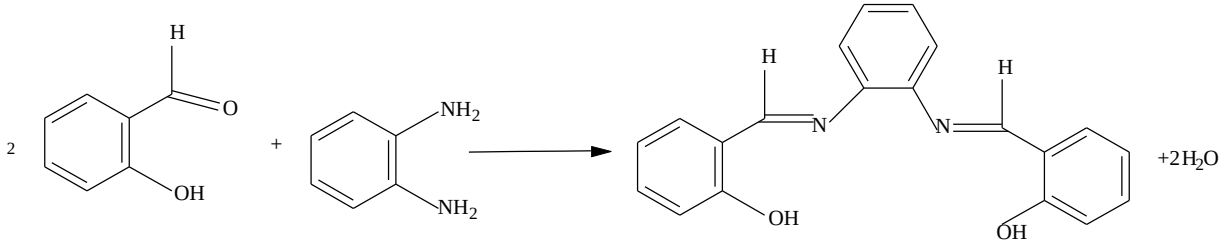

Salicylaldehyde1, 2-phenylenediamine Bis(2-hydroxyphenyl)-1,2benzendiimine

Scheme 3.3: Synthesis of Bis (2-hydroxyphenyl) – 1, 2-benzenediimine.

3.2.1.4 Synthesis of Lanthanide (III) Metal Complexes

0.2 g of Ce (III) nitrate hexahydrate in 20 mL ethanol was added drop by drop to a boiling solution of 0.2 g of SALAN Schiff base, 0.22 g of SAL2AP Schiff base and 0.32 g of SALPD Schiff base in 20 mL ethyl acetate respectively, the mixture was refluxed for 3 hours and the solution concentrated by evaporation. The resultant product was purified and recrystallized from ethanol (Seema, 2015).

3.2.3 Characterization Techniques

The physical and spectral characterization of the synthesized compounds furnishes the important information which is essential for structure elucidation and stereochemistry. The characterization techniques employed for the present research are elemental microanalysis, pH measurement, conductivity measurement, magnetic susceptibility, EDXRF, FT-IR, UV-VIS spectral study, 1H and 13- C NMR, spectroscopy.

3.2.3.1 Elemental Microanalysis

Elemental (CHN) microanalysis supports in the structure determination by providing percentage composition of the elements which are applicable to discover the 40 molecular formulas. Its information is also accessible to ascertain the structure and purity of the synthesized compounds. Elemental analyzer, model CE440, was used to ascertain the elemental compositions of the synthesized compounds.

3.2.3.2 pH Measurement

The legation behavior of Schiff base ligands for the formation of metal complexes are generally driven by deprotonation reaction and the variation in pH value is considered as important evidence of chemical reactions in synthetic chemistry. The formation of metal complex can be predicted by the decrease in pH value in general case. Therefore, the pH values of the synthesized compounds were determined in suitable solvents. For the present research, this measurement was carried out by dissolving the compounds in DMSO and/or methanol solvents. In our work, the pH measurement was done in Elico-16 pH meter in the Electrochemistry and Materials Research Unit (EMRU) in the Department of Chemistry, FUTO.

3.2.3.3 Conductivity Measurement

Conductivity measurement is an important physical technique to gain supportive information about the metal complex formation in coordination chemistry. The molar conductance values of the complexes were measured in M/1000 solution of synthesized compounds in either of DMSO or

methanol solvents. The change in conductance values from ligand to complex formation is a necessary clue for the chelation of ligands with metal ions. The conductivity measurement was done in Labtronics auto digital conductivity meter (Model LT-16)

3.2.3.4 Electronic Absorption Spectroscopy

UV-visible spectroscopy is an important instrumental tool for the coordination chemists to draw the important information about the structural aspects of the complexes (Manfred and Jurgen 2012). For the present research work, the electronic absorption spectral study was achieved in M/1000 solution of the synthesized compounds in DMSO and/or methanol solvents. Electronic UV-Vis spectra were recorded using a UV-1800 Shimadzu spectrophotometer

3.2.3.5 FT-IR Spectral Study

The IR spectral study is another important instrumental tool for the characterization of the ligands and complexes. Basically, it gives information regarding the presence of functional groups, other structural components and the metal ligand bonding parameters. The instrument uses infrared radiations of the electromagnetic spectrum for the vibrations of the bonds in the compounds, from which wealth of information can be achieved. The data of the IR bands can be processed to derive the presence of structural components of the molecules (Rohman and Sugeng, 2014). The bands due to metal-ligand coordination are mainly observed in the far IR region around 500 Cm^{-1}. The IR spectra were recorded as KBr pellets on a Perkin Elmer 783 FT-IR spectrophotometer in the range of 4000-400 cm^{-1}.

3.2.3.6 1H & 13C NMR Spectral Study

The 1H & 13C NMR spectral data provide valuable information regarding the structure of Schiff base ligands and metal complexes. NMR spectroscopy is such a modern instrumental tool without which a chemical researcher cannot think for the design of the proper structure of unknown compounds. The binding mode of the ligand with metal centers in diamagnetic complexes can be well achieved by their 1H & 13C NMR spectral comparison. For the present research work, the 1H & 13C NMR spectra were recorded on Bruker Avance III, 400 MHz spectrometer, using DMSO-d6 as solvent and TMS as the internal reference chemical.

3.2.3.7 EDXRF Study

EDXRF is a convenient technology to screen all kinds of materials for quick identification and quantification of elements with little or no sample preparation. EDXRF is designed to analyze groups of elements simultaneously. It works by separating characteristics x –rays of different

elements into a complete fluorescence energy spectrum which is then processed for qualitative or quantitative analysis. Rapid elemental analysis of regular and irregular samples makes EDXRF an attractive front- end analysis. EDXRF of this present study was carried- out on the Cerium Schiff base complexes to evaluate the percentage of cerium in the synthesized complexes using EDXRF analyzer of software version 10.30.159, voltage 20Kv, and maximum energy of 40 keV

3.2.3.8 AFM Study

Atomic force microscopy (AFM) is a powerful technique that enables the imaging of almost any type of surface, including polymers, ceramics, composites, glass, and biological samples. AFM is used to measure and localize many different forces including adhesion strength, magnetic forces, and mechanical properties. AFM machine, MFP-3D confocal TIRF model was used to analyze the surfaces of the mild- steel after corrosion process. AFM principle involves a nanoscale tip attached to a cantilever which forms a spring. The cantilever bends as the nanoscale tip contacts the surface. The bending is detected using a laser diode and a split photodetector. This bending is indicative of the tip – sample interaction force to keep the deflection constant throughout raster scanning.

3.2.3.9 Magnetic Susceptibility Measurement

Magnetic susceptibility of the cerium Schiff base complexes were determined using Gouy's balance, model, (GMX-02).

3.2.4 Corrosion Inhibition Test by Weight- Loss Method.

3.2.4.1 Preparation corrodent

The corrodent of 1 M HCl solution was prepared by diluting 82 mL of conc. HCl in 1000 cm^3 volumetric flask which is used as corrodent.

3.2.4.2 Preparation of Specimen

Experiments were performed with commercial grade mild - steel, and the elemental analysis carried-out using vacuum emission spectrometer of model BAIRD- DVA. Mild steel specimen of dimension 3 x 3 x 0.1 cm and 1 x 1 x 0.1 cm were used. The weight percentage composition of elements found in the specimen are carbon =1.14 %, silicon = 3.28 %, manganese =2.18, sulphur = 0.226 %, phosphorus =0.012 %, copper = 1.09 %, nickel = 6.08 %, chromium = 0.89 %, and iron = 81.2 % The surface preparation of the specimen was done mechanically using silicon carbides of varying specification (400, 600, 800 and 1000) to achieve a polished surface, which was subsequently cleaned using ethanol before each experiment. Duplicate steel specimens were immersed into 250 mL of the corrodent with and without the inhibitors namely: salicylidene-

aniline, salicylidene-2-aminophenol and salicylidene-1,2- Phenylenediamine and their Ce (III) metal complexes at varying concentrations of the inhibitors, such as 0.1 mmol, 0.2 mmol, 0.4 mmol, 0.6 mmol 0.8 mmol,1.2 mmol, 1.6 mmol, 2.0 mmol. This was carried-out at room temperature (25 ^{o}C). Effect of temperature change at elevated temperature of 40, 50 60, 70 ^{o}C was carried out under three hours. The weight loss measurements were performed according to ASTM standard G 31- 72. The percentage inhibition efficiency (IE) was obtained from the following equation:

$$IE\% = 1 - C_{Rinh} \times \frac{100}{C_{RB}} \quad (1.1)$$

Where C_{Rinh} = Corrosion rate of inhibited system, C_{RB} = Corrosion Rate of Blank

IE = Inhibition Efficiency of inhibitor.

Corrosion rate C_R is given by the equation:

$$C_{R(mdd)} = \frac{\Delta W \times 100}{A \times t} \quad (1.2)$$

Where ΔW = change in weight of coupon, A = area of coupon, t = immersion time

Surface coverage, θ is calculated using the equation:

$$\theta = 1 - \frac{C_{Rinh}}{C_{RB}} \quad (1.3)$$

The activation energies of the corrosion process in free and inhibited acid were calculated using the Arrhenius equation.

$$K = A \exp\frac{E_a}{RT} \quad (1.4)$$

where *Ea* is the activation energy, A is the frequency factor, *T* is the absolute temperature, *R* is the gas constant, and K is the rate constant, which is directly proportional to the corrosion rate. Plotting log k versus 1/T gives a straight line. The slope gives the *Ea* of the adsorption process.

Langmuir adsorption isotherm given by the following equations:

$$\frac{C_{inh}}{\theta} = \frac{1}{b} + C_{inh} \quad (1.5)$$

$$b = \frac{1}{55.5} exp\left(-\frac{\Delta G_{ads}}{RT}\right) \quad (1.6)$$

C_{inh} is the inhibitor concentration, θ is the fraction of the surface covered, b is the adsorption coefficient and G_{ads} is the standard free energy of adsorption.

$$log\frac{C_R}{T} = \left[\left(\frac{logR}{Nh}\right) + \left(\frac{\Delta S^*}{2.303\,R}\right) - \frac{\Delta R^*}{2.303\,RT}\right] \quad (1.7)$$

h is plank's constant, 6.626 x 10-^{34}, N is equal to Avogadro's number, 6.02 x $10^{23.}$, S* is the entropy of activation, R is gas constant, T is temperature in Kelvin. The slope of the linear plot, –H* / 2.303R permits to derive the enthalpy of activation (H*), and an intercept of (log R/Nh) + (ΔS*/2.303 R) is used to calculate the entropy of the activation process, S*.

3.2.5 Molecular Modeling

Molecular modeling is a computer simulation technique to design the molecular graphics and optimize the molecular geometry of the proposed structures. In our investigation, 3D molecular modeling of the proposed structure of the Schiff base ligands and metal complexes was achieved by BioVial Material Studio 7.0 version software program package (Singh et al., 2014). Material studio is molecular modeling software to sketch the chemical structures of the molecules. It is supported by various tools to design the molecules in 2D and 3D forms. The various tools of this software enable us to optimize geometry, calculate energy, build surfaces and perform Gaussian calculations to customize the molecular model. It assists in visualizing molecular orbitals, electron densities, electrostatic potentials and spin densities on the surface of molecules. Electrostatic potential mapped electron density on the surface of molecules can also be visualized. This is also supported by various molecular properties calculations like single point energy calculation and geometry optimization calculation to draw the stable molecular geometry of the proposed molecules.

CHAPTER FOUR

RESULTS AND DISCUSSION

4.1 RESULTS

This chapter presents and discusses the results of the synthesis, characterization, and corrosion inhibition studies of Ce(III) metal complexes derived from salicylidene-aniline, salicylidene-2-aminophenol, and salicylidene-1,2-phenylenediamine Schiff bases. The chapter is structured to address the key objectives of this study, which include the synthesis of the Schiff base ligands and their corresponding Ce(III) metal complexes, comprehensive characterization using various analytical techniques, and the evaluation of their corrosion inhibition properties.

The synthesized Schiff base ligands were characterized by elemental analysis, melting point determination, solubility tests, and conductivity measurements, alongside spectral analyses involving UV-Visible, Infrared (IR), and Proton (^{1}H) and Carbon-13 (^{13}C) Nuclear Magnetic Resonance (NMR) spectroscopy. The resulting Ce(III) complexes were similarly characterized to confirm their successful synthesis and elucidate their structures.

Furthermore, the corrosion inhibition properties of the ligands and their Ce(III) complexes were investigated using both mass loss and electrochemical studies in 1M hydrochloric acid. The adsorption behavior of the inhibitors on carbon steel was studied through the application of adsorption isotherms, including Langmuir, Temkin, and Frumkin models. The effect of temperature on the corrosion inhibition efficiency was analyzed to determine thermodynamic parameters such as activation energy, enthalpy, and entropy.

Finally, molecular modeling and simulation studies were conducted to explore the adsorption mechanism of the Schiff bases and their metal complexes on the metal substrate, providing deeper insights into their interaction with the carbon steel surface. These findings are discussed in detail

in this chapter, highlighting the correlation between the structural properties of the compounds and their performance as corrosion inhibitors.

4.1.1 Physical Measurements for SALAN and CeSALAN

The better understanding of the behavior of metal complexes can be well accomplished by the study of their physical properties, which includes colour, solubility, melting point, pH and conductivity measurements. These are essential to gain supportive information, regarding the ligand and complex formation during the chemical processes. The different compounds have their unique physical properties and their detailed study helps in designing the mechanism of the reaction and also helps in predicting the nature of the compounds.

Table 4.1: Physical Properties, Percentage Yield, and Elemental Analysis of SALAN and CeSALAN

Compounds	Molecular Formular	Colour	pH	Yield (%)	Melting point (^{0}C)	Molecular Composition		
						C	H	N
SALAN	$C_{13}H_{11}NO$	YELLOW	8	88	60	75.56 (75.58)	4.88 (4.73)	7.01 (6.96)
CeSALAN	$C_{26}H_{26}CeN_2O_5$	DULL YELLOW	4	56	88-90	53.61 (53.23)	4.95 (4.47)	4.89 (4.78)

Table 4.1 shows the variation in colour, pH, percentage yield, melting point, and molecular compositions of the synthesized Schiff base SALAN, and its cerium metal complex, CeSALAN. difference in colour, pH, and melting point shows successful synthesis of the compounds.

Table 4.2: Solubility Tests for SALAN and CeSALAN

COMPOUNDS	**SOLVENTS**						
	DI H_2O	ETHANOL	METHANOL	ACETONE	CARBONTETRA-CHLORIDE	DMF	DMSO
SALAN	N/S	S	N/S	S	S/S	S	S
CeSALAN	N/S	N/S	N/S	N/S	N/S	S	S

N/S = not soluble, S = soluble

Table 4.2 shows the solubility of the synthesized compounds in various organic solvents. Both compounds were observed to be soluble in DMF, and DMSO.

Table 4.3 Molar conductivity and Magnetic susceptibility for SALAN and CeSALAN

Compound	Molecular formular	Molecular weight (g/mol)	Molar Conductivity (mS/cm)		Magnetic Susceptibility
			DMSO	DMF	
SALAN	$C_{13}H_{11}NO$	197.24	9.1×10^{-3}	1.01×10^{-2}	-
CeSALAN	$C_{26}H26CeN_2O_5$	586.62	1.44	1.55	006 (paramagnetic)

Molecular formular, weight, molar conductivity, and magnetic susceptibility data of the compounds are shown in Table 4.3. The Schiff base SALAN shows a much lower conductivity values compared to CeSALAN. CeSALAN shows value for magnetic susceptibility for paramagnetic compounds. SALAN recorded no magnetic susceptibility value.

4.1.2 Spectral results for SALAN and CeSALAN

Spectroscopic measurements employed for this present study included: Uv-Visible spectroscopy, FTIR, 1H-NMR, 13-C NMR, and EDXRF. The characterization of the compounds by spectral methods is vital for the structural elucidation of the compounds under study as well as spatial orientation of the bonded atoms.

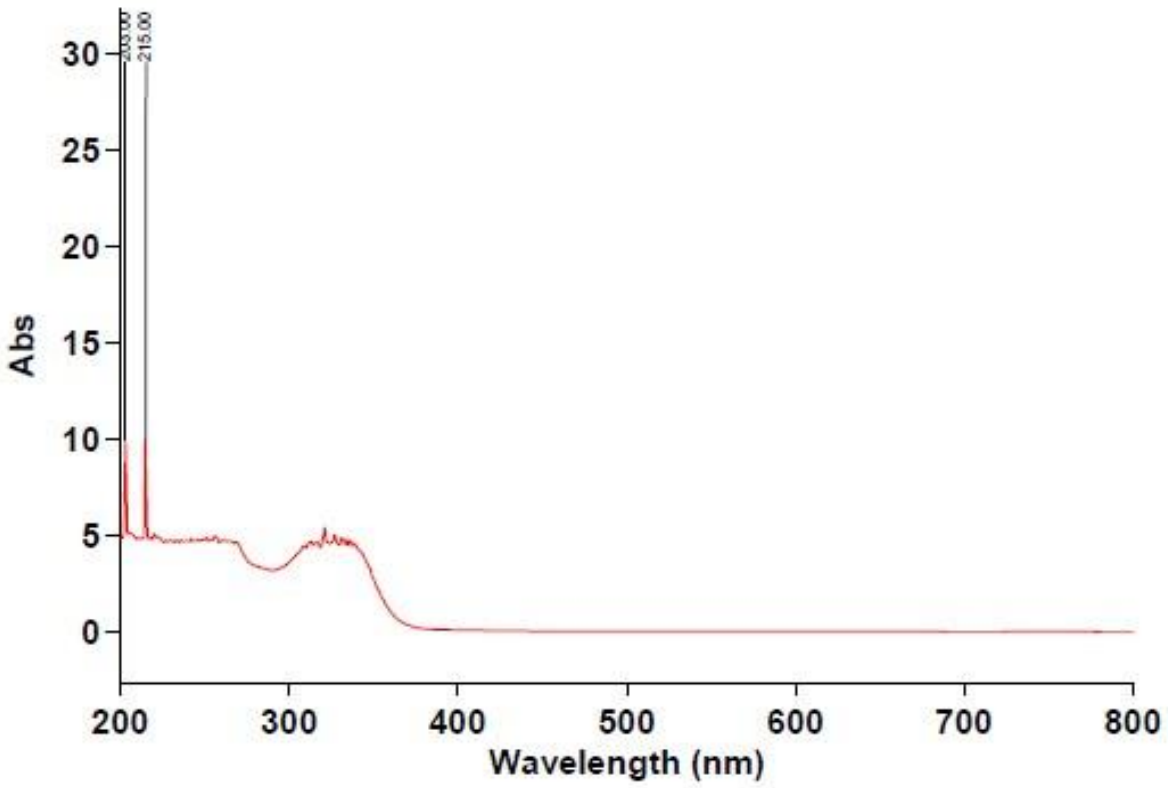

Figure 4.1: UV-Visible Spectrum of SALAN

Uv- visible spectrum of SALAN is shown in Figure 4.1. The maximum absorbance was observed at 215 nm, corresponding to an $n \rightarrow \pi*$ transition.

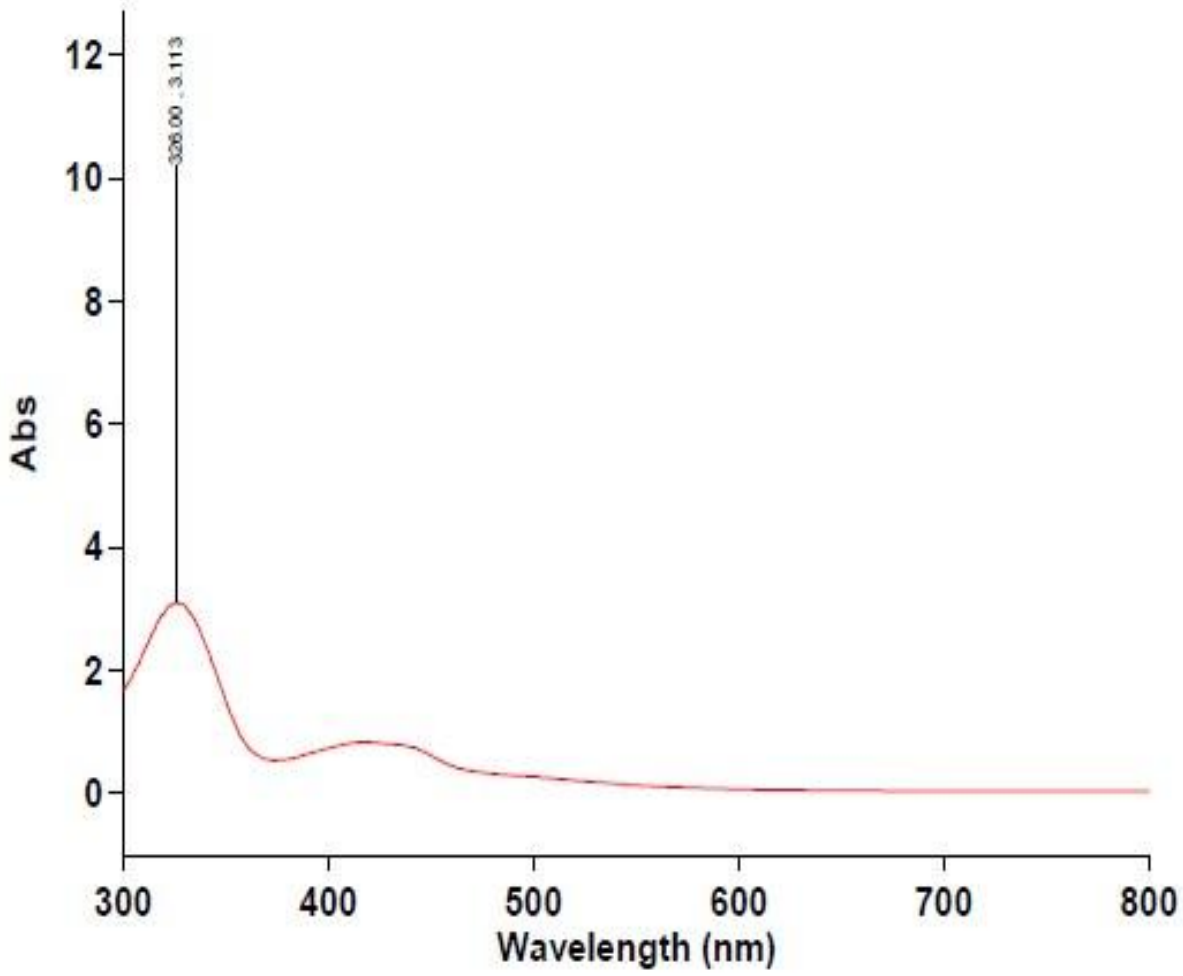

Figure 4.2: Uv –Visible Spectrum of CeSALAN

Maximum absorbance of CeSALAN at 326 nm is observed due to π- π* electronic transition, and formation of the complex.

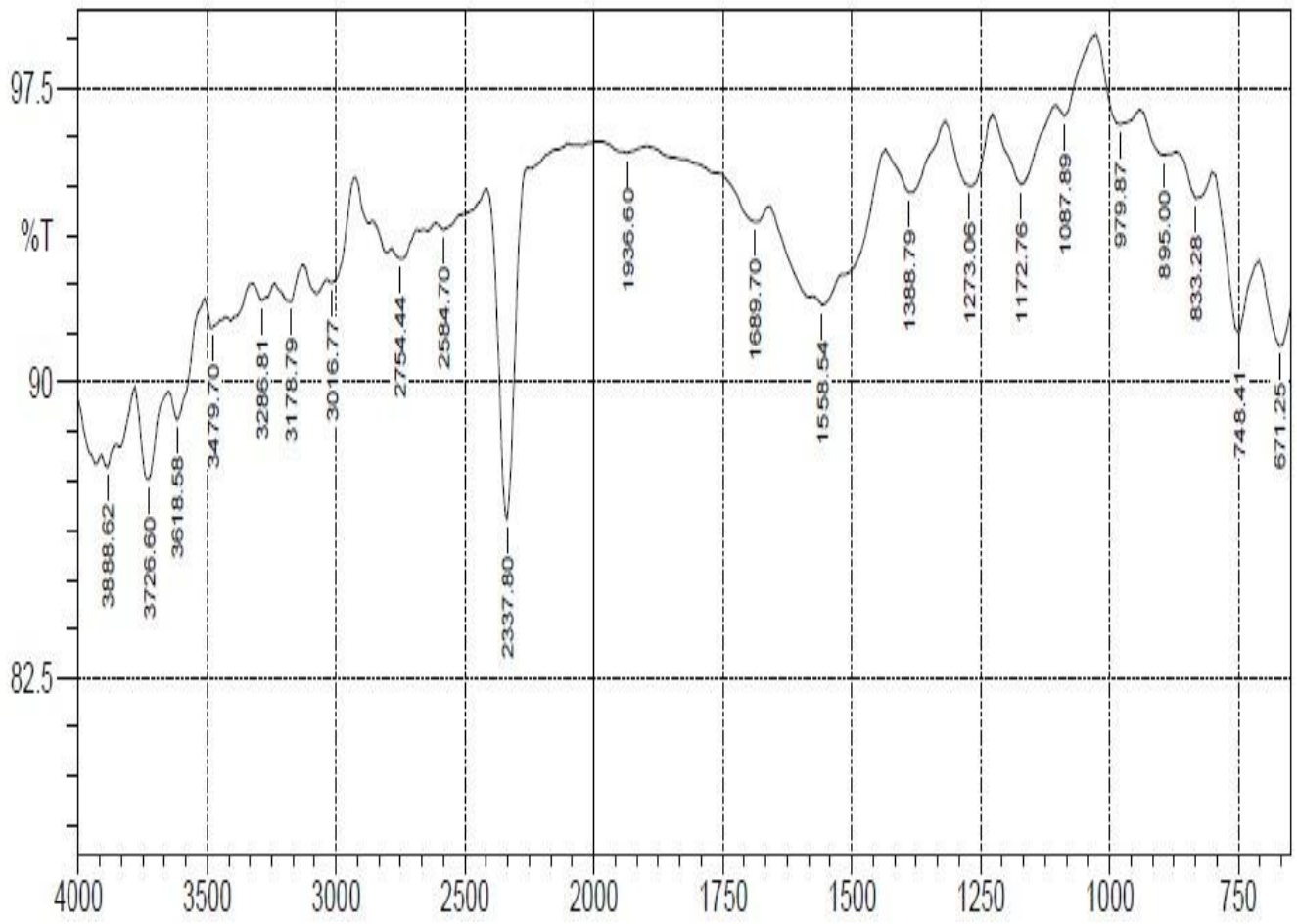

Figure 4.3: Fourier Transform Infrared (FTIR) Spectrum of SALAN

FTIR of SALAN in Fig. 4.3 shows frequencies due to the following vibrations:

v(C-O) at 1273 cm^{-1} , v(OH) at 3479 cm^{-1} , and v(CH=N) at 1689 cm^{-1}.

These characteristics frequencies of Schiff base show successful synthesis of the Schiff base SALAN.

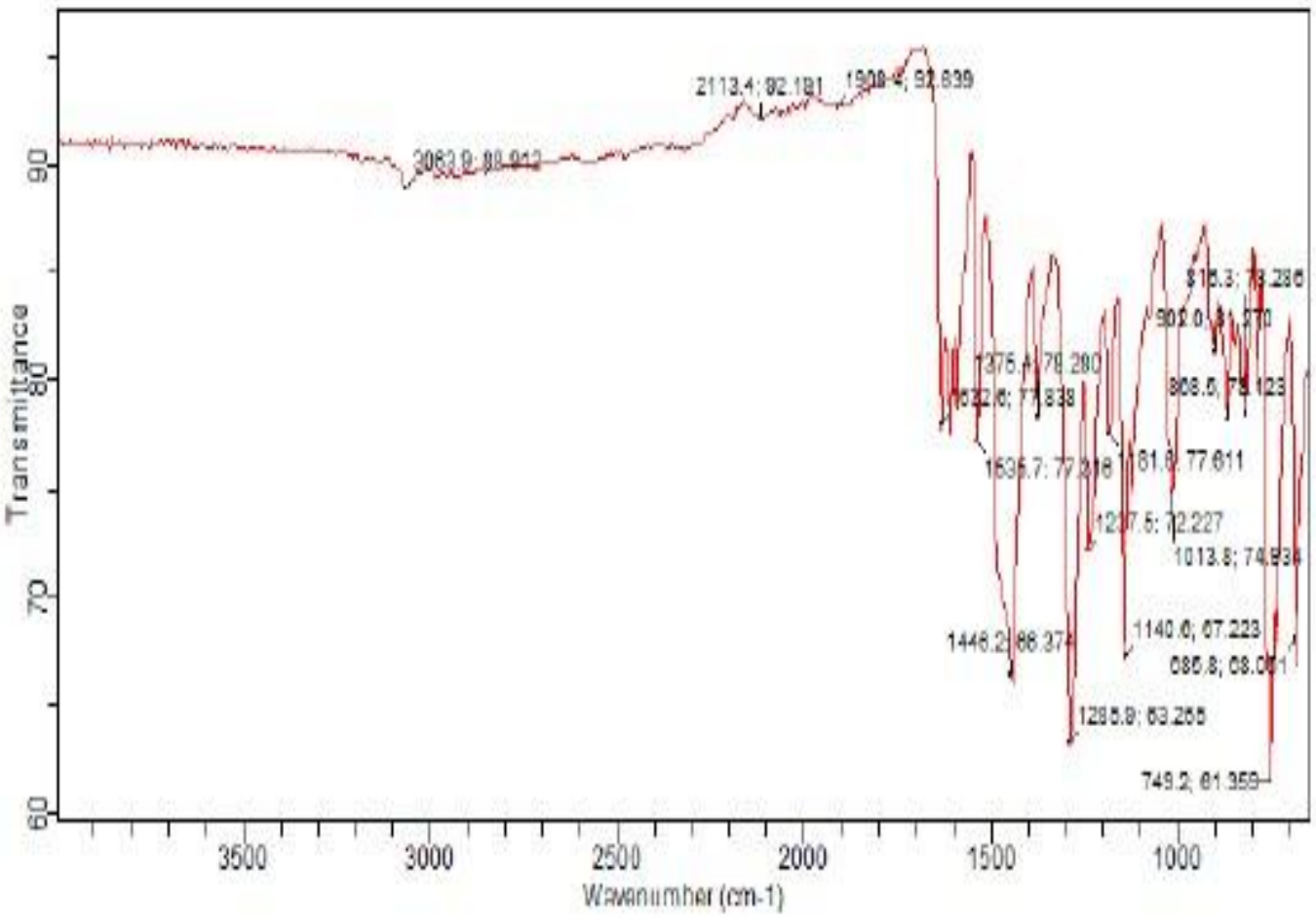

Figure 4.4: Fourier Transform Infrared (FTIR) Spectrum (FTIR) of CeSALAN

FTIR of CeSALAN showed the following vibrational frequencies: v (H_20) at 3063 cm^{-1} ,v (NO_3) at 1446 cm^{-1} , v(M-O) at 685 cm^{-1} , v(C-O) at 1285 cm^{-1}, v(HC=N) at 1632 cm^{-1} .

These characteristics frequencies show successful synthesis of the Schiff base metal complex CeSALAN.

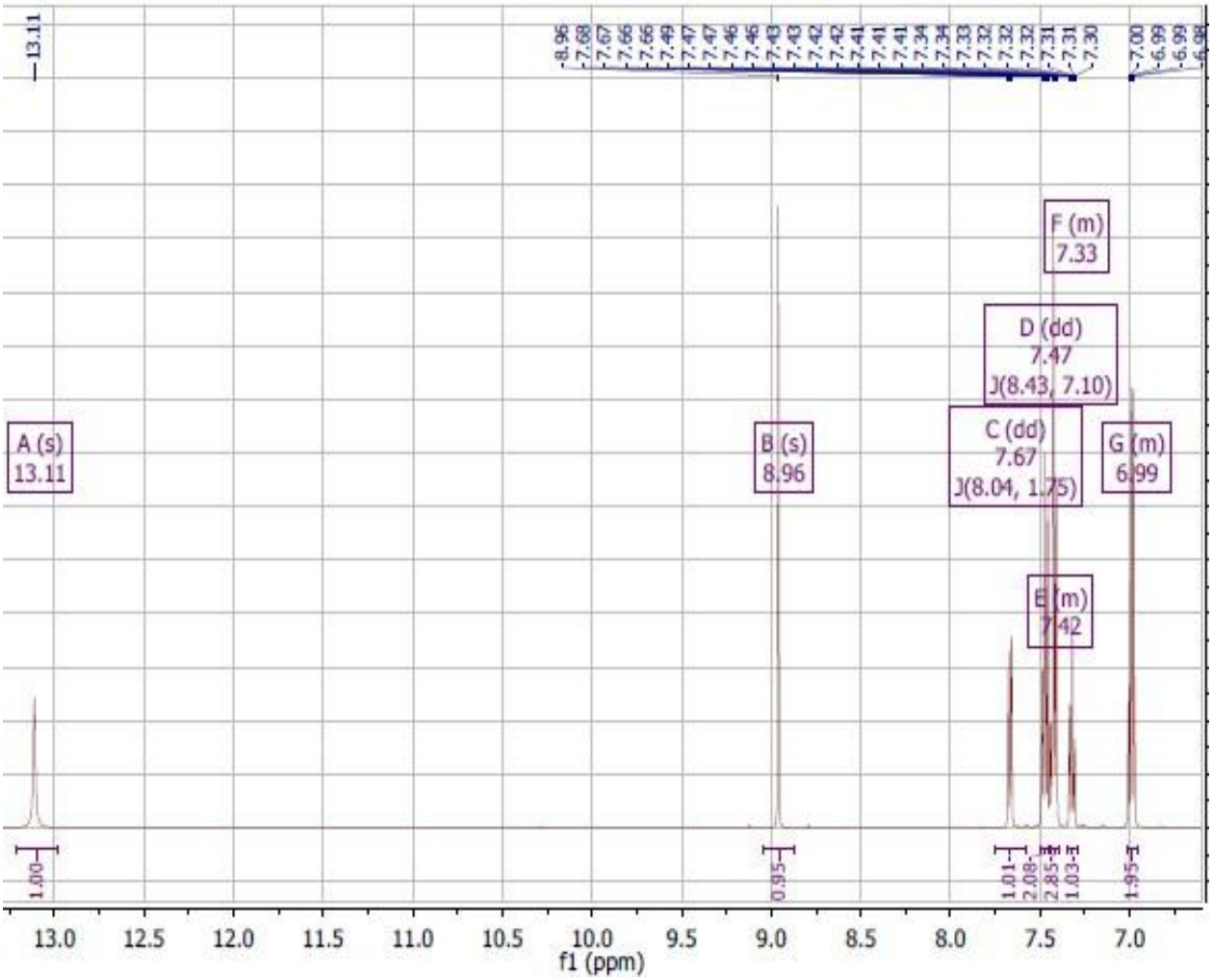

Figure 4.5: Proton ^{1}H NMR Spectrum of SALAN

The key signals exhibited by ^{1}H-NMR spectra of SALAN are due to (H–C=N) proton at δ 8.96 ppm, and hydroxyl (OH) proton of the aldehyde moiety at δ13.11 ppm.

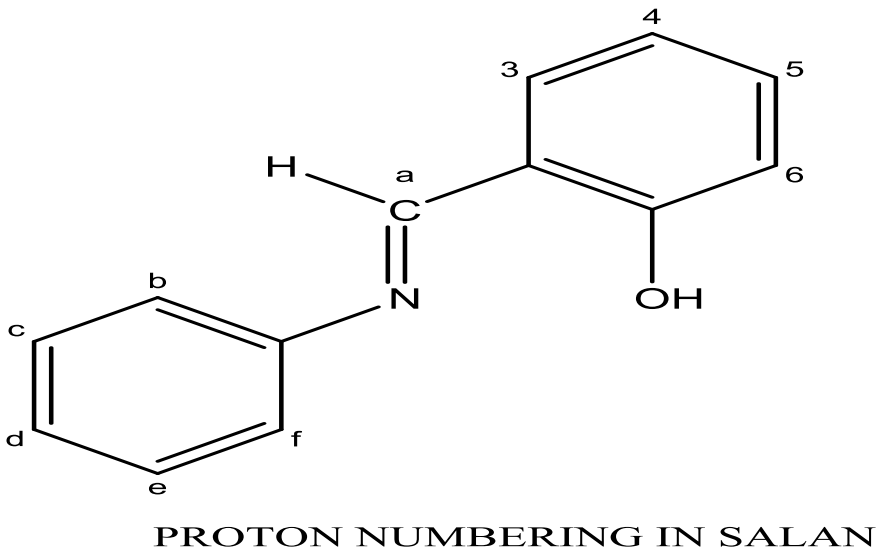

Figure 4.6: Proton numbering in SALAN

Table 4.4: ^{1}H NMR Spectral Data of SALAN

Compound	Chemical Shift (δ) ppm	Assignment
SALAN	13.11	(s, 1H, OH)
	8.96	(s, 1H, HC=N)
	7.42 – 7.32	(m, 5H, b,f,
	7.67- 7.43	H_3,H_4,H_5
	7.68- 7.43	(dd,1H, d)
	7.47- 7.43	(d, 1H, H6)
		(dd, 2H, c, e)

Table 4.4 shows chemical shifts for various proton- signals in the SALAN Schiff base, which identifies the Schiff base.

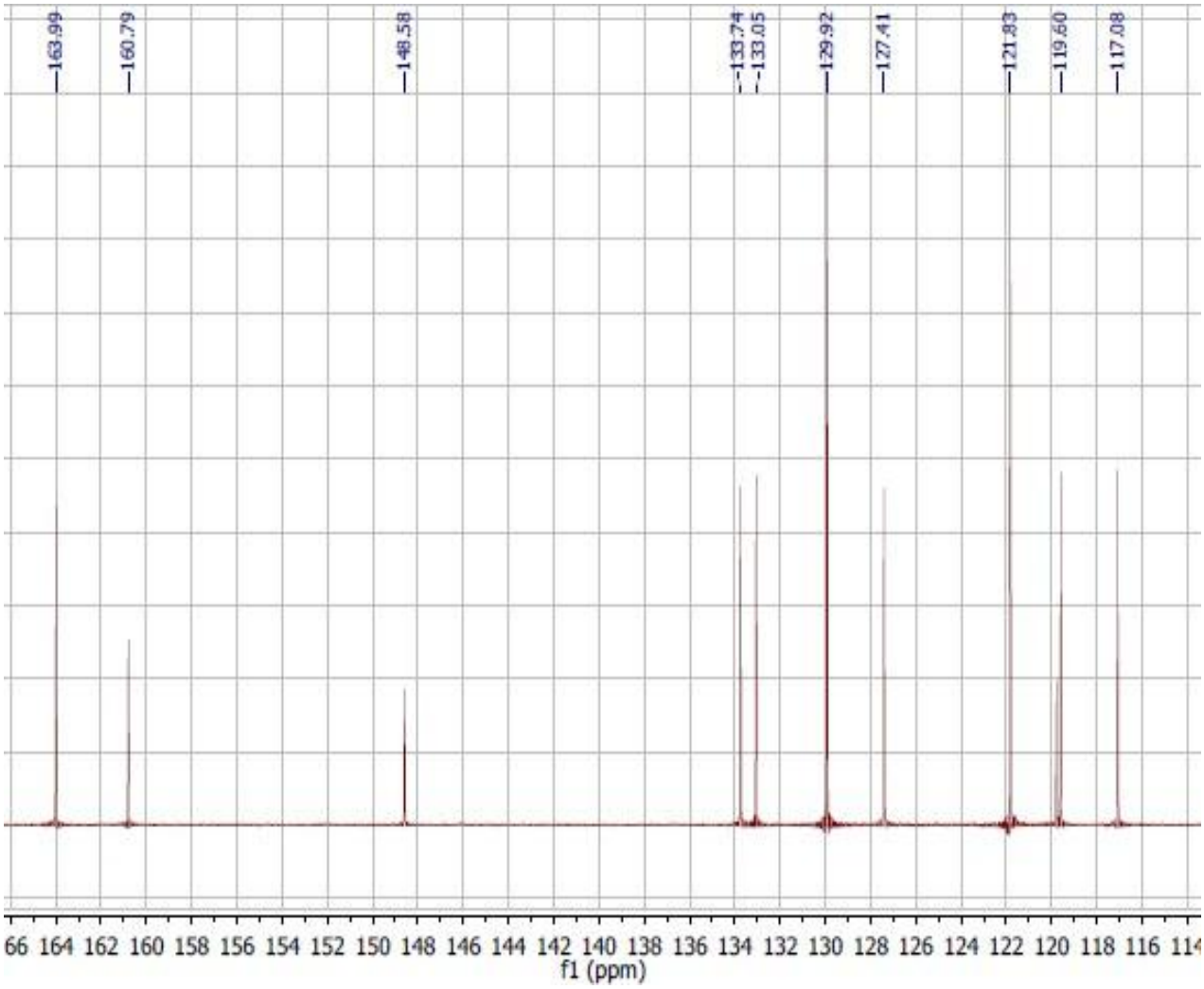

Figure 4.7: Carbon 13 (C-13) NMR Spectrum of SALAN

The signal due to carbon atom of the azomithine group occurred at 163.99 ppm. This confirms the successful synthesis of the Schiff base SALAN.

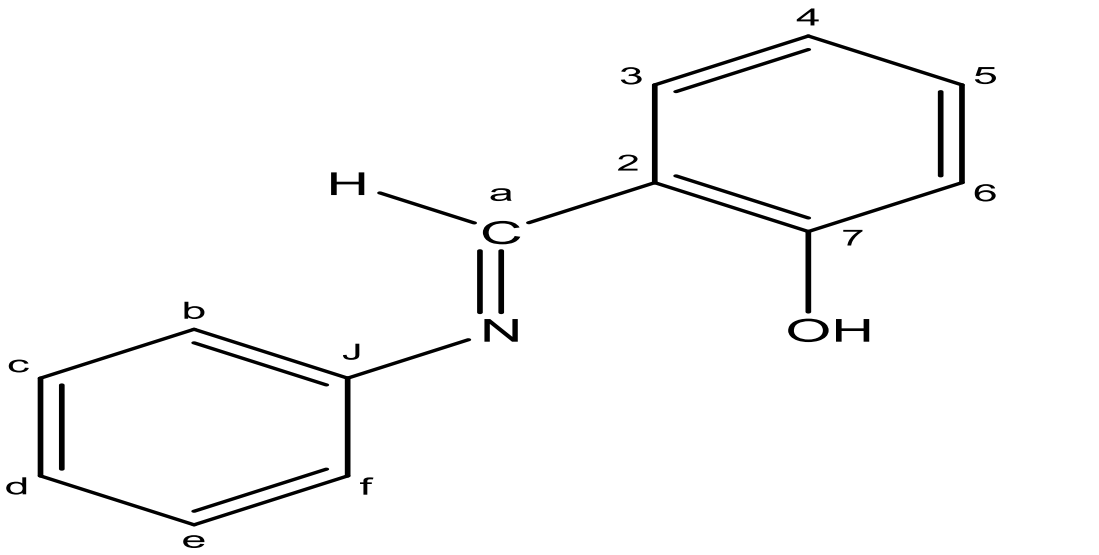

Figure 4.8: Carbon numbering in SALAN

Table 4.5: C-13 NMR Spectral Data of SALAN

Compound	Chemical Shift (δ) ppm (Assignment)
SALAN	117.08 (C6),119.60 (C4), 119.90(C2), 121.83(b,f),127.41(d), 129.92(c,e), 133.05(C3), 133.74(C5), 148.58(J), 160.79(C7), 163.99(C(HC=N)

The spectra data shows chemical shifts due to various constituent protons in SALAN Schiff base.

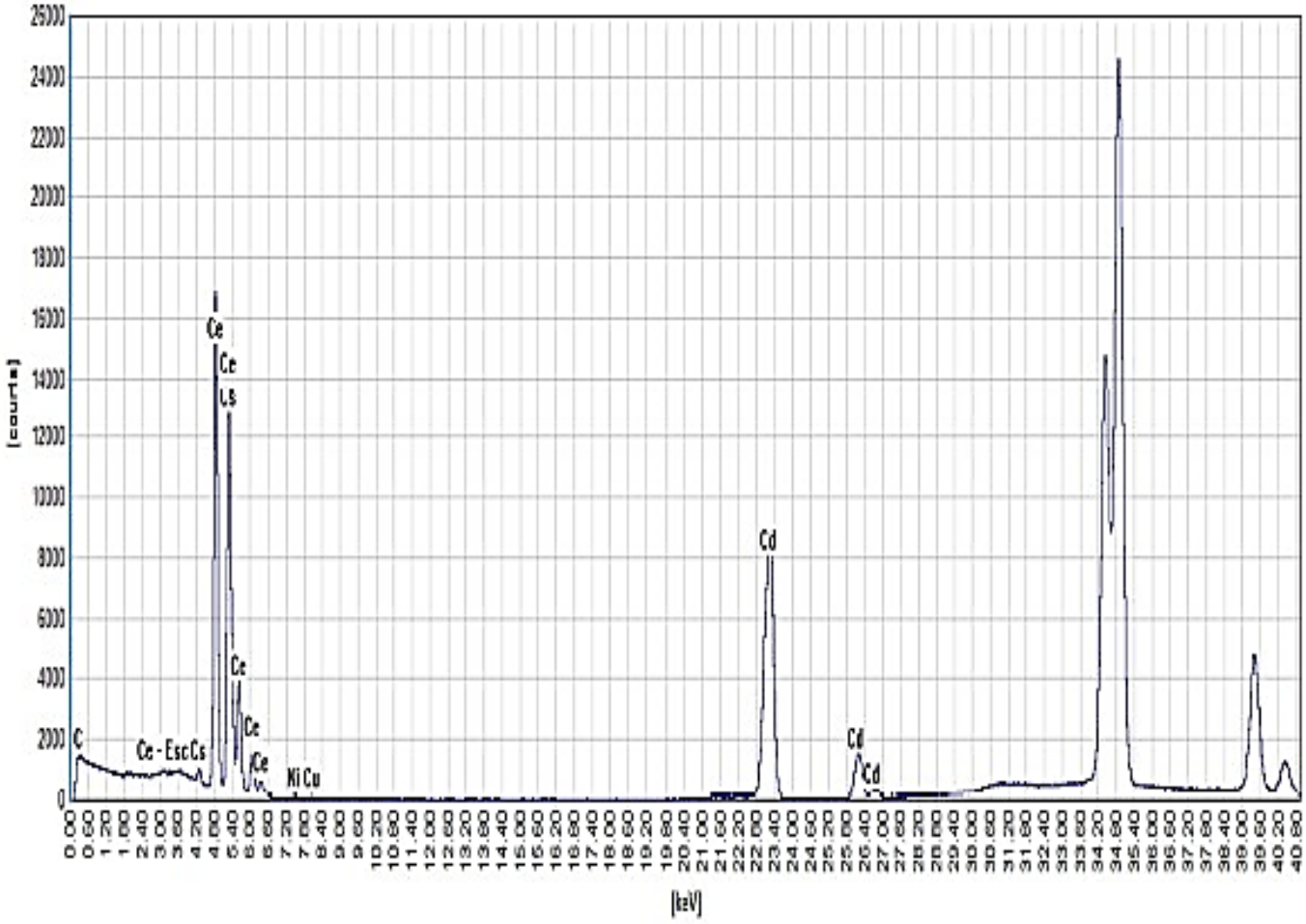

Figure 4.9: EDXRF Spectra of CeSALAN

EDXRF spectra of CeSALAN shows percentage compositions of Cerium found in CeSALAN complex measured as 80.13%.

4.1.3. Inhibitive Action SALAN and CeSALAN

4.1.3.1 Gravimetric results

Table 4.6: Gravimetric Data of Mild Steel in 1M HCl in the presence and absence of SALAN (Lagmuir Adsorption Isotherm)

System (mmol dm^3)	C_R(mdd)	IE%	θ	C/θ
1 $x10^{-1}$	2.07	48.01	0.48	0.21
2 $x10^{-1}$	1.54	61.40	0.61	0.33
4 $x10^{-1}$	1.36	65.76	0.66	0.61
6 $x10^{-1}$	1.29	68.78	0.67	0.90
8 $x10^{-1}$	1.20	73.76	0.74	1.08
12 $x10^{-1}$	1.22	72.78	0.73	1.64
16 $x10^{-1}$	1.23	70.24	0.70	2.28
20 $x10^{-1}$	1.23	69.11	0.69	2.90

Corrosion rate $\mathbf{C_R}$ decreases with increase in Concentration, Surface Coverage **θ**, and Inhibition Efficiency.

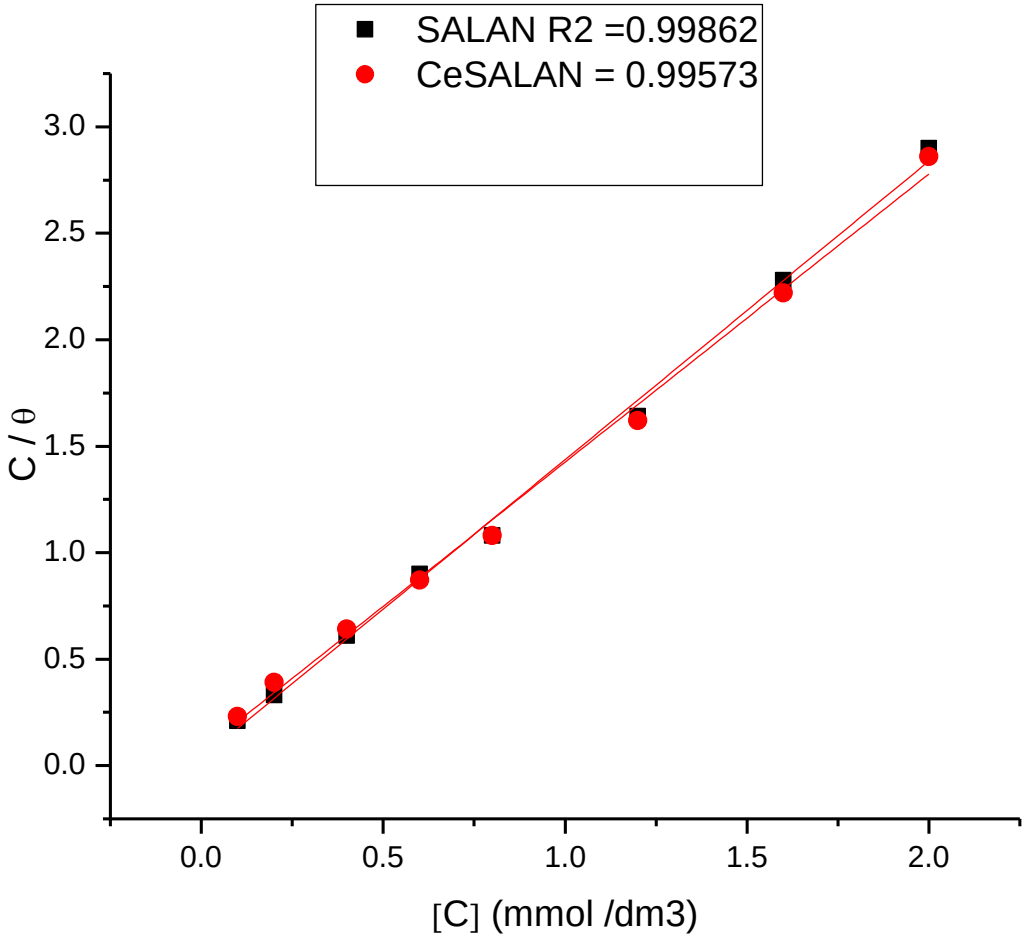

Figure 4.10: Langmuir's Adsorption Plots for Mild Steel in 1 M HCl containing various concentrations of SALAN and CeSALAN.

Table 4.7: Gravimetric Data of Mild Steel in 1M HCl in the presence and absence of SALAN (Temkin Adsorption Isotherm)

System (mmol dm^3)	C_R(mdd)	IE%	Θ	Θ/C	Log(Θ/C)
1 $x10^{-1}$	2.07	48.01	0.48	4.80	0.68
2 $x10^{-1}$	1.54	61.40	0.61	3.05	0.48
4 $x10^{-1}$	1.36	65.76	0.66	1.65	0.22
6 $x10^{-1}$	1.29	68.78	0.67	1.12	0.05
8 $x10^{-1}$	1.20	73.76	0.74	0.93	-0.03
12 $x10^{-1}$	1.22	72.78	0.73	0.61	-0.22
16 $x10^{-1}$	1.23	70.24	0.70	0.44	-0.36
20 $x10^{-1}$	1.23	69.11	0.69	0.35	-0.46

Corrosion rate $\mathbf{C_R}$ decreases with increase in Concentration, Surface Coverage **θ**, and Inhibition Efficiency.

Table 4.8: Gravimetric Data of Mild Steel in 1M HCl in the presence and absence of SALAN (Frumkin's Adsorption Isotherm)

System (mmol dm^3)	C_R(mdd)	IE%	θ	(1-θ)C	Θ (1- θ)C	Log Θ (1- θ)C
1 $x10^{-1}$	2.07	48.01	0.48	0.052	9.23	0.9652
2 $x10^{-1}$	1.54	61.40	0.61	0.078	7.82	0.8932
4 $x10^{-1}$	1.36	65.76	0.66	0.136	4.85	0.6857
6 $x10^{-1}$	1.29	68.78	0.67	0.198	3.38	0.5289
8 $x10^{-1}$	1.20	73.76	0.74	0.208	3.56	0.5514
12 $x10^{-1}$	1.22	72.78	0.73	0.324	2.25	0.3522
16 $x10^{-1}$	1.23	70.24	0.70	0.48	1.46	0.1644
20 $x10^{-1}$	1.23	69.11	0.69	0.62	1.11	0.0453

Corrosion rate $\mathbf{C_R}$ decreases with increase in Concentration, Surface Coverage **θ**, and Inhibition Efficiency.

Table 4.9: Gravimetric Data of Mild Steel in 1M HCl in the presence and absence of CeSALAN (Langmuir's Isotherm)

System (mmol/dm^3)	Corr. Rate	IE%	(θ)	C/θ
1x10^{-1}	2.28	42.71	0.43	0.23
2 x10^{-1}	2.05	51.51	0.52	0.39
4 x10^{-1}	1.46	63.29	0.63	0.64
6 x10^{-1}	1.26	68.64	0.69	0.87
8 x10^{-1}	1.01	74.24	0.74	1.08
12 x10^{-1}	1.07	73.66	0.74	1.62
16 x10^{-1}	1.17	71.36	0.72	2.22
20 x10^{-1}	1.23	70.11	0.70	2.86

Corrosion rate $\mathbf{C_R}$ decreases with increase in Concentration, Surface coverage **θ**, and Inhibition Efficiency.

Table 4.10: Gravimetric Data of Mild Steel in 1M HCl in the presence and absence of CeSALAN (Temkin's Isotherm)

System (mmol/dm^3)	Corr. Rate	IE%	(θ)	θ/C	Log(θ /C)
$1x10^{-1}$	2.28	42.71	0.43	4.30	0.63
$2\ x10^{-1}$	2.05	51.51	0.52	2.60	0.42
$4\ x10^{-1}$	1.46	63.29	0.63	1.58	0.20
$6\ x10^{-1}$	1.26	68.64	0.69	1.15	0.06
$8\ x10^{-1}$	1.01	74.24	0.74	0.93	-0.03
$12\ x10^{-1}$	1.07	73.66	0.74	0.62	-0.21
$16\ x10^{-1}$	1.17	71.36	0.72	0.45	-0.35
$20\ x10^{-1}$	1.23	70.11	0.70	0.35	-0.46

Corrosion rate $\mathbf{C_R}$ decreases with increase in Concentration, Surface Coverage **θ**, and Inhibition Efficiency.

Table 4.11: Gravimetric Data of Mild Steel in 1M HCl in the presence and absence of CeSALAN (Frumkin's Isotherm)

System (mmol/dm^3)	Corr. Rate	IE%	θ	(1-θ) C	θ (1-θ)C	Log θ (1- θ)C
1x10^{-1}	2.28	42.71	0.43	0.057	7.54	0.8774
2 x10^{-1}	2.05	51.51	0.52	0.096	5.42	0.7340
4 x10^{-1}	1.46	63.29	0.63	0.148	4.26	0.6294
6 x10^{-1}	1.26	68.64	0.69	0.186	3.71	0.5694
8 x10^{-1}	1.01	74.24	0.74	0.208	3.56	0.5514
12 x10^{-1}	1.07	73.66	0.74	0.312	2.37	0.3747
16 x10^{-1}	1.17	71.36	0.72	0.448	1.61	0.2068
20 x10^{-1}	1.23	70.11	0.70	0.600	1.16	0.0644

Corrosion rate $\mathbf{C_R}$ decreases with increase in Concentration, Surface Coverage **θ**, and inhibition Efficiency.

Table 4.12: Regression Square (R^2) values obtained for Langmuir, Temkin, and Frumkim Adsorption Isotherms.

Compound	R^2 Langmuir	R^2 Temkin	R^2 Frumkin
SALAN	0.99862	0.62081	0.42973
CeSALAN	0.99573	0.73288	0.49252

Langmuir isotherm model with regression square value upto 0.99 is the model that perfectly fits the adsorption process.

Table 4.13: Influence of Concentration on the Inhibition Efficiency of SALAN and CeSALAN during Mild Steel Corrosion in 1M HCl after 24-hour immersion.

System (mmol/dm^3)	C_R SALAN,	SALAN, IE%	C_R CeSALAN	CeSALAN, IE%
$1x10^{-1}$	2.07	48.01	2.28	42.71
$2\ x10^{-1}$	1.54	61.40	2.05	51.51
$4\ x10^{-1}$	1.36	65.76	1.46	63.29
$6\ x10^{-1}$	1.29	68.78	1.26	68.64
$8\ x10^{-1}$	1.20	73.76	1.01	74.24
$12\ x10^{-1}$	1.22	72.78	1.07	73.66
$16\ x10^{-1}$	1.23	70.24	1.17	71.36
$20\ x10^{-1}$	1.23	69.11	1.23	70.11

IE is observed to increase with increase in concentration, and optimuim IE was recorded for both compounds at 0.8 mmol/$dm^{3,}$ after which reduction in IE occurred.

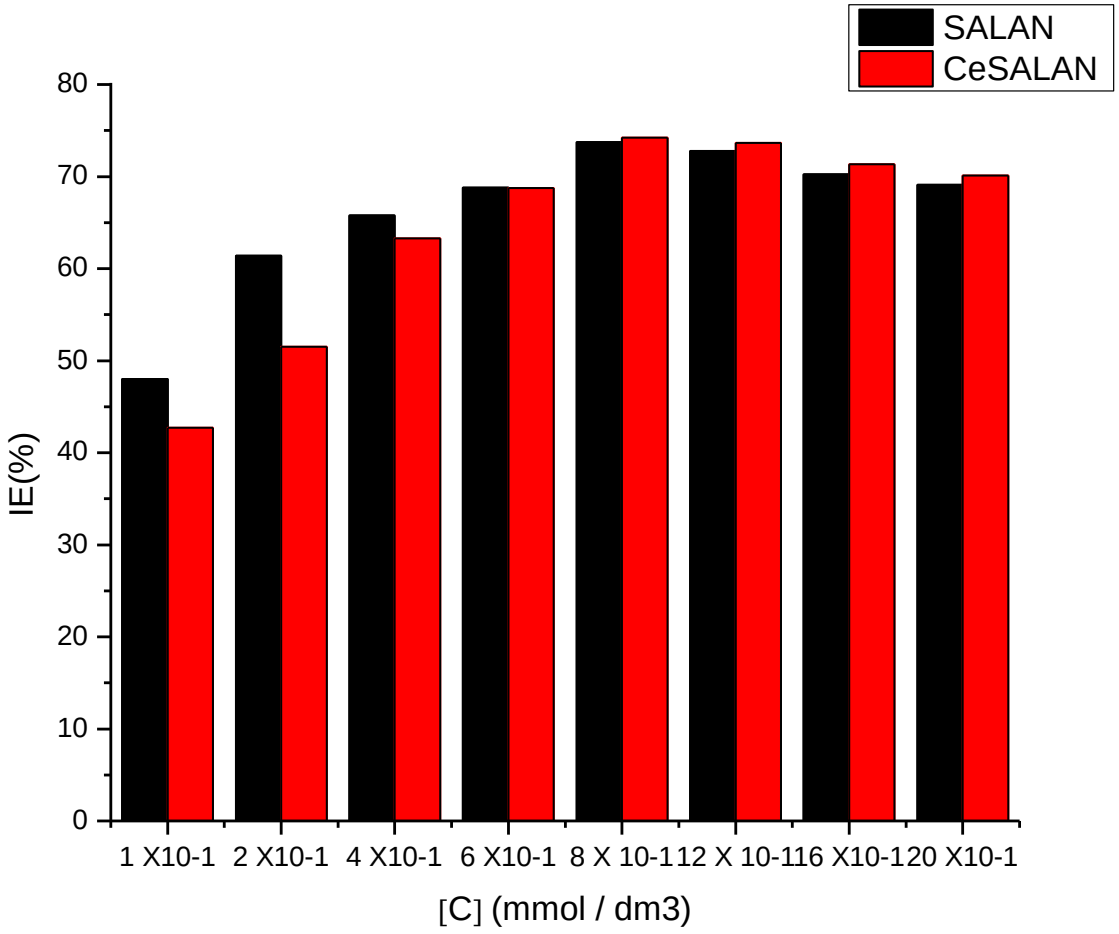

Figure 4.11: Influence of Concentration on the Inhibition Efficiency of SALAN and CeSALAN during Mild Steel Corrosion in 1M HCl after 24-hour immersion

The bar graph illustrates the inhibition efficiency (IE%) as a function of concentration (C) in (mmol/dm^3) for the two compounds: SALAN (black bars) and CeSALAN (red bars). CeSALAN, has enhanced inhibition efficiency compared to the parent Schiff base SALAN from concentrations of 6x10^{-1} to 20 x10^{-1} mmol/dm^3. The optimum efficiency of 73.76 % was recorded for SALAN and 74.24% for CeSALAN at concentration of 8x10^{-1} mmol/ dm^3.

4.1.3.2: Effect of temperature on the performance of the inhibitors

Table 4.14: Effect of Temperature on the inhibition efficiency of SALAN and CeSALAN at optimum concentration

T (K)	I/T (K)	C_R BLANK	Log CR BLANK	C_R SALAN	Log C_R SALAN	IE SALAN	C_R CeSALAN	log C_R CeSALAN	IE CeSALAN
303	0.0033	3.981	0.600	1.044	0.019	73.76	1.010	0.004	74.64
313	0.0032	13.419	1.127	6.093	0.785	54.60	4.419	0.645	67.67
323	0.0031	13.437	1.128	6.256	0.796	53.40	5.841	0.766	56.53
333	0.0030	22.793	1.358	10.870	1.036	52.30	10.674	1.028	53.17
343	0.0029	54.270	1.735	28.30	1.452	47.85	26.893	1.430	50.45

Table 4.14 show relationship between inverse of temperature (I/T) with log C_R of BLANK (uninhibited system), and systems inhibited with SALAN and CeSALAN. C_R decreases on addition of the inhibitors. However, IE decreased with rising temperature.

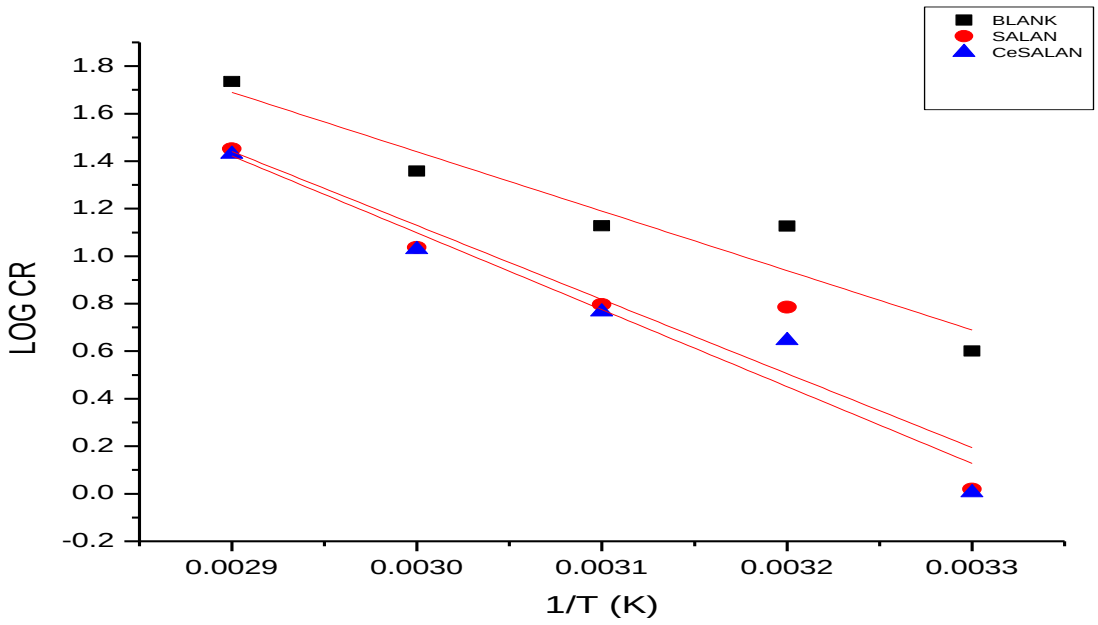

Figure 4.12: Arrhenius plots for Mild Steel in 1 M HCl solution free and systems inhibited by 0.8 mmol/dm^3 of the Inhibitors

Table 4.14 shows data for log C_R vs 1/T for the inhibitor- compounds. Figure 4.12 above show the Arhenius plots for the compounds. Activation energy (E_a) for corrosion of mild steel in the absence and presence of the inhibitors, SALAN and CeSALAN were calculated from slope of Arhenius equation

$$Log\ C_R = \frac{-Ea}{2.303RT + A} \qquad (4.1)$$

Plot of log CR vs 1/T above gives a slope of –Ea/ 2.303 R, from which Ea is calculated.

Table 4.15: Corrosion Data of BLANK, SALAN and CeSALAN for plot of log CR/T vs 1/T

T(K)	1/T(K)	C_R BLANK (mdd)	C_R/T BLANK	log C_R/T BLANK	C_R SALAN (mdd)	C_R/T SALAN	log C_R/T SALAN	C_R CeSALAN (mdd)	C_R/T CeSALAN	log C_R/T CeSALAN
303	0.0033	3.981	0.0131	-1.8827	1.044	0.0034	-2.4685	1.010	0.0033	-2.4815
313	0.0032	13.419	0.0429	-1.3675	6.093	0.0195	-1.7010	4.419	0.0141	-1.8508
323	0.0031	13.437	0.0416	-1.3809	6.256	0.0194	-1.7122	5.841	0.0181	-1.7423
333	0.0030	22.793	0.0684	-1.1649	10.870	0.0326	-1.4868	10.674	0.0321	-1.4935
343	0.0029	54.270	0.1582	-0.8008	28.30	0.0825	-1.0835	26.893	0.0784	-1.1057

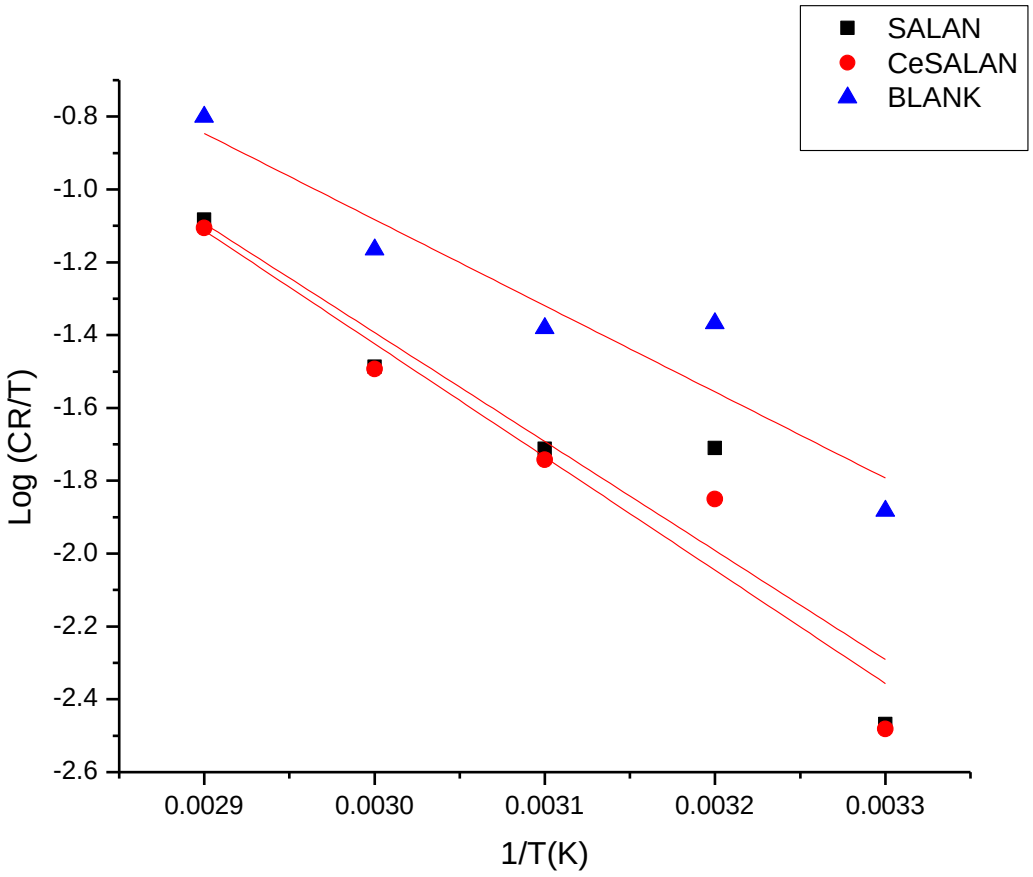

Figure 4.13: Plot of log (C_R/T) Vs 1/ T for BLANK, SALAN, and CeSALAN

Table 4.15 show the data for log (CR/T) vs 1/T for BLANK, SALAN and CeSALAN. Figure 4.13 above shows a plot of log (CR/T) vs 1/T, derived from the relationship.

$Log\ CR/T\ = [(logR/Nh) + (\Delta S*/2.303\ R) - \Delta H*/2.303\ RT]$ equation (1.7), page 32

Where h is plank's constant, 6.626 x 10-^{34}, N is equal to Avagadro's number, 6.02 x 10 $^{23.}$, S* is the entropy of activation, R is gas constant, T is temperature in Kelvin. The slope of the linear plot, –H* / 2.303R permits to derive the enthalpy of activation (H*), and an intercept of (log R/Nh) + (ΔS*/2.303 R) is used to calculate the entropy of the activation process, S*.

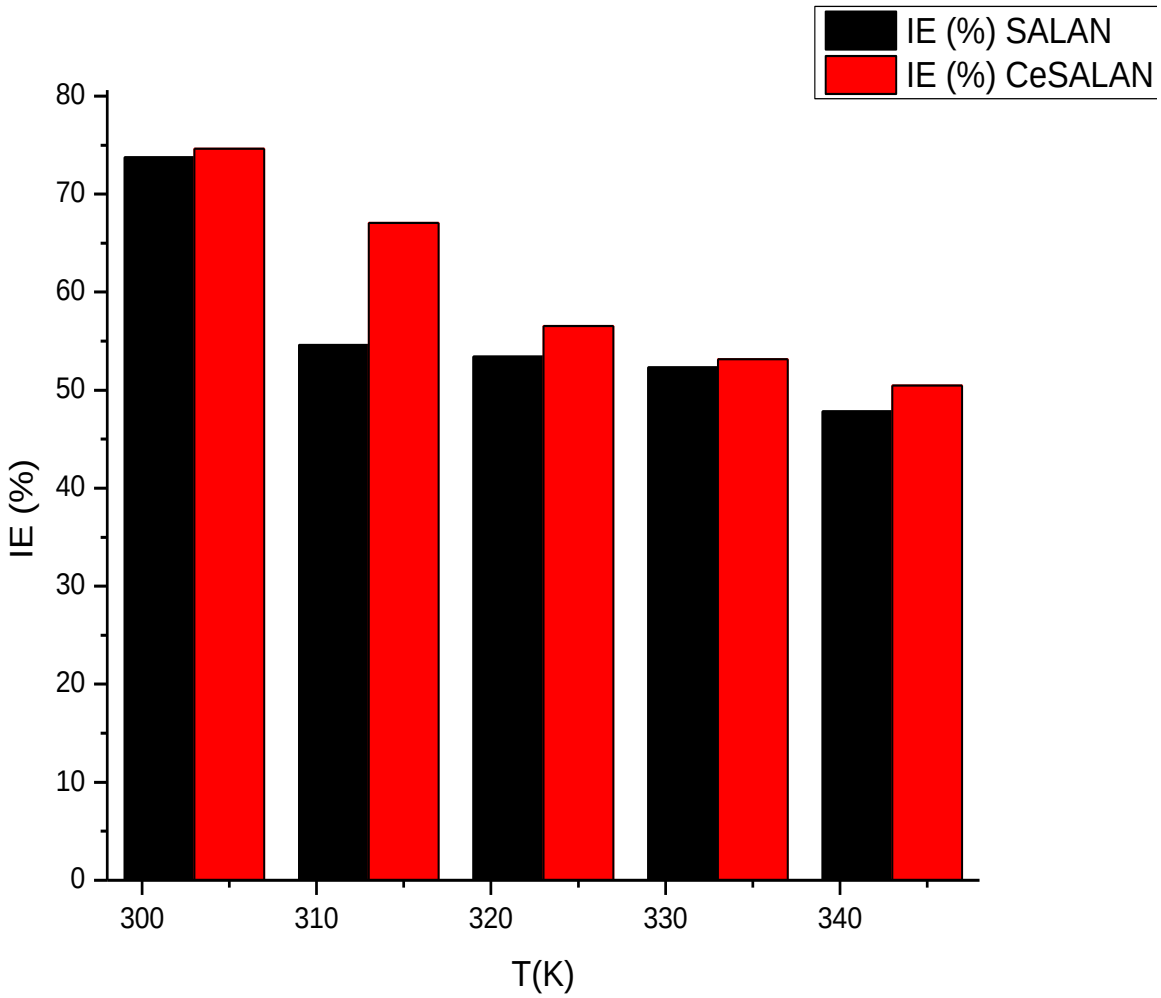

Figure 4.14: Effect of Temperature on the Inhibition efficiency of the compounds at the optimum concentration

Inhibition efficiency decreases with increase in temperature, which is typical for physisorption process of adsorption. However, CeSALAN (red bar) had an enhanced I.E over the parent Schiff base SALAN (black bar).

.

Table 4.16: Values for E_a, ΔG_{ads}, ΔH, and ΔS for BLANK, SALAN and CeSALAN

System	Activation energy (Ea) kJ/Mol	ΔG_{ads}	Enthalpy (ΔH) kJ/ Mol	Entropy (ΔS) kJ/Mol
BLANK	20.31	-	45.79	-82.38
SALAN	25.74	-17.15	57.22	-52.32
CeSALAN	26.79	-11.98	59.55	-46.26

Increase in Ea, Gads, ΔH, and ΔS is observed in the inhibited systems compared to the blank.

Table 4.17: Variation of Inhibition Efficiency with Immersion Time of SALAN and CeSALAN

WEEK	IE (%)	
	SALAN	CeSALAN
1	40.66	45.78
2	27.20	29.85
3	25.41	26.60
4	24.42	25.63

IE of SALAN and CeSALAN is observed to decrease over time, which is suggestive of Physical adsorption process of inhibitor molecules on mild- steel surface.

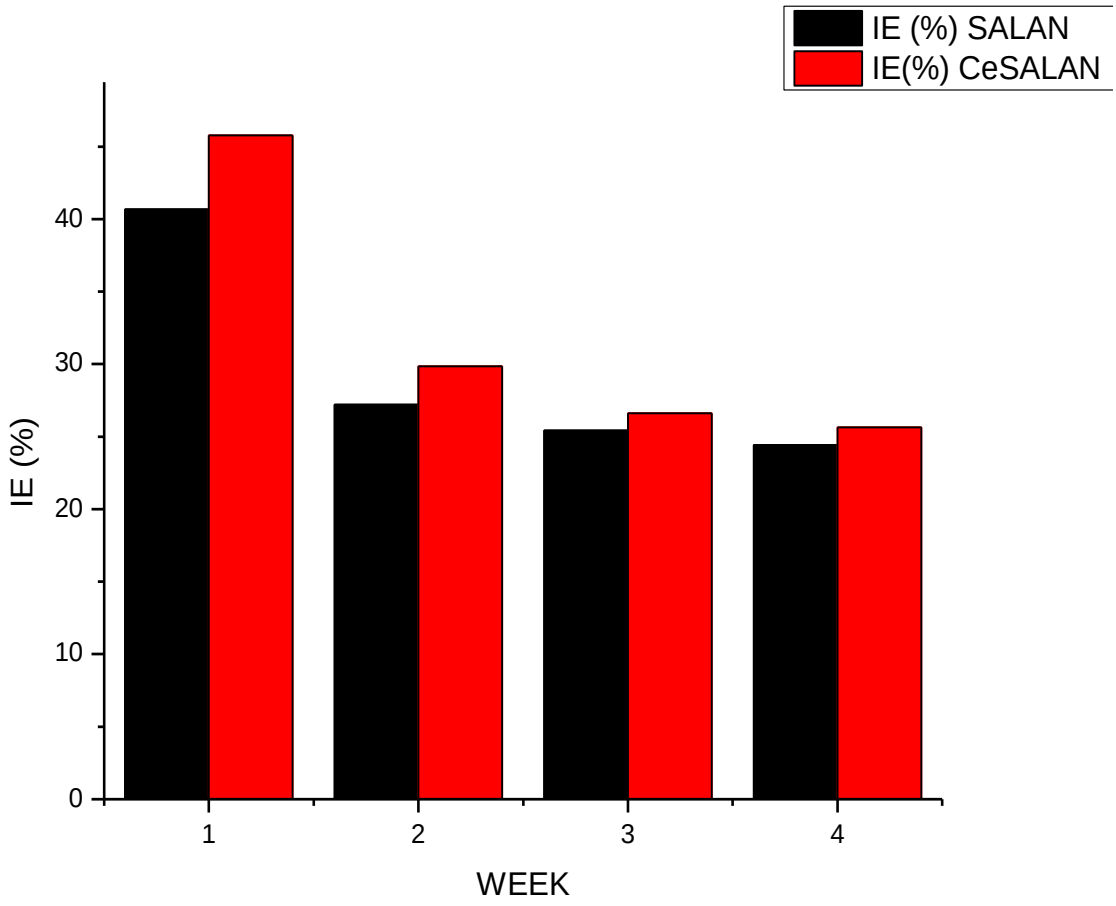

Figure 4.15: The Variation of Inhibition Efficiency of SALAN and CeSALAN with Immersion time

Inhibition efficiency (IE) decreases with time suggesting that the inhibitor was physically adsorbed on the mild steel surface. IE of CeSALAN (red bars) was consistently higher than that of SALAN (black bars) over time.

4.1.4 Surface Studies Using AFM

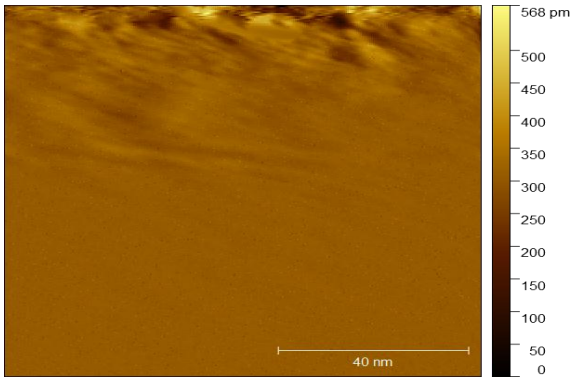

Figure 4.16 (a) BLANK 2D AFM (1M HCl)

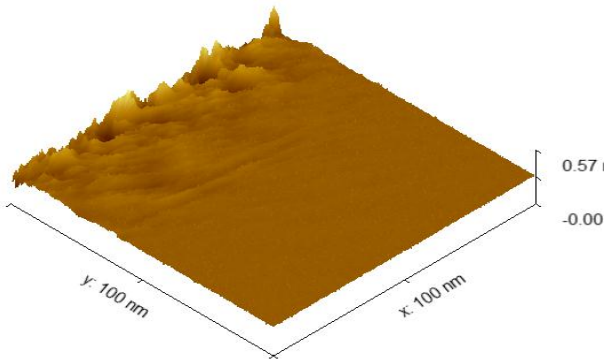

Figure 4.16 (b) BLANK 3D AF(1M HCl)

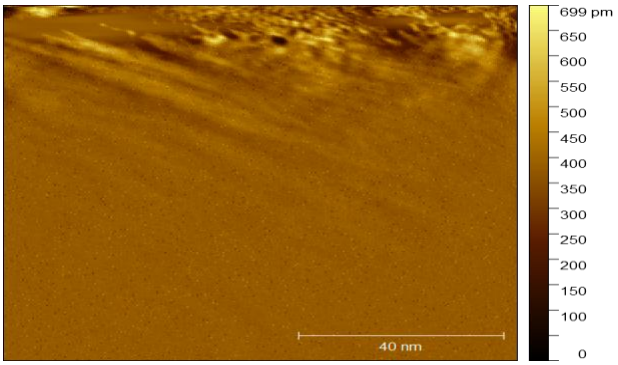

Figure 4.16 (c) SALAN 2D AFM

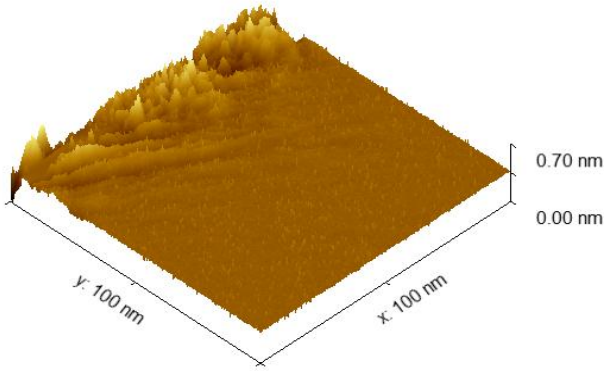

Figure 4.16 (d) SALAN 3D AFM

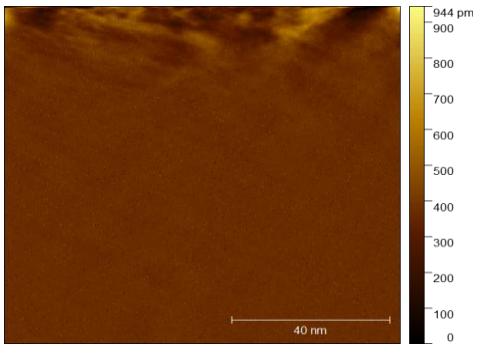

Figure 4.16 (e) CeSALAN 2D AFM

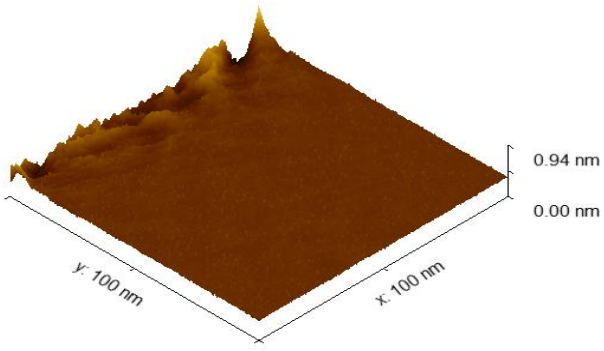

Figure 4.16 (f) CeSALAN 3D AFM

Table 4.18: AFM Parameter Data for Compounds

AFM PARAMETERS	COMPOUNDS		
	BLANK	**SALAN**	**CeSALAN**
Sq value (pm)	44.80	35.07	33.04
Sp value (pm)	574.85	491.73	487.85
Sv value (pm)	399.44	376.81	375.95

Sq value describes overall surface roughness, Sp value indicates defects on a material, Sv value describes the extent of corrosion on a material. These values follow the order, BLANK > SALAN > CeSALAN. Hence, this observation is suggestive that the inhibitors had a protective effect on the mildsteel.

4.1.5 Electrochemical Studies

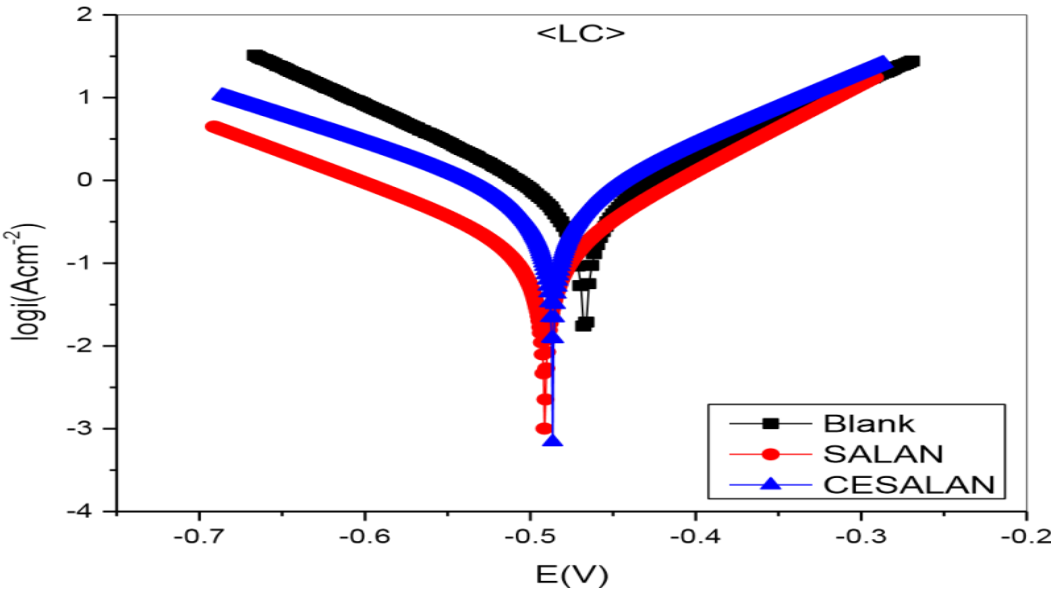

Figure 4.17: Polarization curves of Mild Steel in the absence and in the presence of 0.8 mmol/dm^3 each of SALAN and CeSALAN at 30 °C.

Table 4.19: PDP Parameters of Mild Steel immersed in the presence and absence of 0.8 mmol/dm^3 of the inhibitors in 1M HCl

Environment	Ecorr (mV)	Ba (mV/dec)	Bc (mV/dec)	Icorr (uA/cm^2)	IEPDP (%)
Blank	-467.063	116.0 mV	112.3 mV	543.57	-
SALAN	-485.664	109.5 mV	134.9 mV	207.63	61.80
CeSALAN	-491.225	96.6 mV	135.6 mV	149.96	72.41

Corrosion potential (Ecorr), and corrosion current (Icorr) due to blank is reduced in the presence of the inhibitor- compounds. CeSALAN recorded a higher IE compared to SALAN.

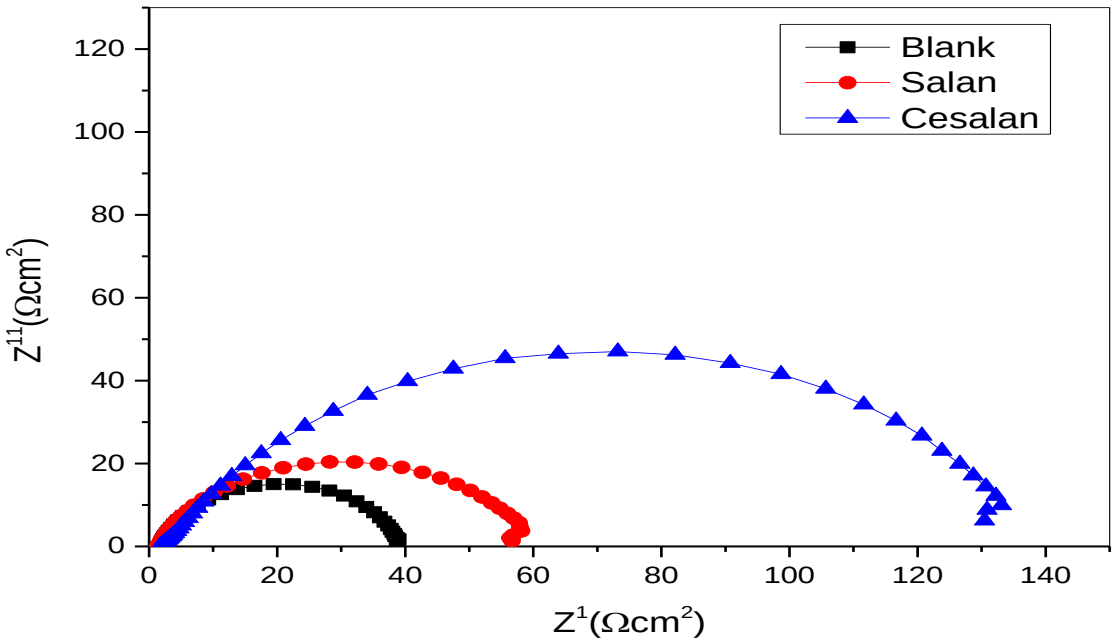

Figure 4.18: Nyquist Curves of Mild Steel in the absence and presence of 0.8mmol/dm^3 Concentrations of SALAN and CeSALAN at 30 °C.

Semi-circle represents resistance to charge transfer (Rct), CeSALAN, having the largest semi-circle diameter suggests its highest corrosion resistance compared to SALAN and Blank. This supports the result from the weight- loss experiment.

Table 4.20: EIS parameters and Inhibition Efficiency at 30 °C of Mild steel in the absence and in the presence of 0.8 mmol/dm^3 concentrations of the inhibitors

Environment	R_S (Ohm)	Rct (Ohm)	Cdl, F/cm^2	IE%$_{EIS}$
Blank	1.6847	37.67	457.95	-
SALAN	1.6901	85.29	439.43	55.83
CeSALAN	2.7894	107.62	355.24	65.03

EIS parameter shows a higher IE for CeSALAN due to complexation. There is decrease in values for double layer capacitance(Cdl), and increase in charge-transfer resistance (Rct) compared to values for blank due to the presence of the inhibitors.

Table 4.21: Inhibition efficiency values obtained for the various Analytical Technique

	Analytical Technique / IE (%)		
Compound	**Weight loss**	**PDP**	**EIS**
SALAN	73.76	61.80	55.83
CeSALAN	74.24	72.41	65.03

The inhibition efficiency obtained for the different analysis techniques ie (Weight loss, EIS, and PDP) for the compounds follow the same order, with the metal complex CeSALAN recording a higher IE compared to the Schiff base SALAN.

4.2 Discussions on SALAN and CeSALAN

4.2.1 Physical Measurements

4.2.1.1 Colour

The interaction of electron cloud of the ligand with degenerate d-orbitals of metal ions split them into different energy levels, corresponding to the geometry of the complexes. Exposure of electromagnetic radiation to such complexes leads to characteristic absorption of energy and electronic transition from lower to higher energy level takes place. If the complex absorbs electromagnetic radiation in the visible region of the spectrum, then it emits energy complementary to absorbed radiation and produces colour of the chemicals. Change in the colour of the complexes is due to the different range of electronic absorption, either by π bonding or nonbonding or by free electrons. Generally, the chromophores in presence of auxochromes show electronic absorption in UV-visible region and provide the characteristic colour of the substances. Conjugation further enhances the intensity of colour. The free electrons of metals in their complexes exhibit electronic absorption and furnish various colours of the metal complexes. The colours of the compounds under study is shown in table 4.1. SALAN (bright yellow), and CeSALAN (dull yellow).

4.2.1.2 pH and Melting point Measurement

The complexation in coordination chemistry is often accompanied by deprotonation of ligand which is the true cause of the variation of pH in the solution phase. In general case, there is drop down in pH values of the solution in moving from Schiff base SALAN to the metal complex CeSALAN. The variation in pH values is committed to being the indication of the complex formation during the reaction. The pH values of Schiff base and the metal complex are reported in the Table 4.1. Moreover, the Schiff base have higher pH value compared to the metal complex.

4.2.1.3 Solubility

The solubility and melting points are the characteristic physical properties of the chemicals. The solubility of the Schiff base and metal complex was examined in water and various organic solvents. Their solubility data are reported in the Table 4.2. The observation of solubility data revealed that the Schiff base and metal complex were insoluble in water but soluble in organic solvents. The Schiff base is soluble in methanol, DMSO, and DMF whereas metal complex is soluble in DMSO and DMF.

4.2.1.4 Molar Conductivity and Magnetic Susceptibility Measurement

The conductivity values help to ascertain the ionic (electrolytic) or nonionic (non-electrolytic) nature of the synthesized Schiff bases and their complexes. The magnetic susceptibility measures the extent at which a material can be attracted or repelled by an externally applied magnetic field. The compounds showed high conductivity, values >0.1 mS/ cm, suggestive of electrolytic (ionic) nature of the Ce(III) Schiff base complexes, and the presence of nitrate ions in the outer coordination sphere of the complexes. The low positive values for magnetic susceptibility recorded for the complexes shows their paramagnetic nature. Table 4.3 compares the Molar conductivities of SALAN and CeSALAN. The Schiff base, SALAN showed low conductivity, values <0.1 mS/cm which shows nonelectrolytic nature of the Schiff base and absence of the nitrate ions in the compound. Magnetic susceptibility value of 006 recordered for the cerium(III) complex, shows paramagnetic nature of the Schiff base metal complex. This implies that the metal complex can be magnetized by an externally applied magnetic field.

4.2.2 Spectral Studies

4.2.2.1 Uv-Vis spectral data of SALAN and CeSALAN

Figures 4.1. and 4.2 display the UV-Visible spectra of SALAN (Schiff base) and CeSALAN respectively in DMSO solvent at room temperature. For SALAN, the maximum absorbance was observed at 215 nm, corresponding to an $\pi \rightarrow \pi*$ transition. This transition arises from the excitation of bonding electrons on the nitrogen atom of the azomethine group to the anti-bonding $\pi*$ orbital. Upon coordination of the nitrogen atom to the metal ion, as seen in the CeSALAN Schiff base complex, a red shift occurs, moving the absorbance to a longer wavelength (lower energy) of 326 nm.

4.2.2.2 Analysis of SALAN and CeSALAN FTIR Spectral

Figures 4.3 and 4.4 show the FTIR F spectral of SALAN and CeSALAN. The infra-red spectra of the Schiff base SALAN showed the characteristics azomethine vibration v(CH=N) at 1689 cm^{-1} which was shifted to a lower frequency of 1632 cm^{-1}, (hypsochromic or blue shift) in the spectrum of the metal complex CeSALAN due to complexation through the azomethine nitrogen. The complexation through the azomethine nitrogen is supported by the appearance of a new frequency at 749 cm^{-1} which may be attributed to v(M-N) due to the newly formed metal–ligand bond. The infrared spectrum of the SALAN Schiff base showed weak broadband in the region 3479 cm^{-1} due to the presence of the phenolic OH group, attributed to the vibration of the intramolecular hydrogen-bonded -OH group. This v(OH) vibration is absent in the spectrum of the metal complex

which shows coordination through the phenolic-OH group of the salicylaldehyde moiety after deprotonation

The strong intensity band observed at 1273 cm^{-1} in the spectrum of the SALAN ligand is due to v(C-O) vibration which was observed at a higher frequency of 1285 cm^{-1} in the spectrum of the complex, confirming complexation through the phenolic oxygen. This shift may be due to the coordination of aldehyde moiety after deprotonation.

A new band assigned to v(M-O) occurred at 685 cm^{-1} which confirms complexation through the oxygen atom of the OH group.

Vibration due to the presence of coordinated water molecule, v(H_2O) is observed at a frequency of 3063 cm^{-1} in the spectrum of the complex. This is confirmed by the presence of a new band at 816 cm^{-1} assigned to vibration due to rocking water. Vibration due to presence of nitrogen v(NO_3) in the spectrum complex is observed at 1446 cm^{-1}.

4.2.2.3 Analysis of 1H-NMR Spectral of SALAN

The 1H-NMR spectra of the Schiff base ligands provide valuable insights into their bonding modes and confirm the presence of specific functional groups. The spectra were recorded in DMSO at room temperature using TMS as an internal standard. The chemical shifts corresponding to the protons in the Schiff base are summarized in Table 4.4, with spectral diagram presented in Figure 4.5

The 1H-NMR spectra of the Schiff base SALAN—exhibited a singlet signal at δ8.96 ppm, attributed to the azomethine (–CH=N–) proton (Enans et al., 2016). Additionally, the hydroxyl proton (−OH) of the aldehyde moiety appeared as a distinct singlet at δ13.11 ppm in the downfield region.

Multiplets observed between δ7.68 and δ7.32 ppm were assigned to the aromatic protons of the Schiff base. These characteristic signals strongly support the successful synthesis and structural integrity of the Schiff base.

4.2.2.4 Analysis of 13-C NMR of SALAN

The 13-C spectrum of SALAN shows signals due to aromatic carbon atoms of the aldehyde moiety at the following frequencies: 117.08, 119.60, 119.90, 133.05, 133.74. 160.79. The signals due to aromatic carbon atoms of the amine moiety occur at the following frequencies: 121.83, 127.41, 129,92, and 148.58. The signal due to carbon atom of the azomithine group occurred at 163.99. This confirms the successful synthesis of the Schiff base (Table 4.5 and Figure 4.7).

4.2.2.5 Discussion on EDXRF of CeSALAN

Figure 4.9 shows EDXRF spectra of CeSALAN, which identifies the percentage compositions of Cerium found in CeSALAN complex as 80.13%, which occurred at a peak of 59947 cps/ MA and characteristics energy for detection of pure cerium in compounds between 6.60- 4.80 keV (Rao et.al., 2022).

4.2.3 Inhibitive Action of SALAN and CeSALAN.

4.2.3.1 Gravimetric Results

4.2.3.2 Analysis of the Results of the Mass-Loss Method

The corrosion rate of mild steel in 1 M HCl solution was studied using the weight loss method, both in the absence and presence of Schiff base and metal complex inhibitors at 30°C. The tt

Table 4.6 to 4.11 show the gravimetric data in presence and absence of SALAN and CeSALAN. The tables present the variation in corrosion rate in (mdd) and inhibition efficiency (expressed as a percentage) with different concentrations of the inhibitors (in mmol/ dm^3). The data demonstrate that the corrosion rate significantly decreased in the presence of the inhibitors. Furthermore, the corrosion rate shows a strong dependency on the concentration of the inhibitors, decreasing progressively with increasing inhibitor concentration.

The reduction in corrosion rate and the corresponding increase in inhibition efficiency are attributed to the adsorption of the inhibitors onto the metal surface. Increased concentration of the inhibitors enhances surface coverage, which in turn increases the number of active sites protected on the metal surface. This phenomenon leads to improved inhibition efficiency. Organic inhibitors with heteroatoms and multiple bonds in their molecular structure are particularly effective in industrial applications due to their strong adsorption capability (Onu et al., 2024; Olasunkanmi et al.,2015)

Figure 4.11 provides a comparative analysis of the inhibition efficiency of the Schiff base and the metal complex after 24hr immersion time. An enhanced inhibition efficiency of CeSALAN over SALAN is recorded at higher concentrations between concentrations of 0.6 to 2.0 mmol/dm^3. Decrease in inhibition efficiency at highest concentration (2.0 mmol/dm3) of both compounds is due to desorption of the inhibition molecules from the surface of the mild steel. Both compounds exhibited good inhibitory performance with optimum IE of 73.76 and 74.24 % for SALAN and CeSALAN respectively.

4.2.3.3 Analysis of Variation of IE with Immersion Time

The variation of inhibition efficiency with immersion time in 1M HCl is shown in Table 4.17 and Figure 4.15. It is found that that the protection factor decreased with time suggesting that the inhibitor was physically adsorbed on the mild steel surface. However, it's observed that the inhibition efficiency of CeSALAN (red bars) was consistently higher than that of SALAN (black bars) over time which is consistent with fact that complexation enhances inhibition efficiency.

4.2.3.4 Analysis of the effect of Temperature on the Performance of the Inhibitors

The effect of temperature on the corrosion of C-steel in free and inhibited 1 M HCl solutions was studied using gravimetric approach in the range of 30–70◦C. The acid solutions were inhibited by addition of 0.8 mmol/dm^3 of the inhibitors. The corrosion parameters calculated from the gravimetric data are given in Table 4.14 and 4.15. Inspection of the listed tables, reveals that the corrosion rate of steel in both free and inhibited acid media increased as the temperature was increased. However, the inhibition efficiency of the additives decreases remarkably with increasing temperature as shown in Figure 4.14. This result supports the idea that the adsorption of inhibitors onto the steel surface is physical in nature. Thus, as the temperature increases, the number of adsorbed molecules decreases, leading to a decrease in the inhibition efficiency. The activation energies of the corrosion process in free and inhibited acid were calculated using the Arrhenius equation.

$$K = A \exp\frac{E_a}{RT}$$ from equation (1.4) page 32

where Ea is the activation energy, A is the frequency factor, T is the absolute temperature, R is the gas constant, and K is the rate constant, which is directly proportional to the corrosion rate. Plotting log k versus 1/T gives a straight line, as revealed by Fig. 4.12. Data of log C_R vs 1/T is given in Table 4.14. The values of activation energy calculated using the lines of Fig. 4.12 are : 20.79 kJ/mol for free system, and 25.74 and 26.79 kJ/mol for system inhibited with SALAN and CeSALAN, respectively. The obtained results suggest that additives inhibit the corrosion reaction by increasing its activation energy. This could be done by adsorption onto the steel surface, making a barrier to mass and charge transfer.

4.2.3.5 Analysis of Thermodynamics Parameters, ΔH, and Δ S

Table 4.15 show the data for log (CR/T) vs 1/T. Figure 4.13 shows a plot of log (C_R/T) vs 1/T , derived from the relationship log CR/ T = [(logR/Nh) + (ΔS*/2.303 R) – Δ H*/2.303 RT]. Where h is plank's constant, 6.626 x 10-^{34}, N is equal to Avagadro's number, 6.02 x 10$^{\cdot}$, S* is the entropy

of activation, R is gas constant, T is temperature in Kelvin. The slope of the linear plot, –H* / 2.303R permits to derive the enthalpy of activation (H*), and an intercept of (log R/Nh) + (ΔS*/2.303 R) is used to calculate the entropy of the activation process, S*. Δ H value obtained for SALAN is 57.22 kJ/ Mol, while CeSALAN ΔH value is 59.54 kJ/ Mol. H* value recorded for the free system (blank) is 45 kJ/ Mol. The positive enthalpies obtained shows the endothermic process of the dissolution process. Entropy values obtained for free system (-82.38 kJ/Mol), system inhibited with SALAN (-52.31 kJ/Mol), system inhibited with CeSALAN (-46.26 kJ/Mol). Increased negative entropy values obtained shows increased orderliness moving from blank system to inhibited systems.

4.2.4 Adsorption Isotherm

It has been assumed that organic inhibitor molecules establish their inhibition action via the adsorption of the inhibitor onto the metal surface. The adsorption processes of inhibitors are influenced by the chemical structures of organic compounds, the nature and surface charge of metal, the distribution of charge in molecule and the type of aggressive media. In general, two modes of adsorption can be considered. The proceeding of physical adsorption requires the presence of electrically charged metal surface and charged species in the bulk of the solution. Chemisorption process involves charge sharing or charge transfer from the inhibitor molecules to the metal surface. The presence, with a transition metal, having vacant, low-energy electron orbital, of an inhibitor molecule having relatively loosely bound electrons or heteroatoms with lone-pair electrons facilitates this adsorption Assuming the corrosion inhibition was caused by the adsorption of SALAN and its metal derivative, and the values of surface coverage (θ) for different concentrations of inhibitors in 1 M HCl were evaluated from weight loss measurements from Equation (1), page 32.

Adsorption isotherms are very important in determining the mechanism of organic electrochemical reactions. The most frequently used adsorption isotherms are Langmuir, Temkin and Frumkin. The listed adsorption isotherms were tested for the description of adsorption behaviour of studied compounds, and it is found that adsorption of SALAN and CeSALAN on mild steel surface in HCl solution obeys the Langmuir adsorption isotherm given by the following equations:

$$\frac{C_{inh}}{\theta} = \frac{1}{b} + C_{inh} \qquad \text{Eqn (1.5) page 32}$$

$$b = \frac{1}{55.5} exp\left(-\frac{\Delta G_{ads}}{RT}\right) \qquad \text{Eqn (1.6) page 32}$$

C_{inh} is the inhibitor concentration, θ is the fraction of the surface covered, b is the adsorption coefficient and G_{ads} is the standard free energy of adsorption. Fig. 4.10 shows the dependence of the fraction of the surface covered C/θ as a function of the concentration (C) of inhibitors. Data showing the calculated parameters for Lagmuir, Temkin, and Frumkin' adsorption isotherm are given in Tables 4.6, 4.7 and 4.8 for SALAN, Tables 4.9, 4.10 and 4.11 for CeSALAN respectively. It should be explained that other adsorption isotherms (Frumkin and Temkin) were checked and Langmuir adsorption isotherm is the best approximate between them. This is why the assumption is true for Langmuir adsorption isotherm. The regression square values obtained for the various listed isotherms are recorded in table 4.12. The obtained plots of the inhibitors are linear with correlation coefficient higher than 0.99. The intercept permits the calculation of the equilibrium constant b which are 20.61 and 10.98 M^{-1} for, SALAN and CeSALAN, respectively. The values of b which indicate the binding power of the inhibitor to the steel surface can lead to calculate the adsorption energy. Values of G_{ads} = −17.15, and, −11.984 kJ mol^{-1}. The negative value of G_{ad}s means that the adsorption of the Schiff base SALAN and its metal complex CeSALAN on mild steel surface is a spontaneous process, and furthermore, the negative values of G_{ads} also show the strong interaction of the inhibitor molecule onto the mild steel surface. Generally, values of Gads around −20 kJ mol^{-1} or lower are consistent with the electrostatic interaction between the charged molecules and the charged metal (physisorption). Those more negative than −40 kJ mol^{-1} involve charge sharing or transfer from the inhibitor molecules to the metal surface to form a coordinate type of bond (chemisorption) (Oguzie et al., 2011). For investigated inhibitors, one can see that the calculated G_{ads} values, were below −20 kJ mol^{-1}, indicating, that the adsorption mechanism of the both inhibitors on mild steel in 1 M HCl solution was typical of physisorption.

4.2.5 Surface Analysis using AFM

Table 4.18 shows AFM parameter data for the compounds under study. Figures (4.16 (a) – 4.16 (f)), show the 2D and 3D AFM diagrams of blank, the Schiff base SALAN, with the metal complex CeSALAN. Table (4.18) show data of the AFM values for Sq, Sp, and Sv for the compounds. The RMS roughness (Sq) values provide a quantitative value that describes the overall surface texture or roughness. A higher Sq indicates a rougher surface while a lower Sq suggests a smoother surface. Maximum peak height (Sp) refers to the height of the tallest peak in a given measurement area relative to the mean plane of the surface. Sp value provides insight into the presence of features such as spikes and protrusions. A high Sp value may indicate defects or irregularities that could compromise a material's performance which in turn signifies higher pits value (Sv), which also indicates the extent of corrosion. The order of the values of the Sq, Sp, and Sv of the blank,

the Schiff base, SALAN, and the metal complex, CeSALAN corrolates with the order of their inhibition efficiency by weight loss experimental technique.

4.2.6 Electrochemical Studies

4.2.6.1: Analysis of the results of Potentiodynamic Polarization Studies

PDP parameters, namely, corrosion potential (E_{corr}), anodic and cathodicTafel slopes (b_a and b_c), corrosion current (i_{corr}), and polarization resistance (Rp) obtained by extrapolation of the polarization curves are grouped in Table 4.19. The inhibition percentage calculated from I_{corr} and R_p are given by equations 4.6 – 4.7

$$E\text{Icorr} = (I\text{corr}' - I\text{corr}) \times 100/I\text{corr}' \quad (4.2)$$

$$E_{Rp} = (Rp - Rp') \times 100/Rp \quad (4.3)$$

Where *Icorr'* and *Rp'*are respectively the corrosion current and the polarization resistance in the absence of inhibitor; *Icorr* and *Rp* are respectively the corrosion current and the polarization resistance in the presence of inhibitor.

A shift in the corrosion potential in presence of the additives compared to the blank corrosion potential can be observed. This shift being less than 85 mV/SCE, suggesting that this compound acts as a mixed-type inhibitor.

Figure 4.17 shows the polarization curves recorded at 30°C in 1 M HCl medium in the absence and in the presence of additives concentrations. The addition of the inhibitor decreases the anodic dissolution and delays the hydrogen ion reduction reaction. This addition shows the shape of almost parallel cathodicTafel branches. This indicates that the mechanism of hydrogen evolution, mainly due to charge transfer, is not modified upon addition of the inhibitor

4.2.6.2 Analysis of the results of EIS studies

Figure 4.18 presents the EIS (AC) impedance spectra of carbon steel in 1M HCl with the inhibitors, while Table 4.20 lists the impedance parameters, including charge transfer resistance and double-layer capacitance The double layer capacitance and EIS inhibitory efficiency were calculated using Equations 5 and 6 respectively (Yadav, et al.,2015; Khalissa et al., 2018):

$$C_{\text{dl}} = Q2^{\frac{1}{a2}}.Rct^{\left(\frac{1-a2}{a2}\right)} \quad (4.4)$$

Where C_{dl} = double layer capacitance. Q = Constant Phase Element (CPE), a^2 = CPE exponent,

Rct = Charge Transfer Resistance.

$$IE_{\mathrm{EIS}}(\%) = \left(\frac{R_{\mathrm{ct}} - R_{\mathrm{ct}}^{\circ}}{R_{\mathrm{ct}}}\right) \times 100 \quad (4.5)$$

Where: Rct° and Rct are the charge transfer resistances without and with inhibitor, respectively.

According to Table 4.20, the values of Rct increase, and those of Cdl decrease with the addition of the additives to the corrosive solution. This can be ascribed to the formation of a protective layer at the metal/acid interface, thus decreasing the direct contact between the mild steel and the aggressive solution (Mohamed et al., 2018; Ansari, et al.2019). In addition to this, the increasing value of the inhibition efficiency. (IE_{EIS}) in the presence of additives further supports the protection ability of the inhibitor, with a higher inhibition efficiency of 65.03 % recorded for CeSALAN against 55.83 % for SALAN.

4.1.2 Physical Measurements for SAL2AP and CeSAL2AP

Table 4.22: Physical properties, percentage yield, and elemental analysis of SAL2AP and CeSAL2AP

Compounds	Molecular Formula	Colour	pH	Yield	Melting point	Molecular Composition		
						C	H	N
SAL2AP	$C_{13}H_{11}NO_2$	WINE RED	6	85	91	74.34 (74.56)	4.93 (4.90)	7.27 (7.59)
CeSAL2AP	$C_{26}H_{20}CeN_2O_5$	DARK BROWN	5	59	168-170	54.02 (53.79)	3.60 (3.47)	4.95 (4.83)

Table 4.22 shows the variation in colour, pH, percentage yield, melting point, and molecular compositions of the synthesized Schiff base SAL2AP, and its cerium metal complex CeSAL2AP. The difference in colour, pH, and melting point shows successful synthesis of the compounds.

Table 4.23: Solubility Tests for Compounds

COMPOUNDS	SOLVENTS						
	DI H_2O	ETHANOL	METHANOL	ACETONE	CARBONTET	DMF	DMSO
SAL2AP	N/S	S	N/S	S	S/S	S	S
CeSAL2AP	N/S	N/S	N/S	N/S	N/S	S	S

N/S = not soluble, S = soluble, S/S = slightly soluble

Table 4.23 shows the solubility of the synthesized compounds in various organic solvents. Both compounds were observed to be soluble in DMF, and DMSO.

Table 4.24: Molar Conductivity and Magnetic Susceptibility of Compounds

Compound	Molecular formular	Molecular weight (g/mol)	Molar Conductivity (mS/cm) DMSO	DMF	Magnetic susceptibility
SAL2AP	$C_{13}H_{11}NO_2$	213.23	4.96 $X10^{-3}$	$6.47x10^{-3}$	-
CeSAL2AP	$C_{26}H_{20}CeN_2O_5$	580.57	1.21	1.04	009(paramagnetic)

The Schiff base SAL2AP shows a much lower conductivity values compared to CeSAL2AP. CeSAL2AP shows value for magnetic susceptibility for paramagnetic compounds, value > 1. SAL2AP recorded no magnetic susceptibility value.

4.1.3 Spectral Results for SAL2AP and CeSAL2AP

Spectroscopic measurements employed for this present study included: Uv-Visible spectroscopy, FTIR, 1H-NMR, 13-C NMR, and EDXRF. The characterization of the compounds by spectral methods is vital for the structural elucidation of the compounds under study as well as spatial orientation of the bonded atoms.

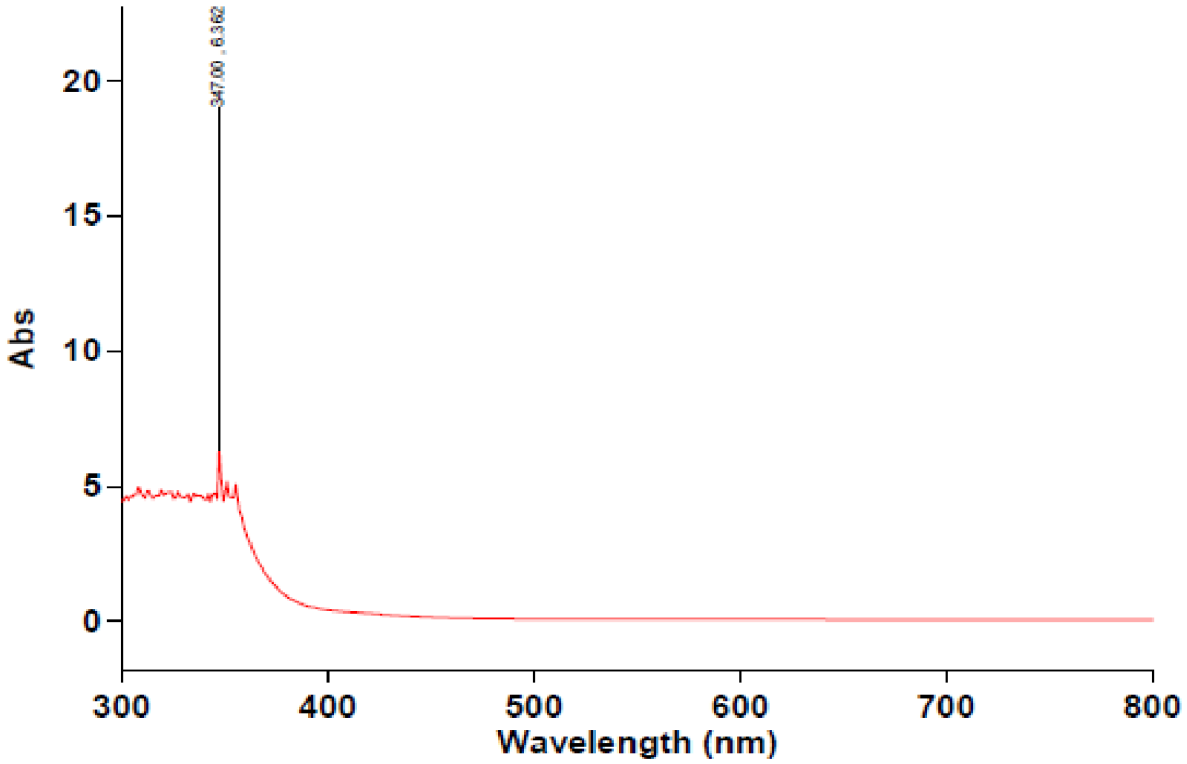

Figure 4.19: UV-Vis. Spectrum of SAL2AP

Maximum absorbance was observed at 347 nm, corresponding to an n→π∗ transition due to transition of non - bonding electrons of the nitrogen atom of the azomethine to the anti –bonding pi (π^*) orbital of the azomethine group.

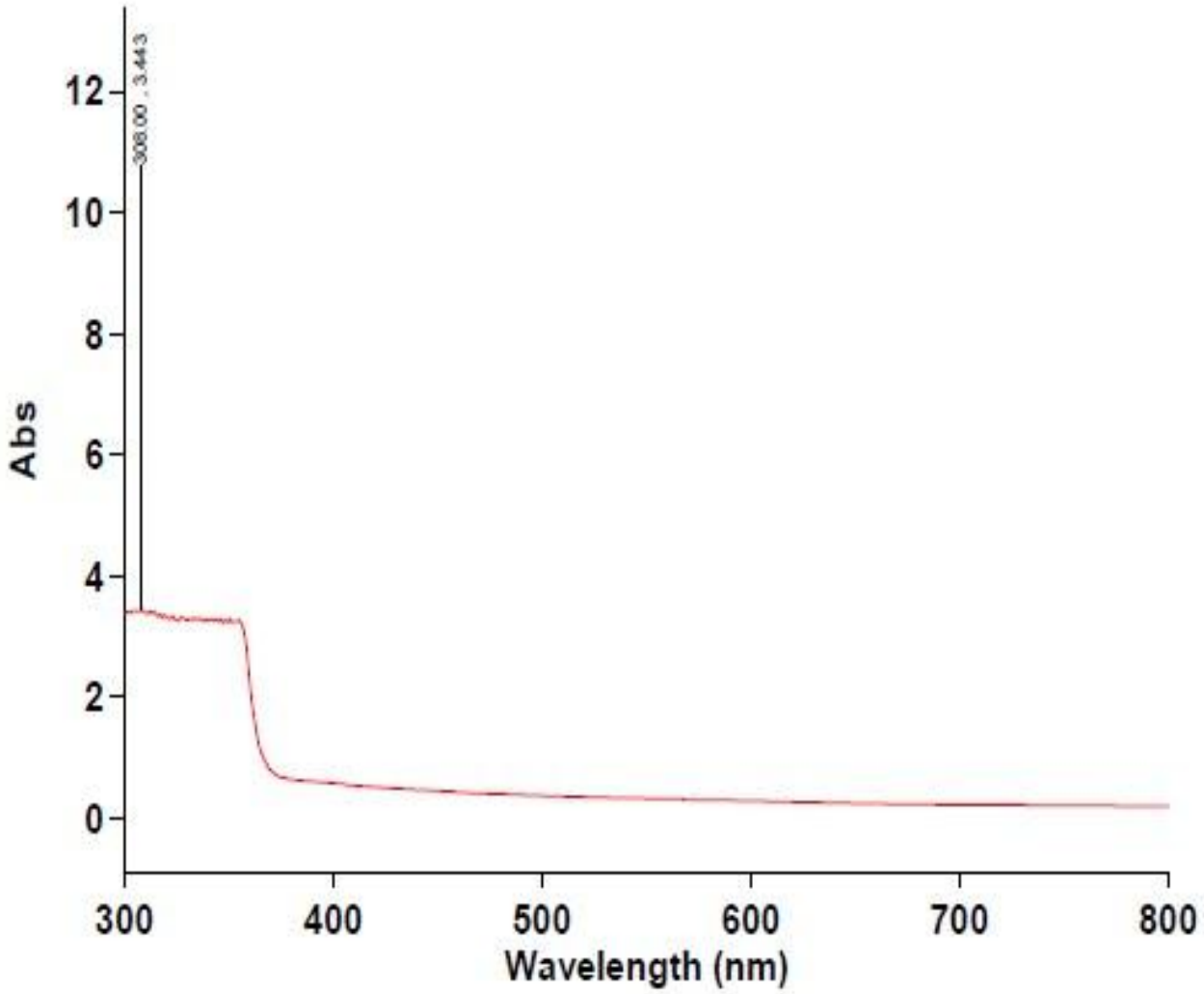

Figure. 4.20: UV- Vis Spectrum of CeSAL2AP

The Uv Spectra of CeSAL2AP shows maximum Absorbance at 308 nm, indicating complex formation.

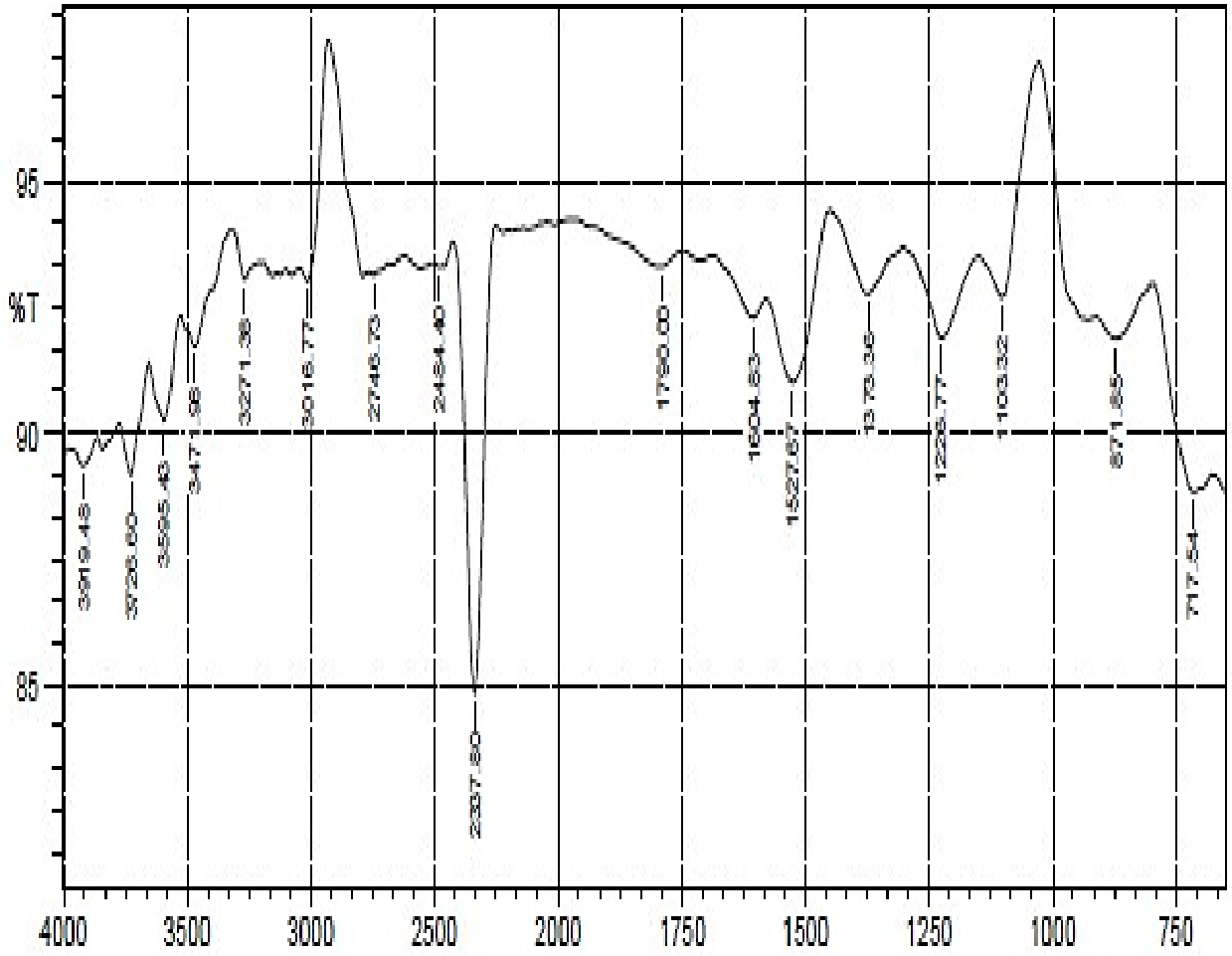

Figure 4.21: FTIR Spectrum of SAL2AP

Frequencies due to the following vibrations of the functional groups were recorded:

v(C-O) at 1226 cm^{-1} , v(OH) at 3471 cm^{-1} , and v(CH=N) at 1604 cm^{-1} .

These characteristics frequencies show successful synthesis of the Schiff base SAL2AP.

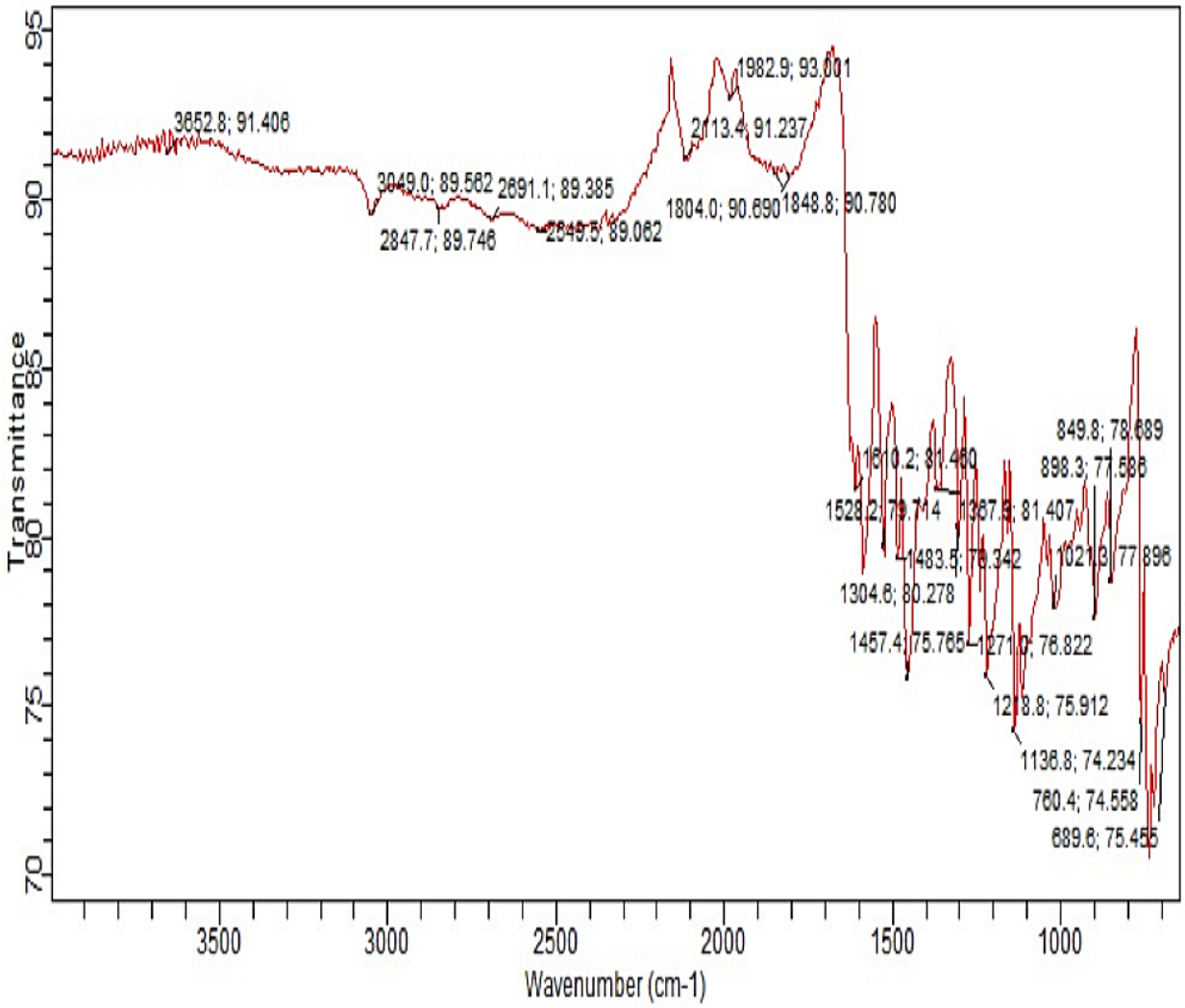

Figure 4.22: FTIR of CeSAL2AP

FTIR of CeSAL2AP showed the following vibrational frequencies: v (H_20) at 3049 cm^{-1} v(NO_3) at 1457 cm^{-1}, v(M-O) at 685 cm^{-1}, v(C-O) at 1218 cm^{-1}, v(HC=N) at 1610 cm^{-1}. These characteristics frequencies show successful synthesis of the Schiff base metal complex CeSAL2AP.

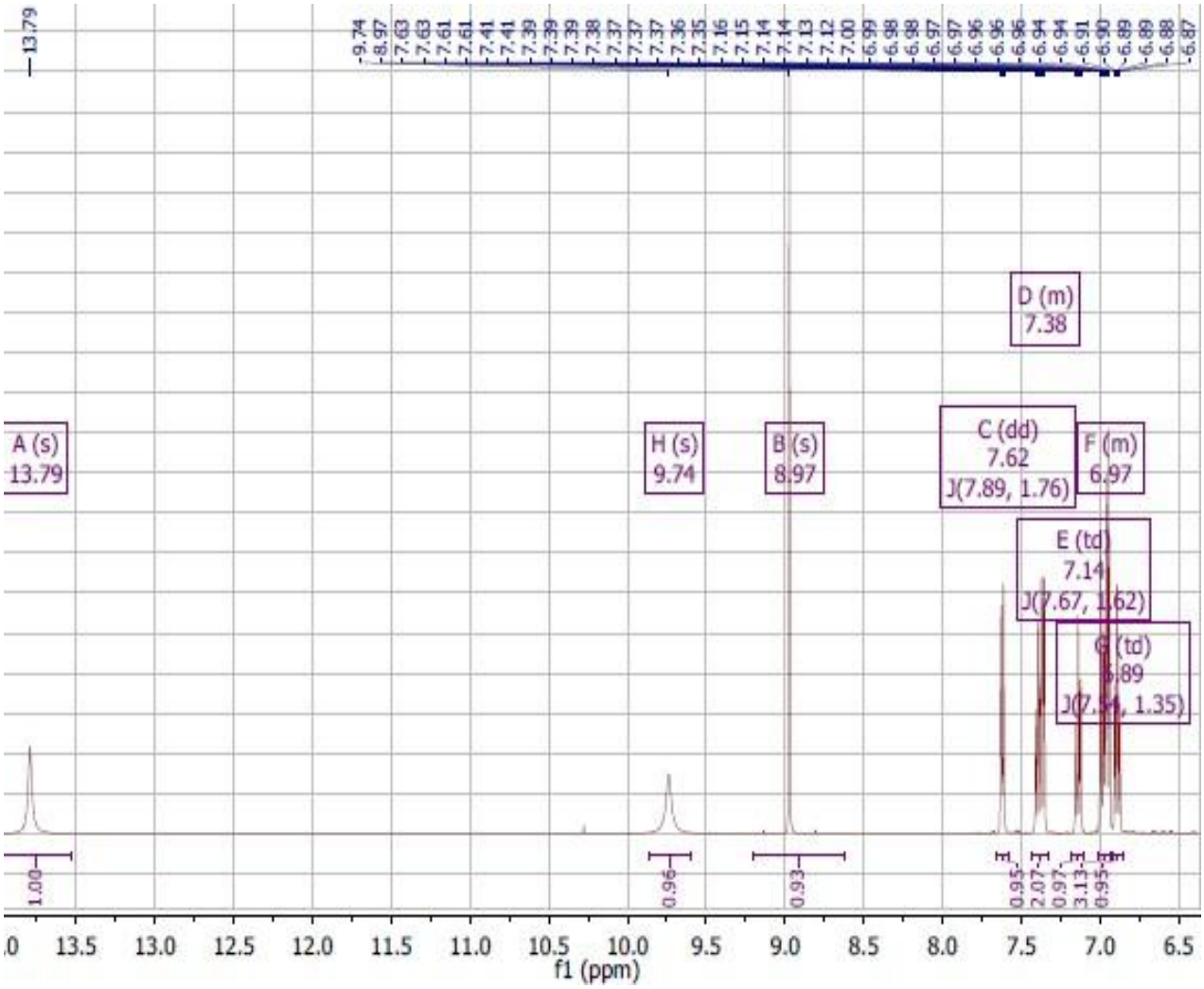

Figure. 4.23: SAL2AP ^{1}H- NMR

The key signals exhibited by the 1H-NMR spectra of the Schiff base, SAL2AP are: a singlet signal at δ 8.97, attributed to the azomethine (–CH=N–) proton, singlet at δ13.79 due to the hydroxyl proton (OH) of the aldehyde moiety, and signal at δ9.74 ppm corresponding to the proton of the aminophenol moiety.

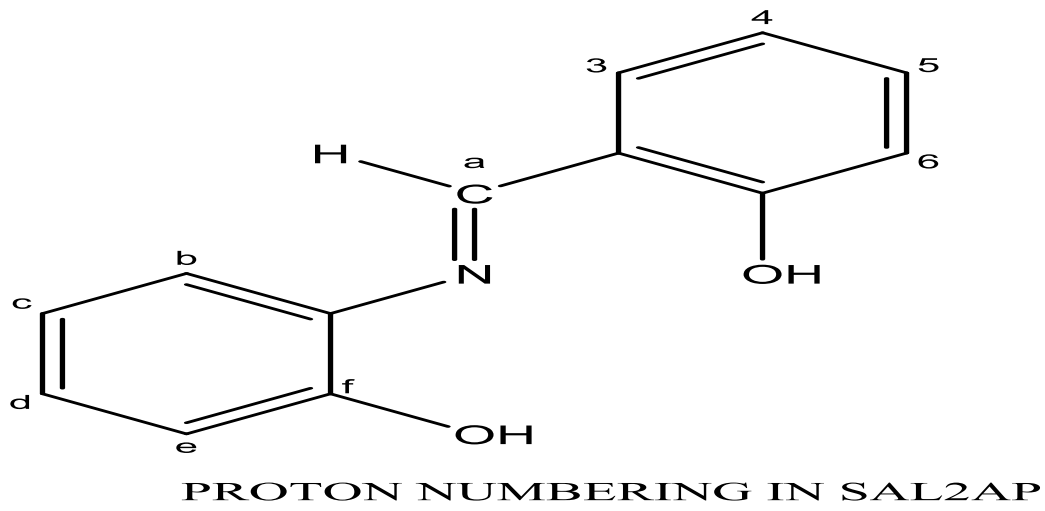

Figure 4.24: Proton numbering in SAL2AP

Table 4.25: ^{1}H NMR Spectral Data of SAL2AP

Compound	Chemical Shift (δ) ppm	Assignment
SAL2AP	7.38 - 6.97	(m, Ar- H)
	8.97	(s,H(HC=N)
	9.74	(s,H(OH)) aminophenol
	13.79	(s, H(OH)) hydroxylaldehyde

Table 4.25 shows chemical shifts for various proton- signals in the SAL2AP Schiff base, which identifies the Schiff base.

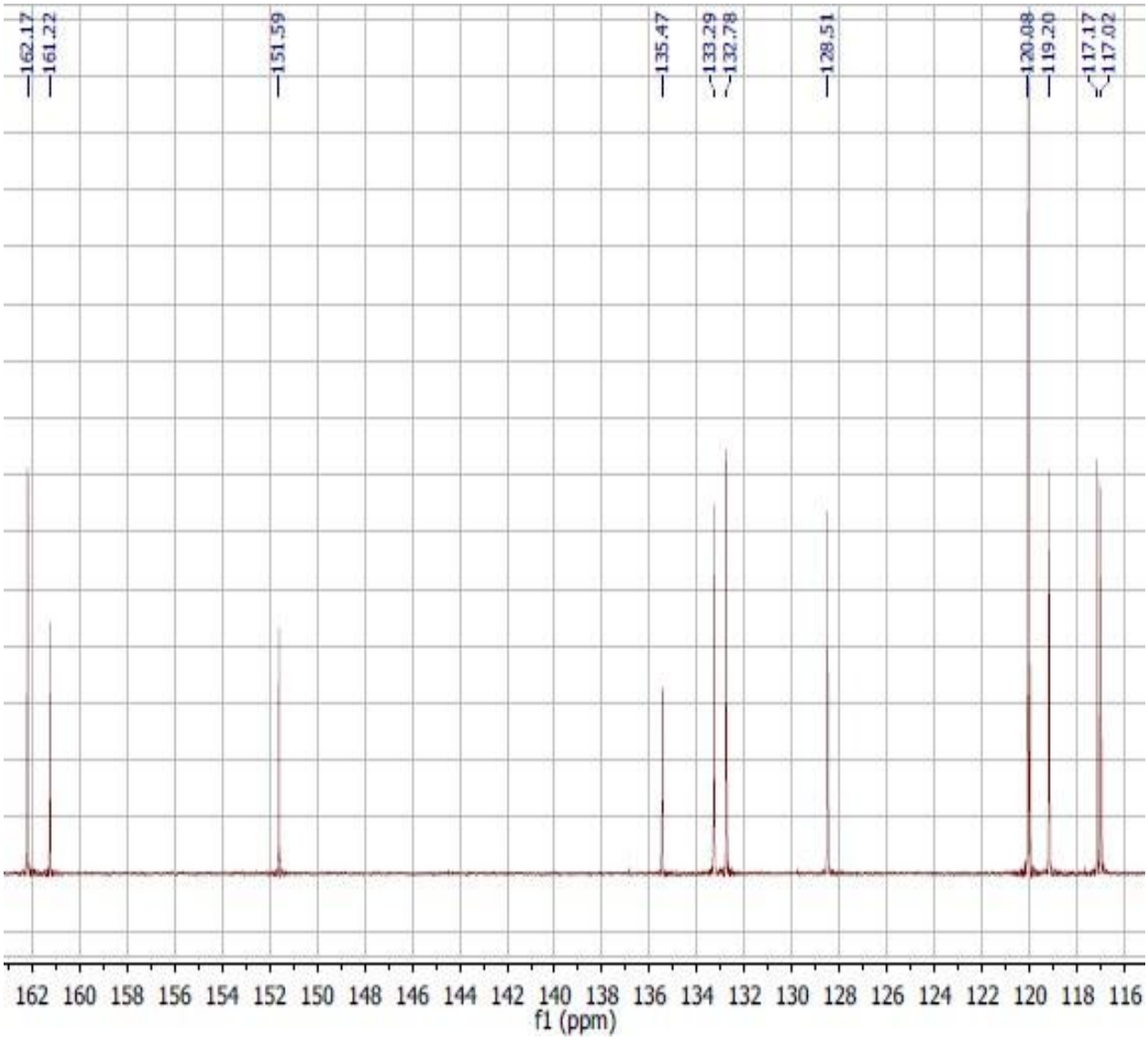

Figure 4.25: C-13 NMR OF SAL2AP

FTIR spectrum of SAL2AP shows key signals for azomithine carbon at 162.17 ppm, hydroxyl carbon of aldehyde moiety at 161.22 ppm, and Signal due to hydroxyl carbon of *o*- aminophenol is at 120.08 ppm.

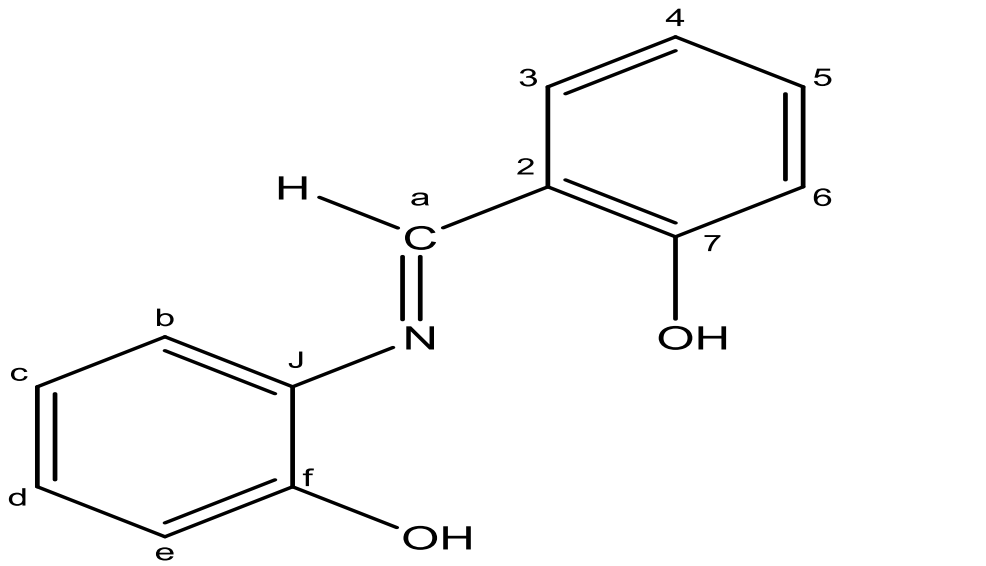

Figure 4.26: Carbon numbering in SAL2AP

Table 4.26: C-13 NMR data of SAL2AP

Compound	Chemical Shift (δ) ppm (Assignment)
SAL2AP	117.02(C6), 117.17 (C4), 119.20(C2), 120.08(b,f), 128.51 (d), 132.78(C,e), 133.29(C3), 135.47(C5), 151.59(j), 161.22(C7), 162.17 (a)

The spectra data in Table 4.25 show chemical shifts due to various constituent protons in SAL2AP Schiff base.

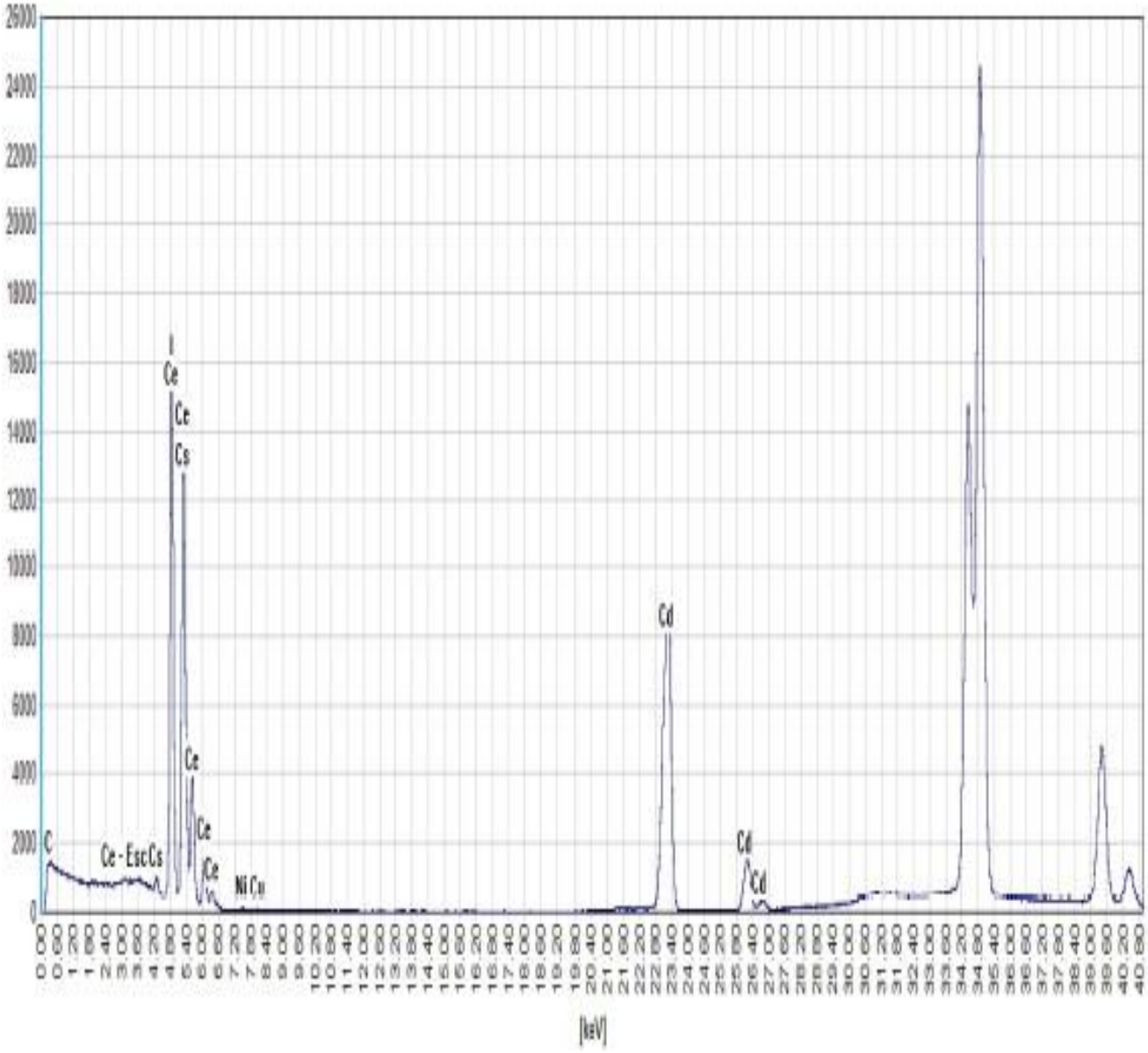

Figure 4.27: Energy Dispersive X-Ray Fluorescence (EDXRF) Spectrum of CeSAL2AP

EDXRF Spectra of CeSAL2AP recorded the percentage composition of Cerium in CeSAL2AP as 45.81%.

4.1.4 Inhibitive Action of SAL2AP and CeSAL2AP

4.1.4.1 Gravimetric Results

Table 4.27: Gravimetric data of Mild Steel in 1M HCl in the presence and absence of SAL2AP (Langmuir Adsorption Isotherm)

System (mmol dm^3)	C_R(mdd) SAL2AP	IE% SAL2AP	θ	C/θ
1 $x10^{-1}$	2.08	47.87	0.48	0.21
2 $x10^{-1}$	1.58	60.27	0.60	0.33
4 $x10^{-1}$	1.48	62.77	0.63	0.64
6 $x10^{-1}$	1.32	66.95	0.67	0.90
8 $x10^{-1}$	1.25	68.75	0.69	1.16
12 $x10^{-1}$	1.18	69.86	0.70	1.71
16 $x10^{-1}$	1.12	71.77	0.72	2.22
20 $x10^{-1}$	1.34	66.24	0.66	2.30

Increase in Surface coverage **θ** and IE is observed with increase in Concentration of SAL2AP and decrease in Corrosion Rate of the system.

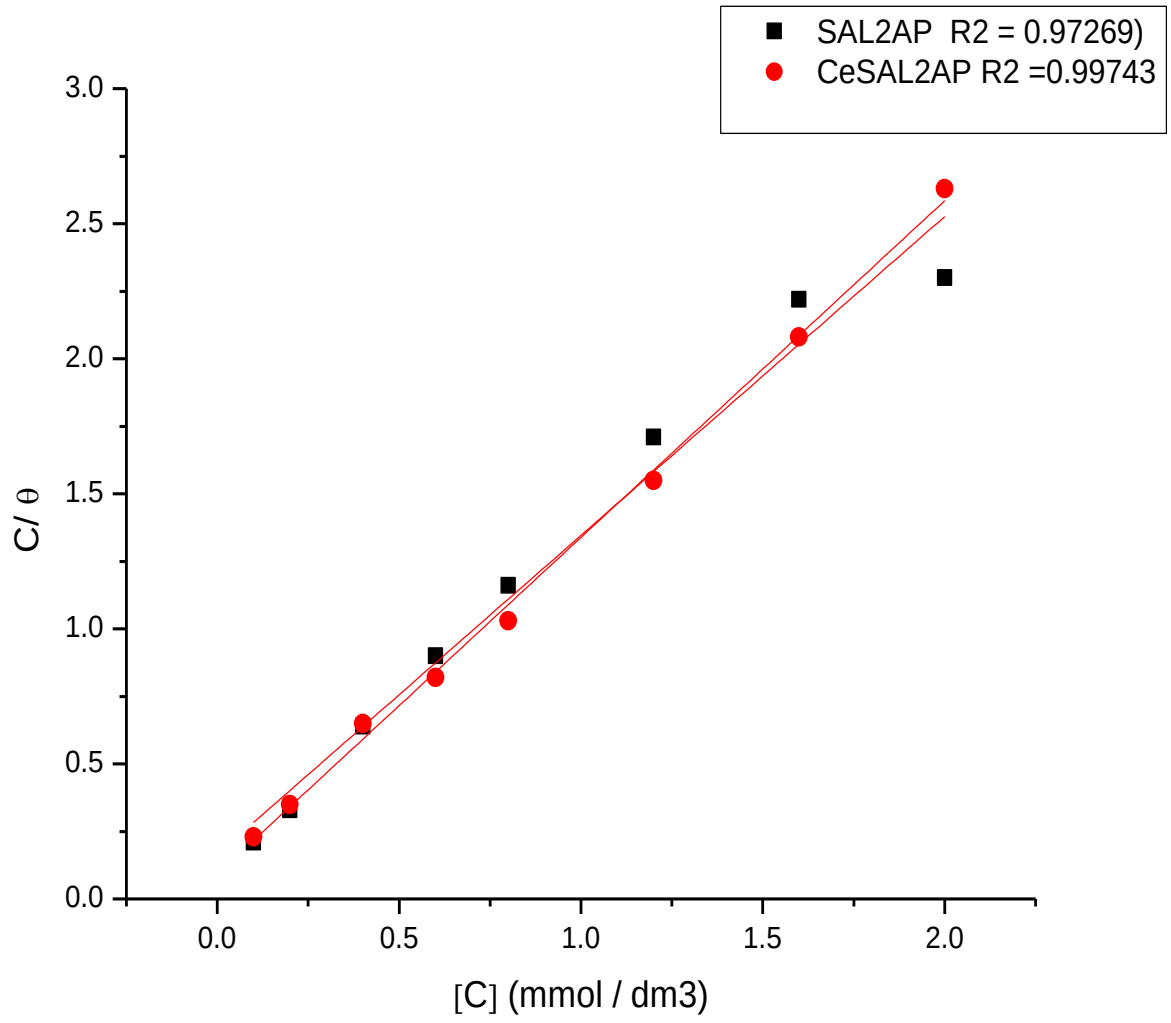

Figure 4.28: Langmuir's Adsorption plots for Mild Steel in 1 M HCl containing various concentrations of SAL2AP and CeSAL2AP

Table 4.28: Gravimetric Data of Mild Steel in 1M HCl in the presence and absence of SAL2AP (Temkin Adsorption Isotherm)

System (mmol/dm3)	Corr. Rate SAL2AP	IE% SAL2AP	θ	θ/C	Log(θ /C)
$1x10^{-1}$	2.08	47.87	0.48	4.80	0.68
$2\ x10^{-1}$	1.58	60.27	0.60	3.00	0.48
$4\ x10^{-1}$	1.48	62.77	0.63	1.58	0.20
$6\ x10^{-1}$	1.32	66.95	0.67	1.12	0.05
$8\ x10^{-1}$	1.25	68.75	0.69	0.86	-0.07
$12\ x10^{-1}$	1.18	69.86	0.70	0.58	-0.24
$16\ x10^{-1}$	1.12	71.77	0.72	0.45	-0.35
$20\ x10^{-1}$	1.34	66.24	0.66	0.33	-0.48

Increase in Surface coverage **θ** and IE is observed with increase in concentration of SAL2AP and decrease in Corrosion rate of the system.

Table 4.29: Gravimetric Data of Carbon Steel in 1M HCl in the presence and absence of SAL2AP (Frumkin's Adsorption Isotherm)

System (mmol dm^3)	C_R(mdd) SAL2AP	IE% SAL2AP	θ	(1-θ)C	θ (1- θ)C	Log θ (1- θ)C
1 $x10^{-1}$	2.08	47.87	0.48	0.052	9.23	0.9652
2 $x10^{-1}$	1.58	60.27	0.60	0.080	7.50	0.8751
4 $x10^{-1}$	1.48	62.77	0.63	0.148	4.26	0.6294
6 $x10^{-1}$	1.32	66.95	0.67	0.198	3.38	0.5289
8 $x10^{-1}$	1.25	68.75	0.69	0.248	2.78	0.4440
12 $x10^{-1}$	1.18	69.86	0.70	0.360	1.94	0.2878
16 $x10^{-1}$	1.12	71.77	0.72	0.448	1.61	0.2068
20 $x10^{-1}$	1.34	66.24	0.66	0.680	0.97	-0.0132

Increase in Surface Coverage and IE is observed with increase in Concentration of SAL2AP and decrease in Corrosion Rate of the system.

Table 4.30: Gravimetric Data of Mild Steel in 1M HCl in the presence and absence of CeSAL2AP (Langmuir's Isotherm)

System (mmol/dm3)	Corr. Rate	IE%	(θ)	C/θ
$1x10^{-1}$	2.26	42.83	0.43	0.23
$2\ x10^{-1}$	1.73	56.61	0.57	0.35
$4\ x10^{-1}$	1.51	62.19	0.62	0.65
$6\ x10^{-1}$	1.08	72.90	0.73	0.82
$8\ x10^{-1}$	0.91	77.55	0.78	1.03
$12\ x10^{-1}$	0.91	77.10	0.77	1.55
$16\ x10^{-1}$	0.94	76.46	0.77	2.08
$20\ x10^{-1}$	0.96	75.94	0.76	2.63

Increase in Surface coverage and IE is observed with increase in concentration of CeSAL2AP and decrease in Corrosion rate of the system.

Table 4.31: Gravimetric Data of Mild Steel in 1M HCl in the presence and absence of CeSAL2AP (Temkin's Isotherm)

System (mmol/dm3)	Corr. Rate	IE%	θ	θ/C	Log(θ /C)
$1x10^{-1}$	2.26	42.83	0.43	0.23	4.30
$2\ x10^{-1}$	1.73	56.61	0.57	0.35	2.85
$4\ x10^{-1}$	1.51	62.19	0.62	0.65	1.55
$6\ x10^{-1}$	1.08	72.90	0.73	0.82	1.22
$8\ x10^{-1}$	0.91	77.55	0.78	1.03	0.98
$12\ x10^{-1}$	0.91	77.10	0.77	1.55	0.64
$16\ x10^{-1}$	0.94	76.46	0.77	2.08	0.48
$20\ x10^{-1}$	0.96	75.94	0.76	2.63	0.38

Increase in Surface Coverage θ and IE is observed with increase in Concentration of CeSAL2AP, and decrease in Corrosion Rate of the system.

Table 4.32: Gravimetric Data of Mild Steel in 1M HCl in the presence and absence of CeSAL2AP (Frumkin's Isotherm)

System (mmol/dm3)	Corr. Rate CeSAL2AP	IE% CeSAL2AP	θ	(1-θ)C	$\frac{\theta}{(1-\theta)C}$	$\frac{Log\ \theta}{(1-\theta)C}$
$1x10^{-1}$	2.26	42.83	0.43	0.052	8.27	0.9175
$2\ x10^{-1}$	1.73	56.61	0.57	0.086	6.63	0.8215
$4\ x10^{-1}$	1.51	62.19	0.62	0.152	4.08	0.6107
$6\ x10^{-1}$	1.08	72.90	0.73	0.162	4.51	0.6542
$8\ x10^{-1}$	0.91	77.55	0.78	0.176	4.43	0.6464
$12\ x10^{-1}$	0.91	77.10	0.77	0.276	2.79	0.4456
$16\ x10^{-1}$	0.94	76.46	0.77	0.368	2.09	0.3201
$20\ x10^{-1}$	0.96	75.94	0.76	0.480	1.58	0.1987

Table 4.33: Regression Square values obtained for Langmuir, Temkin, and Frumkin Adsorption Isotherms.

Compound	R^2 Langmuir	R^2 Temkin	R^2 Frumkin
SAL2AP	0.97269	0.68543	0.54831
CeSAL2AP	0.99743	0.82374	0.48823

Langmuir Isotherm model with regression square value up to 0.99 is the model that perfectly fits the adsorption process.

Table 4.34: Influence of Concentration on the Inhibition Efficiency of SAL2AP and CeSAL2AP during Mild Steel Corrosion in 1M HCl after 24-hour immersion.

System (mmol/dm^3)	C_R SAL2AP	SAL2AP IE%	C_R CeSAL2AP	CeSAL2AP IE%
$1x10^{-1}$	2.08	47.87	2.26	42.83
$2\ x10^{-1}$	1.58	60.27	1.73	56.61
$4\ x10^{-1}$	1.48	62.77	1.51	62.19
$6\ x10^{-1}$	1.32	66.95	1.08	72.90
$8\ x10^{-1}$	1.25	68.75	0.91	77.55
$12\ x10^{-1}$	1.18	69.86	0.91	77.10
$16\ x10^{-1}$	1.12	71.77	0.94	76.46
$20\ x10^{-1}$	1.34	66.24	0.96	75.94

IE increased with increase in concentration, and optimum IE of 71.77 % was recorded for SAL2AP at 1.6 mmol/dm^3 while optimum IE value of 77.55 % was recorded for CeSAL2AP at concentration of 0.8 mmol/dm^3

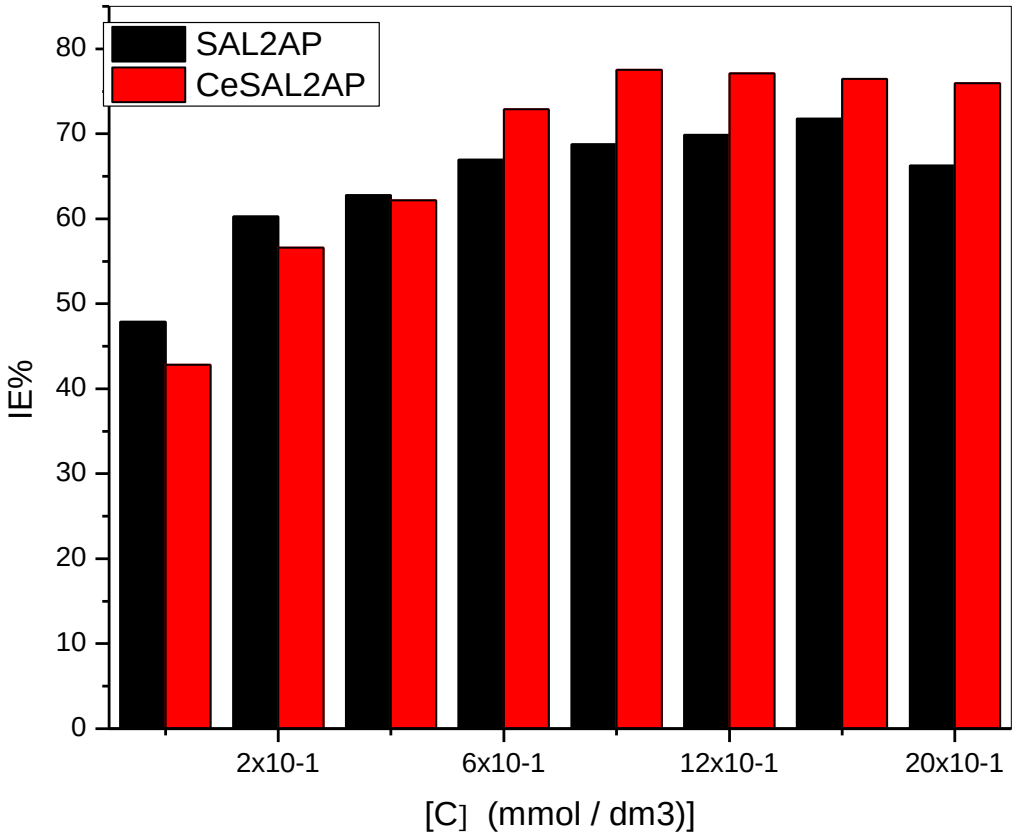

Figure 4.29: Influence of Concentration on the Inhibition Efficiency of SAL2AP and CeSAL2AP during Mild Steel Corrosion in 1M HCl after 24 hr. Immersion.

CeSAL2AP (red bars) consistently shows higher IE% compared to SAL2AP (black bars) from concentrations of 0.6 to 2.0 mmol/dm^3. The IE% increases as the concentration rises for both compounds, with SAL2AP achieving its highest inhibition efficiency, IE of 71.77% at concentration of 1.6 mmol/dm^3, while CeSAL2AP attained optimum IE of 77.55% at lower concentration of 0.8 mmol/dm^3.

4.1.4.2: Effect of Temperature on the Inhibition Efficiency of the Inhibitor- compounds at the optimum concentration

Table 4.35: Effect of Temperature on the Inhibition Efficiency of SAL2AP and CeSAL2AP at optimum concentration

T (K)	I/T (K)	C_R BLANK	log C_R BLANK	C_R SAL2AP	log C_R SAL2AP	IE of SAL2AP	C_R CeSAL2AP	log C_R CeSAL2AP	IE of CeSAL2AP
303	0.0033	3.981	0.600	1.120	0.049	71.77	0.911	-0.040	77.55
313	0.0032	13.419	1.127	6.007	0.779	55.23	4.041	0.6071	69.89
323	0.0031	13.437	1.128	6.030	0.780	55.12	4.437	0.647	66.96
333	0.0030	22.793	1.358	10.248	1.011	55.04	7.630	0.883	66.53
343	0.0029	54.270	1.735	24.478	1.389	54.90	18.463	1.266	65.93

Corrosion rate (C_R) increases with increasing temperature for blank system, and systems containing inhibitor- compounds. Although C_R is higher in blank system compared to inhibited systems.

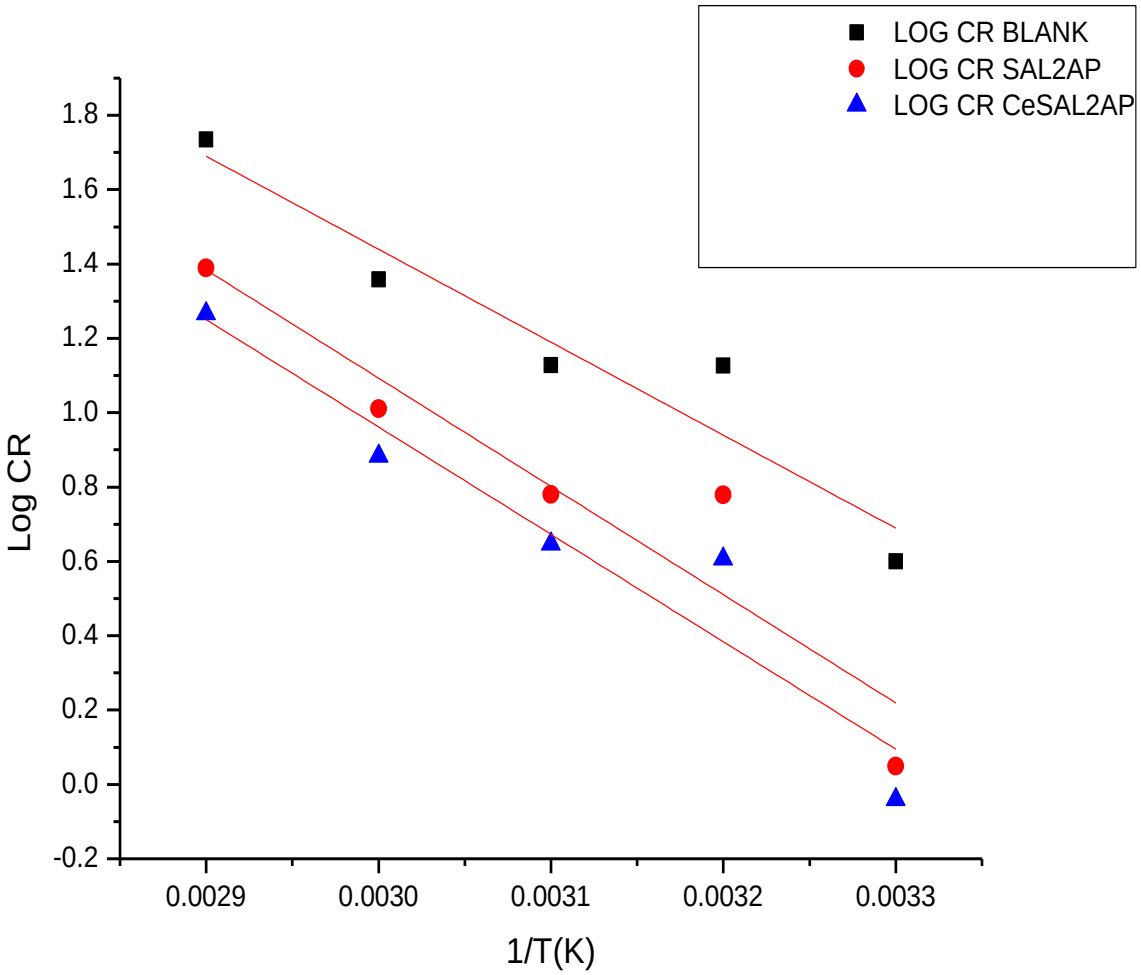

Figure 4.30: Arrhenius Plots for Mild Steel in 1 M HCl Solution free and Inhibited by 0.8 mmol/dm^3 of the Inhibitors

Table 4.35 gives data for log C_R vs I/T for SAL2AP and CeSAL2AP. Arhenius equation is:

log C_R = -Ea / 2.303 RT + A. A plot of log C_R vs 1/T above gives a slope of –Ea/ 2.303 R, from which Ea is calculated.

Table 4.36: Corrosion data of BLANK, SAL2AP and CeSAL2AP, for Plot of log C_R/T vs 1/T

T(K)	1/T(K)	C_R BLANK (mdd)	C_R/T BLANK	LogC_R/T BLANK	C_R SAL2AP (mdd)	C_R/T SAL2AP	log C_R/T SAL2AP	C_RCeSAL2AP (mdd)	C_R/T CeSAL2AP	log C_R/T CeSA2AP
303	0.0033	3.981	0.0131	-1.8827	1.120	0.0037	-2.4318	0.911	0.0030	-2.5229
313	0.0032	13.419	0.0429	-1.3675	6.007	0.0192	-1.7167	4.041	0.0129	-1.8894
323	0.0031	13.437	0.0416	-1.3809	6.030	0.0187	-1.7282	4.437	0.0137	-1.8633
333	0.0030	22.793	0.0684	-1.1649	10.248	0.0308	-1.5114	7.630	0.0229	-1.6402
343	0.0029	54.270	0.1582	-0.8008	24.478	0.0714	-1.1463	18.463	0.0538	-1.2692

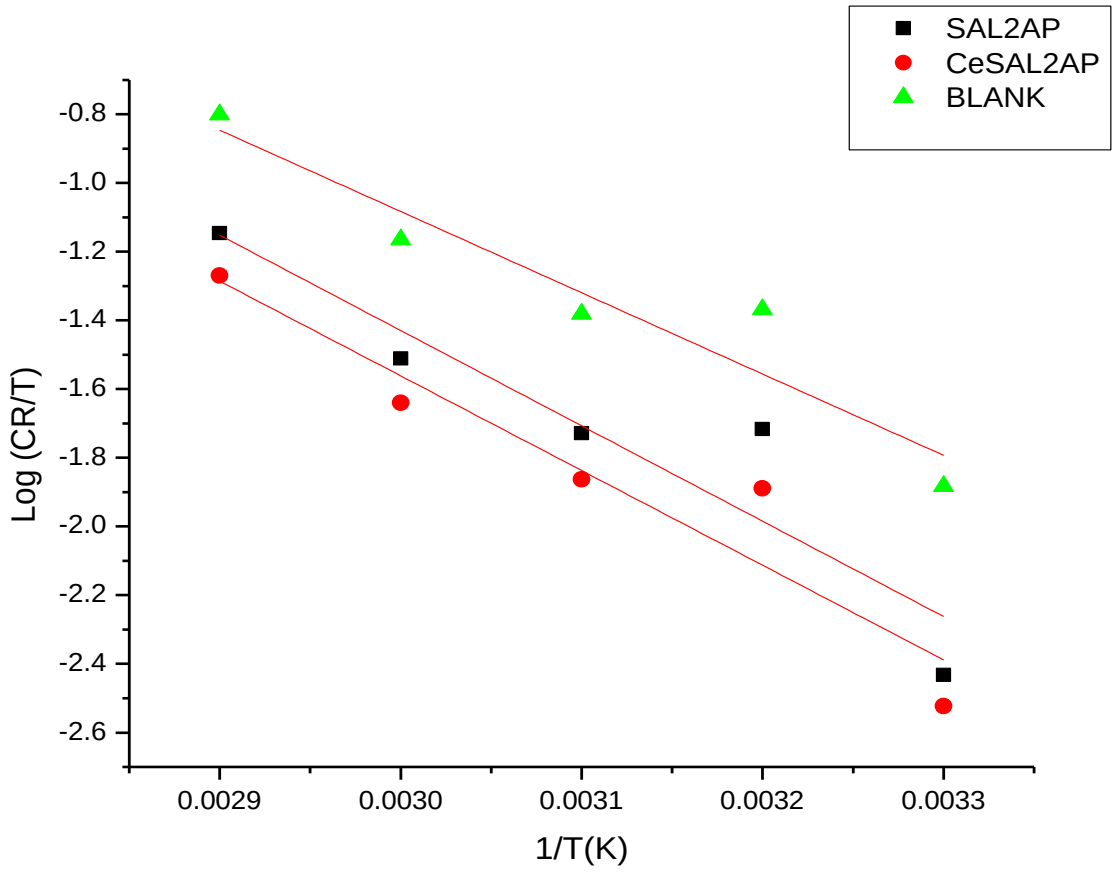

Figure 4.31: Plot of log of C_R/T vs I/T for Blank, SAL2AP and CeSAL2AP

Figure 4.31 above shows a plot of log C_R/T vs 1/T, derived from the relationship log C_R/ T = [(logR/Nh) + (ΔS*/2.303 R) – Δ H*/2.303 RT]. Where h is plank's constant, 6.626 x 10^{-34}, N is equal to Avagadro's number, 6.02 x $10^{.23}$, S* is the entropy of activation, R is gas constant, T is temperature in Kelvin. The slope of the linear plot, –H* / 2.303R, permits to derive the enthalpy of activation (H*), and an intercept of (log R/Nh) + (ΔS*/2.303 R) is used to calculate the entropy of the activation process, S*.

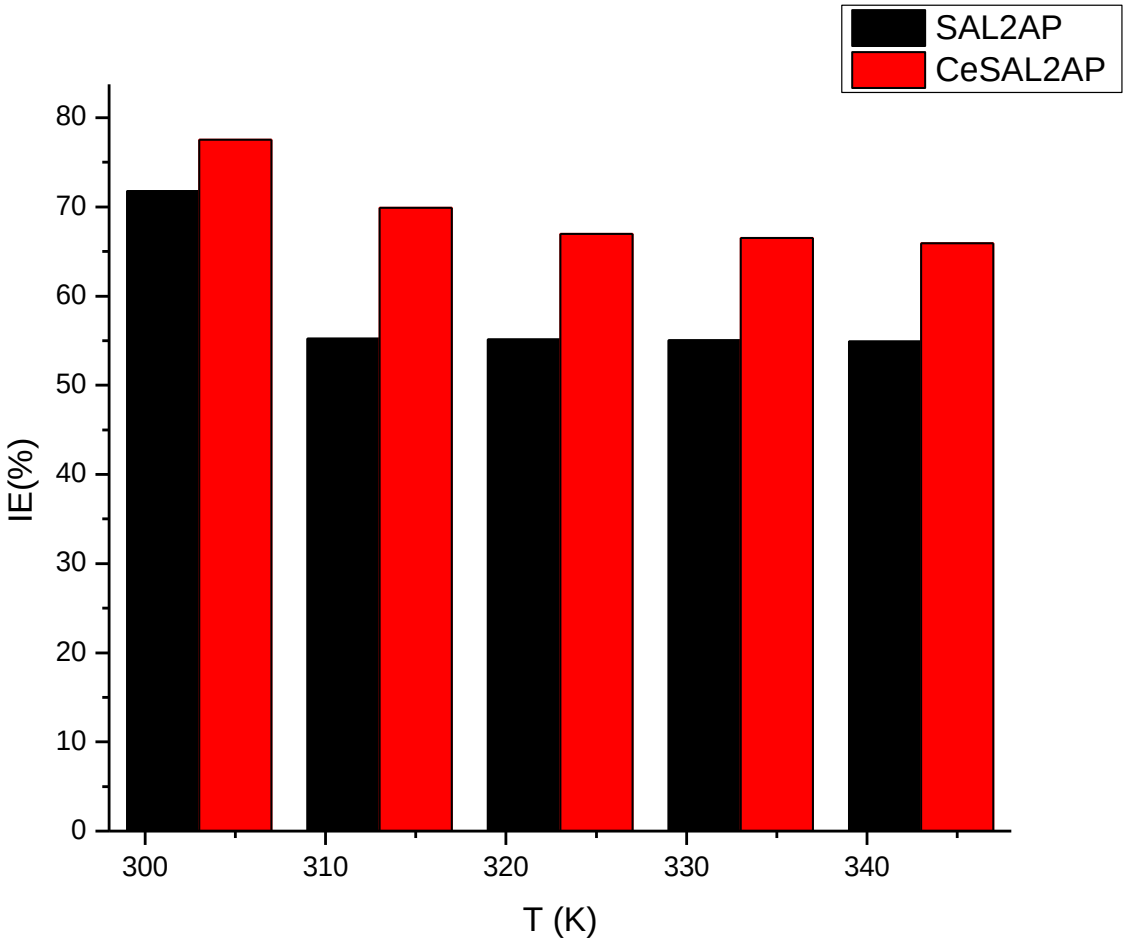

Figure 4.32: Effect of Temperature on the Inhibition Efficiency of the compounds at Optimum Concentration

A decrease in IE is observed in the compounds with increase in temperature, which is typical for physisorption process of adsorption. However, CeSAL2AP (red bar) had an enhanced I.E over the parent Schiff base SAL2AP (black bar).

Table 4.37: Values for Ea, ΔGads, ΔH, and ΔS for Blank, SAL2AP and CeSAL2AP

System	Ea (kJ/Mol)	ΔG_{ads}	Δ H (kJ/MOL)	Δ S kJ/Mol
BLANK	20.31	-	45.79	- 82.38
SAL2AP	24.21	-16.5	53.21	- 65.47
CeSAL2AP	24.01	-14.8	52.01	- 69.13

Table 4.38: Variation of Inhibition Efficiency with Immersion Time for SAL2AP and CeSAL2AP

WEEK	IE % OF COMPOUND	
	SAL2AP	CeSAL2AP
1	41.90	65.90
2	30.62	38.04
3	25.99	30.79
4	25.61	30.51

IE of SAL2AP and CeSAL2AP is observed to decrease over time, which is suggestive of physical adsorption process of inhibitor molecules on mild- steel surface.

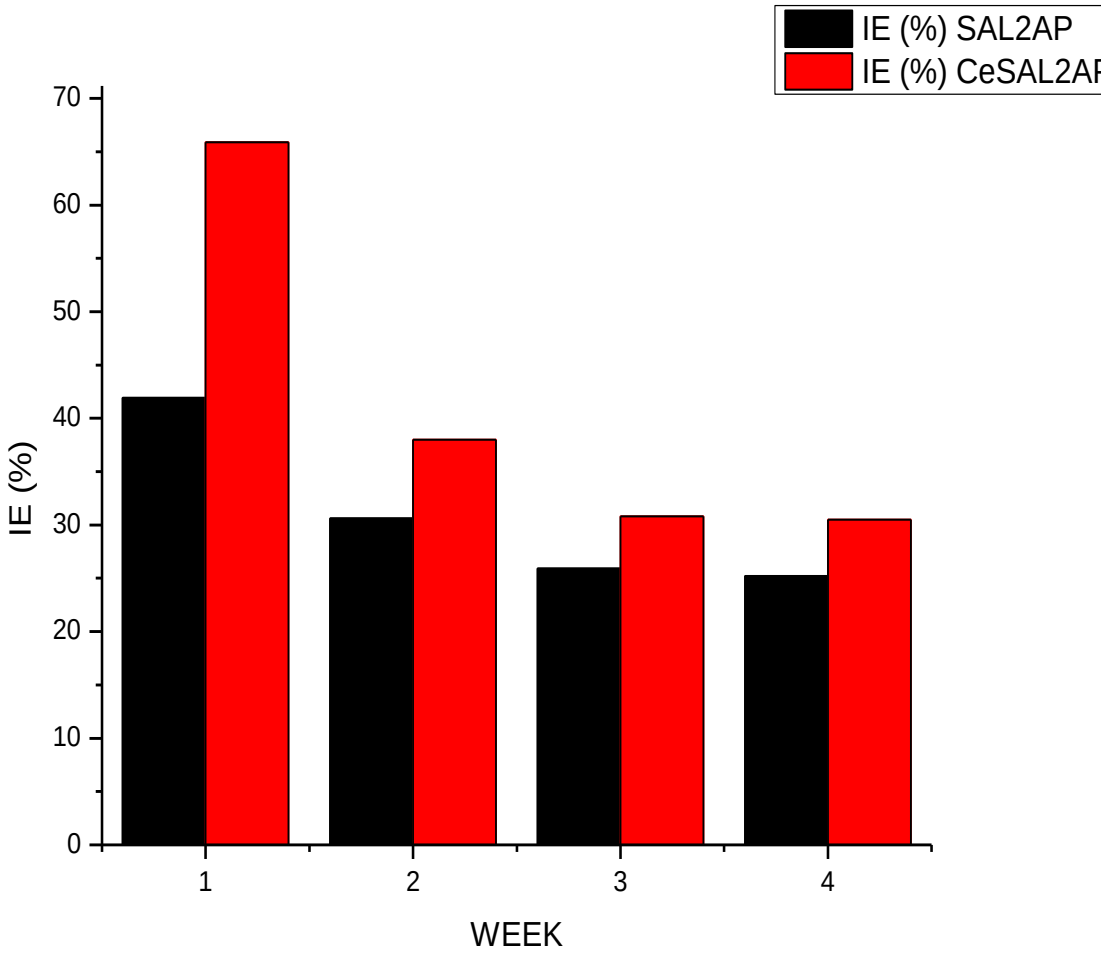

Figure 4.33: Variation of Inhibition Efficiency of SAL2AP, and CeSAL2AP with Immersion Time

The bar chart shows that IE decreased with time suggesting that the inhibitors were physically adsorbed on the mild steel surface. Additionally, IE of the complex CeSAL2AP (red bar) was consistently above that of the parent Schiff base SAL2AP (black bar).

4.1.5 Surface Studies Using AFM

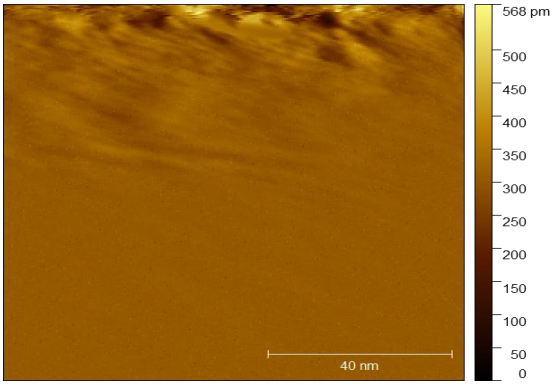

Figure 4.34 (a) BLANK 2D AFM (1M HCl)

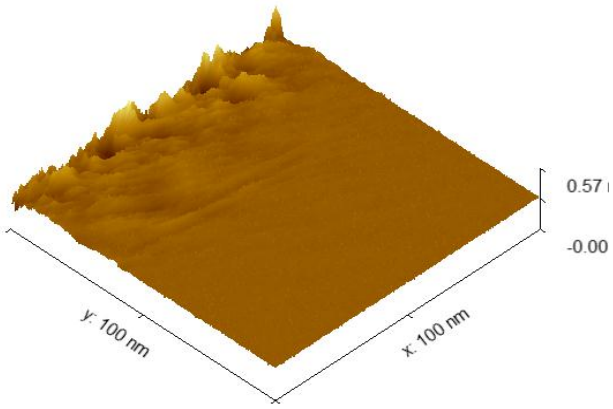

Figure 4.34(b) BLANK 3D AFM (1 M HCl)

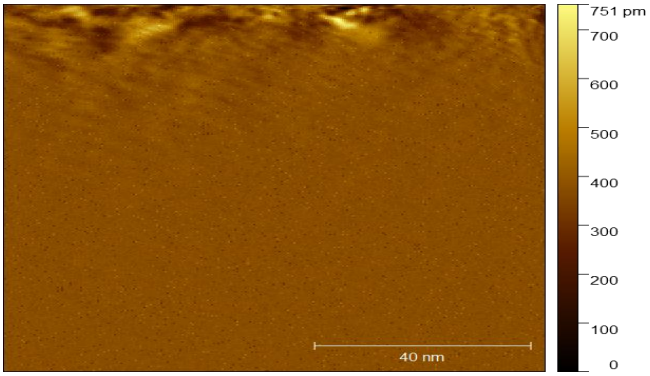

Figure 4.34 (c) SAL2AP 2D AFM

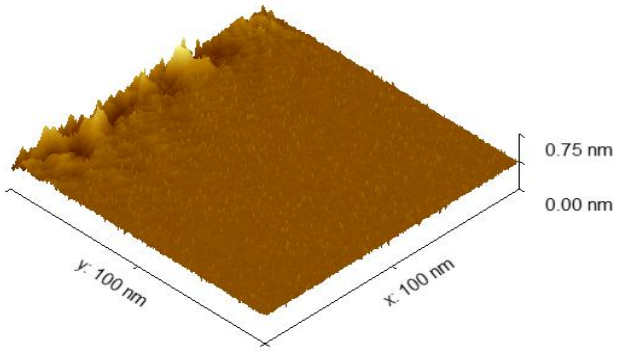

Figure 4.34 (d) SAL2AP 3D AFM

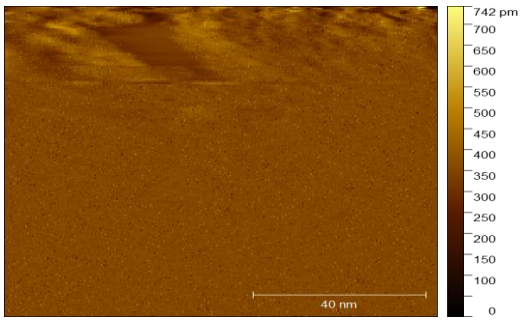

Figure 4.34 (e) CeSAL2AP 2D AFM

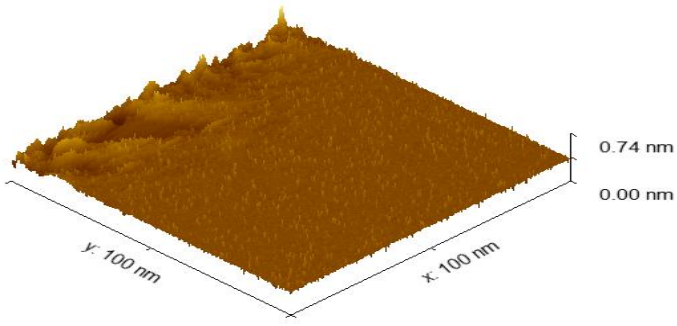

Figure 4.34 (f) CeSAL2AP 3D AFM

Table 4.39: AFM Parameters of Compounds

AFM PARAMETERS	COMPOUNDS		
	BLANK	**SAL2AP**	**CeSAL2AP**
Sq value (pm)	44.80	29.04	26.54
Sp value (pm)	574.85	386. 34	375.21
Sv value (pm)	**399.44**	**371.21**	**369.12**

The RMS roughness (Sq) values provides a quantitative value that describes the overall surface texture or roughness. Maximum peak height (Sp) refers to the height of the tallest peak in a given measurement area relative to the mean plane of the surface. Sp value provides insight into the presence of features such as spikes and protrusions. (Sv) value indicates the extent of corrosion.

4.1.6 Electrochemical Results

4.1.6.1 Potentiodynamic (PDP) Results

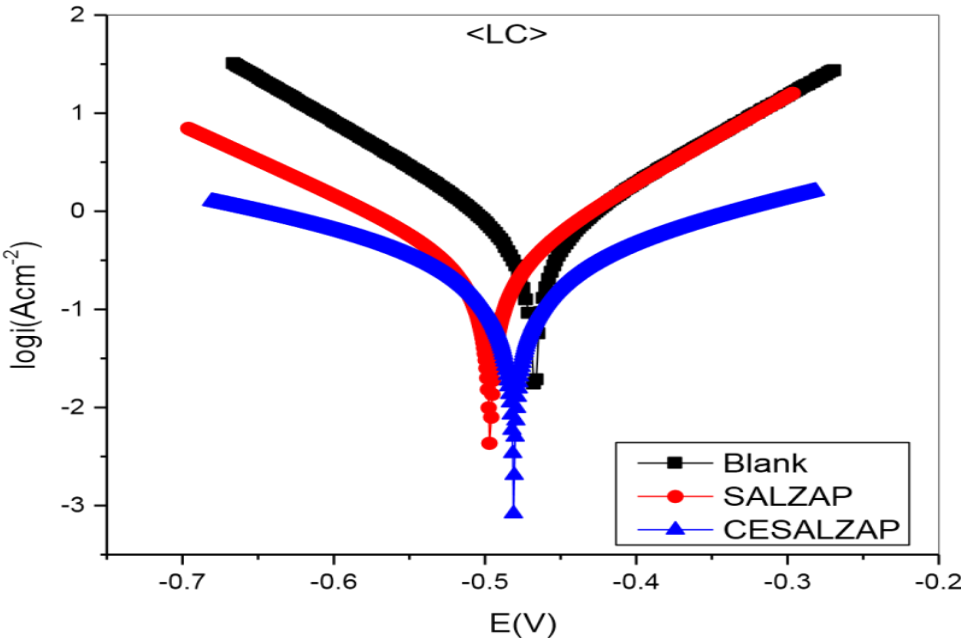

Figure 4.35: Polarization curves of Mild Steel in the absence and in the presence of 0.8 mmol/dm^3 each of SAL2AP and CeSAL2AP at 30 °C

Table 4.40: PDP parameters of Mild Steel immersed in the presence and absence of 0.8 mmol /dm^3 of the inhibitors in 1M HCl

Environment	Ecorr (mV)	ba (mV/dec)	bc (mV/dec)	Icorr. (uA/cm2)	R_P	IE $_{PDP}$ (%)
BLANK	-467.06	116.0	112.3	543.58	45.1	-
SAL2AP	-481.03	297.4	352.4	364.83	95.2	32.90
CeSAL2AP	-496.58	114.2	143.2	282.65	191	48.02

Icorr and Ecorr decreases while IE increases in the presence of the inhibitors.

4.1.6.2 EIS Results

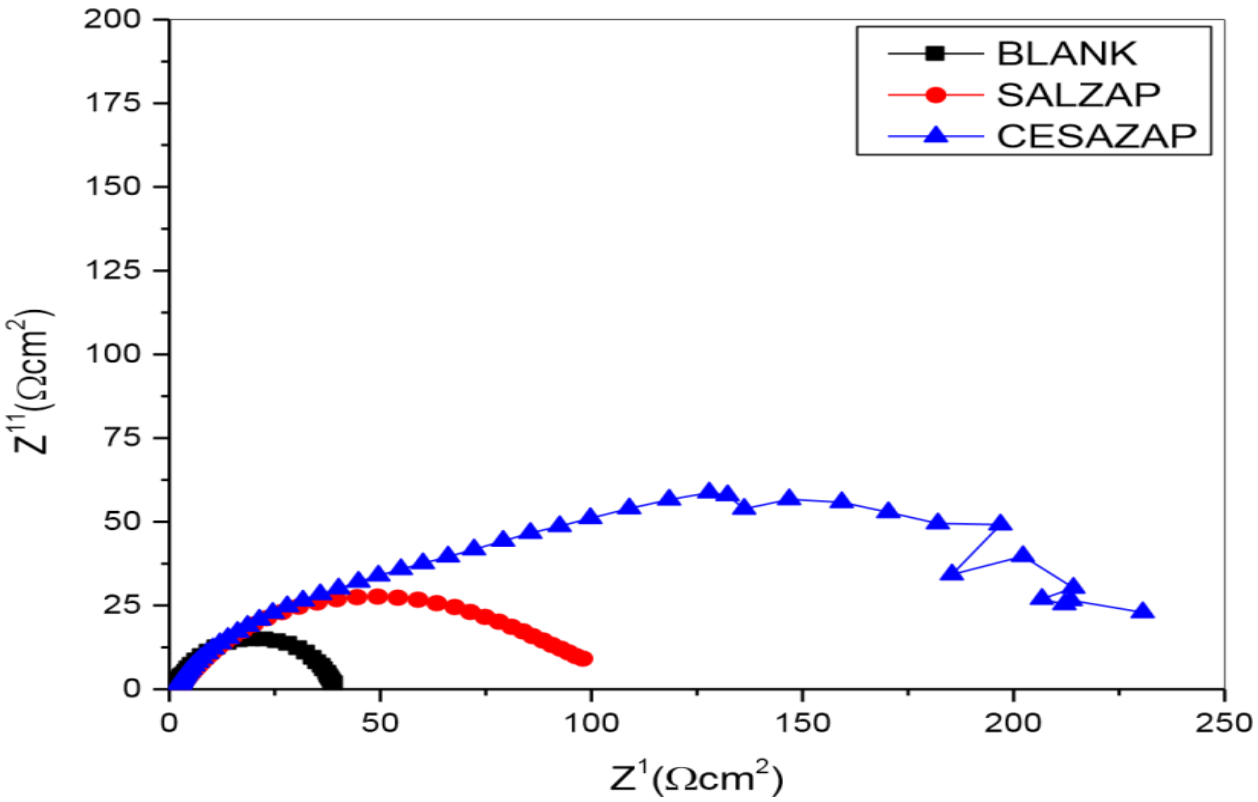

Figure 4.36: Nyquist curves of Mild Steel in the Absence and Presence of 0.8 mmol /dm^3 concentrations at of SAL2AP and CeSAL2AP at 30 °C.

Semi- circle represents resistance to charge transfer (Rct). CeSAL2AP with wider semi- circle suggests its highest corrosion resistance compared to SAL2AP and BLANK.

Table 4.41: EIS Parameters and Inhibition Efficiency at 30 °C of Mild Steel in the absence and in the presence of 0.8 mmol /dm3 concentrations of the inhibitors

Environment	R_S (Ohm)	Rct (Ohm)	Cdl, (μF/cm^2)	IE%$_{EIS}$
BLANK	1.6848	37.67	458.23	-
SAL2AP	2.5425	94.93	425.11	60.32
CeSAL2AP	1.5074	211.68	138.23	82.21

Cdl value is reduced while Rct and IE value is increased in the presence of the inhibitors

Table 4.42: Inhibition Efficiency values obtained for the various Analytical Techniques

	Analytical Technique / IE (%)		
Compound	**Weight loss**	**PDP**	**EIS**
SAL2AP	71.77	32.90	60.32
CeSAL2AP	77.55	48.02	82.21

The data obtained shows agreement in the order of IE values obtained for the Schiff base SAL2AP, and its metal complex, CeSAL2AP from the various analysis techniques.

4.2.1 Discussion on SAL2AP and CeSAL2AP

4.2.1.1 Physical Measurements

4.2.1.1.1 Colour

The different colours of the synthesized compounds have been referenced in the Table 4.22. The variation in color of the synthesized Schiff bases compared to their corresponding cerium complexes gives credence to the successful synthesis of the metal complexes.

4.2.1.1.2 Melting Point and pH Measurement

The complexation in coordination chemistry is often accompanied by deprotonation of ligand which is the true cause of the variation of pH in the solution phase. In the general case, there is drop down in pH values of the solution in moving from Schiff base to metal complex. The variation in pH values is committed to being the indication of the complex formation during the reaction. The pH values of Schiff base and its metal complex are reported in the Table 4.22. Moreover, the Schiff base SAL2AP have higher pH (6) value than the metal complex, CeSAL2AP, pH (5).

4.2.1.1.3 Solubility Analysis

The solubility of the Schiff base and metal complex was examined in water and various organic solvents. Their solubility data are reported in the Table 4.23. The observation of solubility data revealed that the Schiff base and its metal complex were insoluble in water but soluble in organic solvents. The Schiff base, SAL2AP is soluble in methanol, DMSO, and DMF, whereas metal complex, CeSAL2AP is soluble in DMSO and DMF.

4.2.1.1.4 Molar Conductivity and Magnetic Susceptibility Measurement

Molar conductivity in DMSO and DMF of the compounds measured in mS/Cm at a concentration of 10^{-3}M shown in Table 4.24. Magnetic susceptibility values are also showed in Table 4.24. The compound showed high conductivity values, 1.21 and 1.04 mS/Cm, values >0.1 mS/ Cm, suggestive of electrolytic (ionic) nature of the Ce (III) Schiff base complex, and the presence of nitrate ions in the outer coordination sphere of the complex . The Schiff base showed low conductivity values of 4.96 X $10^{-3}$and 6.47x10^{-3} mS/Cm , values <0.1 mS/Cm which shows non electrolytic nature of the Schiff base and absence of the nitrate ions in the compounds . The magnetic properties of the compounds were studied using Gouy balance, Sherwood scientific limited UK. Serial number, 29275. The value of 009 obtained for the cerium complex, (Table 4.24) is suggestive of paramagnetic nature of the Cerium complex, ie (value>1), meaning that the

compound can be attracted by an external magnetic field. The Schiff base, SAL2AP showed no magnetic properties.

4.2.1.2 Spectral Measurements

4.2.1.2.1 UV-Vis Spectral data of SAL2AP and CeSAL2AP

Figures 4.19 and 4.20 show the Uv- Visible spectra of the SAL2AP and CeSAL2AP at room temperature in DMSO solvent**.** Maximum absorbance observed for SAL2AP Schiff base was at 347nm, attributed to $n \rightarrow \pi^*$ transition due to transition of non -bonding electrons of the nitrogen atom of the azomethine to the anti –bonding pi (π^*) orbital of the azomethine group, which experienced a blue shift to a lower wave length (and higher energy) of 308 nm in the CeSAL2AP Schiff base complex due to coordination of the nitrogen atom to the metal ion.

4.2.1.2.2 FTIR Spectral Studies of SAL2AP and CeSAL2AP

The spectra of the Schiff base and Cerium metal complex are given in figures 4.21 and 4.22. V(C=N) vibration observed in the spectrum of SAL2AP at 1604 cm-1 occurred at a higher frequency in the spectrum of the complex CeSAL2AP at 1610 cm^{-1} which explains coordination through the azomithine nitrogen. This is confirmed by the appearance of a new band at 760 cm^{-1} assigned to v (M-N) vibration due to the formation of metal- nitrogen bond in the complex.
v(C-O) vibration in the spectrum of the ligand is observed at 1226 cm^{-1} , which experienced a blue shift to 1218 cm-1 in the spectrum of the complex. This may be due to deprotonation of –OH of the phenolic group before complexation. Disappearance of v (OH) phenolic band at 3471 cm^{-1} originally present in SAL2AP confirms coordination through phenolic oxygen after deprotonation. Appearance of a new frequency at 685 cm^{-1} in the spectrum of the complex attributed to v(M-O) further supports complexation due to formation of new metal- oxygen bond.

The presence of coordinated water molecules is indicated by the appearance of a broad band in the region of 3049 cm^{-1}. This is confirmed by the appearance of of a new band at 849 cm-1 assigned to vibration of rocking water.

v(NO_3) vibration due to presence of nitrate group in the outer coordination sphere of the complex is indicated by the appearance of a new band at 1457 cm^{-1} in the spectrum of the complex.

4.2.1.2.3 Analysis of ^{1}H-NMR Spectral of SAL2AP

The 1H-NMR spectra of Schiff base ligands provide valuable insights into their bonding modes and confirm the presence of specific functional groups. The spectra of SAL2AP Schiff base was recorded in DMSO at room temperature using TMS as an internal standard. The chemical shifts

corresponding to the protons in the Schiff base are summarized in Table 4.25, with spectral diagram presented in Figures 4.23, while Figure 4.24 shows the proton numbering in the Schiff base.

The ^{1}H-NMR spectra of the Schiff base, SAL2AP exhibited a singlet signal at δ8.97, attributed to the azomethine (–CH=N–) proton (Enans et al., 2016). Additionally, the hydroxyl proton (OH) of the aldehyde moiety appeared as a distinct singlet at δ13.79.

Multiplets observed between δ 7.38 and δ 6.97 ppm were assigned to the aromatic protons of the Schiff base. Notably, the singlet signal at δ 9.74 ppm in SAL2AP corresponds to the proton of the aminophenol moiety. These characteristic signals strongly support the successful synthesis and structural integrity of the Schiff base.

4.2.1.2.4 13-C NMR Spectra of SAL2AP Schiff Base

13-C NMR spectral study furnishes idea about the different kinds of carbon atoms and their electronic environment in the molecules. The 13C NMR spectrum of SAL2AP Schiff base - ligand delivers a signal for azomithine carbon at 162.17 ppm, hydroxyl carbon of aldehyde moiety at 161.22 ppm, Aromatic carbon atoms of aldehyde moiety exhibit signals at 117.02, 117. 17, 119.20, 133.29, 135.47 ppm.

Signal due to hydroxyl carbon of *o*- aminophenol is at 120.08 ppm. Signals at 128.51, 132.78, 151.59 ppm, are signals due to aromatic carbon atoms of *o*- aminophenol. The carbon numbering is shown in Figure 4.26, and the spectrum displayed in Figure 4.25. The 13- C NMR data is shown in Table 4.26.

4.2.1.2.5 Energy Dispersive X- ray Fluorescence (EDXRF) Spectroscopy Analysis of CeSAL2AP

Figure 4.27 is an Energy Dispersive X-Ray Fluorescence (EDXRF) spectrum of CeSAL2AP, which shows the characteristic X-ray peaks of elements present in the analyzed sample. CeSAL2AP showed a cerium composition of 45.81%, with a peak intensity of 40,535 cps/MA, within the energy range of 6.60–4.80 keV for occurrence of cerium. This confirms the successful synthesis of the cerium complex.

4.2.1.3 Inhibitive Action SAL2AP and CeSAL2AP

4.2.1.3.1 Analysis of Gravimetric Results

The corrosion rate of mild steel in 1 M HCl solution is studied by weight loss method in the absence and presence of Schiff base and the metal complex at 30°C and the percentage of inhibition efficiency is calculated. Tables 4.27 – 4.32 show the variation of corrosion rate (mdd) and inhibition efficiency, IE, in (%) with varying concentrations of inhibitors in (mmol/dm^3) for SAL2AP and CeSAL2AP. From the data, it is observed that corrosion rate is significantly lowered in the presence of the inhibitor. The corrosion rate is found to be dependent on the concentration of the inhibitor. With increase in concentration, the corrosion rate decreases gradually.

The data reveals that inhibition efficiency increases with increase in the concentration of the inhibitors in 1 M HCl solution. In the case of SAL2AP maximum inhibition efficiency of (71.77%) is recorded at 1.6 mmol /dm^3 of the inhibitor concentration, and with CeSAL2AP, it is found to be 77.55%, at concentration of 0.8 mmol/dm^3.

The decreasing corrosion rate and increasing inhibition efficiency are attributed to the adsorption of inhibitor on the metal surface. The increase in the concentration increases the surface coverage due to adsorption which increases the number of active sites protected on the metal surface. Hence, the inhibition efficiency increases with increase in the concentration. It is evident that the cerium complex, CeSAL2AP outperformed the parent Schiff base, SAL2AP considering the difference in their inhibition efficiencies, and also taking into consideration the lower concentration of 0.8 mmol/dm^3 at which the cerium complex attained optimum inhibition compared to a higher concentration of 1.6 mmol/dm^3 at which SAL2AP optimum inhibition efficiency occurred.

4.2.1.3.2 Analysis of variation of IE with Immersion time

The variation of inhibition efficiency with immersion time in HCl is shown in Table 4.35 and Figure 4.33. It is found that that the protection factor decreased with time suggesting that the inhibitors were physically adsorbed on the mild steel surface. Additionally, IE of the complex CeSAL2AP (red bar) was consistently above that of the parent Schiff base SAL2AP (black bar). This observation is in agreement with enhanced I.E of Schiff bases due to complexation.

4.2.1.3.3 Analysis of the effect of temperature on the performance of the inhibitors

The effect of temperature on the corrosion of C-steel in free and inhibited 1 M HCl solutions was studied using gravimetric approach in the range of 30–70◦C. The attack by acid solutions on the mild steel were inhibited by addition of 0.8 mmol/dm^3 of the inhibitors. The corrosion parameters

calculated from the gravimetric data are given in Table 4.35. Inspection of the Table reveals that the corrosion rate of steel in both free and inhibited acid media increased as the temperature was increased. However, the inhibition efficiency of the inhibitors decreased remarkably with increasing temperature (Figure 4.32). This result supports the idea that the adsorption of inhibitors onto the steel surface is physical in nature. Thus, as the temperature increases, the number of adsorbed molecules decreases, leading to a decrease in the inhibition efficiency. It is also observed that higher inhibition efficiency was recorded for the cerium complex, CeSAL2AP compared to the parent Schiff base SAL2AP at all temperatures. This gives credence to the fact that complexation enhances inhibition efficiency of Schiff base compounds. The activation energies of the corrosion process in free and inhibited acid were calculated using the Arrhenius equation [equation 1.4] page 32.

$$K = A \exp \frac{Ea}{RT}$$

Where Ea is the activation energy, A is the frequency factor, T is the absolute temperature, R is the gas constant, and K is the rate constant, which is directly proportion to the corrosion rate. Plotting log k versus 1/T gives a straight line, as revealed by Figure 4.30. The values of activation energy calculated using the lines of Fig. 4.30 are 20.79, for free, and 24.21and 24.01 kJ/mol for acid solutions inhibited with SAL2AP and CeSAL2AP, respectively. The obtained results suggest that the compounds inhibited the corrosion reaction by increasing its activation energy. This could be done by adsorption of the inhibitors onto the steel surface, making a barrier to mass and charge transfer.

4.2.1.3.4 Analysis of Thermodynamics Parameters, ΔH, and Δ S

Figure 4.31 shows a plot of log C_R/T vs 1/T, derived from the relationship Log C_R/ T = [(logR/Nh) + (ΔS*/2.303 R) – Δ H*/2.303 RT]. Where h is plank's constant, 6.626 x 10-^{34}, N is equal to Avagadro's number, 6.02 x $10^{23.}$, S* is the entropy of activation, R is gas constant, T is temperature in Kelvin. The slope of the linear plot, –H* / 2.303R permits to derive the enthalpy of activation (H*), and an intercept of (log R/Nh) + (ΔS*/2.303 R) is used to calculate the entropy of the activation process, S*. Data of the log CR/ T vs 1/ T are listed in Table 4.36. ΔH* value obtained for SAL2AP is 53.21 kJ/ Mol, while CeSAL2AP Δ H value is 52.01 kJ/ Mol. Δ H value recorded for the free system (blank) is 45.79 kJ/ Mol. The positive enthalpies obtained shows the endothermic process of the dissolution process. ΔS values obtained for SAL2AP and CeSAL2AP are -65.47 and -69.13 kJ/Mol respectively. The negative entropies shows increased orderliness moving from the uninhibited to inhibited systems.

4.2.1.4 Adsorption Isotherms

It has been assumed that organic inhibitor molecules establish their inhibition action via the adsorption of the inhibitor onto the metal surface. The adsorption processes of inhibitors are influenced by the chemical structures of organic compounds, the nature and surface charge of metal, the distribution of charge in molecule and the type of aggressive media. In general, two modes of adsorption can be considered. The proceeding of physical adsorption requires the presence of electrically charged metal surface and charged species in the bulk of the solution. Chemisorption process involves charge sharing or charge transfer from the inhibitor molecules to the metal surface. The presence of an inhibitor molecule having relatively loosely bound electrons or heteroatoms with lone-pair electrons, and a lanthanide or transition metal, having vacant, low-energy electron orbital, facilitates this adsorption. Assuming the corrosion inhibition was caused by the adsorption of SAL2AP and its metal complex CeSAL2AP, and the values of surface coverage (θ) for different concentrations of inhibitors in 1 M HCl were evaluated from weight loss measurements from Eq. (3.1). Adsorption isotherms are very important in determining the mechanism of organic electrochemical reactions. The most frequently used adsorption isotherms are Langmuir Table 4.27 and 4.30. and Figure 4.28. Temkin, Table 4.28 and 4.31, and Frumkin Table 4.29 and 4.32). The listed adsorption isotherms were tested for the description of adsorption behaviour of studied compounds and it was found that adsorption of SAL2AP and CeSAL2AP on mild steel surface in HCl solution obeys the Langmuir adsorption isotherm given by equations (1.5) and (1.6) page 32.

$$\frac{C_{inh}}{\theta} = \frac{1}{b} + C_{inh} \qquad (1.5)$$

$$b = \frac{1}{55.5} exp\left(-\frac{\Delta G_{ads}}{RT}\right) \qquad (1.6)$$

C_{inh} is the inhibitor concentration, θ is the fraction of the surface covered, b is the adsorption coefficient and G_{ads} is the standard free energy of adsorption. Figure 4.28 shows the dependence of the fraction of the surface covered C/θ as a function of the concentration (C) of inhibitors. It should be explained that other adsorption isotherms (Frumkin and Temkin) were checked and Langmuir adsorption isotherm is the best approximate between them. This is why the assumption is true for Langmuir adsorption isotherm. Regression square (R^2) values for the various isotherms are listed in Table 4.33.

The obtained plots of the inhibitors are linear with correlation coefficient higher than 0.99. The intercept permits the calculation of the equilibrium constant b which are 27.0 M^{-1} , and 10.8 M^{-1}

for, SAL2AP and CeSAL2AP, respectively. The values of b which indicate the binding power of the inhibitor to the steel surface can lead to calculate the adsorption energy. Values of G_{ads} = −16.6 kJ mol−1, and, −14.8 kJ mol^{-1}. The negative value of G_{ads} means that the adsorption of the inhibitors on mild steel surface is a spontaneous process, and furthermore the negative values of G_{ads} also show the strong interaction of the inhibitor molecule onto the mild steel surface. Generally, values of Gads around −20 kJ mol^{-1} or lower are consistent with the electrostatic interaction between the charged molecules and the charged metal (physisorption). Those more negative than −40 kJ mol^{-1} involve charge sharing or transfer from the inhibitor molecules to the metal surface to form a coordinate type of bond (chemisorption) . For investigate inhibitors, it is observed that the calculated G_{ads} values, were below −20 kJ mol^{-1}, indicating that the adsorption mechanism of the both inhibitors on mild steel in 1 M HCl solution was typical of physisorption.

4.2.1.5 Surface Analysis using AFM

Figures 4.34(a) – 4.34(f), show the 2D and 3D AFM diagrams for blank, Schiff base SAL2AP with its metal complex CeSAL2AP. Table 4.39 shows the AFM data for Sq, Sp, and Sv.

The RMS roughness (Sq) values provide a quantitative value that describes the overall surface texture or roughness. A higher Sq indicates a rougher surface while a lower Sq suggests a smoother surface. Maximum peak height (Sp) refers to the height of the tallest peak in a given measurement area relative to the mean plane of the surface. Sp value provides insight into the presence of features such as spikes and protrusions. A high Sp value may indicate defects or irregularities that could compromise a material's performance which in turn signifies higher pits value (Sv), which also indicates the extent of corrosion. The order of the values of the Sq, Sp, and Sv of the blank, the Schiff bases with their metal complexes correlates with the order of their inhibition efficiencies based on the weight loss experiment

4.2.1.6 Electrochemical Studies

4.2.1.6.1 Analysis of the results of Potentiodynamic polarization studies

The Potentiodynamic polarization curve of mild steel immersed in acid solution. The presence and absence of SAL2AP and CeSAL2AP is given in Figure 4.35. The PDP corrosion parameters of carbon steel immersed in the presence and absence of 0.8 mmol/dm3 of the two inhibitors in 1M HCl are given in Table 4.40. When mild steel is immersed in acidic medium without inhibitor the corrosion potential (Ecorr) is -467.06 mV Vs SCE and the corrosion current is 543.58(uA/cm^2). When the additives were added to the acidic medium the Ecorr value is found to be -496.58 Vs SCE in the medium containing CeSAL2AP and -481.03 mV Vs SCE in the medium containing

SAL2AP. The icorr decreased to 282.65 uA/cm^2 with CeSAL2AP and to 364.83 uA/cm2 with SAL2AP. The decrease in the corrosion current values indicates that the compounds functions as inhibitors and reduces the corrosion of mild steel in acidic medium. The shift in the Ecorr value to a less negative value and the changes in the cathodic and anodic slopes shows that the inhibitor controls both the cathodic and anodic reactions and behaves as mixed inhibitor. The effect of complexation is observed in an enhanced inhibition efficiency, IE PDP due to addition of the Schiff base metal complex CeSAL2AP (48.02 %), compared to that of the Schiff base SAL2AP (32.90%). PDP parameters, namely, corrosion potential (E_{corr}), anodic and cathodicTafel slopes (b_a and b_c), corrosion current (i_{corr}), and polarization resistance (Rp) obtained by extrapolation of the polarization curves. The inhibition percentage calculated from I_{corr} and R_p are given by equations 4.2 and 4.3

$$E\text{Icorr} = (I\text{corr}' - I\text{corr}) \times 100/I\text{corr}' \quad (4.2)$$

$$E_{Rp} = (Rp - Rp') \times 100/Rp \quad (4.3)$$

Where *Icorr'* and *Rp'*are respectively the corrosion current and the polarization resistance in the absence of inhibitor; *Icorr* and *Rp* are respectively the corrosion current and the polarization resistance in the presence of inhibitor.

4.2.1.6.2 Analysis of the Results of EIS Studies

The EIS spectrum (Niquisit plot) of carbon steel immersed in 1M HCl containing the inhibitor is shown in Figure 4.36. Table 4.41 contains the impedance parameters namely, charge transfer resistance and the double layer capacitance.

The double layer capacitance and EIS inhibitory efficiency were calculated using Equations (4.4) and (4.5) respectively (Yadav, et al., 2015; Khalissa et al., 2018):

$$C_{\text{dl}} = Q2^{\frac{1}{a2}}.Rct^{\left(\frac{1-a2}{a2}\right)} \quad (4.4)$$

Where C_{dl} = double layer capacitance. $Q = \text{Constant Phase Element (CPE)}$, $a2$ = CPE exponent,

Rct = Charge Transfer Resistance.

$$IE_{\text{EIS}}(\%) = \left(\frac{R_{\text{ct}} - R_{\text{ct}}^{\circ}}{R_{\text{ct}}}\right) \times 100 \quad (4.5)$$

Where Rct° and Rct are the charge transfer resistances without and with inhibitor, respectively.

According to Table 4.41, the values of Rct increase, and those of Cdl decrease with the addition of the inhibitors to the corrosive solution. This can be ascribed to the formation of a protective layer at the metal/acid interface, thus decreasing the direct contact between the mild steel and the aggressive solution (Mohamed et al., 2018; Ansari, et al.2019). In addition to this, the increasing value of the inhibition efficiency in the presence of inhibitors further supports the protection ability of the inhibitors, with CeSAL2AP recording a higher inhibition efficiency of 82.21% compared to SAL2AP with IE value of 60.32%.

4.1.3 Physical Measurements for SALPD and CeSALPD

Table 4.43: Physical Properties, Percentage Yield, and Elemental Analysis of SALPD and CeSALPD

Compounds	**Molecular Formular**	**Colour**	**pH**	**Yield**	**Melting point**	**Molecular Composition**		
						C	**H**	**N**
SALPD	$C_{20}H_{16}N_2O_2$	Orange	6	74	150-155	77.59 (77.01)	4.97 (4.99)	8.52 (8.36)
CeSALPD	$C_{40}H_{30}CeN_4O_5$	Brown	3	54	178-180	61.21 (61.06)	4.01 (3.84)	7.23 (7.12)

Table 4.42 shows the variation in colour, PH, percentage yield, melting point, and molecular compositions of the synthesized Schiff base SALPD, and its cerium metal complex, CeSALPD. The difference in colour, PH, and melting point shows successful synthesis of the compounds

Table 4.44: Solubility Tests for SALPD and CeSALPD in different Organic Solvents

COMPOUNDS	**SOLVENTS**						
	DI H_2O	ETHANOL	METHANOL	ACETONE	CARBONTET	DMF	DMSO
SALPD	N/S	N/S	N/S	N/S	S/S	S	S

CeSALPD	N/S	N/S	N/S	N/S	N/S	S	S

N/S= non- soluble, S= soluble

The solubility tests of the synthesized compounds in various organic solvents shows that both compounds are observed to be soluble in DMF, and DMSO.

Table 4.45: Molar Conductivity and Magnetic Susceptibility of SALPD and CeSALPD in DMSO and DMF

Compound	**Molecular formular**	**Molecular weight (g/mol)**	**Molar Conductivity (mS/cm)**		**Magnetic susceptibility (Assignment)**
			DMSO	**DMF**	
SALPD	$C_{20}H_{16}N_{2O}$	316.12	3.44x10-3	$5.11x10^{-3}$	-
CeSALPD	$C_{40}H_{30}CeN_4O_5$	786.82	0.41	0.29	015 (paramagnetic)

The Schiff base SALPD shows a much lower conductivity values compared to CeSALPD. CeSALPD shows value for magnetic susceptibility for paramagnetic compounds, SALAN recorded no magnetic susceptibility value.

4.1.4 Spectral Results

Spectroscopic measurements employed for this present study included: Uv-Visible spectroscopy, FTIR, 1H-NMR, 13-C NMR, and EDXRF. The characterization of the compounds by spectral methods is vital for the structural elucidation of the compounds under study as well as spatial orientation of the bonded atoms.

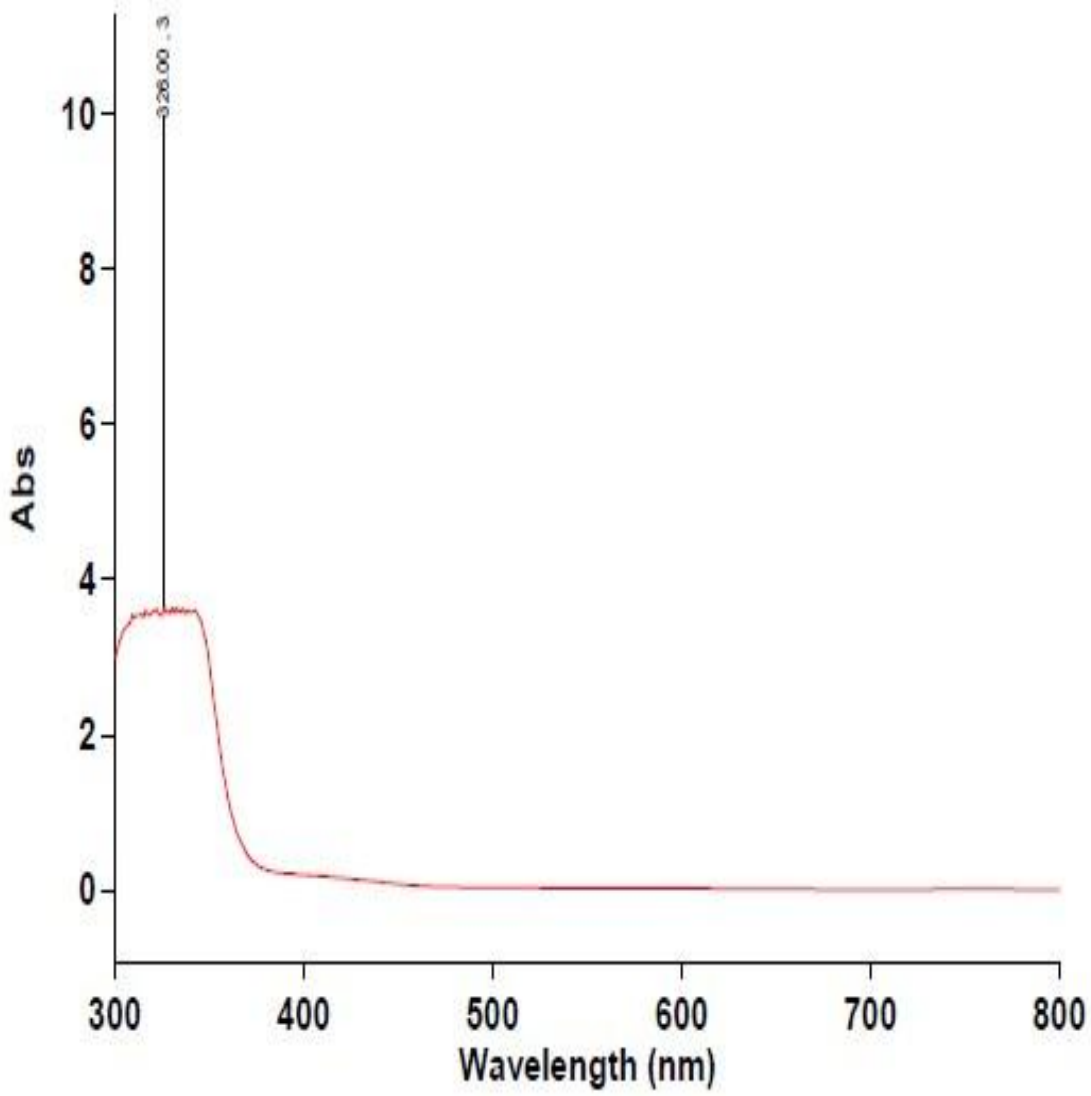

Figure 4.37: UV- VIS Spectrum of SALPD

The maximum absorbance was observed at 326 nm, corresponding to an $n \rightarrow \pi^*$ transition. This transition arises from the excitation of non-bonding electrons on the nitrogen atom of the azomethine group to the anti-bonding π^* orbital.

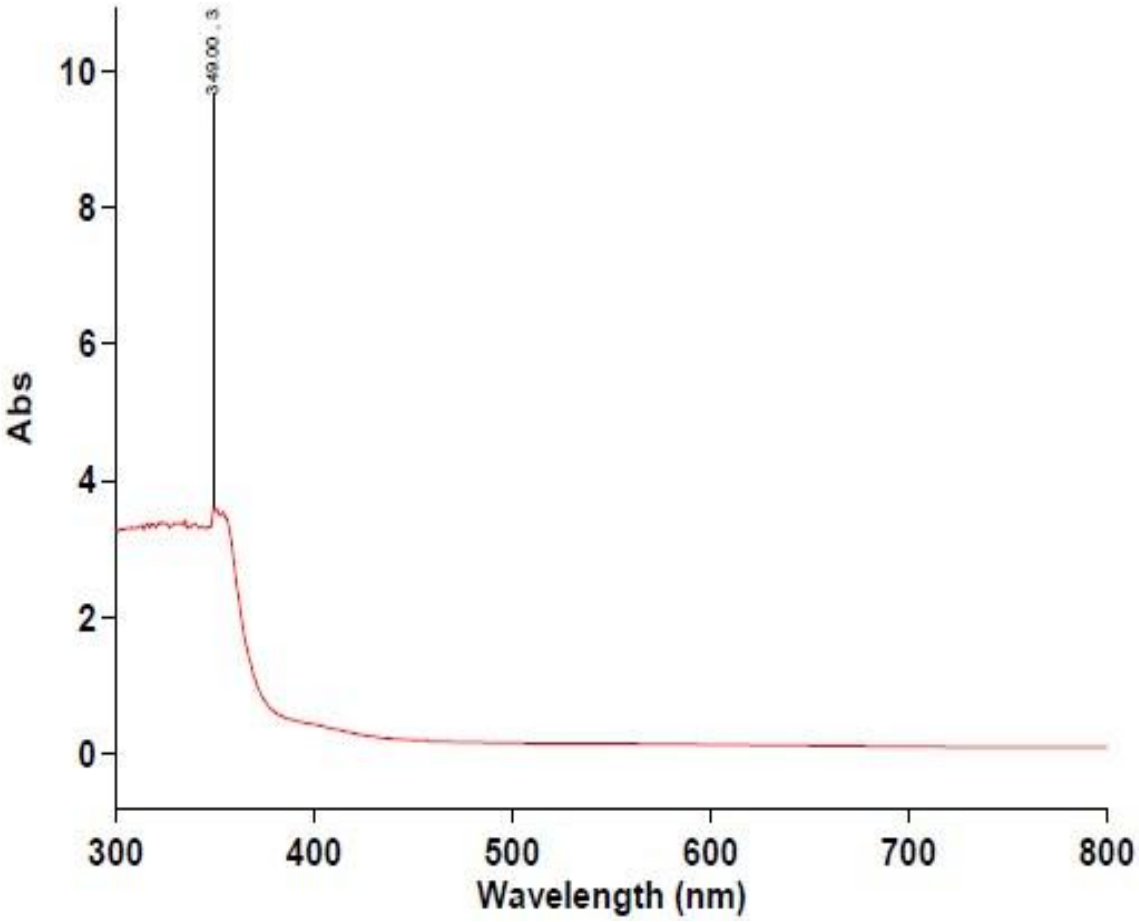

Figure 4.38: UV-VIS. SPECTRUM OF CeSALPD

Maximum Absorbance of CeSALPD occurred at 349 nm which confirms the formation of the complex.

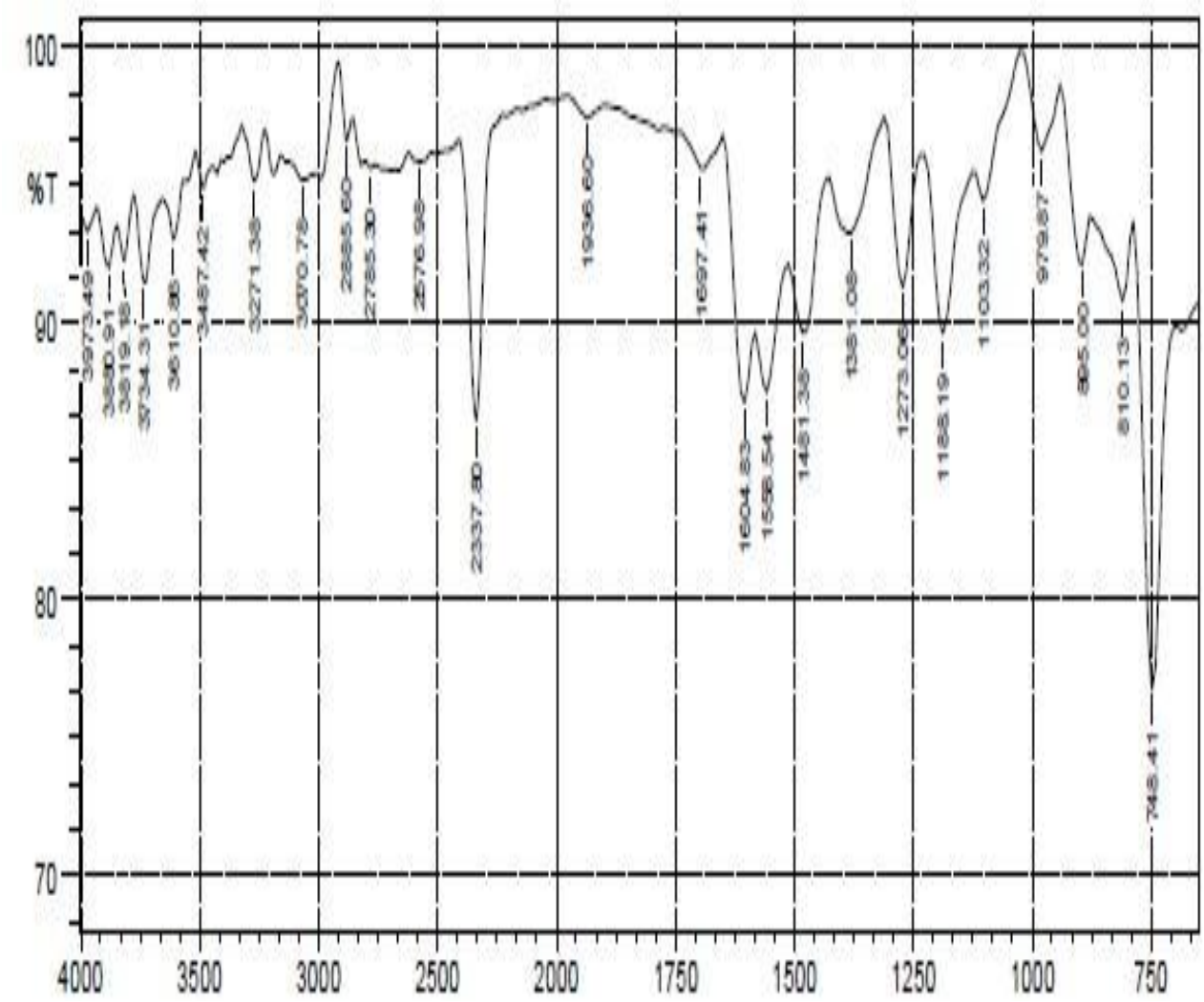

Figure 4.39: Furia Transform Infrared (FTIR) Spectrum of SALPD

Frequencies due to the following vibrations were detected: v(C-O) at 1273 cm^{-1} , v(OH) at 3487 cm^{-1} , and v(CH=N) at 1697 cm^{-1}.

These characteristics frequencies show successful synthesis of the Schiff base SALPD.

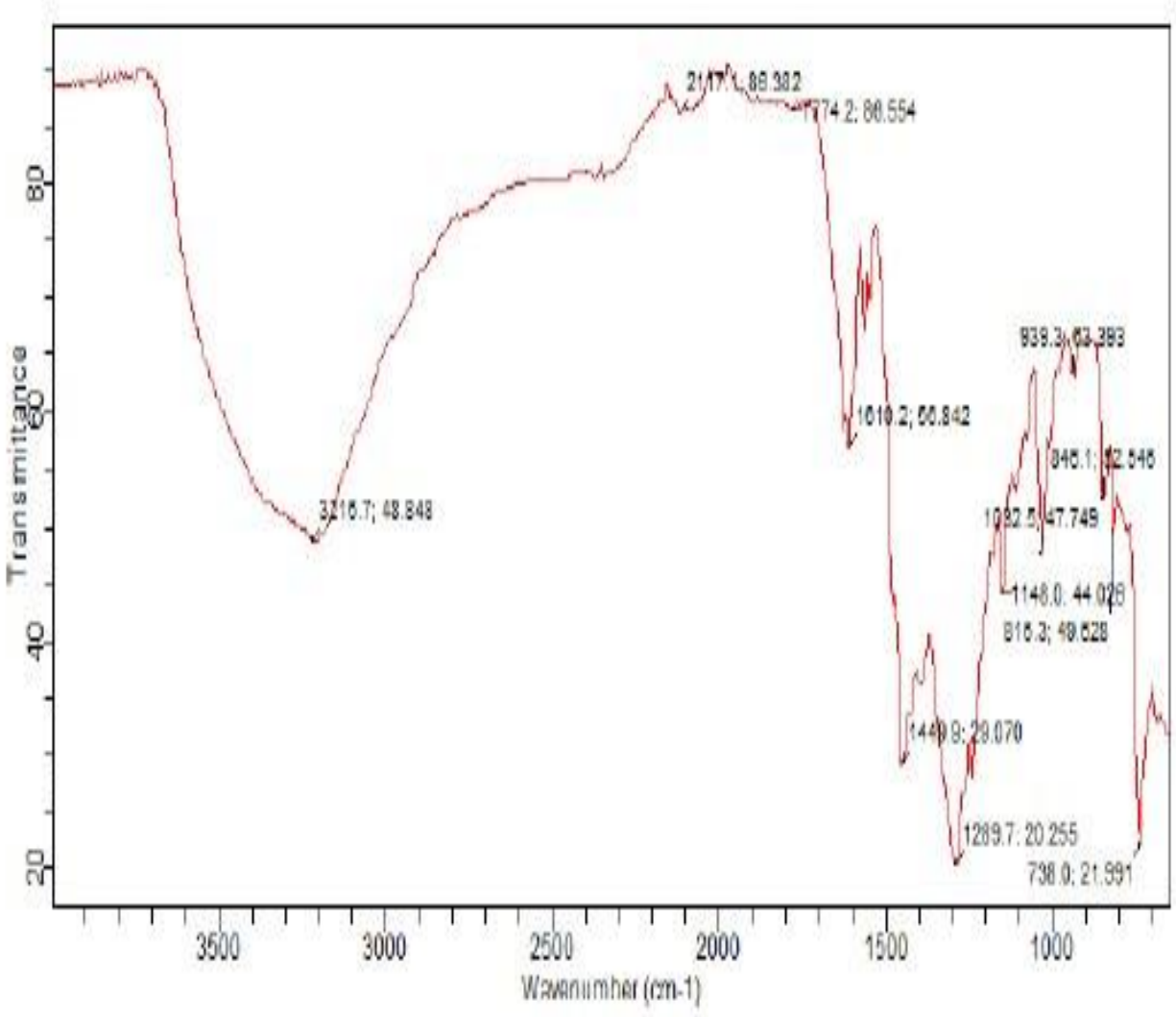

Figure 4.40: Fourier Transform Infrared (FTIR) Spectrum of CeSALPD

FTIR of CeSALPD showed the following vibrational frequencies: v (H_20) at 3216 cm^{-1}, V(NO_3) at 1449 cm^{-1}, v(M-O) at 738 cm^{-1}, v(C-O) at 1273 cm^{-1}, v(HC=N) at 1610 cm^{-1}. These characteristics frequencies show successful synthesis of the Schiff base metal complex CeSALPD.

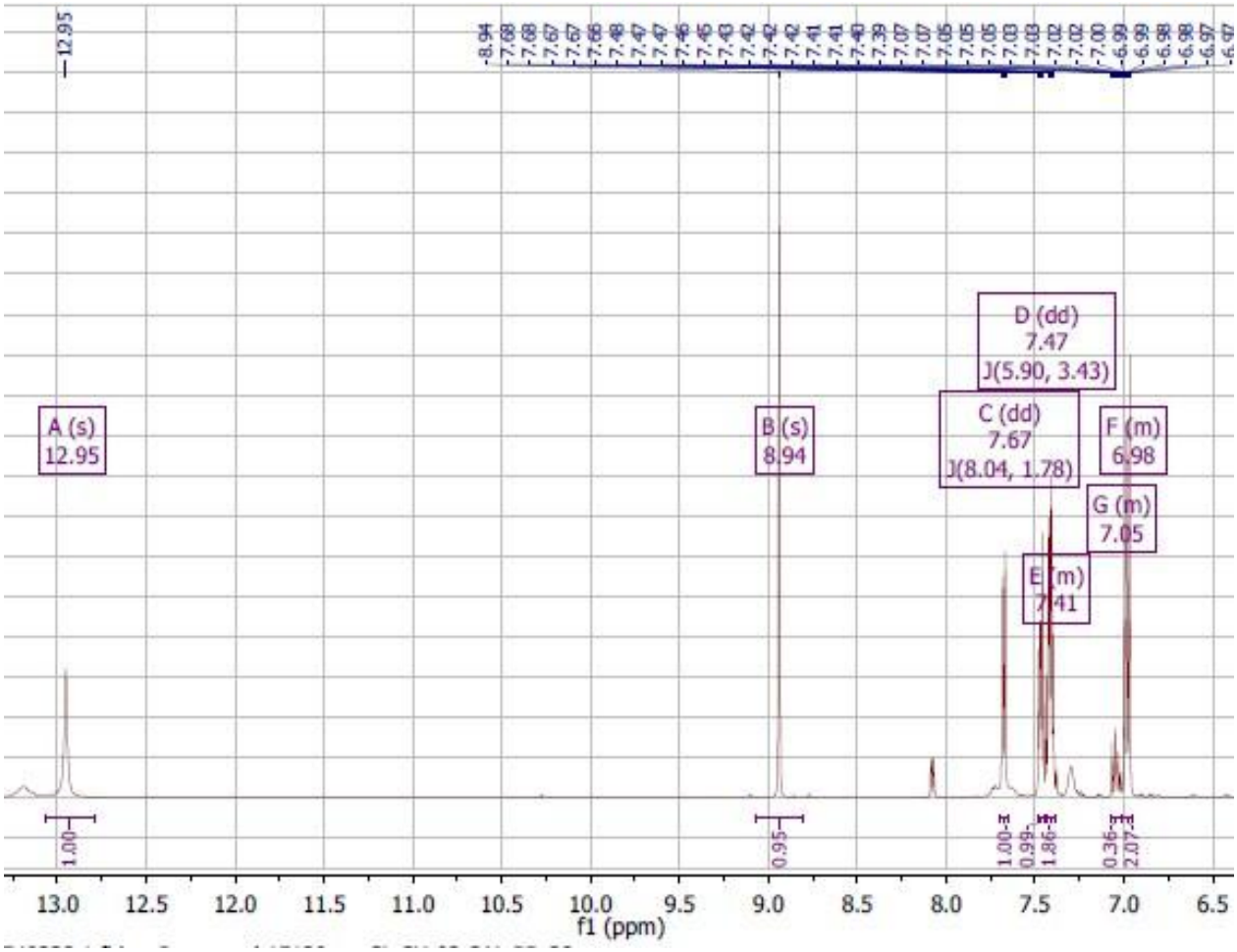

Figure 4.41: Proton NMR (^{1}H- NMR) Spectrum of SALPD

The key signals exhibited by ^{1}H-NMR spectra of SALPD are due to (HC=N) proton at δ 8.94 ppm, and hydroxyl (OH) proton of the aldehyde moiety at δ12.95 ppm.

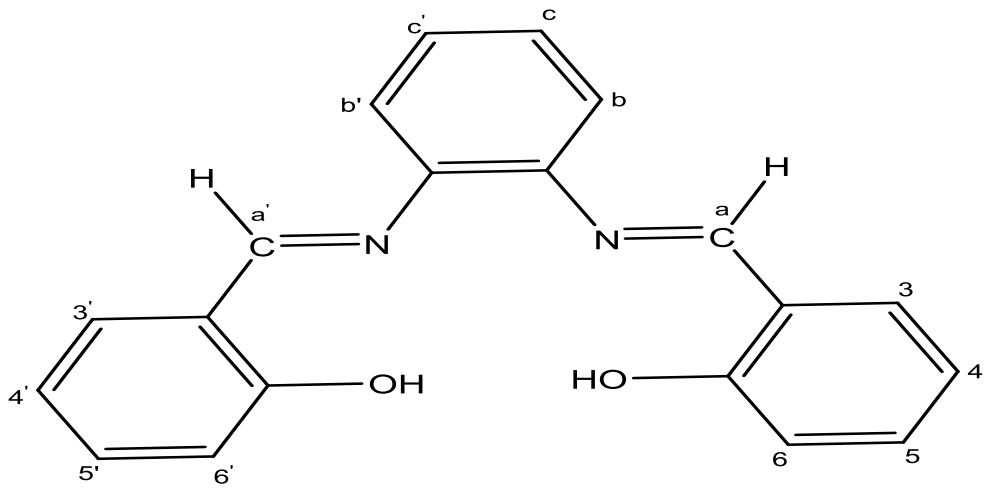

PROTON NUMBERING IN SALPD

Figure 4.42: Proton numbering in SALPD

Table 4.46: ^{1}H NMR Spectral Data of SALPD

Compound	Chemical Shift (δ) ppm	Assignment
SALPD	8.94	(s, 2H, HC=N)
	12.95	(s, 2H, OH)
	6.98 – 6.97	(m, 2H, H_5 H_5^I)
	7.05 – 7.00	(m, 6H, C, C^1, H_4, H_4^I, H_6, H_6^I)
	7.41- 7.03	(m, 4H, b, b^1, H_3, H_3^I)

Table 4.46 shows chemical shifts for various proton- signals in the SALPD Schiff base, which identifies the Schiff base.

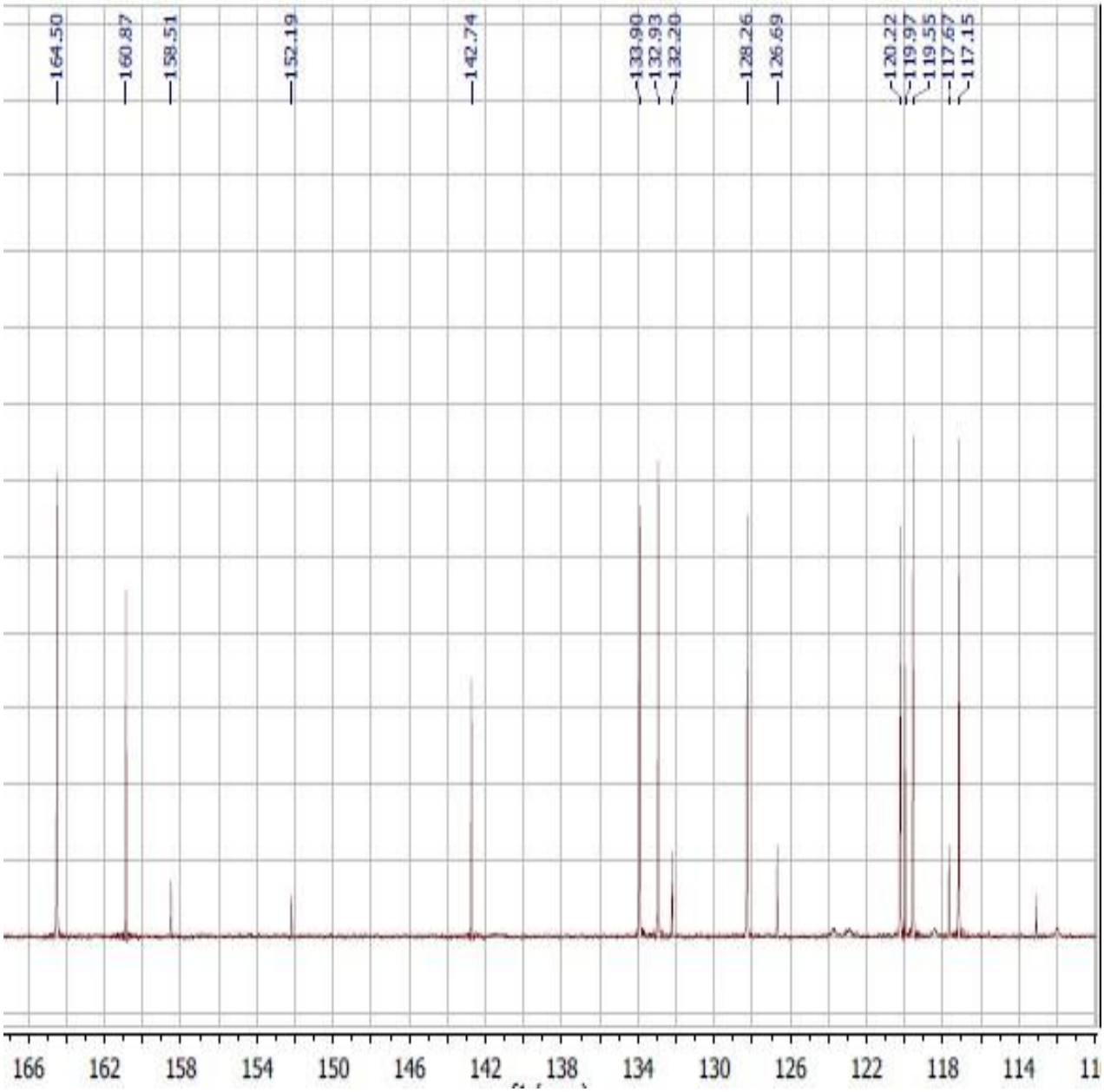

Figure 4.43: Carbon-13 (C-13) NMR OF SALPD

The signal due to carbon atom of the azomithine group occurred at 164.50 ppm. This confirms the successful synthesis of the Schiff base SALPD.

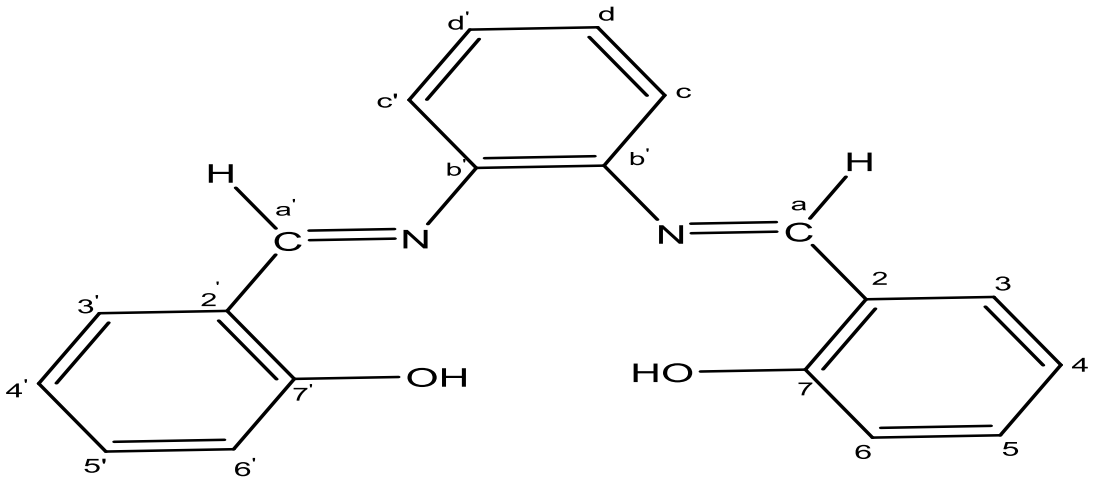

CARBON NUMBERING IN SALPD

Figure 4.44: Carbon numbering in SALPD

Table 4.47: C-13 NMR Data of SALPD

Compound	Chemical Shift (δ) ppm(Assignment)
SALPD	117.67(C_6,C_6^I),119.55(C_2,C_2^I),120.22(C_4,C_4^I), 126.69(C,C^1),128.26(d,d^I),132.20(C_3,C_3^I)132.93(C_5,C_5^I),133.90(b,b^I), 160.87(C_7,C_7^I), 164.50(a, a^I)

The spectra data in table 4.47 shows chemical shifts due to various constituent protons in SALPD Schiff base.

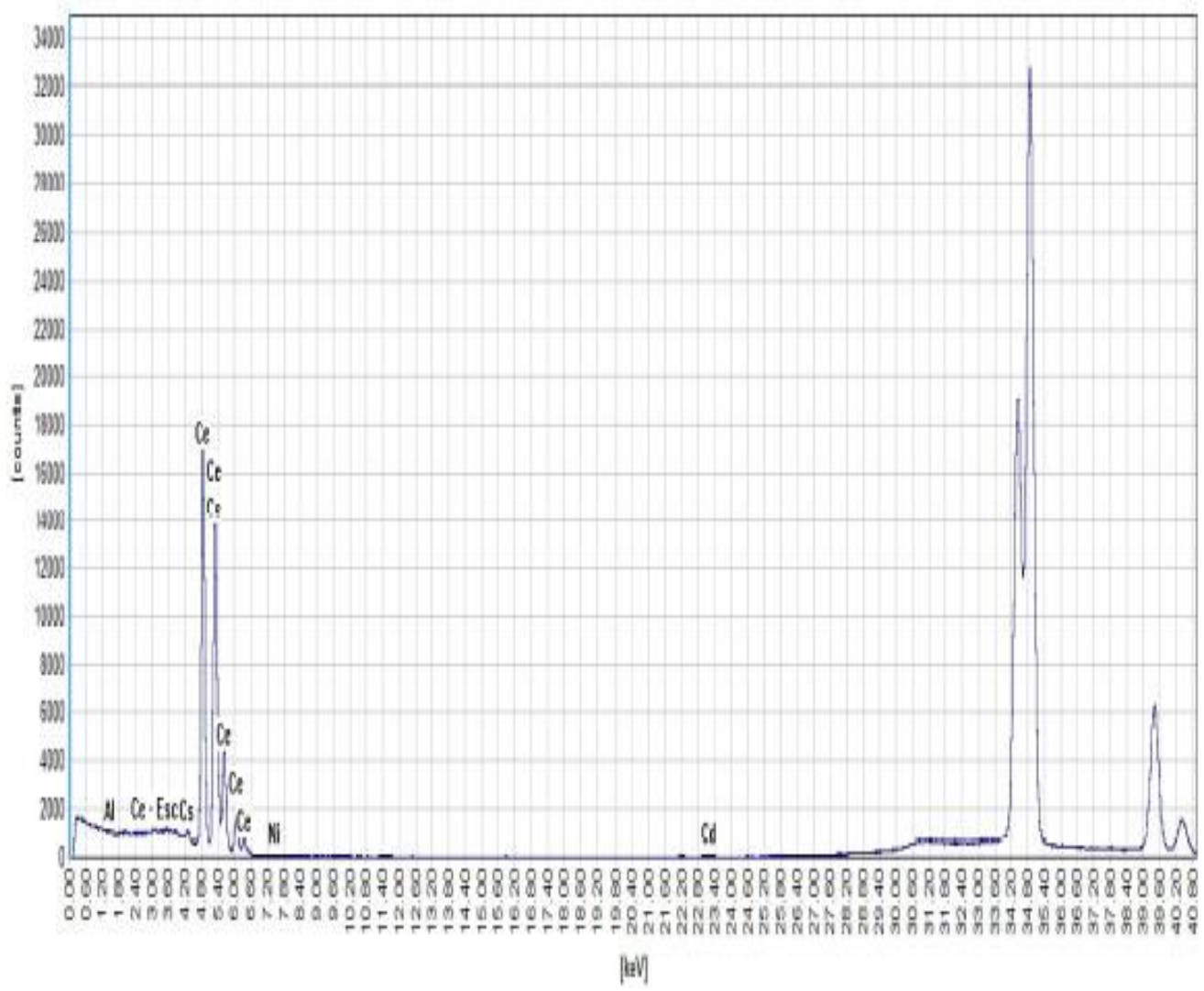

Figure 4.45: Energy Dispersive X-Ray Fluorescence (EDXRF) OF CeSALPD

CeSALPD displayed the highest cerium composition at 83.24%, with a peak intensity of 62,497 cps/MA, also within the 6.60–4.80 keV energy range for detection of cerium.

4.1.5 Inhibitive Action of SALPD and CeSALPD.

4.1.5.1 Gravimetric Results

Table 4.48: Gravimetric data of Mild Steel in 1M HCl in the presence and absence of SALPD (Lagmuir Adsorption Isotherm)

System (mmol dm^3)	C_R(mdd)	IE%	θ	C/θ
1 $x10^{-1}$	1.94	51.19	0.51	0.20
2 $x10^{-1}$	1.56	60.84	0.61	0.33
4 $x10^{-1}$	0.94	76.47	0.77	0.52
6 $x10^{-1}$	0.82	79.46	0.80	0.75
8 $x10^{-1}$	0.78	81.17	0.81	0.99
12 $x10^{-1}$	0.69	82.74	0.83	1.45
16 $x10^{-1}$	0.86	78.23	0.78	2.05
20 $x10^{-1}$	0.88	77.80	0.78	2.56

Corrosion rate C_R decreases with increase in concentration, surface coverage **θ** and Inhibition Efficiency IE.

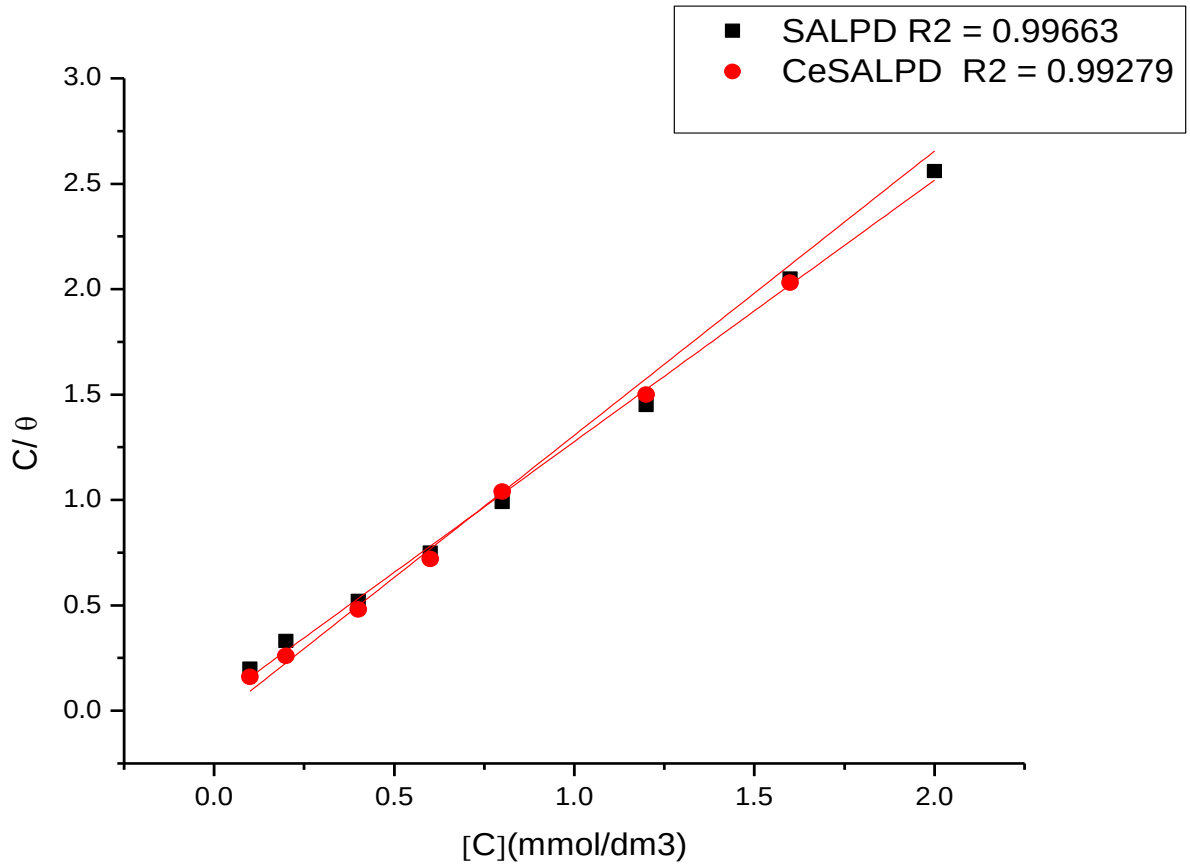

Figure 4.46: Langmuir's Adsorption Plots for mild steel in 1 M HCl containing various concentrations of SALPD and CeSALPD

Table 4.49: Gravimetric data of Mild Steel in 1M HCl in the presence and absence of SALPD (Temkin Adsorption Isotherm)

System (mmol dm^3)	C_R(mdd)	IE%	θ	θ /C	log(θ /C)
1 $x10^{-1}$	1.94	51.19	0.51	5.10	0.71
2 $x10^{-1}$	1.56	60.84	0.61	3.05	0.48
4 $x10^{-1}$	0.94	76.47	0.77	1.93	0.29
6 $x10^{-1}$	0.82	79.46	0.80	1.33	0.12
8 $x10^{-1}$	0.78	81.17	0.81	1.01	0.004
12 $x10^{-1}$	0.69	82.74	0.83	0.69	-0.16
16 $x10^{-1}$	0.86	78.23	0.78	0.49	-0.31
20 $x10^{-1}$	0.88	77.80	0.78	0.39	-0.41

Corrosion rate C_R decreases with increase in Concentration, Surface Coverage θ and Inhibition Efficiency IE.

Table 4.50: Gravimetric Data of Mild Steel in 1M HCl in the presence and absence of SALPD (Frumkin's Adsorption Isotherm)

System (mmol dm^3)	C_R(mdd)	IE%	θ	(1-θ)C	$\frac{\theta}{(1-\theta)C}$	$\frac{log\ \theta}{(1-\theta)C}$
1 $x10^{-1}$	1.94	51.19	0.51	0.049	10.41	1.0175
2 $x10^{-1}$	1.56	60.84	0.61	0.078	7.82	0.8932
4 $x10^{-1}$	0.94	76.47	0.77	0.092	8.37	0.9227
6 $x10^{-1}$	0.82	79.46	0.80	0.120	6.67	0.8241
8 $x10^{-1}$	0.78	81.17	0.81	0.152	5.33	0.7267
12 $x10^{-1}$	0.69	82.74	0.83	0.204	4.07	0.6096
16 $x10^{-1}$	0.86	78.23	0.78	0.352	2.22	0.3464
20 $x10^{-1}$	0.88	77.80	0.78	0.440	1.77	0.2480

Corrosion rate C_R decreases with increase in Concentration, Surface coverage **θ** and Inhibition Efficiency, IE.

Table 4.51: Gravimetric Data of Mild steel in 1M HCl in the presence and absence of CeSALPD (Langmuir's Isotherm)

System (mmol/dm3)	Corr. Rate	IE%	(θ)	C/θ
$1x10^{-1}$	1.55	61.09	0.61	0.16
$2\ x10^{-1}$	0.96	75.76	0.76	0.26
$4\ x10^{-1}$	0.68	82.95	0.83	0.48
$6\ x10^{-1}$	0.69	82.63	0.83	0.72
$8\ x10^{-1}$	0.92	76.67	0.77	1.04
$12\ x10^{-1}$	0.82	79.50	0.80	1.50
$16\ x10^{-1}$	0.85	78.74	0.79	2.03
$20\ x10^{-1}$	1.12	71.85	0.72	2.78

Corrosion rate $\mathbf{C_R}$ decreases with increase in Concentration, Surface Coverage, **θ** and Inhibition Efficiency, IE.

Table 4.52: Gravimetric Data of Mild Steel in 1M HCl in the presence and absence of CeSALPD (Temkin's Isotherm)

System (mmol/dm3)	Corr. Rate	IE%	(θ)	θ/C	log(Θ/C)
$1x10^{-1}$	1.55	61.09	0.61	6.10	0.79
$2\ x10^{-1}$	0.96	75.76	0.76	3.80	0.58
$4\ x10^{-1}$	0.68	82.95	0.83	2.08	0.32
$6\ x10^{-1}$	0.69	82.63	0.83	1.38	0.14
$8\ x10^{-1}$	0.92	76.67	0.77	0.96	-0.02
$12\ x10^{-1}$	0.82	79.50	0.80	0.66	-0.18
$16\ x10^{-1}$	0.85	78.74	0.79	0.49	-0.31
$20\ x10^{-1}$	1.12	71.85	0.72	0.36	-0.44

Table 4.53: Gravimetric data of Mild Steel in 1M HCl in the presence and absence of CeSALPD (Frumkin's Isotherm)

System (mmol/dm^3)	Corr. Rate	IE%	θ	(1-θ) C	$\frac{\theta}{(1-\theta)C}$	$\frac{Log\ \theta}{(1-\theta)C}$
1x10^{-1}	1.55	61.09	0.61	0.039	15.64	1.1942
2 x10^{-1}	0.96	75.76	0.76	0.048	15.83	1.1995
4 x10^{-1}	0.68	82.95	0.83	0.068	12.21	1.0867
6 x10^{-1}	0.69	82.63	0.83	0.102	8.14	0.9106
8 x10^{-1}	0.92	76.67	0.77	0.184	4.18	0.6212
12 x10^{-1}	0.82	79.50	0.80	0.240	3.33	0.5224
16 x10^{-1}	0.85	78.74	0.79	0.336	2.35	0.3711
20 x10^{-1}	1.12	71.85	0.72	0.560	1.29	0.1106

Corrosion rate C_R decreases with increase in Concentration, Surface Coverage **θ** and Inhibition Efficiency IE.

Table 4.54: Regression Square values obtained for Langmuir, Temkin, and Frumkin adsorption isotherms.

Compound	R^2 Langmuir	R^2 Temkin	R^2 Frumkin
SALPD	0.99663	-0.14489	0.19143
CeSALPD	0.99279	0.02616	0.14664

Langmuir isotherm model with regression square value up to 0.99 is the model that perfectly fits the adsorption process.

Table 4.55: Influence of concentration on the inhibition efficiency of SALPD and CeSALPD during Mild Steel corrosion in 1M HCl after 24-hour immersion.

System (mmol/dm^3)	C_R SALPD	SALPD, IE%	C_R CeSALPD	CeSALPD, IE%
$1x10^{-1}$	1.94	51.19	1.55	61.09
$2\ x10^{-1}$	1.56	60.84	0.96	75.76
$4\ x10^{-1}$	0.94	76.47	0.68	82.95
$6\ x10^{-1}$	0.82	79.46	0.69	82.63
$8\ x10^{-1}$	0.78	81.17	0.92	76.67
$12\ x10^{-1}$	0.69	82.74	0.82	79.50
$16\ x10^{-1}$	0.86	78.23	0.85	78.74
$20\ x10^{-1}$	0.88	77.80	1.12	71.85

IE increases with increase in Concentration, and optimum IE of 82.74 % was recorded for SALPD at 1.2 mmol/dm^{3,} and CeSALPD IE of 82.95 % at lower concentration of 0.4 mmol/ dm^3.

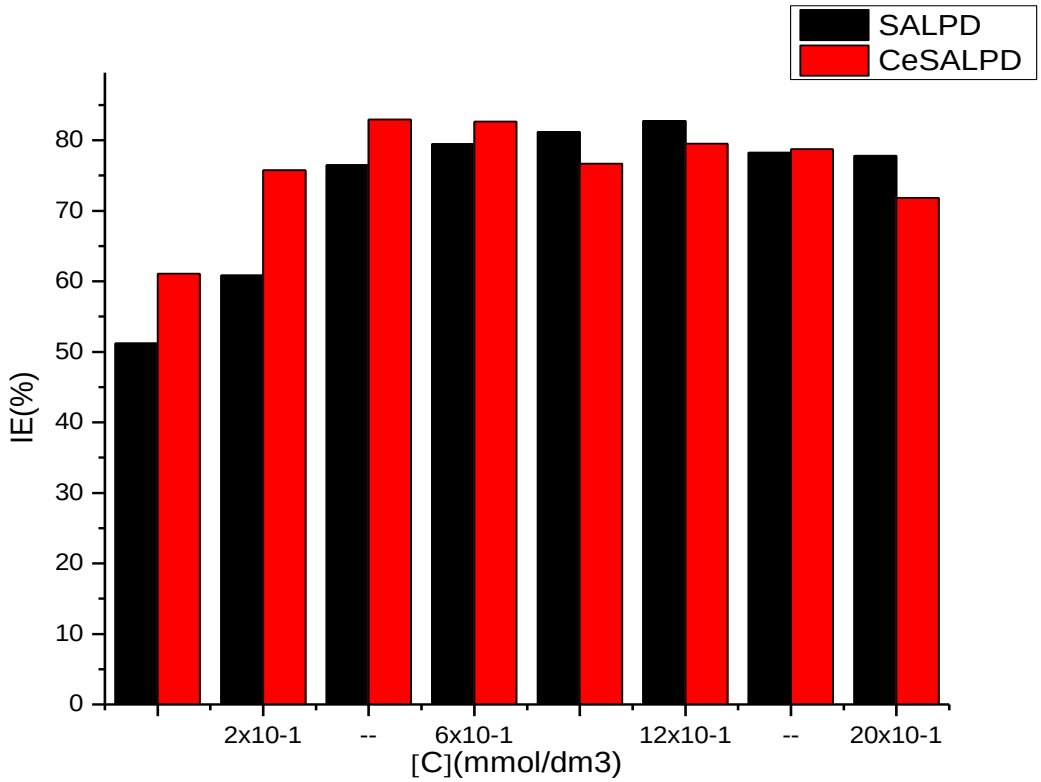

Figure 4.47: Effect of Concentration on the Inhibition Efficiency of SALPD and CeSALPD during Mild Steel Corrosion in 1M HCl after 24-hour immersion

CeSALPD (red bars) consistently shows higher IE% compared to SALPD (black bars) from concentrations of 0.1 to 0.6 mmol/dm^3.

4.1.5.2: Effect of temperature on the performance of the inhibitors

Table 4.56: Effect of Temperature on the inhibition efficiency of SALPD and CeSALPD at optimum concentration

T (K)	I/T (K)	C_R BLANK	logC_R BLANK	C_R SALPD	logC_R SALPD	IE SALPD	C_R CeSALPD	logC_R CeSALPD	IE CeSALPD
303	0.0033	3.981	0.600	0.690	0.1612	82.74	0.664	-0.1778	83.32
313	0.0032	13.419	1.127	4.715	0.6735	64.87	4.160	0.6191	68.96
323	0.0031	13.437	1.128	4.926	0.6925	63.34	4.489	0.6521	66.59
333	0.0030	22.793	1.358	8.556	0.9323	62.46	7.648	0.8835	66.45
343	0.0029	54.270	1.735	21.133	1.3250	61.06	18.333	1.2632	66.22

Table 4.55 shows relationship between inverse of temperature (I/T) with log C_R of BLANK (uninhibited system), and systems inhibited with SALPD and CeSALPD. C_R decreases on addition of the inhibitors. However, a decrease in IE is observed with increasing temperature of the systems.

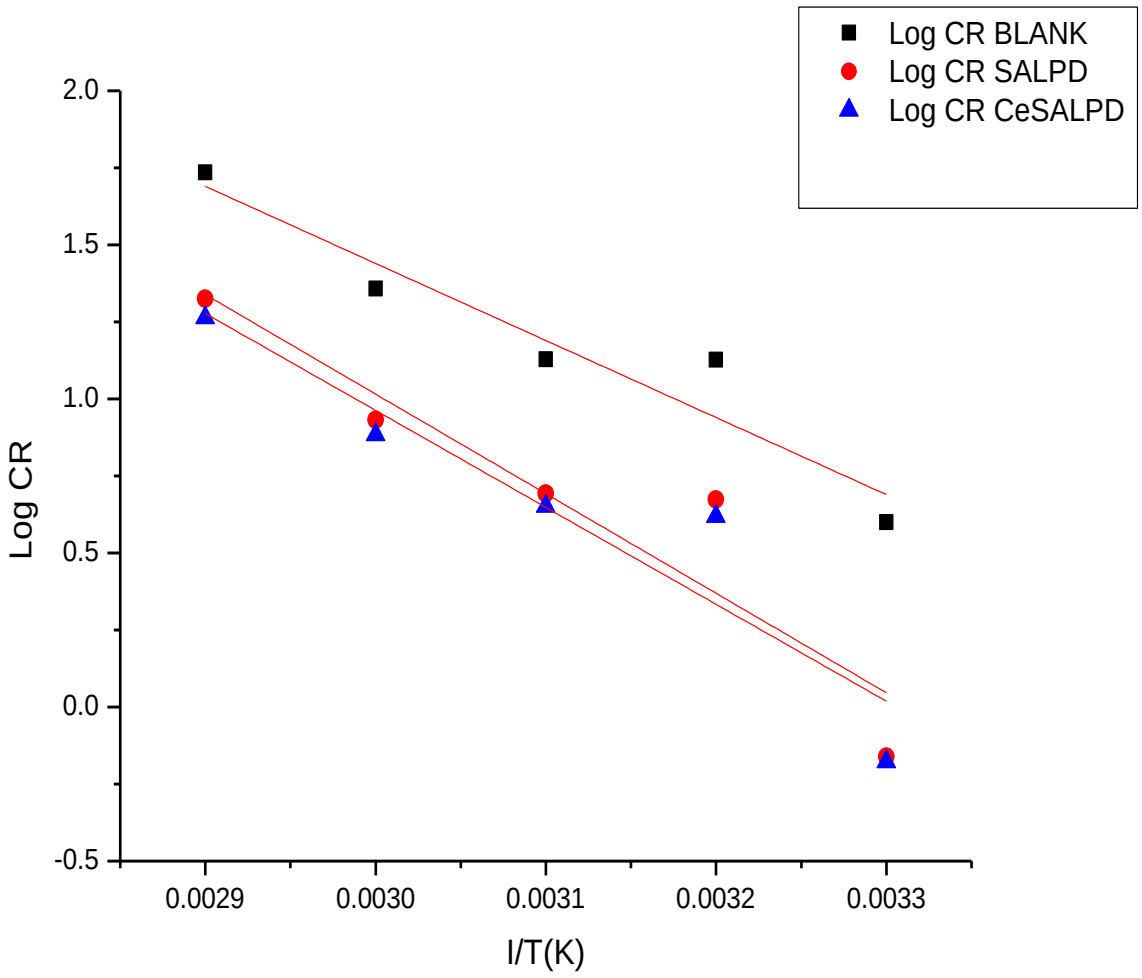

Figure 4.48: Arrhenius plots for Mild Steel in 1 M HCl solution free and inhibited by 0.8 mmol/dm^3 of the Inhibitors.

Tables 4.55 show data for log C_R vs 1/T for SALPD and CeSALPD. Activation energy (E_a) for corrosion of mild steel in the absence and presence of the inhibitors, SALPD and CeSALPD were calculated from slope of Arhenius equation log C_R = -Ea / 2.303 RT + A. Plot of log CR vs 1/T above gives a slope of –Ea/ 2.303 R, from which Ea is calculated.

Table 4.57: Corrosion Data of BLANK, SALPD and CeSALPD for plot of log CR/T vs 1/T

T(K)	1/T(K)	C_R BLANK (mdd)	C_R/T BLANK	log C_R/T BLANK	C_R SALPD (mdd)	C_R/T SALPD	log C_R/T SALPD	C_R CeSALPD (mdd)	C_R/T CeSALPD	log C_R/T CeSALPD
303	0.0033	3.981	0.0131	-1.8827	0.690	0.0023	-2.6383	0.664	0.0022	-2.6576
313	0.0032	13.419	0.0429	-1.3675	4.715	0.0151	-1.8210	4.160	0.0133	-1.701
323	0.0031	13.437	0.0416	-1.3809	4.926	0.0153	-1.8153	4.489	0.0139	-1.8570
333	0.0030	22.793	0.0684	-1.1649	8.556	0.0257	-1.5901	7.648	0.0230	-1.6383
343	0.0029	54.270	0.1582	-0.8008	21.133	0.0616	-1.2104	18.333	0.0534	-1.2725

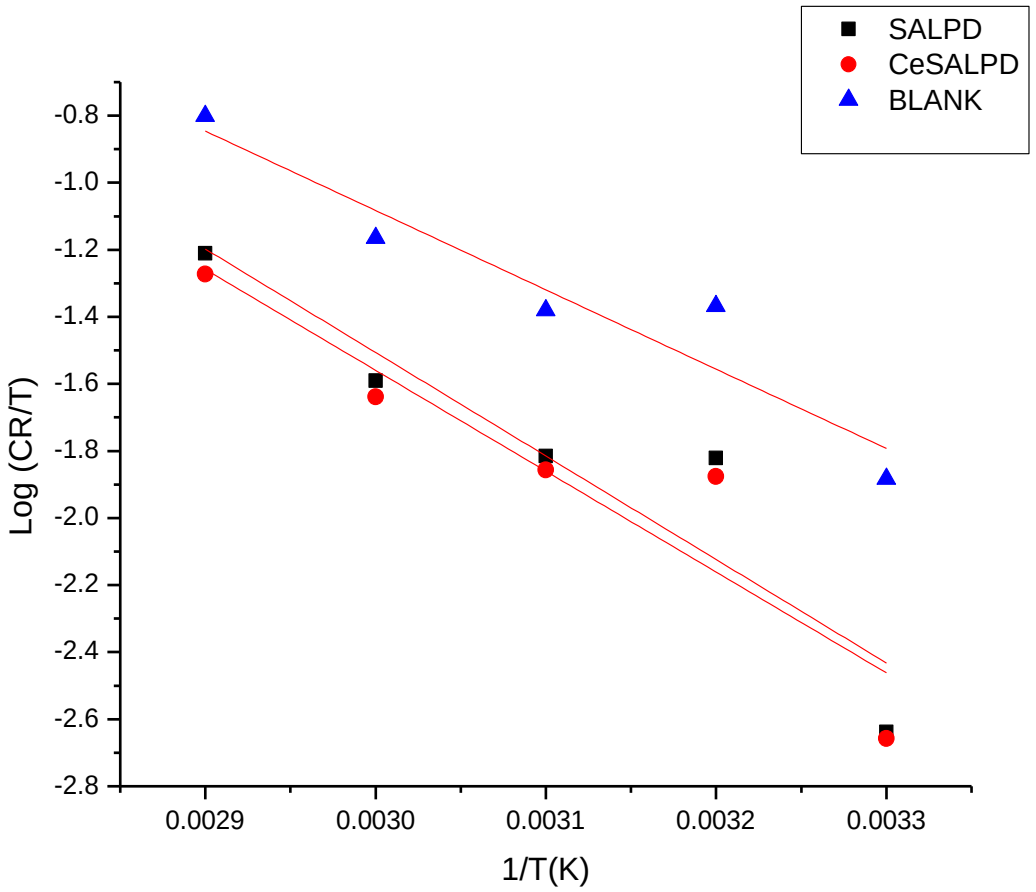

Figure 4.49: Plot of log (CR/T) Vs 1/T

Figure 4.49 above shows a plot of log C_R/T vs 1/T, derived from the relationship log C_R/T = [(logR/Nh) + (ΔS*/2.303 R) – Δ H*/2.303 RT]. Where h is plank's constant, 6.626 x 10^{-34}, N is equal to Avagadro's number, 6.02 x $10^{\cdot}$, S* is the entropy of activation, R is gas constant, T is temperature in Kelvin. The slope of the linear plot, –H* / 2.303R permits to derive the enthalpy of activation (H*), and an intercept of (log R/Nh) + (ΔS*/2.303 R) is used to calculate the entropy of the activation process, S*.

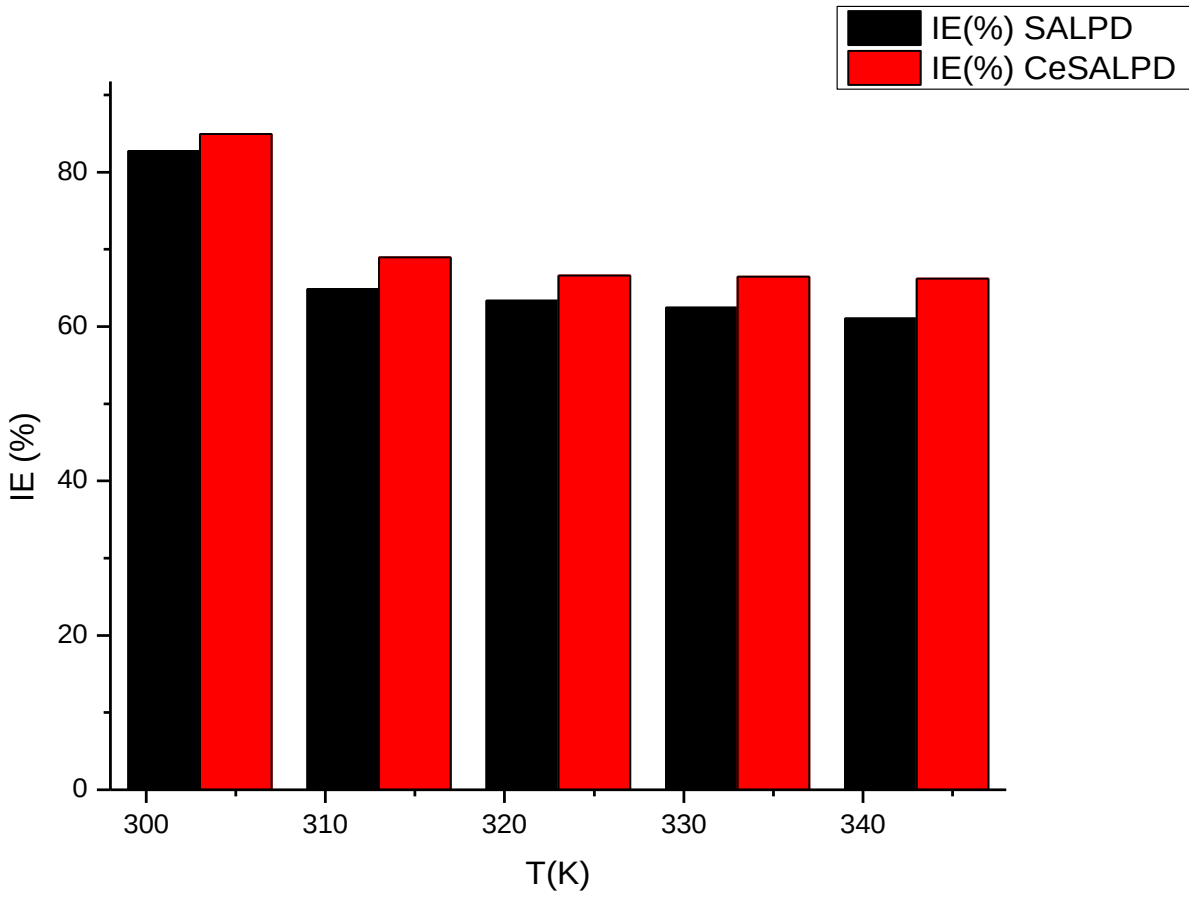

Figure 4.50: Effect of Temperature on the Inhibition Efficiency of the Compounds at the Optimum Concentration

The inhibition efficiency of the additives decreases remarkedly with increasing temperature, with CeSALPD outperforming the parent Schiff base SALPD at all temperatures, this observation is consistent with an enhanced corrosion inhibition with Schiff base metal complexes.

Table 4.58: Values for E_a, ΔG_{ads}, ΔH, and ΔS for Blank, SALPD and CeSALPD

System	Ea (KJ/Mol)	G_{ads}	ΔH KJ/ Mol	ΔS KJ/Mol
Blank	20.31	-	45.79	-82.38
SALPD	26.27	-17.86	59.48	-49.12
CeSALPD	26.16	-15.64	57.60	-54.66

Table 4.59: Effect of Immersion time on Inhibition Efficiency of SALPD and CeSALPD at Optimuim Concentration of Inhibitors

	COMPOUNDS IE (%)	
WEEK	SALPD	CeSALPD
1	63.20	77.15
2	37.20	45.90
3	32.40	41.00
4	30.80	37.30

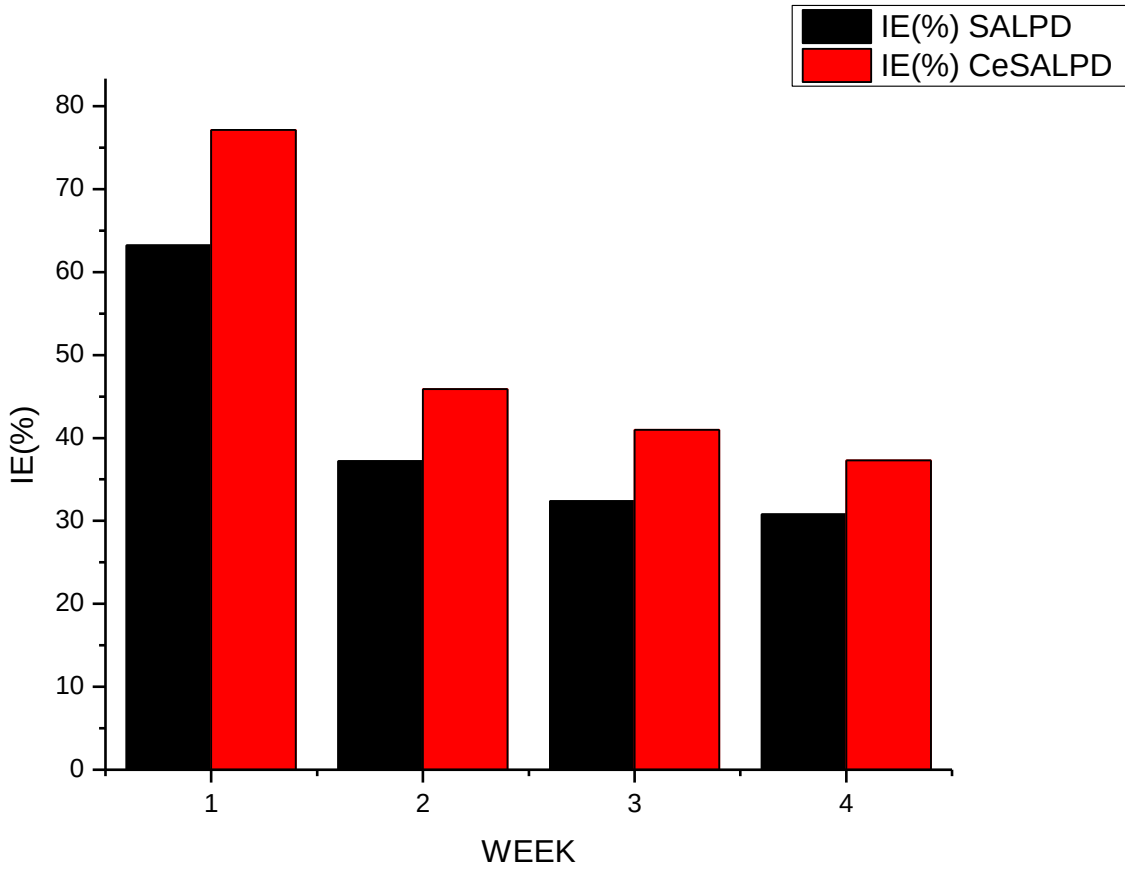

Figure 4.51: Variation of Inhibition Efficiency of SALPD, and CeSALPD with Immersion Time

It is found that that IE decreased with time suggesting that the inhibitors were physically adsorbed on the mild steel surface. Additionally, IE of the complex CeSALPD (red bar) was consistently above that of the parent Schiff base SALPD (black bar).

4.1.6 Surface Analysis Using AFM

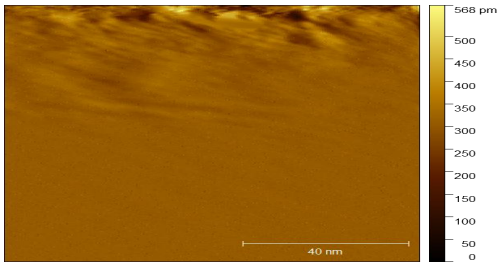

Figure 4.52: (a) 2D AFM FOR BLANK

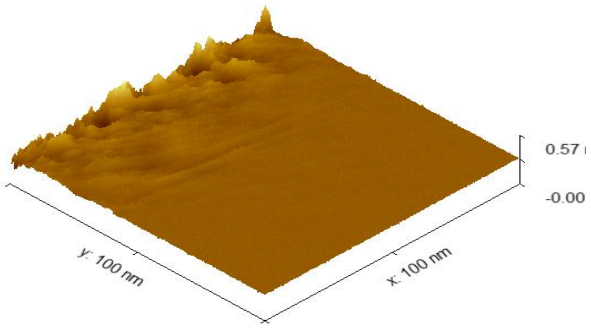

Figure 4.52: (b) 3D AFM FOR BLANK

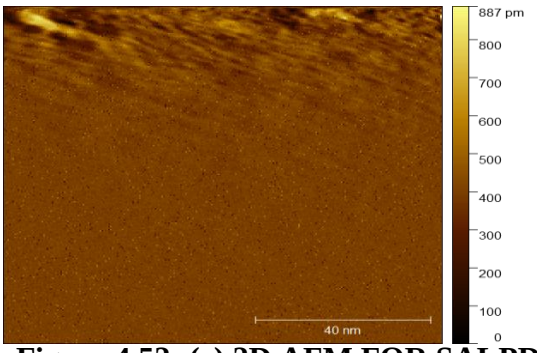

Figure 4.52: (c) 2D AFM FOR SALPD

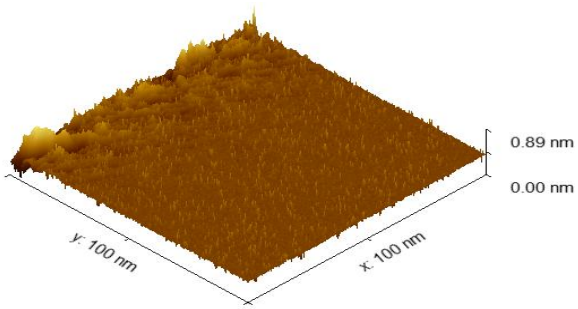

Figure 4.52: (d) 3D AFM FOR SALPD

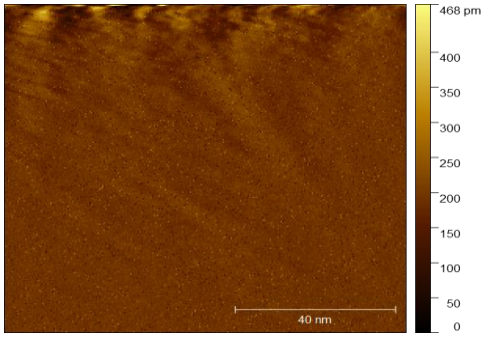

Figure 4.52: (e) 2D AFM FOR CeSALPD

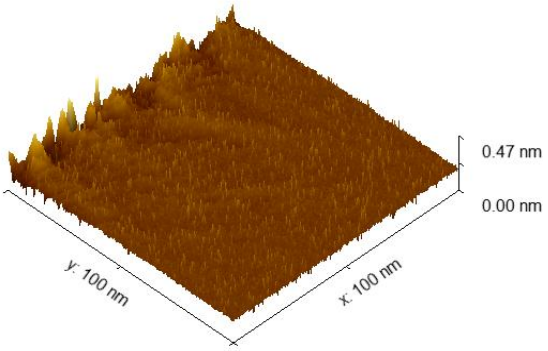

Figure 4.52: (f) 3D AFM FOR CeSALPD

Table 4.60: AFM Parameters of Inhibitor Compounds

AFM PARAMETERS	COMPOUNDS		
	BLANK	**SALPD**	**CeSALPD**
Sq value (pm)	44.80	21.52	20.88
Sp value(pm)	574.85	274.84	261.01
Sv value(pm)	**399.44**	307.44	**192.94**

Figures 4.52 (a) – 4.52 (f), show the 2D and 3D AFM results of blank, the Schiff base SALPD with its metal complex CeSALPD.Table (4.60) above show the AFM values for Sq, Sp, and Sv. Sq value describes overall surface roughness, Sp value indicates defects on a material, Sv value describes the extent of corrosion on a material. These values follow the order, BLANK > SALPD > CeSALPD. Hence, this observation is suggestive that the inhibitors had a protective effect on the mildsteel.

4.1.7 Electrochemical Results

4.1.7.1 Potentiodynamic (PDP) Results

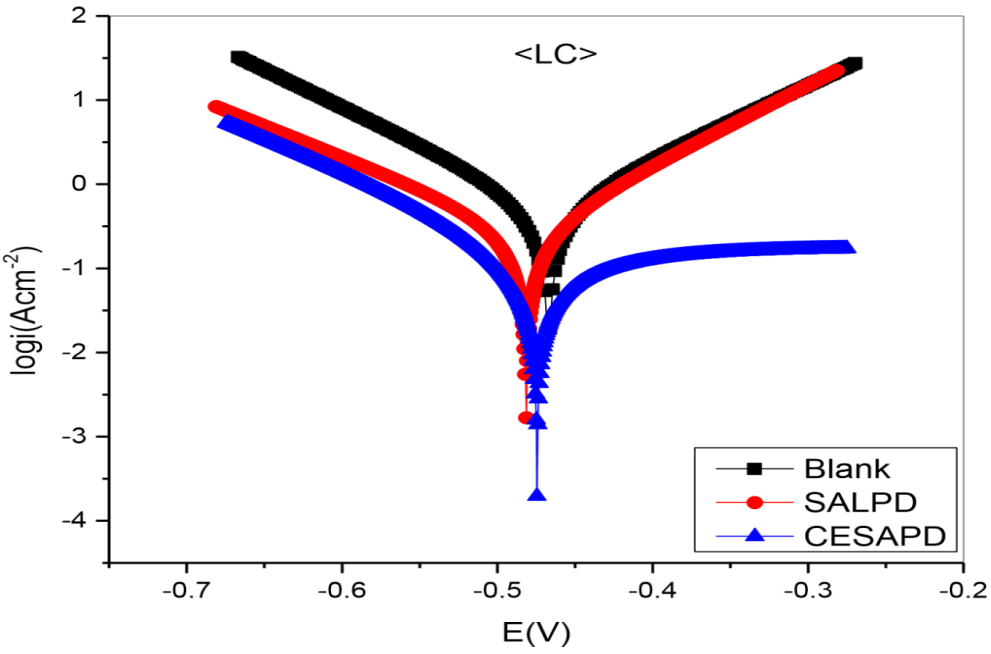

Figure 4.53: Polarization curves of Mild Steel in the absence and presence of 0.8 mmol / dm3 each of SALPD and CeSALPD of at 30 °C.

Table 4.61: The PDP Parameters of Mild Steel immersed in the presence and absence of 0.8 mmol/dm^3 of the inhibitors in 1M HCl

Environment	Ecorr. (mV)	ba (mV/dec)	bc (mV/dec)	Icorr. (A/cm2)	IE%icorr
Blank	-467.063	116.0	112.3	543.58	-
SALPD	-474.475	225	133.6	177.44	67.36
CeSALPD	-483.068	326	135.3	134.07	75.34

There is decrease in corrosion current (Icorr) and decrease in corrosion potential in the presence of the inhibitors compared to values for Blank system. However, CeSALPD recorded a higher IE value (75.34 %) compare to SALPD (67.36 %).

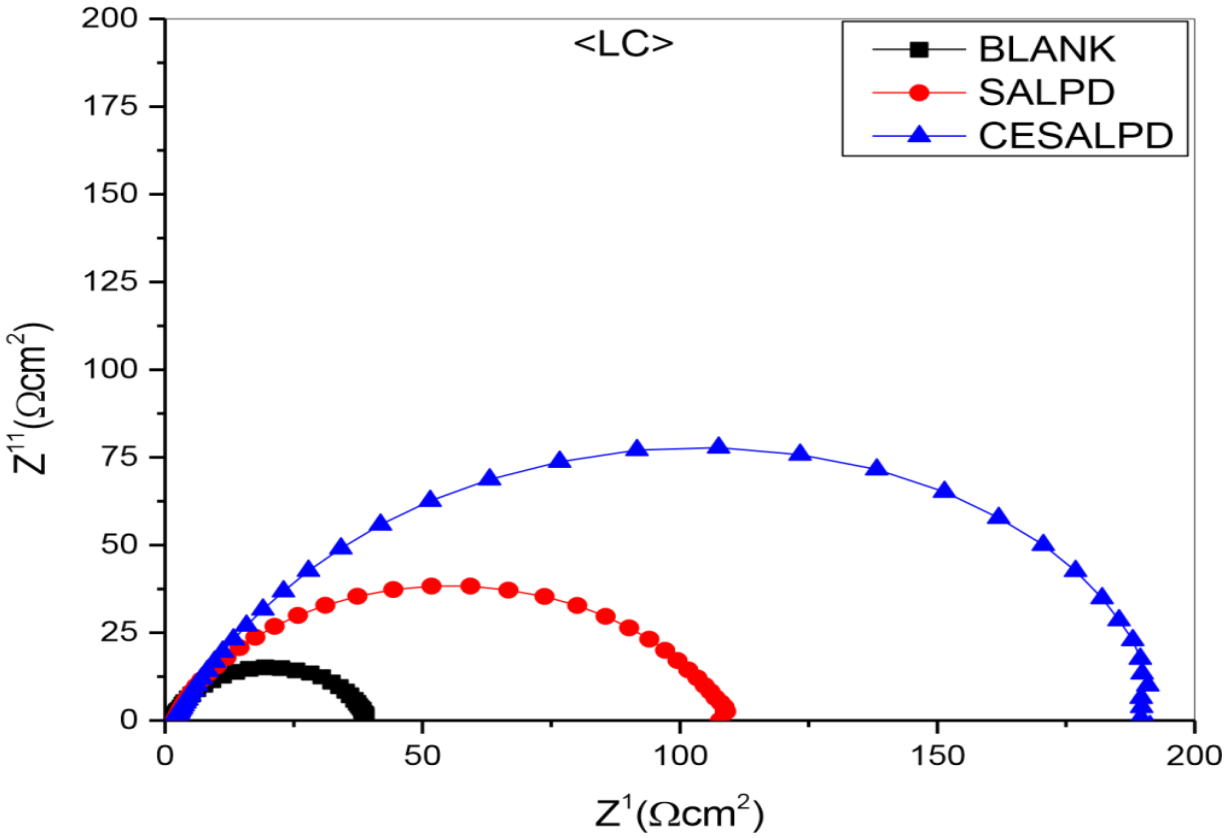

Figure 4.54: Nyquisit Plot for inhibitors at 0.8 mmol/dm^3

In Figure 4.54, Semi circle represents resistance to charge transfer (Rct), CeSALPD, having the largest semi- circle diameter suggests its highest corrosion resistance compared to SALPD and Blank. This supports the result from the weight- loss experiment.

Table 4.62: EIS Parameters and Inhibition Efficiency at 30°C of Mild Steel in the absence and in the presence of 0.8mmol/dm^3 concentrations of the inhibitors

Environment	RS (Ohm)	Rct (Ohm)	Cdl, (µF/cm2)	IE%$_{EIS}$
Blank	1.6847	37.67	457.95	
SALPD	1.9917	107.13	211.33	64.84
CeSALPD	1.7191	185.34	191.34	79.68

Value for double layer capacitance (Cdl) is observed to decrease while Charge transfer resistance (Rct) increases with addition of the inhibitors. CeSALPD recorded a higher IE (79.68 %) compared to SALPD (64.84 %).

Table 4.63: Inhibition Efficiency values obtained for the various Analytical Techniques

	Analysis Technique / IE (%)		
Compound	**Weight loss**	**PDP**	**EIS**
SALPD	82.74 (at 1.2 mmol/dm^3)	67.36	64.84
CeSALPD	82.95 (at 0.4 mmol/ dm^3)	75.34	79.68

Data in Table 4.63 shows agreement in the order of IE obtained for the compounds from the various analysis techniques.

4.2.2 Discussion on SALPD and CeSALPD

4.2.2.1 Physical Measurements

4.2.2.1.1 Colour

The different colours of the synthesized compounds have been referenced in the Table 4.42 . The variation in colour of Schiff bases compared to their Schiff base metal complexes confirms the successful synthesis of the cerium complexes.

4.2.2.1.2 pH and Melting Points Measurement

Complexation in coordination chemistry is often accompanied by deprotonation of ligand which is the true cause of the variation of pH in the solution phase. In the general case, there is drop down in pH values of the solution in moving from ligand to metal complexes. The variation in pH values is indicative of the complex formation during the reaction. The pH values of Schiff base SALPD and the metal complex CeSALPD are reported in the Table 4.42. Moreover, the Schiff base have higher pH values (6) than the metal complex, pH (3).

4.2.2.1.3 Solubility Analysis

The solubility and melting points are the characteristic physical properties of compounds. The solubility of the Schiff base and the metal complex was examined in water and various organic solvents. Their solubility data are reported in the Table 4.43. The observation of solubility data revealed that the Schiff base -ligand SALPD and metal complex CeSALPD were insoluble in water but soluble in organic solvents. The Schiff base is soluble in methanol, DMSO, and DMF whereas metal complex is soluble in DMSO and DMF.

4.2.2.1.2 Molar Conductivity Measurement and Magnetic Susceptibility measurements

The conductivity values help to ascertain the ionic (electrolytic) or non-ionic (non -electrolytic) nature of the synthesized Schiff base and the metal complex.

Molar conductivity in DMSO and DMF of the compounds measured in mS/cm at a concentration of 10^{-3} M shown in Table 4.44. Magnetic susceptibility values are also showed in Table 4.44. The Schiff base compound showed high conductivity values, 0.41 and 0.29 mS/cm respectively in DMSO and DMF, values >0.1 mS/ cm, suggestive of electrolytic (ionic) nature of the Ce (III) Schiff base complex CeSALPD, and the presence of nitrate ions in the outer coordination sphere of the complex . The Schiff base showed low conductivity values of 3.44 X $10^{-3}$and 5.11 x10^{-3} mS/cm , values <0.1 mS/Cm which shows non electrolytic nature of the Schiff base and absence of the nitrate ions in the compounds. The magnetic properties of the compounds were studied using Gouy balance, Sherwood scientific limited UK. Serial number, 29275. The value of 015 obtained for the cerium complex, (Table 4.44) is suggestive of paramagnetic nature of the Cerium complex, ie (value>1), meaning that the compound can be attracted by an external magnetic field. The Schiff base, SAL2AP showed no magnetic properties.

4.2.2.2 Spectral Measurements

4.2.2.2.1 Electronic Absorption Spectra Analysis of SALPD and CeSALPD

Maximum absorbance of SALPD Schiff base at 326 nm attributed to $n \rightarrow \pi^*$transition due to transition of non -bonding electrons of the nitrogen atom of the azomethine to the anti –bonding pi (π^*) orbital of the azomethine group. This value shifted to a higher wavelength of 349 nm in the CeSALPD metal complex due to coordination of the nitrogen atom to the metal ion (Figures 4.37, and 4.38).

4.2.2.2.2 FTIR Spectral Studies of SALPD and CeSALPD

The FTIR spectra of SALPD and CeSALPD are given in Figures 4.39, and 4.40 respectively. V(C=N) vibration due azomithine group in the Schiff base SALPD occurred at 1697 cm-1 which experienced a blue shift to 1610 cm-1 in the spectrum of the metal complex CeSALPD. This shift in frequency signifies the involvement of the nitrogen atom of the azomithine group in complexation. This is confirmed by the appearance of a new band at 738 cm^{-1} assigned to vibration due to v (M-N) stretching frequency. V (C-O) vibration was observed in the spectra of the ligand at 1273 cm-1 which shifted to a higher wavelength at 1289 cm^{-1} in the spectrum of the complex. This shift in frequency is as a result of coordination to the metal through the oxygen atom of the phenol group after deprotonation. The appearance of a new band due to v(M-O) occuring at 628 cm^{-1} in the spectrum of the complex further confirms the formation of M-O bond due to complexation. v (H_2O) due to coordinated water in the spectrum of the complex is observed as a broad band at 3216 cm^{1}. Vibration due to v(OH) in the spectrum of the ligand was observed at 3487 cm^{-1}, which disappears in the spectrum of the complex after deprotonation.
V($N0_3$) vibration occurred in the complex in the region 1449 cm^{-1}.

4.2.2.2.3 ^{1}H Spectral Study of SALPD

The proton NMR, (1H-NMR) spectrum of SALPD (Figure 4.41) reveals distinct chemical environments for the protons in the molecule. The spectrum confirms the presence of key functional groups in SALPD: a phenolic proton, an imine proton, and aromatic protons. The chemical shifts and splitting patterns align with the structure of a Schiff base derived from salicylaldehyde, indicating the successful synthesis of the ligand. Table 4.45 presents Proton (^{1}H) NMR Spectral data of SALPD. Proton numbering of SALPD is shown in Figure 4.42.

Key Features:

1. **Signal at 12.95 ppm (A)**: This singlet corresponds to the proton on the phenolic –OH group. Its downfield position is due to strong hydrogen bonding or electronegative deshielding effects.
2. **Signal at 8.94 ppm (B)**: This singlet represents the imine (-C=NH) proton, characteristic of Schiff bases. The deshielded nature is due to the electron-withdrawing nature of the imine group.

3. **Signals in the range 7.47–7.05 ppm (C, D, F, G)**: These peaks belong to aromatic protons on the benzene ring. The multiplets and doublets indicate the protons' coupling interactions, consistent with the substitution pattern of the aromatic ring.

4. **Splitting and Coupling Constants**: The doublet of doublets (dd) at 7.47 ppm (D) and 7.67 ppm (C) indicates coupling with adjacent protons, with coupling constants J = 5.90 Hz and 3.43 Hz for D, and J = 8.04 Hz and 1.78 Hz for C.

   Multiplet at ~6.98 ppm (F), 7.41 ppm (E), and 7.05 ppm (G) suggests overlapping peaks of aromatic protons.

4.2.2.2.4 13-C NMR Spectral Study of SALPD

The spectrum (Figure 4.43) confirms the presence of the imine group (distinct peak at ~164.50 ppm) and the aromatic ring structure with varying electronic environments. The distribution and chemical shifts of aromatic carbons align with the expected structure of SALPD, validating the Schiff base ligand's formation. Carbon numbering in SALPD is shown in Figure 4.44. Table 4.46 records the carbon-13 (C-13) NMR data for SALPD **with following Key Observations:**

1. **Signal at ~164.50 ppm**: This peak corresponds to the carbon in the imine group (-C=NH). The highly deshielded nature of this carbon is due to the electron-withdrawing effect of the nitrogen atom and the double bond.

2. **Signals at ~160.87 ppm**: These peaks represent the carbons attached to the hydroxyl group (-OH) and aromatic carbons directly bonded to electronegative groups. The deshielding is due to resonance and inductive effects.

3. **Signals at ~117.67,**120.22, 132.20, and 132.93 ppm belong aromatic carbons of the aldehyde moiety.

4. **Signals at 119**.55 ppm is assigned to carbon atoms directly bonded to the imine carbon. 120.22, 132.20, and 132.93 ppm belong aromatic carbons of the aldehyde moiety

5. **Signals at 126**.69, 128.26, 133.90 ppm, are assigned to aromatic carbons of the diamine moiety.

4.2.2.2.5 EDXRF Spectral Analysis of CeSALPD

Figure 4.45 displays CeSALPD spectrum analysis. CeSALPD showed the highest cerium composition compared to the other complexes. The percentage composition of cerium found is 83.24%, with a peak intensity of 62,497 cps/MA, also within the 6.60–4.80 keV energy range.

4.2.2.3 Inhibitive Action SALPD and CeSALPD

4.2.2.3.1 Analysis of gravimetric Results

The corrosion rate of mild steel in 1 M HCl solution is studied by weight loss method in the absence and presence of Schiff base and metal complex at 30°C and the percentage of inhibition efficiency is calculated. Table 4.48 to 4.53 show the variation of corrosion rate (mdd) and inhibition efficiency (IE in %) with varying concentration of inhibitor in (mmol/dm3). From the data it is observed that corrosion rate is significantly lowered down in the presence of the inhibitor. The corrosion rate is found to be dependent on the concentration of the inhibitor. With the increase in concentration, the corrosion rate decreases gradually.

Figure 4.47 shows the variation of percentage inhibition efficiency (IE%) with concentration of inhibitor in (mmol/dm^3) and the bar chart reveals that inhibition efficiency increases with increase in the concentration of the inhibitors in 1M HCl medium. In the medium containing SALPD a maximum inhibition efficiency of (82.74%) was attained at 1.2 mmol/ldm^3 of the inhibitor concentration while that containing CeSALPD, it is found to be 82.63% efficiency at 0.8 mmol/dm3 concentration of the inhibitor. At lower concentrations of the inhibitors between 0.1 to 0.8 mmol/ dm^3, its observed that CeSALPD had a higher inhibition efficiency compared to the parent Schiff base SALPD. This observation confirms that little quantity of CeSALPD order than large quantity is required to achieve an excellent inhibition of corrosion of mild steel in acidic medium which has economic advantage. It also gives credence to the fact that complexation enhances the inhibition efficiency of Schiff base compounds. The decreasing corrosion rate and increasing inhibition efficiency are attributed to the adsorption of inhibitor on the metal surface. The increase in the concentration increases the surface coverage due to adsorption which decreases the active sites on the metal surface. Hence, the inhibition efficiency increases with increase in the concentration.

4.2.2.3.2 Analysis of variation of Inhibition Efficiency with Immersion Time

Table 4.59 and Figure 4.51 show the variation of inhibition efficiency as a function of immersion time. It could be observed from the Table and Figure that inhibition efficiency of the compounds decreased with immersion time, which is due to physisorption process of adsorption of the inhibitor molecules on the surface of the mild steel. There is dissolution of the inhibitor molecules from the mild- steel surface with prolonged immersion in the aggressive medium. The exposed surface is attacked by the corrodent (1 M HCl), and I.E decreases. However, I.E of CeSALPD (red bars) was

consistently higher than that of SALPD over the whole period of immersion. This correlates with the fact that complexation in Schiff base- compounds gives rise to enhanced I.E of the Schiff bases.

4.2.2.3.3 Analysis of the Effect of Temperature on the Performance of the Inhibitors

The effect of temperature on the corrosion of mild steel in free and inhibited 1 M HCl solutions was studied using gravimetric approach in the range of 30–70 ^{o}C.

The acid solutions were inhibited by addition of 0.8 mmol/dm^3 of the compounds. The corrosion parameters calculated from the gravimetric data are given in Table 4.57. Inspection of the data reveals, that the corrosion rate of steel in both free and inhibited acid media increased as the temperature was increased. However, the inhibition efficiency of the compounds decreases remarkedly with increasing temperature (Figure 4.50), with CeSALPD outperforming the parent Schiff base SALPD at all temperatures, this observation is consistent with an enhanced corrosion inhibition with Schiff base metal complexes. This result supports the idea that the adsorption of inhibitors onto the steel surface is physical in nature. Thus, as the temperature increases, the number of adsorbed molecules decreases, leading to a decrease in the inhibition efficiency. The activation energies of the corrosion process in free and inhibited acid were calculated using the Arrhenius equation, equation (1.4).

$$K = A\, exp \frac{Ea}{RT} \qquad Eqn.(4.3)$$

Where Ea is the activation energy, A is the frequency factor, T is the absolute temperature, R is the gas constant, and K is the rate constant, which is directly proportion to the corrosion rate. Plotting log k versus 1/T gives a straight line, as revealed by Fig. 4.48. The values of activation energy calculated using the lines of Figure. 4.48 are 20.79 for free acid solution, 26.79 and 26.16 kJ/mol for acid solutions inhibited with SALPD and CeSALPD, respectively. The obtained results suggest that compounds inhibited the corrosion reaction by increasing its activation energy. This could be done by adsorption onto the steel surface, making a barrier to mass and charge transfer.

4.2.2.3.4 Analysis of Thermodynamics Parameters, Δ H and ΔS.

Figure 4.49 shows a plot of log CR/T vs 1/T, derived from the relationship log C_R/ T = [(log R/Nh) + (ΔS*/2.303 R) – Δ H*/2.303 RT]. Where h is plank's constant, 6.626 x 10-^{34}, N is equal to Avagadro's number, 6.02 x $10^{23.}$, S* is the entropy of activation, R is gas constant, T is temperature in Kelvin. The slope of the linear plot, –H* / 2.303R permits to derive the enthalpy of activation (H*), and an intercept of (log R/Nh) + (ΔS*/2.303 R) is used to calculate the entropy of the

activation process, S*. Data of the CR/ T vs 1/ T are listed in Table 4.57. The positive enthalpies obtained shows the endothermic process of the dissolution process. ΔH and Δ S values obtained for SALPD are 59.48 kJ/ Mol and - 49-12 kJ/ Mol respectively, while CeSALPD Δ H value is 57.60 kJ/ Mol, and ΔS value is -54.66 kJ/Mol, H* value recorded for the free system (blank) is 45.79 kJ/ Mol, and Δ S is -82.38 kJ/Mol. The negative entropy shows increased orderliness moving from the uninhibited system to the inhibited systems

4.2.2.4 Adsorption Isotherm

It has been assumed that organic inhibitor molecules establish their inhibition action via the adsorption of the inhibitor onto the metal surface. The adsorption processes of inhibitors are influenced by the chemical structures of organic compounds, the nature and surface charge of metal, the distribution of charge in molecule and the type of aggressive media. In general, two modes of adsorption can be considered. The proceeding of physical adsorption requires the presence of electrically charged metal surface and charged species in the bulk of the solution. Chemisorption process involves charge sharing or charge transfer from the inhibitor molecules to the metal surface. The presence of an inhibitor molecule having relatively loosely bound electrons or heteroatoms with lone-pair of electrons, with a lanthanide or transition metal, having vacant, low-energy electron orbital, facilitates this adsorption. Assuming the corrosion inhibition was caused by the adsorption of SALPD and its metal derivatives, and the values of surface coverage (θ) for different concentrations of inhibitors in 1 M HCl were evaluated from weight loss measurements from Eq. (3.1). Adsorption isotherms are very important in determining the mechanism of organic electrochemical reactions. The most frequently used adsorption isotherms are Langmuir Tables 4.48 and 4.51. and Figure 4.46. Temkin, Table 4.49 and 4.52, and Frumkin Table 4.50 and 4.53). The adsorption isotherms were tested for the description of adsorption behaviour of studied compounds and it is found that adsorption of SALPD and CeSALPD on mild steel surface in HCl solution obeys the Langmuir adsorption isotherm given by the equations (1.5) and (1.6) page 32

$$\frac{C_{inh}}{\theta} = \frac{1}{b} + C_{inh} \quad (1.5)$$

$$b = \frac{1}{55.5} exp\left(-\frac{\Delta G_{ads}}{RT}\right) \quad (1.6)$$

C_{inh} is the inhibitor concentration, θ is the fraction of the surface covered, b is the adsorption coefficient and G_{ads} is the standard free energy of adsorption. Figure. 4.46 shows the dependence of the fraction of the surface covered C/θ as a function of the concentration (C) of inhibitors. It

should be explained that other adsorption isotherms (Frumkin and Temkin) were checked and Langmuir adsorption isotherm is the best approximate between them. This is why the assumption is true for Langmuir adsorption isotherm. The regression square values obtained for the various isotherms are recorded in Table 4.54.

The obtained plots of the inhibitors are linear with correlation coefficient higher than 0.99. The intercept permits the calculation of the equilibrium constant b which are 27.62, and 23.76 M^{-1} for, SALPD and CeSALPD, respectively. The values of b which indicate the binding power of the inhibitor to the steel surface can lead to calculate the adsorption energy. Values of G_{ads}= −17.86, and, −15.64 kJ mol^{-1}. The negative value of G_{ad}s means that the adsorption of the additives on mild steel surface is a spontaneous process, and furthermore the negative values of G_{ads} also show the strong interaction of the inhibitor molecule onto the mild steel surface . Generally, values of Gads around −20 kJ mol^{-1} or lower are consistent with the electrostatic interaction between the charged molecules and the charged metal (physisorption). Those more negative than −40 kJ mol^{-1} involve charge sharing or transfer from the inhibitor molecules to the metal surface to form a coordinate type of bond (chemisorption) . For investigate inhibitors, one can see that the calculated G_{ads} value were less than – 20 kJ mol-1, indicating, that the adsorption mechanism of the both inhibitors on mild steel in 1 M HCl solution was typical of physisorption.

4.2.2.5 Surface Analysis using AFM

Figures 4.52(a) – 4.52 (f), show the 2D and 3D AFM results of blank, the Schiff base SALPD with its metal complex CeSALPD. Table (4.60) show the AFM values for Sq, Sp, and Sv. The RMS roughness (Sq) values provide a quantitative value that describes the overall surface texture or roughness. A higher Sq indicates a rougher surface while a lower Sq suggests a smoother surface. Maximum peak height (Sp) refers to the height of the tallest peak in a given measurement area relative to the mean plane of the surface. Sp value provides insight into the presence of features such as spikes and protrusions. A high Sp value may indicate defects or irregularities that could compromise a material's performance which in turn signifies higher pits value (Sv), which also indicates the extent of corrosion. The order of the values of the Sq, Sp, and Sv of the blank, the Schiff base with the metal complex correlates with the order of their inhibition efficiencies based on the weight loss experiment.

4.2.2.6 Electrochemical Studies

4.2.2.6.1 Analysis of the Results of Potentiodynamic Polarization Studies

The Potentiodynamic polarization curves of mild steel immersed in acidic medium in the presence and absence of 0.8 mmol/dm^3 of SALPD and CeSALPD is given in Figure 4.53, while the corrosion parameters of the two inhibitors are given in Table 4.61. When mild steel is immersed in acidic medium without inhibitor the corrosion potential (Ecorr) is -467.06 mV vs SCE and the corrosion current is 543.58(uA/cm^2). When the inhibitors were added to the acidic medium the Ecorr value is found to be -474.48 vs SCE in the medium containing SALPD and -483.07 mV vs SCE in the medium containing CeSALPD. The icorr decreased from 543.58 in the blank solution to 177.44 uA/cm^2 with SALPD and to 134.07 uA/cm^2 with CeSALPD. The decrease in the corrosion current values indicates that the additives functions as an inhibitor and reduces the corrosion of mild steel in acidic medium. The shift in the Ecorr value to a less negative value and the changes in the cathodic and anodic slopes shows that the inhibitor controls both the cathodic and anodic reactions and behaves as mixed inhibitor. IE recorded for SALPD is 67.36%. While 75.34 % was recorded for CeSALPD. These values are in agreement with weight loss method.

PDP parameters, namely, corrosion potential (Ecorr), anodic and cathodicTafel slopes (ba and bc), corrosion current (Icorr), and polarization resistance (Rp) obtained by extrapolation of the polarization curves. The inhibition percentage calculated from Icorr and Rp are given by equations 4.2 - 4.3

$$E\text{Icorr} = (I\text{corr}' - I\text{corr}) \times 100/I\text{corr}' \quad (4.2)$$

$$ERp = (Rp - Rp') \times 100/Rp \quad (4.3)$$

4.2.2.6.2 Analysis of the Results of EIS Studies

Figure 4.54 presents the EIS spectra of carbon steel, (Niqusit plot) in 1M HCl with the inhibitors, while Table 4.62 lists the impedance parameters, including charge transfer resistance and double-layer capacitance. The double layer capacitance and EIS inhibitory efficiency were calculated using equations 4.4 and 4.5 respectively (Yadav, et al., 2015; Khalissa et al., 2018):

$$\frac{1}{C_{dl}} = \frac{(1 - a2)}{Q2a2.Rct\ a2} \quad (4.4)$$

Where; C_{dl} = double layer capacitance

$Q =$ Constant Phase Element (CPE),

$a2$ = CPE exponent,

Rct = Charge Transfer Resistance.

$$IE_{EIS}(\%) = (Rct_R - ct^{Rct} \times 100 \quad (4.5)$$

Where: Rct° and Rct are the charge transfer resistances without and with inhibitor, respectively.

According to Table 4.62, the values of Rct increases, and those of Cdl decrease with the addition of the inhibitors to the corrosive solution. This can be ascribed to the formation of a protective layer at the metal/acid interface, thus decreasing the direct contact between the mild steel and the aggressive solution (Mohamed et al., 2018; Ansari, et al.2019). In addition to this, the increasing value of the inhibition efficiency in the presence of additives further supports the protection ability of the inhibitor. CeSALPD has enhanced I.E (79.68%) over SALPD (64.84%). These values are in agreement with weight loss method.

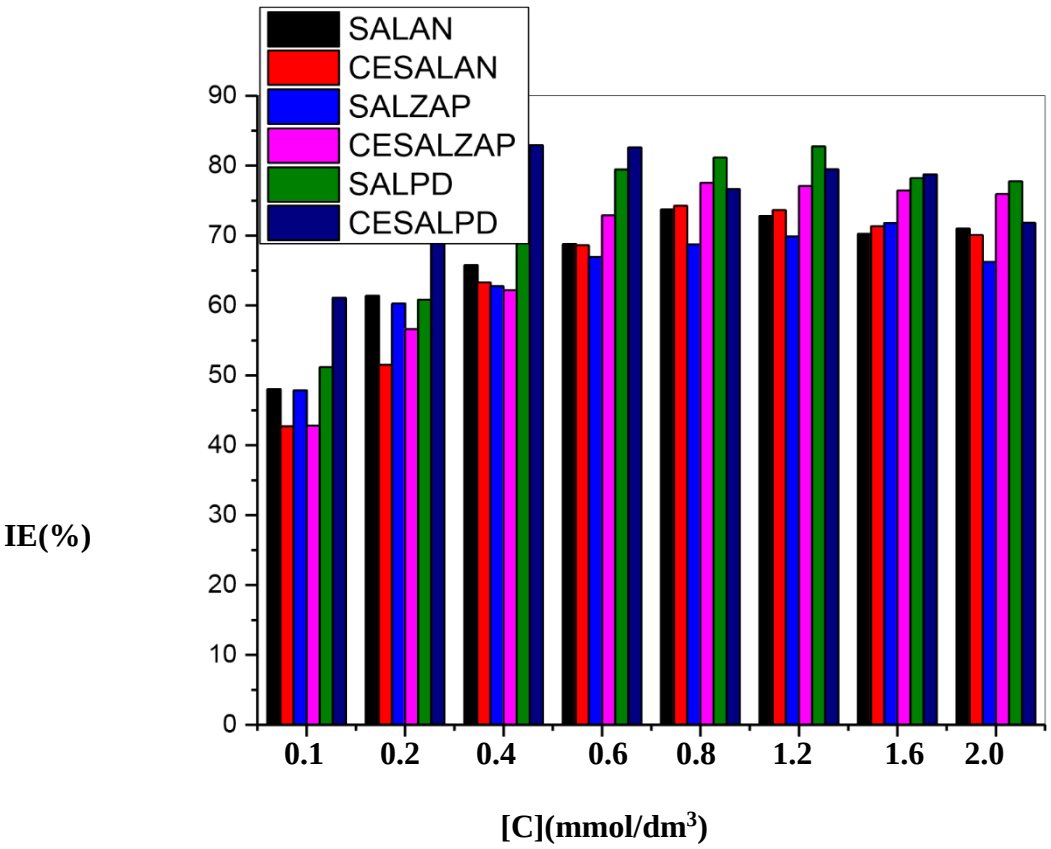

Figure 4.55: Comparism Plot of the Inhibition Efficiency vs Concentration of the Schiff bases and their Metal Complexes

The plot in Figure 4.55 above shows comparism of inhibition efficiency (IE %), of the various Schiff bases with their metal complexes. It can be deduced from the plot that the Schiff base metal complexes got to their optimum IE at much lower concentrations compared to their parent Schiff base compounds. This implies that less quantities of the Schiff base metal complexes are required to inhibit corrosion of mild steel in aggressive medium compared to their parent Schiff bases, which is of economic advantage to the industrial sector. This finding is agreement that metal complexes of Schiff bases exhibit enhanced IE compared to their parent Schiff bases.

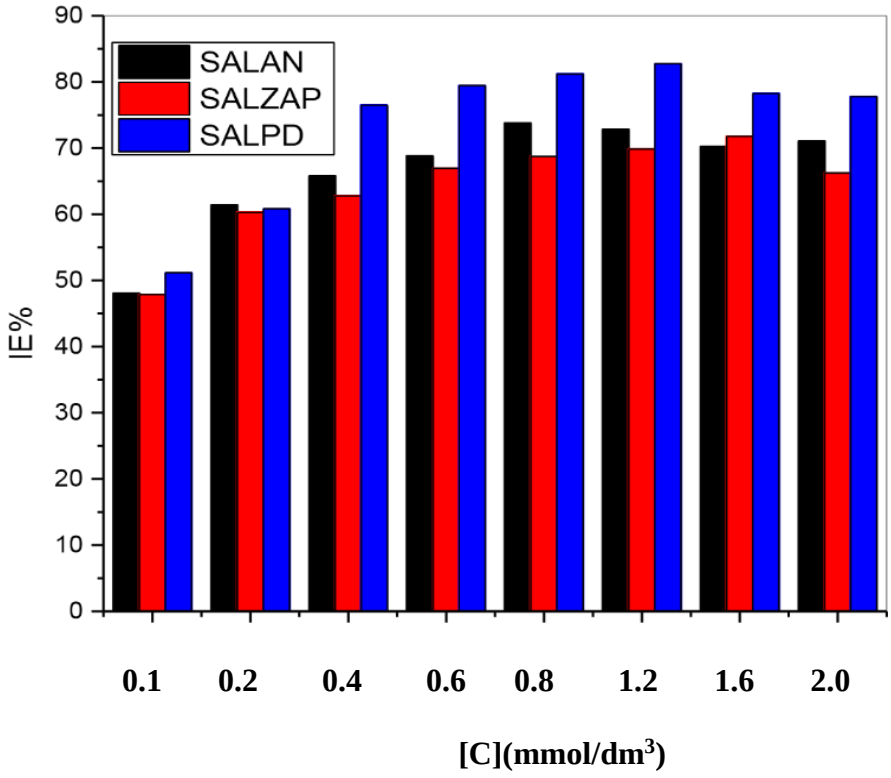

Figure 4. 56: Plot of Inhibition Efficiency vs Concentration of the Schiff base Compounds after 24 hr. Immersion

The plot in Figure 4.56 above compares the IE % of the various Schiff bases under study after 24 hours immersion time. The order of inhibitive performances of the Schiff bases are thus: SALPD>SALAN> SAL2AP, which is in agreement with the computational analysis of reactivity of the Schiff base compounds.

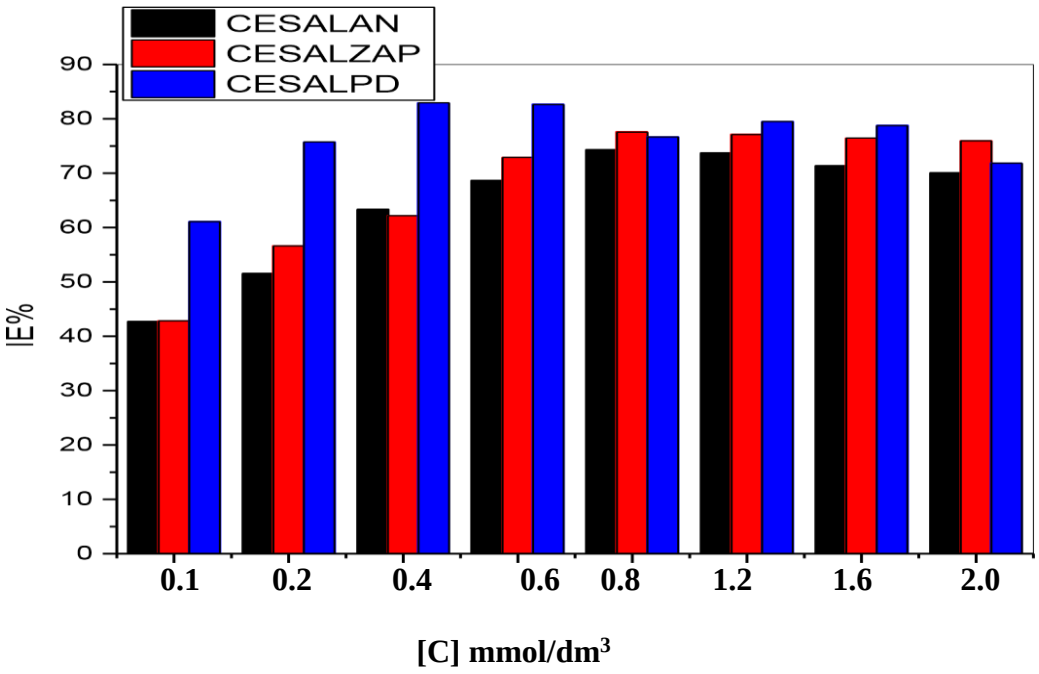

Figure 4.57: Comparism plot of Inhibition Efficiency of the Cerium Metal Complexes

The plot shown in figure 4.57 above compares the IE of the cerium (III) Schiff base complexes. It is observed that CeSALPD (blue bar) recorded the highest IE compared to CeSALAN (black bar), and CeSAL2AP (red bar). This observation can be explained using the effect of chelation on reactivity, while considering the structures of the Schiff base compounds and the number of heteroatoms with non- bonding electrons present in their molecules. Chelation gives rise to stability in coordination compounds. And stability enhances reactivity. The greater the number of chelate rings in the structure of a compound, the bulkier it becomes. Bulky compounds have a higher ability to cover more corrosion active sites on the mild steel surface than lighter compounds, therefore, they have greater potentials of inhibiting corrosion. Again, the greater the number of heteroatoms in a compound, the more it can furnish electrons, and greater its reactivity. Considering the fact that CeSALPD is the most bulky of all the Cerium Schiff base compounds, having highest numbers of chelate rings (six), aswell as highest number of heteroatoms(eight), ie (4 N, 4 O) atoms, outperformed the others in protective efficiency. CeSAL2AP having six heteroatoms (2N, 4O), outperformed CeSALAN with four heteroatoms, (2 N,2 O) atoms in its molecules.

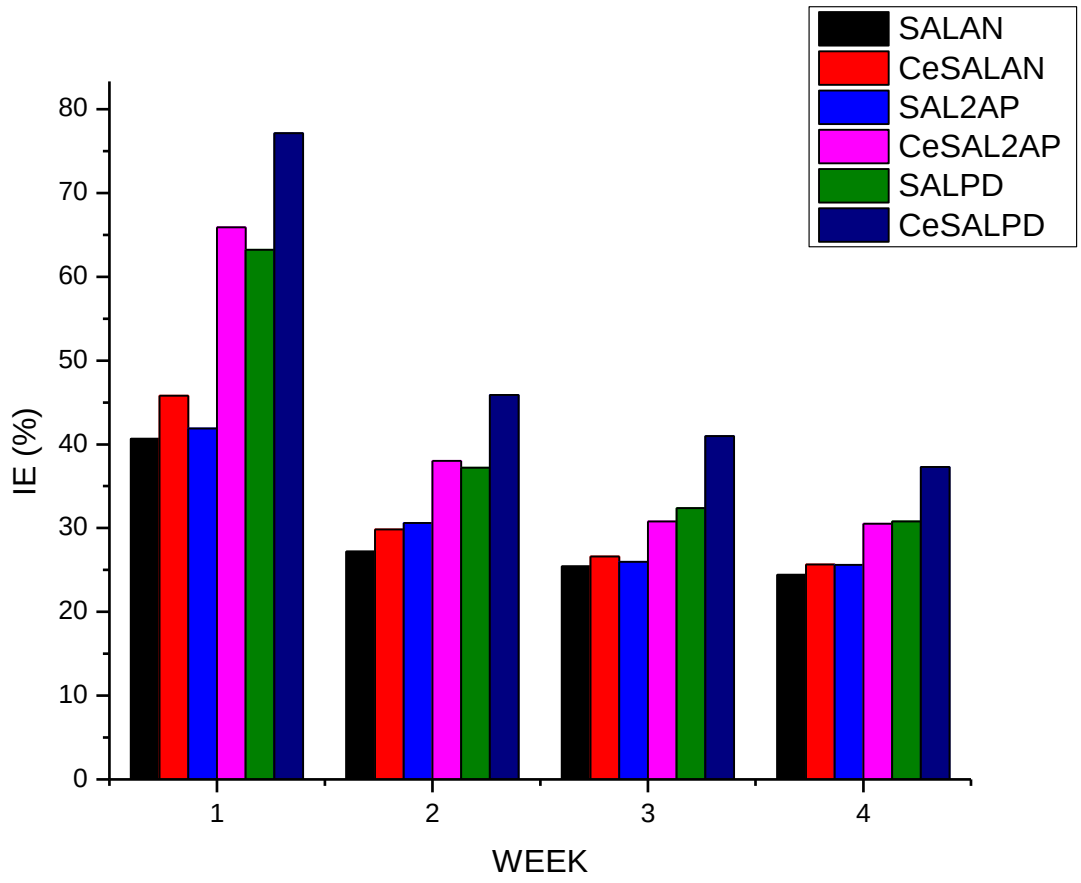

Figure 4.58: Comparism of Inhibition Efficiency of Compounds with Immersion Time

Figure 4.58 above compares the IE of the various compounds with immersion time. From the bar chart, a continuous decrease in IE of the compounds with immersion time could be observed, which is due to physical adsorption of the inhibitor molecules on the mild steel, this leads to dissolution of the inhibitor molecules from the surface of the mild steel over time. The IE of the metal complexes outperformed those of their parent Schiff bases, giving credence that complexation enhances IE of Schiff base compounds. CeSALPD being the best inhibitor – compound due to its molecular structure, i.e., highest number of heteroatoms and chelate rings, towered over the rest to the compounds.

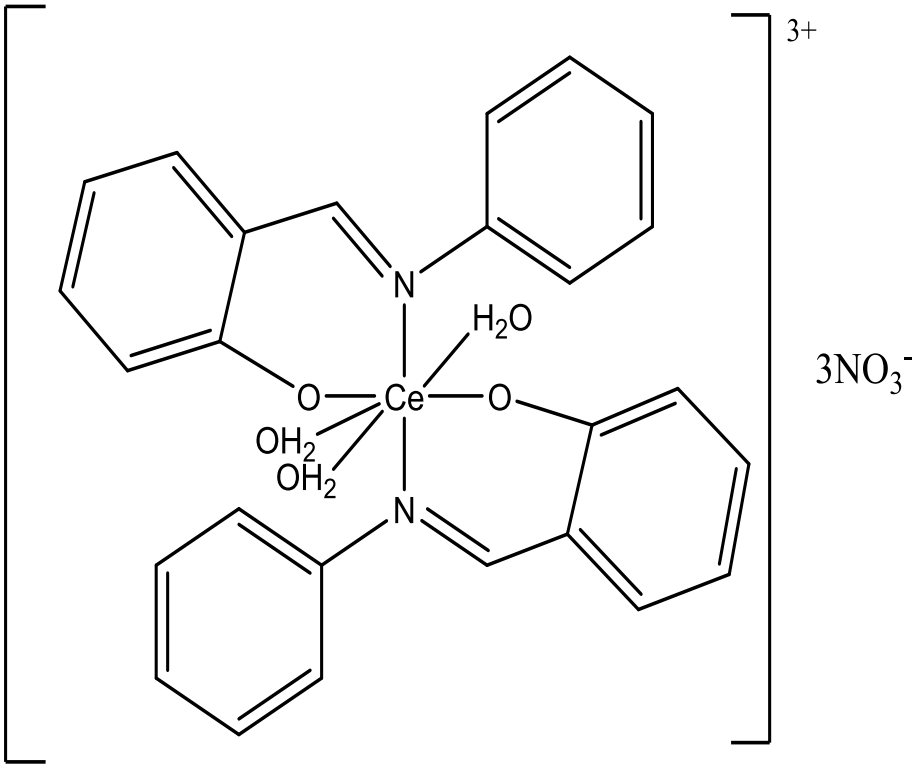

CeSALAN

Figure 4.59: Proposed structure for Ce (III) - 2-hydroxyphenyl-phenylimine or (Cerium (III) Salicyalideneaniline)

(Distorted pentagonal bipyramid)

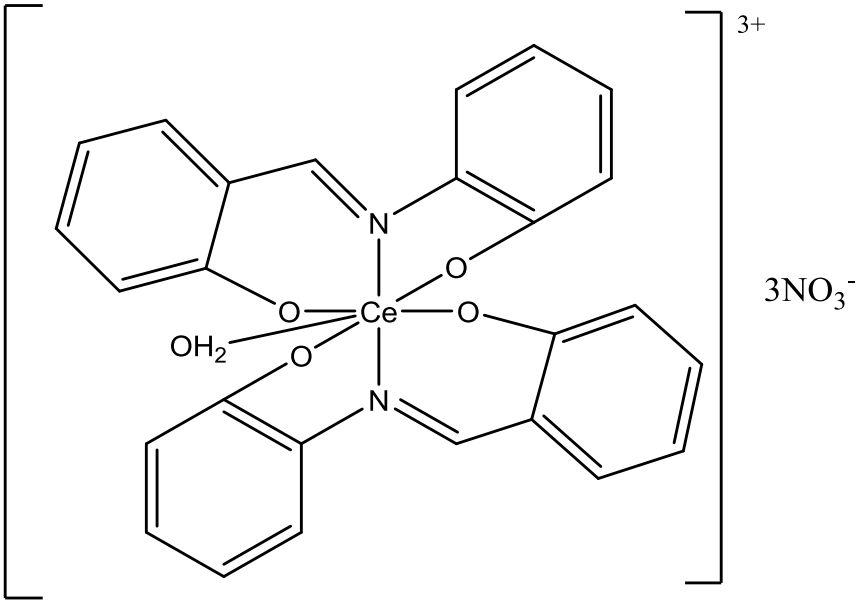

CeSAL2AP

Figure 4.60: Proposed Structure for Ce (III) -Bis (2-hydroxyphenyl) imine or (Cerium (III) Salicyalidene-2-aminophenol)

(Distorted pentagonal bipyramid).

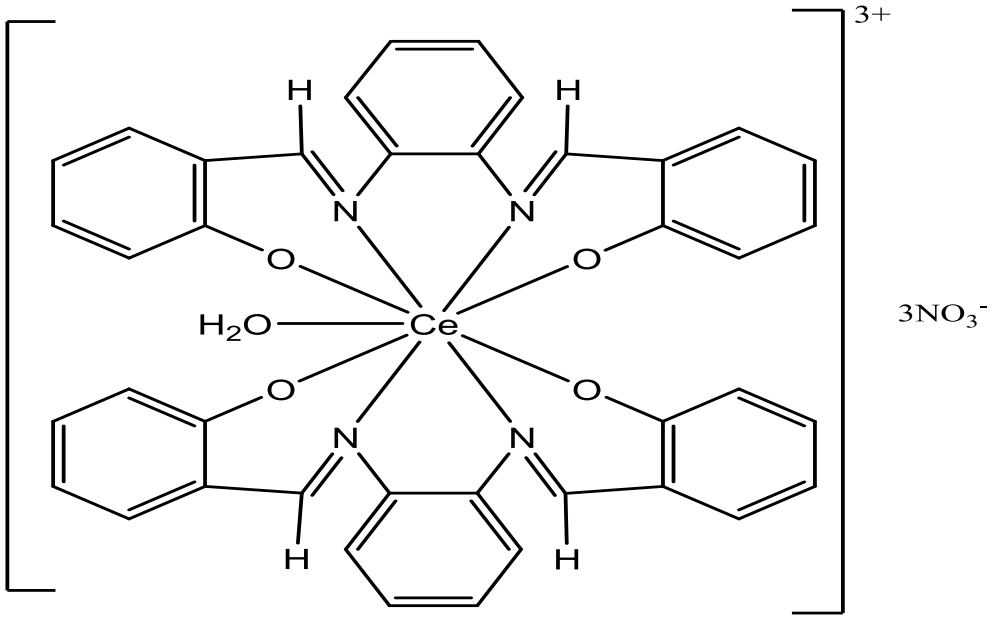

CeSALPD,

Figure 4.61: Proposed structure for Ce (III)- Bis (2-hydroxyphenyl) -1,2-Benzenediimine or (Cerium (III) Salicyalidene-O-phenylindiamine)

(Tricapped trigonal prism)

4.2.2.7 Molecular Modeling Study

Molecular modeling is a computational tool to give a much more accurate assessment of theoretical predictions regarding the structure of the molecules. Various physical and chemical information of the molecules can be best achieved by molecular modeling software program package (Pirhadi et al., 2016). Theoretical predictions like electron density and electrostatic potential maps provide a clear picture of the behavior of the molecules. In our investigation, the correct stereochemistry of the Schiff bases has been assured through, manipulation and modification of the molecular coordinates to obtain reasonable and low energy molecular geometries. Figures 4.62 (a)(b)(c) represents the optimized structures of the three Schiff bases from which the molecular orbitals evolved. Figure 4.63 (a)(b)(c) shows HOMO OF SALAN, SAL2AP and SALPD. Figure 4.64 (a)(b)(c) shows LUMO OF SALAN, SAL2AP, and SALPD.

Figures 4.65 (a)(b), Figures 4.66 (a)(b), Figures 4.67(a)(b) shows a flat adsorption mode for SALAN, SALPD and CeSALPD respectively on mild steel surface.

SALAN (a)	SAL2AP (b)	SALPD (c)
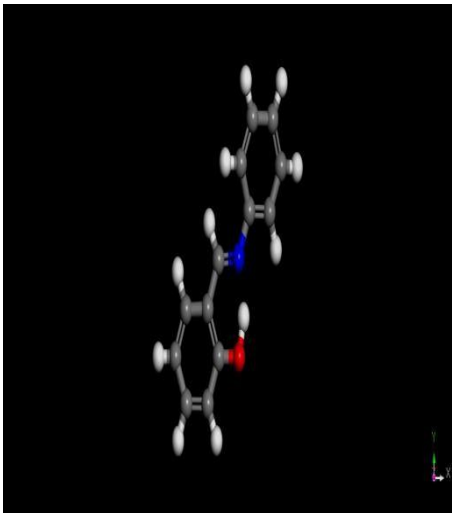	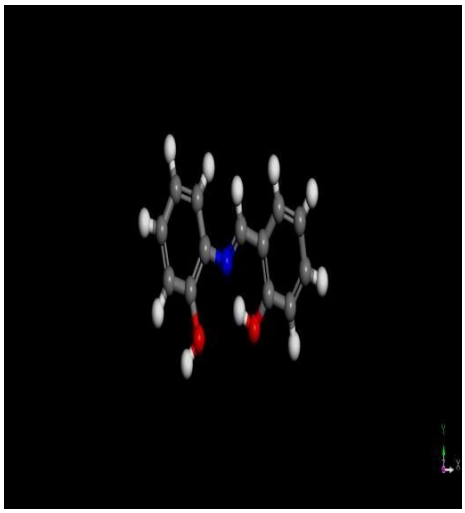	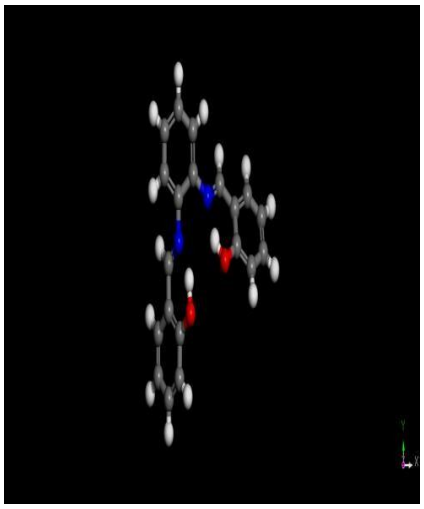

Figures 4.62: (a) (b) (c) OPTIMIZED STRUCTURE OF SALAN, SAL2AP and SALPD

SALAN (a)	SAL2AP (b)	SALPD (c)
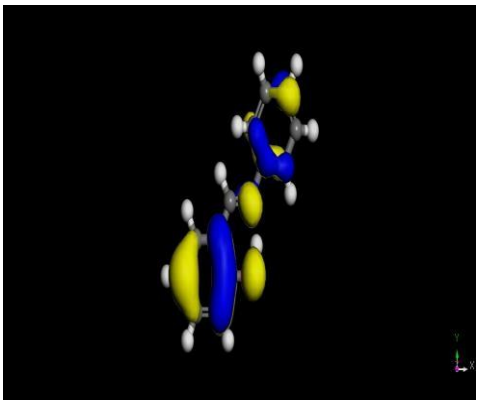	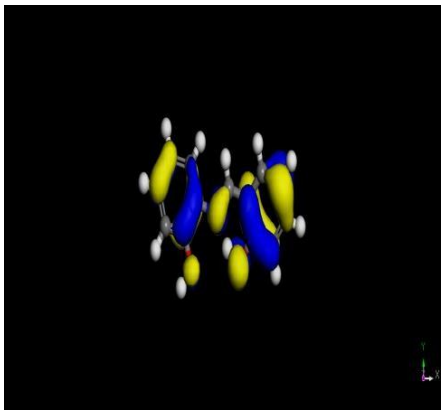	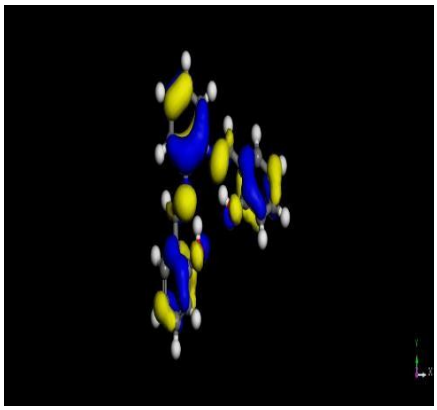

Figure 4.63: (a) (b)(c) HOMO OF SALAN, SAL2AP and SALPD

SALAN (a)	SAL2AP (b)	SALPD (c)
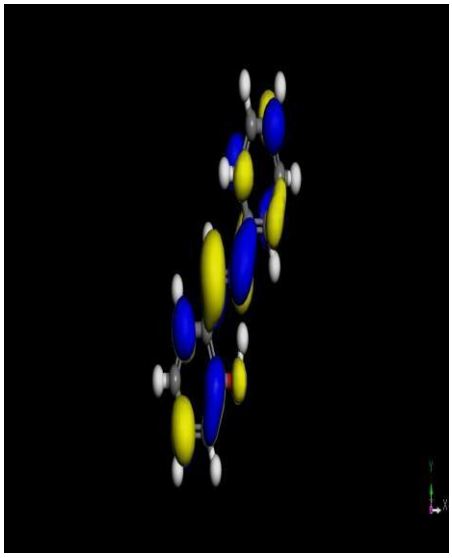	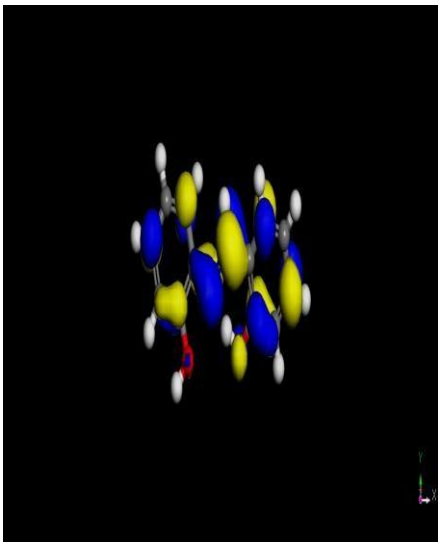	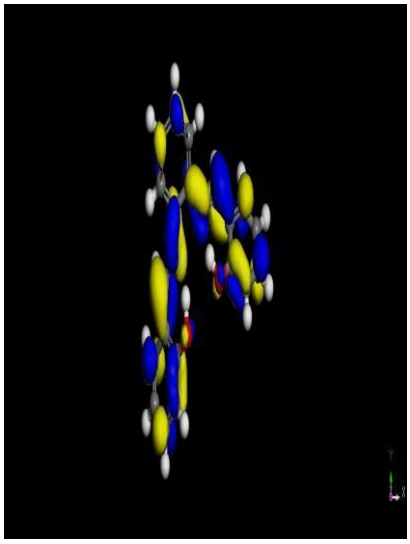

Figures 4.64: (a) (b) (c) LUMO OF SALAN, SAL2AP, and SALPD

Table 4.64: Quantum Chemical Parameter Data of Schiff Bases

Parameters	EHOMO	ELUMO	ΔE(ev)	*I*(ev)	A(ev)	*X*(ev)	η (ev)	∂ (ev)	μ(ev)
SALAN	-5.2920	-2.729	2.5630	5.2920	2.7290	4.0105	1.2815	0.7803	3.1797
SAL2AP	-5.3070	-2.707	2.6000	5.3070	2.7070	4.0070	1.3000	0.7692	2.4947
SALPD	-5.2060	-2.906	2.3000	5.2060	2.9060	4.0560	1.1500	0.8696	3.7121

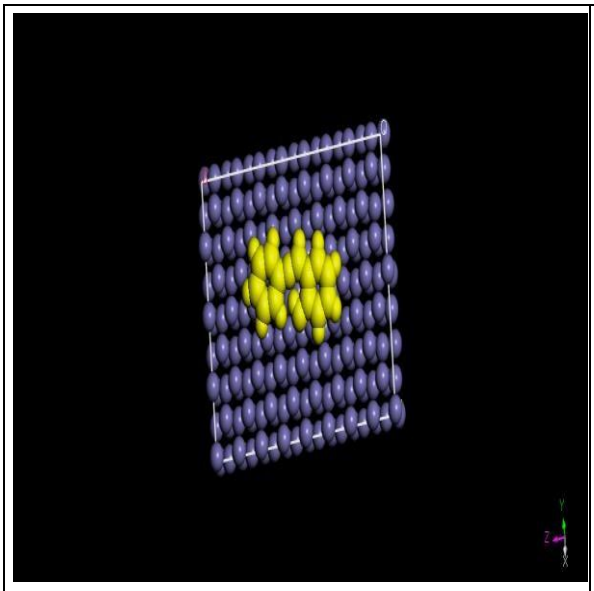	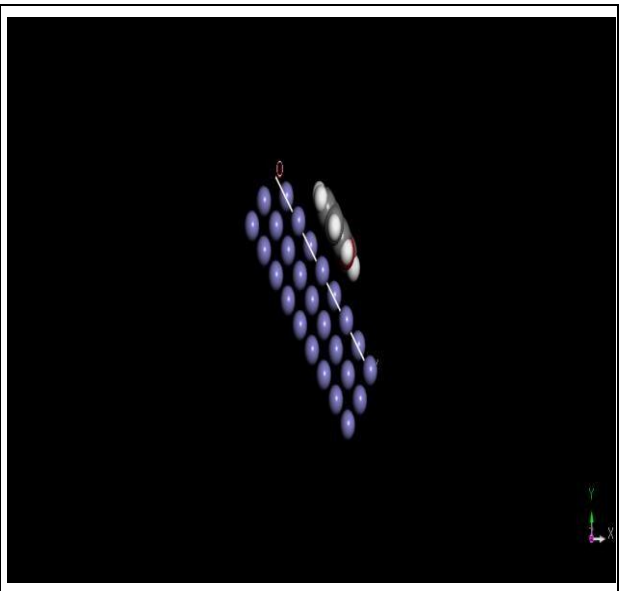
(a)	(b)
Top view of adsorption mode of SALAN on mild- steel surface	**Side- view of adsorption mode of SALAN on mild steel surface**

Figures 4.65: (a) (b) Top and Side view of adsorption mode of SALAN on Mild Steel surface

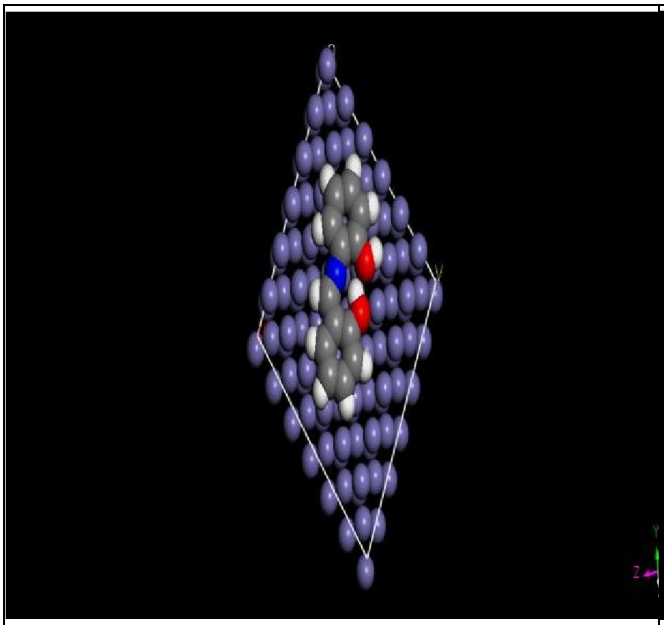	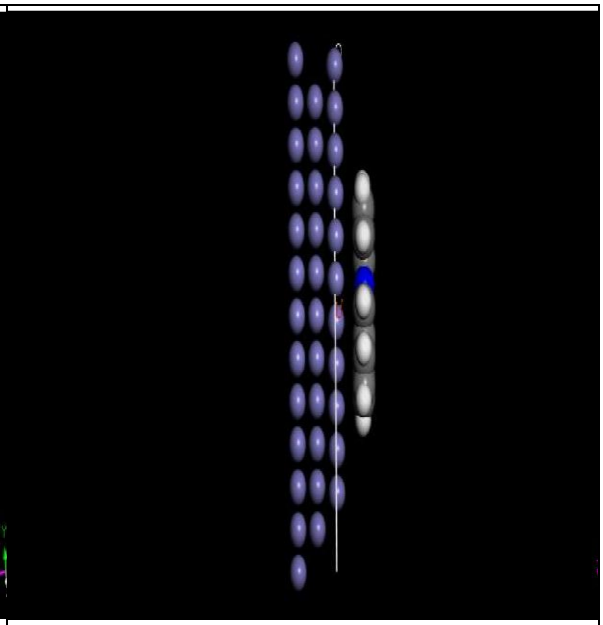
(a)	(b)
Top view of adsorption mode of SAL2AP on mild steel	**Side- view of adsorption mode of SAL2AP on mild steel surface**

Figures 4.66 (a)(b) Top and Side views of adsorption mode of SAL2AP on Mild Steel surface

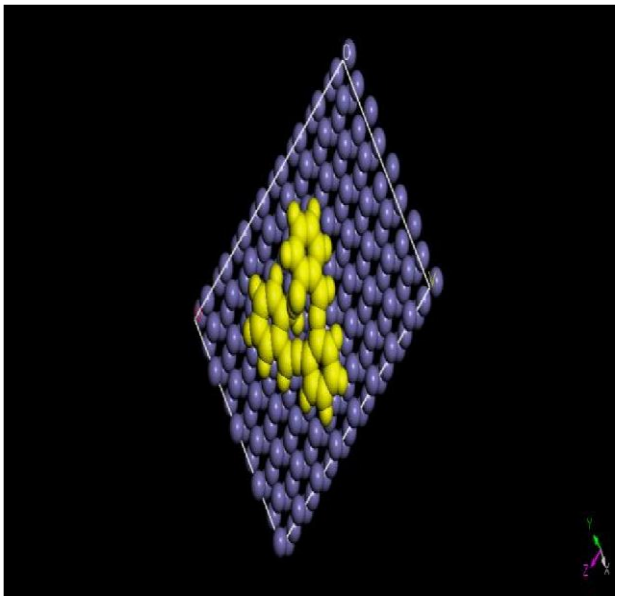	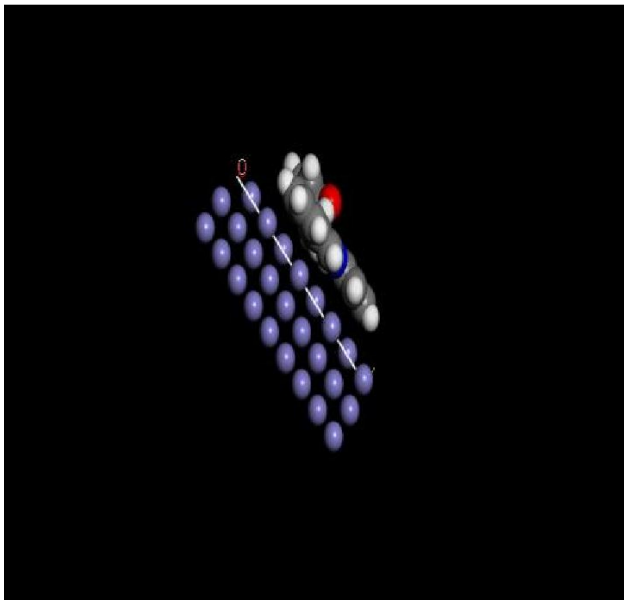
(a)	(b)
Top view of adsorption mode of SALPD on mild steel surface	**Side- view of adsorption of SALPD on mild steel cleaved surface**

Figure 4.67: (a) (b) Top and Side views of Adsorption mode of SALPD on Mild Steel Surface

4.2.2.8 Analysis of Molecular Modelling of Schiff Bases

The HOMO electron density surface reveals the parts of a molecule with the highest donating electrons into appropriate vacant orbitals of an acceptor. The electron density distribution of the frontier molecular orbitals (Figures 4.63(c)) showed that the HOMO orbitals of SALPD is predominantly of pi-character and the electron density is extended over the entire aromatic system and the pi-electron networks which might favor forward electron donation to the vacant d-orbital of the metal (Fe in mild steel) for donor-acceptor interactions. Additionally, inhibition efficiency of imine compounds is enhanced with increase in the number of aromatic rings on their molecule (Olasunkanmi et al., 2016). The number of aromatic rings electron – rich center) on the entire molecule of SALPD are more in number compared to number of aromatic rings on SALAN and SAL2AP, therefore SALPD is predisposed to furnish more electrons for interaction with the d-orbital of Fe of mild steel and a better inhibition efficiency compared to SALAN and SAL2AP molecules. Presence of more heteroatoms on SALPD molecule provides more sites of interaction and enhanced adsorption on the mild steel surface and higher inhibition performance.

The HOMO orbital of SALAN (Figure 4.63 (a)) is spread over the aromatic system and therefore of pi- character. However, the electron density is predominantly on the salicylaldehyde moiety. Hence the pi- electron network which might favor forward electron donation to the vacant d-orbital of the metal (Fe in mild steel) for donor-acceptor interactions may come from the salicylaldehye moiety. Also, the density of electron on the salicylaldehyde moiety of SALAN is slightly higher than the electron density on salicylaldehyde moiety of SAL2AP. Therefore, SALAN having similar molecular structure with SAL2AP may likely furnish more electrons for interaction with the d- orbital of Fe of mild steel, conferring more protection to the mild steel than SAL2AP. Electron density of SAL2AP (Figure 4.63 (b)) is more on the 2-aminophenol moiety which is suggestive that the electron flow to the empty d- orbital of Fe of mild steel will come from the 2- aminophenol moiety.

LUMO electron density shows the parts of a molecule with the highest chance of accepting electrons from the filled d- orbital of a donor which gives rise to back-bonding, complexation, increase in interaction with the d-orbitals of Fe of mild steel and formation of stronger covalent bond which gives rise to enhanced adsorption and protection of the mild steel . LUMO electron density of SALPD (Figure 4.64 (c)) with greater number of available lowest unoccupied molecular orbital has the highest tendency to furnish empty orbitals for electron interaction and feedback-bonding. This invariably enhances adsorption of the molecules on the surface of mild steel and

increased inhibition performance compared to both SALAN (Figure 4.64(a)) and SAL2AP (Figure 4.64(b)) with lesser available LUMO orbitals.

4.2.2.8 HSAB-type Analysis

Quantum chemical parameters obtained from the calculations which are responsible for inhibitor efficiency such as the energy of highest occupied molecular orbital (E_{HOMO}), energy of lowest unoccupied molecular orbital

(E_{LUMO}), the separation energy (E_{LUMO}-E_{HOMO}), ΔE, representing the function of reactivity, dipole moment (μ), the electronegativity χ, the global hardness (η), and softness (σ), are collected in Tables 4.64. Out of the whole lot, only the $_{HOMO}$, E_{LUMO}, and the dipole moment were obtained directly from the software. Following the Koopman's HSAB principle**,** the eigen values of HOMO and LUMO were related to ionization potential (I) and electron affinity (A) as:

$-E_{HOMO}$ and, $-E_{LUMO}$ respectively. (4.6)

Absolute electronegativity, X, and absolute hardness, η of the inhibitor molecules are given by Pearson [Pearson, 1988] as:

$$X = \frac{1}{2}(I + A) \text{ and } \eta = \frac{1}{2}(I - A) \quad (4.7)$$

Where I = ionization energy,

A = electron affinity.

Chemical softness (σ) is the measure of the capacity of an atom or group of atoms to receive electrons; it is estimated by using the equation: $\sigma = 1/\eta$. (4.8)

The obtained values of X and η were used to calculate the fraction of electron transferred, ΔN, from the inhibitor to metallic surface as follow [Kovacevic et al., 2011]:

$$\Delta N = 1 - \frac{X^{Fe-Xinh}}{\eta Fe + \eta inh} \quad (4.9)$$

In the equations above, for iron as a bulk metal, a theoretical electronegativity value of 7.0 was used, and absolute hardness is considered to be zero.

Hardness and softness are the basic chemical concepts, called global reactivity descriptors have been theoretically justified within the framework of density functional theory [Hohenberg& Kohn,

1964]. These are the important properties to measure the molecular stability and reactivity. Chemical hardness fundamentally signifies the resistance towards the deformation or polarization of the electron cloud of the atoms, ions or molecules under small perturbation of chemical reaction. A hard molecule has a large energy gap and a soft molecule has a small energy gap [Obi-Egbedi et al., 2011]. The dipole moment is another crucial molecular property that comes into play during the assessment of an additive as a potential corrosion inhibitor [Udhayakalaa et al., 2013; Ju et al., 2018]. Molecules with larger dipole moments exhibit greater polarity, enabling stronger electrostatic interactions with charged metal surfaces, which enhances the adsorption of the inhibitor onto the metal. The sign of ΔN can be used to determine the tendency of electrons to transfer between iron atoms and organic molecules [Khaled, 2010]. If ΔN is greater than zero, electrons tend to move from molecules to the metal surface [Feng, et al., 2011]. Conversely, electrons are more easily transferred from iron atoms to organic molecules. If for a molecule, the value of ΔN with an iron atom falls in the range of 0−3.6, then this molecule may have good inhibition performance. Within the same range, the larger the ΔN value is, the better the inhibition efficiency the molecule may have. The values obtained in this study show the Schiff base compounds are good inhibitors.

Table 4.64 collects all the quantum chemical parameters obtained in this study. From these parameters, we derived the following insight:

(1) **Electron Donation/Acceptance**: **SALPD** is the best **electron donor** (highest EHOMO) and the best **electron acceptor** (lowest ELUMO), indicating a balanced ability for both donating and accepting electrons.

(2) **Reactivity**: Reactivity decreases in the order: **SALPD > SALAN > SAL2AP** (based on ΔE values). **SALPD** is the most reactive due to its smallest energy gap (2.300 eV) and lowest hardness.

(3) **Polarity**: **SALPD also** exhibits the highest dipole moment (3.7121 eV), suggesting it has the strongest molecular polarity, which could influence its interactions in polar environments.

4.2.2.9 Inhibitor Adsorption Simulation.

To simulate the interaction between the corrosion inhibitor and the steel surface, an adsorption module is carried out to obtain the adsorption structure and energy for the Schiff base compounds on a Fe (110) surface. The simulated spatial structures are shown in Figure 4.65, 4.66 and 4.67.

By careful examination of the images, it could be observed that all the inhibitors adsorbed nearly parallel to the iron surface where a chemical bond could occur through donation of pi electrons of the aromatic ring and the lone pair of the hetero-atoms to the metal, which explains the excellent inhibiting performances of the Schiff base compounds on mild steel in acidic medium.

CHAPTER FIVE

CONCLUSION AND RECOMMENDATION

5.1 Conclusion

The corrosion inhibition potentials of Cerium (III) metal complexes of some salicylaldehyde based Schiff bases have been successfully evaluated. The three Schiff bases employed for this present work are salicylideneaniline(SALAN), salicylalidene-2- aminophenol (SAL2AP), and salicylalidene –*o*-phenylene(SALPD) with their cerium (III) metal complexes namely Cerium(III) salicylalideneaniline(CeSALAN), Cerium(III) salicylidene-2- aminophenol (CeSAL2AP), and *Cerium* (III)salicylalidene-*o*-phenylene diamine (CeSALPD) were successfully synthesized, and characterized by spectral technique such as NMR, UV, EDXRF, and FTIR techniques. The spectral results obtained such as shift in maximum absorbance wavelength of the Schiff bases compared to their metal complexes, presence of signal due to proton and carbon of azomithine functional group in the NMR spectral of the Schiff bases, presence of characteristics functional groups of Schiff bases in the compounds and the detection of Cerium metal in the EDXRF spectral of the metal complexes, confirms the successful synthesis of the inhibitor- compounds. Their physical properties were analyzed using colour, melting point analysis, pH, and solubility. Some chemical properties of the compounds such as molar conductivity, and magnetic susceptibility were also analyzed. AFM technique was used to analyze the surface of the mild steel after corrosion. Molecular modeling was used to predict the reactivity of the Schiff bases. Results from the molecular modeling shows that the Schiff base-compounds have electron- rich HOMO orbitals, and sufficient number of LUMO orbitals for donor- acceptor interaction with the d- orbital of Fe of the mild- steel. The inhibitor – compounds were observed to adsorb in a flat mode on the mild-steel surface which encourages an effective electron- acceptor interaction between the inhibitor - compounds and the Fe of the mild- steel, which could lead to enhanced inhibition by the Schiff base compounds. Other quantum chemical parameters such as hardness, softness, energy gap, electronegativity, ionization potentials were also calculated. Molecular result obtained shows the reactivity of the Schiff bases follows the order SALPD.> SALAN> SAL2AP. Gravimetric method was used to analyze the corrosion inhibition potentials of the compounds, and electrochemical method was used to confirm the results of the weight loss method. Results generated from electrochemical studies such as the PDP showed that the addition of the inhibitors in the corrosion medium increased the values of the cathodic (bc) and anodic tafel (ba) slope which is suggestive that the inhibitors acted as mixed- type inhibitors. The results from EIS measurement showed that

addition of the inhibitors to the corrosion medium reduced the values of corrosion potential (E_{corr}) in absence of the inhibitors, and lowered the values of the corrosion current (I_{corr}). Evaluation of inhibition efficiency with immersion time showed decrease in inhibition with immersion time. The effect of temperature on the inhibitive performances of the compounds were evaluated, and it was confirmed that the inhibition efficiency of the compounds decreased with increasing temperature. These observations are consistent with physisorption adsorption process of inhibitor molecules. The thermodynamic parameters obtained from the temperature experiment shows that the inhibitors inhibited corrosion of the mild steel by increasing the activation energy (Ea) of the reaction due to the blank. The positive values of enthalpy (ΔH) shows endothermic adsorption process, while negative entropy (ΔS) shows movement towards increased orderliness of the system due to the inhibitive activities of the inhibitors. The negative values of Gibb's free energy of reaction due to the presence of the inhibitors shows the reaction was spontaneous. Three adsorption isotherms namely: Langmuir, Temkin, and Frumkin models were used to study the adsorption mode of the inhibitor molecules on the mild- steel surface. The regression square values obtained from the various adsorption models show that Langmuir isotherm best fits into the adsorption process with R^2 value up to 0.99. The results obtained by the gravimetric method, electrochemical method, and computational modeling were in agreement. Data obtained from the present study showed excellent inhibitory performances of the Schiff bases and their Cerium metal complexes, with SALPD and CeSALPD recording the highest inhibition efficiency compared to other Schiff bases and their metal complexes. Results, also confirmed that complexation enhanced the corrosion inhibition potentials of Schiff base compounds.

5.2 Recommendations

Based on the physisorption process of absorbance of the studied- inhibitor compounds on the mild steel- surface, which gave rise to reduction in IE of the compounds over time, the studied compounds may not be efficient to protect a mild steel over a long duration. Therefore, it could be helpful to employ synergism with nano metal oxides such as ZnO, Al_2O_3, and TiO_2. Nano materials are widely used as inhibitors due to their excellent barrier properties, high chemical stabilities and reactivities. They have ability to increase surface coverage, and adherence due to their small size and high surface area to volume ratio. Additionally, further research could be done on the compounds to study their catalytic abilities, which could be employed in industrial processes that require catalysis.

5.3 Contributions to Knowledge

1. This work has provided a detailed data base on the protective efficiency of the six studied compounds in acidic medium with CeSALPD emerging as the best inhibitor compound at concentration as low as 0.4 mmol/dm3 with inhibition efficiency of 82.95 %.
2. It has provided an insight into the geometry of the complexes, and the coordination chemistry of the Schiff bases as well as their physico-chemical and spectral characterization.
3. The results obtained from this research will help to build a data base on the use of lanthanides compounds for corrosion inhibition.
4. The investigated compounds can successfully be used in place of long- used carcinogenic chromate- based compounds as inhibitors of mild- steel in acidic medium due to their low health - risks.

REFERENCES

Abdel Aziz, A.A., Salem, A.N. M., Sayed, M. A., & Aboaly, M.M. (2012). Synthesis, structural characterization, thermal studies, catalytic efficiency, and antimicrobial activity of some M(II) complexes with ONO tridentate Schiff base N-Salicylidene-o-aminophenol ($SaphH_2$) *Journal of Molecular Structure,* 1010, 130-138

Abdel- basset. R., Fatiha, B., Linda, T., Nourelhonda, B., Malika, F., Buzhayehu, A., & Mir, W.A. (2025). Electrochemical, quantum chemical and thermodynamic investigation of a Schiff base Corrosion inhibition for XC70 Steel. Scientific reports, 15, 19350.

Abdel- Rahman, L.H., Abu-Dief, A.M., Mohammed, I., Mounir, A.A., & Mohammed, N.A.H. (2016). Synthesis, structure elucidation, biological screening, molecular modelling and DNA binding of some Cu(II) chelates incorporating imines derived from amino acids. *Journal of Molecular Structure,* 1103, 232-244.

Abdel-Gaber, A.M., Abd-El-Nabey, B.A., Khamis, E., & Abd-El-Khalek, D.E. (2011). A natural extract as scale and corrosion inhibitor for steel surface in brine solution. *Disalination,* 278(1-2), 337-342.

Abu-Dief, A.M., & Mohamed, I.M.A. (2015). A Review on versatile applications pf transition metal complexes incorporating Schiff bases. Benisuef university, *Journal of Basic Applied Sciences,* 4, 119-133.

Ahmed, A., Taghried, A.S., Khalida, F.A., Lina, M.S., Abdul, A.H.K., & Mohd, S.T. (2019). Quantum chemical elucidation on corrosion inhibition efficiency of Schiff base: DFT investigations supported by weight loss and SEM techniques. *International Journal of Low-carbon Techniques*, 15(2); 202-209.

Ahmed, A.A. (2024). Schiff bases as Corrosion inhibitors: A mini- Review. *Journal of Materials and Engineering*, 02(3) 61-67.

Al- Momani, N.N., Taha, Z.A., Ajloani, A.M., Shagra, Q. M., & Al Zouby, M. (2013). A study of in-vitro antibacterial activity of Lanthanide complexes with tetradentate Schiff base ligand. *Asian Pacific Journal of Tropical Biomedicine*, 3(5), 367.

Almi, S., Rais, Z., Seridi, S., Benakcha, R., Almi, K., Hadjeb, R., Menasra, H., & Adjal, F. (2025). Synthesis and corrosion inhibition efficiency of Schiff bases derived from salicylideneaniline – a review. *New Journal of Chemistry, 49*, 5639–5664.

Amer, S, Nadia, E.W., & Hoda, E. G. (2013). Synthesis, spectral, antitumour and antimicrobial studies on Cu(II) complexes of pourine and triazole Schiff bases derivatives. *Journal of Molecular Structure*, 10(49), 326-335.

Amin, M.A., Khaled, K.F., Mohgen, Q., & Arida, H.A. (2010). A study of the inhibition of iron in HCl solutions by some aminoacids, *Corrosion science*, 52, 1684-1695.

Ammar, Z., Salah, N.N., Salem, A., Latifa, K., Aicha, K., Abasse, K., Mousa, A., Djamel, G., Mohamed, A., Ali, A. A. L and Noureddine, E. (2023). Corrosion Inhibitiency of Azo Compounds Derived from Schiff bases on Mild steel (XC70) in (HCl, in 1 M DMSO) Medium: An experimental and theoretical Study. ACS Omega, 8(24), 21571 – 21584: https // .

Anancona, J.R, Natiana, N., & Juan, C. (2015). Synthesis, characterization and antibacterial activity of a tridentate Schiff base derived from Cephalothin and sulfadiazine, and its transition metal complexes: Spectrochimica Acta Part A: *Molecular and Biomolecular Spectroscopy*, 137, 16-22.

Ansari, S., Ansari, G., Ghori, M. U., & Kazi, A. G. (2019). Impact of Brand Awareness and Social Media Content Marketing on Consumer Purchase Decision. *Journal of Public Value and Administrative Insight, 2*(2), 5–10.

Aouniti, A., Elmsellem, H., Tighadouini, S., Elazzouzi, M., Radi, S., Chetouani, A, Hammouti, B., & Zarrouk, A. (2016). Schiff bases derived from2-acetylthiophene as corrosion inhibitor of steel in acidic medium. *Journal of Taibah University for Science*, 10,774-785.

Arjmand, F., Sayeid, F., & Muddassir, M. (2011) Synthesis of new chiral heterocyclic Schiff base modulated Cu(II)/Zn(II) complexes their comparative binding studies with CT-DNA, mononucleotides and cleavage activity. *Journal of Photochemistry and Photobiology B: Biology*, *103*(2), 166-179.

Athira, C.J., Sujamol, M.S., Sindyhu, Y., & Mohanan, K. (2021). Synthesis, spectroscopic characterization, corrosion inhibition studies and dyeing properties of lanthanide(III) complexes of 1-[(3-carboxyethyl-4,5- dimethylthiophen-2-yl) azo]-2 -napthol. Indian *Journal of Chemistry*, 60 A, 489-498.

Bhawna, C, Ashish, K.S., Sanjeele, T., Balaram, P., Hassane, L.Ill-Min, C., Ranjana, J., &Eno, E.E. (2020). Comparative investigation of corrosion – mitigation behaviour of thiadiazole-derived bis- Schiff bases for mild steel in acid medium: Experimental, theoretical, and surface study. *ACS Omega*, 5, 13503-13520.

Biswas, S., Chandam, K.M., Rahu, N., Das, A., & Mondal, K.T. (2015). Synthesis of new Rhodium(III) complex by benzylic C-S bond cleavage of thio ether containing NNS donor Schiff base ligand: investigation of catalytic activity towards transfer hydrogenation of ketones. *Inorganica Chimica Acta*, 515, 120096.

Brodowska, K., & Łodyga-Chruscinska, E. (2014). Schiff bases – interesting range of applications in various fields of science. *CHEMIK, 68*, 129–134.Jia, Y., & Li, J. (2013). Molecular assembly of Schiff base interactions: construction and application. *Chemical Reviews*.

Cao, Y., Cenlan, Y., Hongmei, L., Haixia, L, Qipeng, L, Zeli, Y, & Gang, W. (2016). Synthesis, crystal structures and invitro anticancer activities of oxovanadium(IV) complexes of amino acid Schiff base and 1,10- Phenanthroline ligands. *Transition Metal Chemistry*, 41, 531-538.

Ceyhan, G., Muhammet, K., Mehmet, T., Ibrahim, D., Ayse, S.V. & Vickie, M. (2013). Structural characterization of some Schiff base compounds Investigation of their electrochemical, photoluminescence, thermal and anticancer activity properties. *Journal of Luminescence*, 143, 623-634.

Chakraborty, A., Kumar, P., Ghosh, K, & Roy Partha (2010). Evaluation of Schiff base copper complex compound as potent anticancer molecule with multiple targets of action. *European Journal of Pharmacology*, 647(1-3), 1-12.

Da Silva, C. M., Da Silva, D. L., Modolo, L. V., Alves, R. B., De Resende, M. A., Martins, C. V. B., & De Fátima, Â. (2011). Schiff bases: A short review of their antimicrobial activities. *Journal of Advanced Research*, *2*, 1–8.

Denissen, P.J., & Garcia, S.J. (2017). Cerium- loaded algae exoskeletons for active corrosion protection 8of coated AA2024-T3. *Corrosion Science* 128, 164-175.

Ebenso, E.E, Verma, C., Lukman, O.O., Akpan, E.D., Verma, D., Lgaz, H., Guo, L., Kaya, S. & Quaraishi, M.A. (2021). Molecular modelling of compounds used for corrosion inhibition studies: *Physical Chemistry Chemical Physics,*1(89).

Ebenso, Eno, E., Isabirye, David, A., & Eddy, N. O. (2010). Adsorption and quatum chemical studies on the inhibition potentials of some thiosemicarbazone for the corrosion of mild steel in acidic medium. *International Journal of Molecular Science,* 11(6), 2473-2498.

El- Arrouji, S, Karrouchi, K., Barisha, A., Ismaily, K., Warad, I., Rais, Z., Radi, S., Taleb, M., Ansar, M. & Zarrouk, A. (2020). New pyrazole derivatives as effective corrosion inhibitors on steel – electrolyte interface in HCl: Electrochemical surface morphological (SEM) and computational analysis. *Colloid surface* A.604, 125325.

El-Baradie, K.Y., El- Wakiel, N.A, ElGhamry, H.A. (2014). Synthesis, characterization and corrosion inhibition in acid medium of L-histidine Schiff base complexes. *Applied Organometallic Chemistry*, 29(3), 117-125.

El-Sherif, A.A., Shehata, M.R., Shoukry, M.M., & Barakat M.H. (2012). Synth-Synthesis, characterization, equilibrium study and biological activity Of Cu(II), Ni(II) and Co(II)

metal complexes of polydentate Schiff Base ligand. *Spectrochimica Acta Part A: Molecular and Biomolecular Spectroscopy*, 96: 889 -97.SA.

Enas, V., Lena, R. & Mona, A. (2016). Synthesis 0f Co(II) and Cu(II) Complexes with NO and N_2O_2 Ligand Derived from Salicylaldehyde. *Chemistry and Materials Research*, 8 (7), 82-93.

Fatma, N., Sayed, and Gehad, G.M. (2022). Newly Synthesized Lanthanide Complexes of Ferrocene- based Schiff bases with high biological activities, and improved molecular docking date. *Journal of Organometallic Chemistry*: https// doi.org/ 1010161jorganchem.2022.122450.

Feng, N., Guo, X., Liang, S., Zhu, Y., & Liu, J. (2011). Biosorption of heavy metals from aqueous solutions by chemically modified orange peel. *Journal of Hazardous Materials*, *185*(1), 49–54.

Fu, J., Li, S., Wang, Y., Cao, L., & Lu, L. (2010). Computational and electrochemical studies of some amino acid compounds as corrosion inhibitors for mild steel in hydrochloric acid solution. *Journal of Materials Chemistry*, *20*(5), 913–920.

Gece, G. (2018). The use of quantum chemical methods in corrosion inhibition studies, *Corrosion* science, 50(II), 2981-2992.

Gece, G., Bilgic, S., & Turksen, O. (2010). Quantum chemical studies of some amino acids on the corrosion of cobalt in sulfuric acid solution. *Materials and corrosion*, 6(2), 141-146.

Gupta, R., Agrawal, N., & Grupta, K.C. (2012). Synthesis IR Spectrual studies and biological activities of rare earth metal complexes with biochemical relevant ligand. *Research Journal of Pharmaceutical Biological and Chemical Sciences*, 3(2), 6-50.

Hamak, K. F., & Eissa, H. H. (2013). Synthesis, characterization, biological evaluation and anticorrosion activity of some heterocyclic compounds: Oxazepane derivatives from Schiff bases. *Journal of Molecular Structure*, *1048*, 334–341.

Hameed, A., Al-Rashida, M., Uroos, M., Ali, S. A., & Khan, K. M. (2017). Schiff bases in medicinal chemistry: a patent review (2010-2015). *Expert Opinion on Therapeutic Patents*, *27*, 63–79.

Hitesh, P., Bhautadiya, L.S., Jabali, J.V., and Toral, H.V. (2019). Rare earth metal complexes with Schiff base ligand: Synthesis, characterization and biochemical evaluation. Research *Journal of Life Sciences, Bioinformatics Pharmaceutical and Chemical sciences*, 5(3),1-14.

Ingale, V.D, Shinde, V.G., Dighore, N.R., Rajbhoj, A.S. and Gaikwad, S.T. (2015). Synthesis characterization and antimicrobial activity of a biovalent Schiff base derived from

Salicylaldehyde and 4-methoxyaniline and it's lanthande(III) complexes. *Journal of Chemical and Pharmaceutical Research*, 7(9), 493-499.

Jiang, Z., Zhang, H., Bian, X., Li, J., & Zhang, H. (2019). Insight into the Building of ACE inhibitory peptides to Angiotension-converting Enzyme: A molecular simulation. *Molecular Simulation*, 45,215-222.

Ju, M.-G., Chen, M., Zhou, Y., Dai, J., Ma, L., Padture, N. P., & Zeng, X. C. (2018). Toward Eco-friendly and Stable Perovskite Materials for Photovoltaics. *Joule*, *2*(7), 1231–1241.

Jun, Z., GUIMIN, Q., Songqing, H., Youguo, Y., Zhenjia, R, Lijun, Y. (2010). Theoretical evaluation of corrosion inhibition performance of imidazoline compounds with different hydrophilic groups. *Corrosion Science*, 53, 147-152.

Kapoor, P., Fahmni, N. and Singh, R.V. (2012). Microwave assisted synthesis, spectroscopic, electrochemical and DNA cleavage studies of lanthanide (III) complexes with Coumaria based imines. Spectrochemica Acta Part A: *Molecular and Biomolecular Spectroscopy*, 83(1), 74-81. from Reaction of 4, 4 – MethyleneDiantipyrene with Ethylenediamine: Indonesian Journal of Chemistry, 22(5): 1365.

Kawther, A. H., & Naser, D. S. (2022). Synthesis, characterization, and antibacterial activity of lanthanide metal complexes with Schiff base ligand produced. *Egyptian Journal of Chemistry*, *65*(12), 67–76.

Keypour, H., Mozhdeh, L., Malid, R., & Hamid, R. (2014), Synthesis and characterization of some new cd(II) and zn(II) macrocyclic Schiff base complexes derived from cyclo condensation of three new linear aromatic(N4) amines. *Journal of The Iranian Chemical Society*, 11, 1473-1482.

Khaled, K.F. (2010). Corrosion control of copper in nitric acid solutions using Some amino acids-A combined experimental and theoretical study. *Corrosion Science*, 52,3225-3234.

Khalissa, C., & Lynda-Maya, M. (2018). Contribution to the Agro-Morphological Characterization of Three Vetch Species (Vicia Spp.) in the Setif Semi-Arid Region by Discriminant Factorial Analysis (ADF). *International Journal of Innovative Approaches in Agricultural Research, 2*(2), 79–102.

Khlood, S.A., Gamil, A.A., Ismail, A., Arwa, A., Ali. A.K., Fathy, S., & Nashwa, E. (2021). Spectral, molecular modelling, and biological activity studies on new Schiff base of acenaphthaquinone transition metal complexes. *Bioinorganic Chemistry and Applications*. Doi.org/10.1155/2021/6674394.

Kostova, I., & Saso, L. (2013). Advances in research of Schiff-base metal Complexes as potent antioxidants. *Current Medicinal Chemistry*, (20):4609–4632.

Kovacevic, A. V., Parker, Q. A., Jacoby, G. H., Sharp, R., Miszalski, B., & Frew, D. J. (2011). Planetary Nebulae towards the Galactic bulge - I. [O iii] fluxes. *Monthly Notices of the Royal Astronomical Society*, *414*(2), 860–878.

Luz, Teodorico and Ramalho, C. (2010). Removal of Metal Ions from Aqueous Solution by Chelating Polymeric Hydrogel. *Environmental Chemistry Letters*, 8, 4, 343-348.

Madkour, L. H., & Elroby, S. K. (2015). Inhibitive properties, thermodynamic, kinetics and quantum chemical calculations of polydentate Schiff base compounds as corrosion inhibitors for iron in acidic and alkaline media. *International Journal of Industrial Chemistry*, *6*, 165–184.

Manfred, R., & Jurgen, P. (2012). Electronic absorption spectroscopy. Doi: 10.10071978-3-62-24390-5-3.

Maryam, C., Abdelkarim, C., Hassane, Lgaz, Rachid, S., Santosh, L., Gaonkar, K., & Subraumanya, B. (2019). Synthesis and corrosion inhibition evaluation of a new Schiff base hydrazine for mild steel corrosion in HCL medium: electrochemical, DFT, & molecular dynamics simulation studies. *Journal of adhesion Science and technology*, 34(12), 90-97.

Migahed, M.A., Farag, A.A, Elsaed, S.M., Kamal, R., Mostfa, AbdEl-Bary, H. (2011). Synthesis of a new family of Schiff base non-ionic surfactants and evaluation of their corrosion inhibition effect on X- type tubing steel in deep oil wells formation water. *Material Chemistry and Physics*, 125(1-2), 125-135.

Mohamed, K. A., Mohamed, R.M., & Mohamed, M.A. (2010). Computational Simulation of the molecular structure of some triazoles as inhibitors for the corrosion of metal surface. *Journal of molecular structure: Theochem*, 95(9), 66-67.

Mohamed, T. M. A., Ang, Y.-S., Radzinsky, E., Zhou, P., Huang, Y., Elfenbein, A., Foley, A., Magnitsky, S., & Srivastava, D. (2018). Regulation of Cell Cycle to Stimulate Adult Cardiomyocyte Proliferation and Cardiac Regeneration. *Cell*, *173*(1), 104-116.e12.

Mounika, K., Anupama, B., Pragathi, J., & Gyanakumari, C. (2010). Synthesis, characterization and biological activity of a Schiff base derived from 3-ethoxysalicylaldehyde and 2-aminobenzoic acid and its transition metal complexes. *Journal of Scientific Research*, *2*(3), 513–524.

Navneet, K., Pratima, S., & Astha, P. (2013). Synthesis of New Schiff base complexes and their application. *International Journal of Applied Research and Studies*, 2(2), 1-4.

Negm, N.A, Ghuiba, F, M., & Tawfik, S.M. (2011). Novel isoxazolium cationic Schiff base compounds as corrosion inhibitors for carbon steel in hydrochloric acid. *Corrosion Science*, 53(11), 35566-3575.

Negm, N.A, Mandile, N.G, Badr, E.A., & Mohammed, A. (2012). Gravimetric and electrochemical evaluation of environmentally friendly non-ion-corrosion inhibitors for carbon steel in 1M HCl. *Corrosion science*, 6, 94-103.

Ni, H., Wu, J., Sun, Z., Lu, G., & Yu, J. (2019). Molecular simulation of the structure and physical properties of Alkali nitrate salts for thermal energy Storage. *Renew Energy*, 136, 955-967.

Nidli, Siddharam, Davendra, P.R., Armit, K.G., Aishish, V., and Yashveer, G. (2025). Schiff bases and their Possible therapeutic applications: *A Review Results in Chemistry*. Doi: https://doi.org/10.1016/j.rechem. 2024.101941.

Nizor, E. G., Basim, H. A., Mohammed, R.S. (2024). Novel thiazole derived Schiff bases as efficient Corrosion inhibitors for Mild steel in acidic Media: Synthesis, electrochemical and computational insights. *Arabian Journal of Chemistry*, https:// doi.org/10.10161j.arabjc. 2024.105867.

Obi-Egbedi, N. O., & Obot, I. B. (2011). Inhibitive properties, thermodynamic and quantum chemical studies of alloxazine on mild steel corrosion in H2SO4. *Corrosion Science, 53*(1), 263–275.

Oguzie, E.E., Li, Y., Wang, S.G., & Wanga, F. (2011). Understanding corrosion inhibition mechanisms- experimental and theoretical approach, *RSC Advances*, 1,866-873.

Olasunkanmi, L. O., Kabanda, M. M., & Ebenso, E. E. (2016). Quinoxaline derivatives as corrosion inhibitors for mild steel in hydrochloric acid medium: Electrochemical and quantum chemical studies. *Physica E: Low-dimensional Systems and Nanostructures*, *80*, 82–90.

Olasunkanmi, L. O., Obot, I. B., & Ebenso, E. E. (2016). Adsorption and corrosion inhibition properties of N-{n-[1-R-5-(quinoxalin-6-yl)-4,5-dihydropyrazol-3-yl]phenyl} methanesulfonamides on mild steel in 1 M HCl: experimental and theoretical studies. *RSC Advances, 6*(90), 86782–86797.

Olasunkanmi, L.O, Obot, I.B, Kabanda. M. M., & Ebenso, E. E. (2015). Some quinoxalin-6-yl derivatives as corrosion inhibitors for mild steel in hydrochloric acid: experimental and theoretical studies, *The Journal of Physical Chemistry*, 119, 16004–16019.

Onu, L.U., Akalezi, C.O., and Ogwuegbu, M.O.C. (2024). Assessment of newly synthesized salicylaldehyde - based Schiff base as corrosion inhibitors for carbon steel in aqueous environment. *Journal of Chemical Society of Nigeria*, 49(5): 683-704.

Osowole, A.A., and Balogun, S.A. (2012). Spectral, magnetic, thermal and antibacterial properties of some metal (II) complexes of aminoindanyl Schiff bases. *European Journal of Applied Sciences*, 4, 1, 6-13.

Pirhadi, S., Sunseri, J., & Koes, D. R. (2016). Open-source molecular modeling. *Journal of Molecular Graphics and Modelling, 69*, 127–143.

Prakash, A. & Adhikari, D, (2011). Applications of Schiff bases and their metal complexes: A Review. *International Journal of ChemTech. Research*, 3, 1891-1896.

Preethi, K., Lavanya, M. (2021). Optimization of inhibition efficiency of a Schiff base on mild steel in acid medium: Electrochemical and RSM approach. *Journal of Bio-and Tribo-corrosion*, 7: 110.

Rajewar, V. R., Dharmale, M. K. & Pingalkar, S. R. (2014). Synthesis and spectral characterization of lanthanide complexes derived from 2-[(4-Bromo-2,6-dichlorophyenylimino)-methyl]-4,6-diiodo-phenol. *Oriental Journal of Chemistry*, 30(4), 2049-2058.

Rawat, M. S. M., Mal, S., & Singh, P. (2015). Photochromism in anils - A review. *Open Chemistry Journal*, *2*, 7–19.

Rohman, D.L., & Sugeng, R. (2014). FTIR spectroscopy combined with partial least square for analysis of red fruit oil in ternary mixture system. *International Journal of Spectroscopy*. Doi'org 10.1155/2014/785914

Sagar, Y, S., Raju, M.P., & Rams, S.D. (2013). Corrosion inhibition of mild steel by using mixed ligand metal complexes. *International Journal of Chemical Science.*11(1), 503-517.

Samide, A. & Tutunam, B. (2011). Adsorption and inhibitive properties of a Schiff base for the corrosion control of carbon steel in saline water. *Journal of Environmental Science and Health A: Toxic Hazardous Substances and Environmental Engineering*, 46(14), 1713- 20.

Seem, V. (2015). Biological activity based on structural aspects of some phenolic Schiff base complexes. *Chemistry and materials research*, 9, 41- 50.

Sherif, O.E. and Abdel- Kader, N.S. (2014). Spectroscopic and biological activities studies on biovalent transition metal complexes of Schiff bases derived from condensation of 1,4-Phynelendiamine and benzopyrine derivatives. Spectrochima Acta Part A: *Molecular and Biomolecular Spectroscopy*, 117, 519-526.

Shivakumar, S, & Mohana, K. (2013). Corrosion behaviour and adsorption thermodynamics of some Schiff base on mild steel corrosion in industrial water medium. *International Journal of Corrosion*. Doi:10.1155/2013/5432.

Shobha, B., Sanaulla, P.F. Tegene, D., Ananda, Mucthy, H.C, & Bheemaraju, V. (2021). Evaluation of corrosion inhibition efficiency of Aluminum alloy 2024 by diaminostilbene and azobenzene Schiff bases in Hydrochlololoric acid. *International journal of corrosion*. https//doi.org/10.115512021/5869915.

Singh, A.K. & Quaishi, M.A. (2012). Study of some bidentate Schiff bases of Isatin as corrosion inhibitors for mild steel in hydrochloric acid solution. *International Journal of Electrochemical Science,* 7(4), 3222-3241.

Suraj, B.A., Balasaheb, U.J., Subhash, M.L. & Nana, V.S. (2020). A role of Schiff base and their metal complexes used as corrosion inhibitor in different corrosive medium. *Journal of Emerging Technologies and Innovative Research,* 7(1), 167-173.

Synthesis and corrosion inhibitiency efficiency of Schiff bases derived from Salicylideneaniline – a review. *New journal of Chemistry*: https:// doi.org/ 10.10391D4NJ05497K.

Tahani, I.K. & Khadijah, M.E. (2016). New Schiff bases as corrosion inhibition and biological activities of their metal complexes. *International Journal of Engineering Research and Management,* 3(8),106-166.

Tahmasebi, V., Grivani, G., & Bruno, G. (2016). Synthesis, characterization, crystal structure determination and catalytic activity in apoxidation reaction of two new oxovanadium(IV) Schiff base complexes. *Journal of Molecular Structure*,1123, 367-374.

Tian, H., Li, W., Cao, K., & Hou, B. (2013). Potent inhibition of copper corrosion in neutral chloride media by novel non- toxic thiadazole derivatives. *Corrosion Science* 73, 281-291.

Udhayakalaa, P., Rajendiranb, T. V., & Gunasekaran, S. (2013). Theoretical study using DFT calculations on inhibitory action of some pyrazole derivatives on steel. *Journal of Advanced Scientific Research, 4*(02), 31-37.

Verma, C., Lgaz, H., Verma, D. K, Ebenso, E.E. Bahadur, I. & Quraishi M.A. (2018). Molecular dynamics and monte-Carlo simulation as Powerful tools for study of interfacial adsorption behaviour of corrosion inhibitors in aqueous phase: A review. *Journal of Molecular Liquids* 260, 99-120.

Vimal, P., Pranav, T., Hardik, G. and Disha, K. (2014). Synthesis and characterization of Schiff base of *P*-chloro aniline and their metal complexes and their evaluation for antibacterial activity.

Yadav, A., Kon, K., Kratosova, G., Duran, N., Ingle, A. P., & Rai, M. (2015). Fungi as an efficient mycosystem for the synthesis of metal nanoparticles: progress and key aspects of research. *Biotechnology Letters, 37*(11), 2099–2120.

Yousif, E., Khulood, A.S., Nadia, S., Jumat, S. and Bashar, A. (2013). Metal complexes of Schiff base: Preparation characterization and antibacterial activity. *Arabian Journal of Chemistry*, 1-5.

Zahraa, A., & Aisha, G. (2019). Synthesis, characterization and anti-corrosion properties of an 8-hydroxyquinoline derivative. *Heliyon* 5(1):e02895.

Zhang, Bin, Lin, Yan, Tang, Xiaoning, Xu, Yinhua and Xie, Gang (2010). Mechanism of antibacterial activity of silver and praseodymium loaded white carbon black. *Journal. Of Rare earths,* 28, 442-448.

Zhang, H.H, Qin, C.K, Chen, Y., & Zhang, Z. (2019). Inhibition behavior of mild steel by three new benzaldehydethiosemicarbazone derivatives in 0.5M H_2SO_4: experimental and computational study, *Corrosion science*. 6,1-16.

APPENDIX

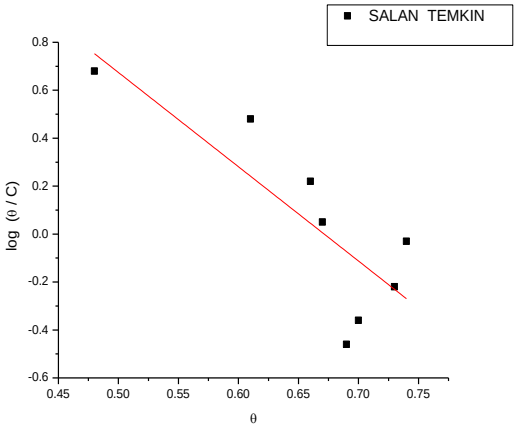

Figure 1: Temkin'S Plot for SALAN

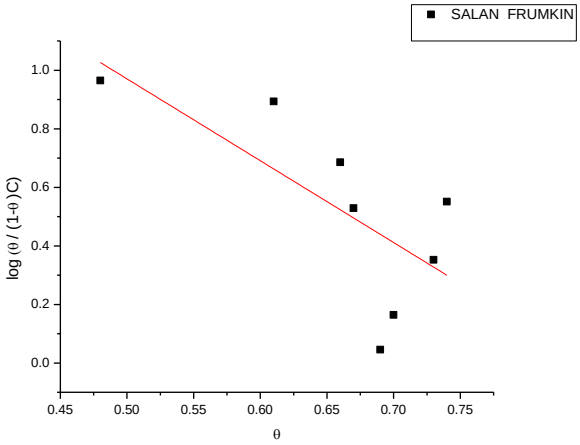

Figure 2: Frumkin's Plot for SALAN

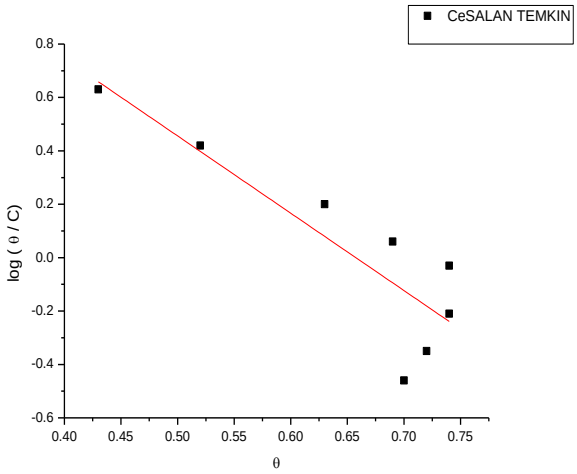

Figure 3. Temkin's Plot for CeSALAN

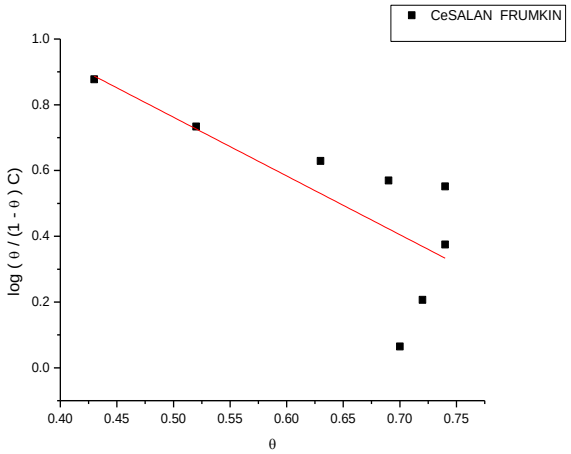

Figure 4. Frumkin's Plot for CeSALAN

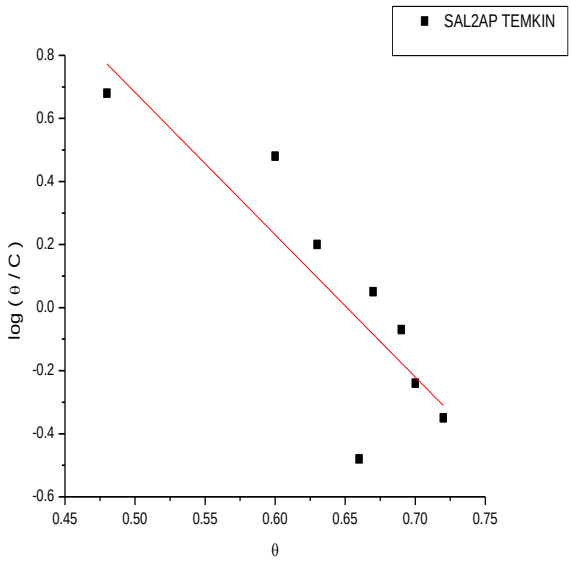

Figure 5. Temkin's Plot for SAL2AP

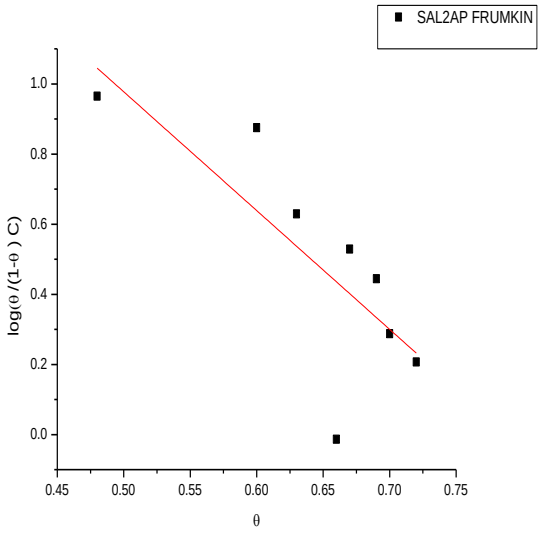

Figure 6. Frumkin's Plot for SAL2AP

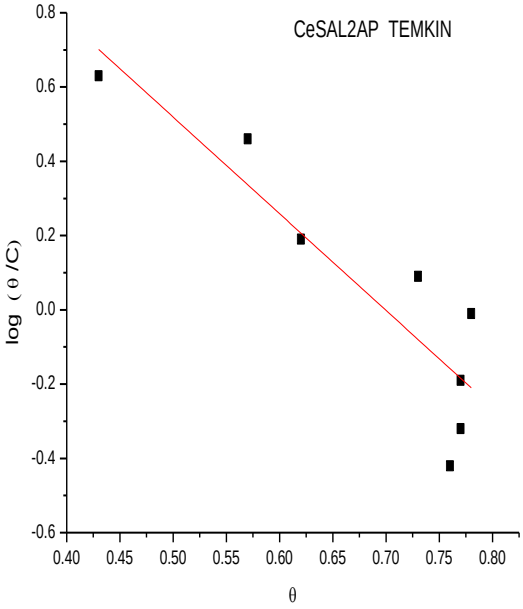

Figure 7. Temkin's Plot for CeSAL2AP

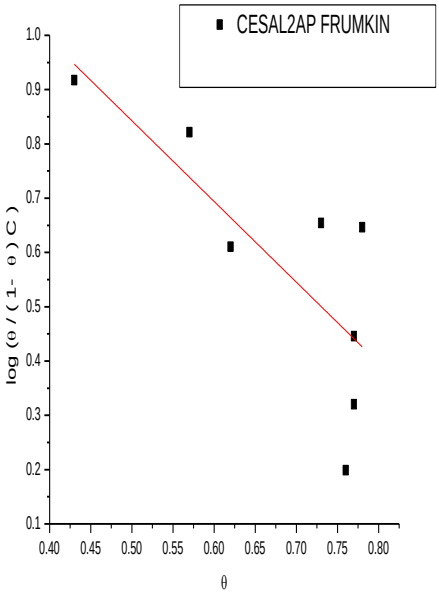

Figure 8. CeSAL2AP Frumkin's Plot

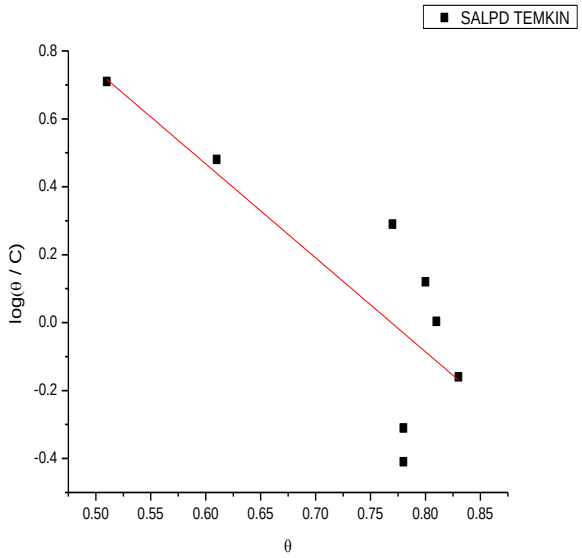

Figure 9. Temkin's Plot for SALPD

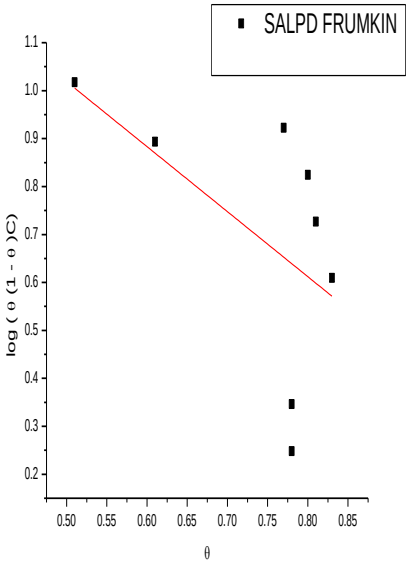

Figure 10. Frumkin's Plot for SALPD

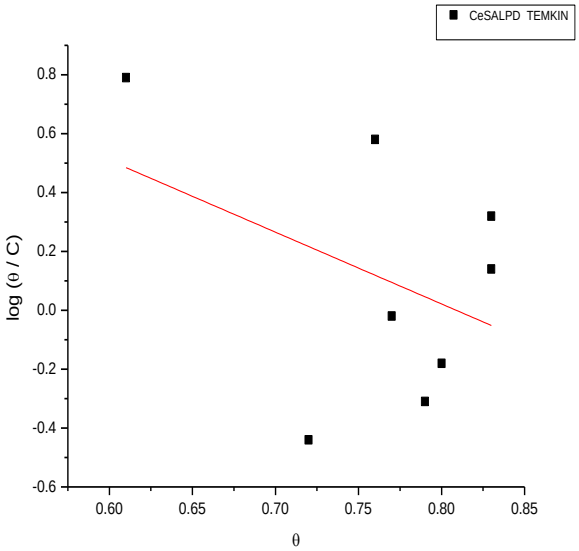

Figure 11. Temkin's Plot for CeSALPD

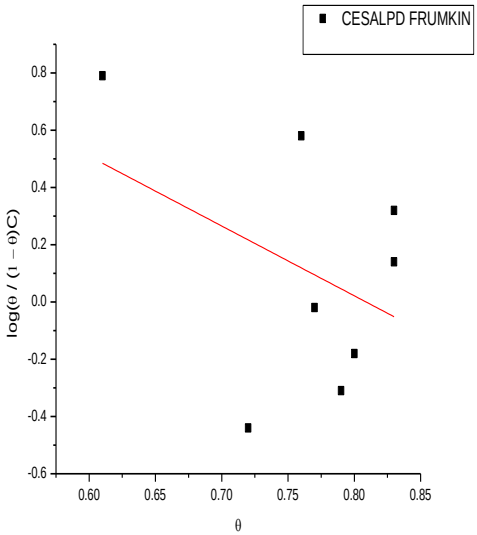

Figure 12. Frumkin's Plot for CeSALPD